Twelfth International Conference on Time-Resolved Vibrational Spectroscopy (TRVS XII)

National Institute of Standards and Technology (NIST)
Gaithersburg, MD 20899

May 23-27, 2005

TRVS XII Meeting in Review

The twelfth in a long-standing series of "Time-Resolved Vibrational Spectroscopy" (TRVS) meetings was held May 23rd through 27th, 2005 at the National Institute of Standards and Technology in Gaithersburg, MD. This world-renowned international conference continued the illustrious tradition of the original 1982 meeting that took place in Lake Placid, NY. This series of meetings was initiated by leading experts in the field of ultrafast laser spectroscopy, and continues to be overseen by its original founder, Prof. George Atkinson (Univ. of Arizona, now Science Advisor at the US State Department). In its current format, the conference promotes the traditional areas of pulsed laser vibrational spectroscopies including infrared, Raman and related coherent optical methods for emerging technology areas including basic science, energy related research and advancing novel commercial applications. Since monitoring time-dependent phenomena in molecular systems is key to many developing research programs in academia, government and industry, the conference focuses on molecular dynamics topics of interest to a wide attendance base.

The latest meeting on Time Resolved Vibrational Spectroscopy promoted science that is at the heart of the physical sciences, including chemistry, physics, biophysics, biology, and materials science. Vibrational spectra are molecule and bond-specific. Thus, time-resolved vibrational studies provide detailed structural and kinetic information about primary dynamical processes. From this perspective, the goal of achieving a complete understanding of complex chemical and physical phenomena at the molecular level is well served by fostering a venue for recent progress in experimental and theoretical vibrational studies in condensed phase and interfacial environments. In these respects TRVS XII was a complete success!

Our scientific program included sessions and invited speakers (8 plenary, 17 invited) that addressed multi-disciplinary topics including advances, recent developments and novel applications of vibrational spectroscopy to molecular systems. This year's meeting featured world-renowned invited speakers and attracted forty-five graduate students, many postdoctoral researchers and starting investigators interested in using infrared, Raman and related vibrational spectroscopies in their careers. Ninety-three people from all over the world attended. In parallel to experimental research, highlights of related theoretical investigations were also presented. The seven topical sessions (see program) and "Future TRVS Directions" session enabled contributors and participants engaged in modern applications and uses of vibrational spectroscopy to "cross-fertilize" and this venue lead to exciting future scientific developments and collaborations in this expanding and active field. Two Poster sessions including thirty posters allowed everyone the opportunity to present their work in open discussion formats. We also must recognize the significant contributions and support given by our fourteen Government agency and corporate sponsors some of whom exhibited their wares in the lounge during the meeting and generously helped reimburse registrations and travel expenses for many of our speakers and younger attending scientists. All meeting sessions were video taped and are available from the conference co-chairs in DVD format for those wishing copies of specific sessions or oral presentations.

In addition to the scientific sessions, we had numerous opportunities to discuss our recent work with new acquaintances and form collaborations. We circulated through the first poster session Monday afternoon that was complemented by our on-site meeting reception. We also enjoyed a Wednesday afternoon excursion to the Washington DC Mall where we visited many US National landmarks and Smithsonian Museums. After touring the museums, we gathered at the International Spy Museum to see their unusual exhibits. The self-guided museum tour was followed by our Banquet which featured awards presentations in recognition of work performed by our senior scientists (Profs. F. Siebert, M. El-Sayed and T. Kobayashi). We were also privileged to hear an after-dinner speech by the TRVS meeting founder, Prof. George Atkinson where he discussed potential avenues for fostering scientific cooperation through developing US State Department postdoctoral and international programs. On Friday, at then end of the "Future Directions" session, four awards supported by Newport/Spectra Physics were presented to student participants for their outstanding poster presentations.

The Twelfth Time-Resolved Vibrational Spectroscopy Conferences provided a unique opportunity to assemble a critical number of the leading researchers from academia, industry and government from the US and other nations of the world. It can now be recognized as the "leading venue" for researchers to discuss their findings and meet with their peers every two years. It is hoped that this meeting will continue to attract new people interested in diversifying their work and that you and your colleagues will attend the next meeting scheduled to take place in the summer of 2007 in Munich, Germany (W. Zinth and A. Laubereau, co-chairs).

With our thanks and best wishes to all our scientific colleagues and future TRVS meetings,

Ted Heilweil, Co-Chair
Tel: 301-975-2370
edwin.heilweil@nist.gov

Terry L. Gustafson, Co-Chair
Tel: 614-292-1832
gustafson.5@osu.edu

Previous Time-Resolved Vibrational Spectroscopy Meetings

The following list encompasses the last two decades of recorded meetings since 1982. The origin of the conference was in 1982, organized and chaired by Prof. George Atkinson.

Dates	Title	Location	Chair(s)
June 1982	TRVS I	Lake Placid, NY, USA	G. Atkinson
July 1985	TRVS II	Bischofsgrün, Germany	A. Laubereau and M. Stockburger
August 1987	TRVS III	Amersfoort, Netherlands	J.D.W. van Voorst
May 1989	TRVS IV	Princeton, NJ, USA	T. Spiro
May 1991	TRVS V	Tokyo, Japan	H. Takahashi
May 1993	TRVS VI	Berlin, Germany	A. Lau, F. Siebert and W. Werncke
June 1995	TRVS VII	Sante Fe, NM, USA	W. Woodruff
April 1997	TRVS VIII	Oxford, UK	A. W. Parker
May 1999	TRVS IX	Tuscon, AZ, USA	G. Atkinson
May-June 2001	TRVS X	Okazaki, Japan	H. Hamaguchi and T. Kitagawa
May 2003	TRVS XI	Castiglione, Italy	A. Califano and R. Righini

Names and Addresses International Organizing Committee
Time-Resolved Vibrational Spectroscopy (TRVS XII) - 2005

Professor George H. Atkinson
Department of Chemistry
University of Arizona
PO Box 210041
Tucson, AZ 85721-0041
atkinsog@u.arizona.edu

Professor Salvatore Califano
LENS, University of Florence
Via N. Carrara 1,
500019 Sesto Fiorentino
Italy
califano@lens.unifi.it

Professor Paul M. Champion
Physics Department
Northeastern University
306 Huntington Avenue
Boston, MA 02115
champ@neu.edu

Professor Thomas Elsaesser
Max-Born –Institute
Max-Born-Strasse 2A
Berlin, Germany
elsasser@mbi-berlin.de

Professor Mostafa A.El-Sayed
Georgia Institute of Technology
School of Chemistry & Biochemistry
Atlanta, GA 30332-0400
mostafa.el-sayed@chemistry.gatech.edu

Professor Marloes Groot
Vrije Universiteit
Faculty of Science, Biophysics
De Boelelaan 1081
Amsterdam, The Netherlands
marloes@nat.vu.nl

Professor Terry L. Gustafson
Department of Chemistry
The Ohio State University
100 West 18th Avenue
Columbus OH 43210-1185
gustafson@chemistry.ohio-state.edu

Professor Hiro-O Hamaguchi
The University of Tokyo
7-3-1 Hongo, Bunkyo-ku, 113 Japan
hhama@chem.s.u-tokyo.ac.jp

.

Dr. Edwin J. Heilweil
Optical Technology Division
National Inst. of STDS & Technology
B208 Building 221
Gaithersburg, MD 20899
edwin.heilweil@nist.gov

Professor Robin Hochstrasser
University of Pennsylvania
Department of Chemistry
231 South 34th Street
Philadelphia, PA 19104-6323
hochstra@sas.upenn.edu

Professor Teizo Kitagawa
Institute for Molecular Science
Okazaki National Research Institute
Myodaiji, 444 Japan
teizo@ims.ac.jp

Professor Takayoshi Kobayashi
The University of Tokyo
Dept. of Physics
Faculty of Science
Hongo 7-3-1 Bunkyo, 113 Japan
kobayashi@phys.s.u-tokyo.ac.jp

Professor Yasushi Koyama
Kwansei Gakuin University
Faculty of Science
Wegahara, 662 Japan
ykoyama@kwansei.ac.jp

Professor Alfred Laubereau
Technical Univesity of Munich
Physik--Department E11
Technische Universitat Muenchen
James Frank Strassee
Garching - D85748, Germany
alfred.laubereau@physik.tu-muenchen.de

Professor Jean-Louis Martin
Ecole Polytechnique
INSERM
Palaiseau, 91761 Cedex
France, Metropolita
jean-louis.martin@polytechnique.fr

Professor Stephen Meech
University of East Anglia
School of Chemical Sciences and Pharmacy
Norwich, UK
s.meech@uea.ac.uk

Professor Anne B. Myers-Kelley
Kansas State University
Department of Chemistry
Manhattan, KS 66506
amkelley@ksu.edu

Professor Dwayne Miller
Departments of Chemistry and Physics
80 St. George Street
Toronto, ONT
M5S 3H6, Canada
dmiller@lphys.chem.utoronot.ca

Professor Shaul Mukamel
Department of Chemistry
516 Rowland Hall, Ste. RH434
University of California (08/15/03)
Irvine, CA 92697-2025
smukamel@uci.edu

Professor Anthony Parker
Rutherford Appleton Laboratory
Central Laser Facility
Chilton Diodcot, OX1 0QX
United Kingdom
a.w.parker@rl.ac.uk

Professor Roberto Righini
LENS, University of Florence
Via N. Carrara 1
500019 Sesto Fiorentino
Italy
righini@lens.unifi.it

Professor Friedrich Siebert
Sektion Biophysik
Instit fur Moleculare Medizin
und Zellforschung
Albert-Ludwigs-Universitat
Herman Herderstr. 9 D79104
Freiburg, Germany
frisi@biophysik.uni-freiburg.de

Professor Thomas G. Spiro
Department of Chemistry
Princeton University
Princeton NJ 08644
spiro@chemvax.princeton.edu

Professor Hiroaki Takahashi
Waseda University
3-4-1 Ohkubo, Shinjyuku, 169 Japan
takahash@mn.waseda.ac.jp

Professor Andrei Tokmakoff
Department of Chemistry
Massachusetts Institute of Technology
77 Massachusetts Ave.
Cambridge, MA 02139
takmakof@MIT.edu

Professor Siva Umapathy
Inorganic and Physical Chemistry
Indian Institute of Science
BANGALORE 560 012 India
umapathy@ipc.iisc.ernet.in

Professor Larry Ziegler
Boston University
Dept. of Chemistry
Metcalf Center for Science and Engineering
590 Commonwealth Avenue
Boston, MA 02215
lziegler@chem.bu.edu

Professor Wolfgang Zinth
Inst. f. Med. Optik
University of Munich
Barbara Str. 16
Munchen, 80797 Germany
Wolfgang.Zinth@physik.uni-muenchen.de

Corporate and Agency Sponsors*

http://www.brimrose.com

http://www.cmrx.com

http://www.cohr.com

http://www.princetoninstruments.com

http://www.irassociates.com

http://physics.nist.gov/otd

http://www.newport.com"

http://www.newport.com"

http://www.sc.doe.gov/bes/BES.html

http://www.nrl.navy.mil

http://www.jascoinc.com

http://www.jobinyvon.com

http://physics.nist.gov

http://www.brukeroptics.com

*NIST does not endorse any commercial products that may be mentioned on these sites.

Table of Contents

ORGANIC SPECTROSCOPY			
Page	*Talk Number*	*Authors*	*Title*
1	MA-01	Heinz Frei	Observing Reaction Intermediates in Nanoporous Solids by Time-Resolved FT-IR Spectroscopy
4	MA-02	Omar F. Mohammed, Dina Pines, Jens Dreyer, Ehud Pines, and Erik T. J. Nibbering	Sequential Proton Transfer Through Water Bridges in Acid-base Reactions
5	MA-03	Mike George	Organometallic Reactions in Conventional and Supercritical Fluids: Intermediates, Mechanisms and Spin
6	MA-04	Sarah M. Mandel, George Holinga, and Matthew S. Platz	Detection of the Hoffman Intermediate by Time Resolved Infrared Spectroscopy
9	MA-05	Eric C. Fulmer, Feng Ding, and Martin T. Zanni	New Pulse Sequence Developments in Two-Dimensional Infrared Spectroscopy

BIOLOGICAL TRVS			
12	MP-01	Philipp Kukura, Sangwoon Yoon and Richard A. Mathies	Femtosecond Broadband Stimulated Raman Spectroscopy: A New Approach for Time-Resolved Vibrational Structural Studies
16	MP-02	Ullas Gurudas and Johannes P. M. Schelvis	Detection of a Tryptophan Neutral Radical in DNA Photolyase by Resonance Raman Spectroscopy
19	MP-03	Anthony W. Parker	Excited State and Photoionisation of DNA – A Time-resolved Vibrational Spectroscopy Study
20	MP-04	Sergei Kruglik, Audrius Jasaitis, Latifa Bouzhir-Sima, Jean-Louis Martin, Ursula Liebl, and Marten H. Vos	Ultrafast Heme Structural Changes Upon Ligand Dissociation from the Heme-Based Bacterial Oxygen Sensor FixL
21	MP-05	Effie Pinakoulaki and Costas Varotsis	Time-Resolved Resonance Raman and Time-Resolved Step-Scan FTIR Studies of Nitric Oxide Reductase from *Paracoccus denitrificans*; Comparison of the Heme b_3 – Fe_B Site to that of the Heme-Cu_B in Oxidases
22	MP-06	P.M. Champion, D. Ionascu, F. Gruia , A. Yu and X. Ye	Experimental Studies of Structure, Function, and Coherent Oscillations in Biomolecules
23	MP-07	J. Terner, I.P. Torres-Filho, K.R. Ward, R.W. Barbee, M.A. Tiba, R. Pittman, and L. Torres	Noninvasive Remote Monitoring of Tissue Oxygen Saturation
27	MP-08	Shin Sato, Chikako Kudo and Hiro-o Hamaguchi	Reverse Proton Transfer Reaction Dynamics of 2-aminopyridine-acetic Acid Complex with Nanosecond Time-Resolved Infrared Spectroscopy

NANOPARTICLES			
Page	*Talk Number*	*Authors*	*Title*
30	TA-01	Gregory V. Hartland	Coherent Excitation of Vibrational Modes in Metallic Nanoparticles by Laser-Induced Heating
33	TA-02	Gregory D. Scholes, Vanessa M. Huxter, Karolina Fritz, Jeongho Kim, and Cathy Wong	Exciton Spin Flip Dynamics in Colloidal Quantum Dots
34	TA-03	M. Bonn, E. Hendry, M. Koeberg, C. de Mello Donega, D. Vanmaekelbergh, F. Wang and T.F. Heinz	Ultrafast THz Studies of Carrier Cooling in CdSe Nanocrystals
35	TA-04	Mostafa El-Sayed	Some Interesting Properties and Application of Plasmonic Nanoparticles of Different Shapes
36	TA-05	Jeffrey C. Owrutsky, Gerald M. Sando, and Kevin Dahl	Ultrafast Infrared Spectroscopy of Anions in Reverse Micelles
39	TA-06	Yoonsoo Pang, Zhaohui Wang, John C. Deàk, and Dana D. Dlott	Vibrational Energy Transfer in Reverse Micelle Molecular Nanostructures

TRANSIENT RAMAN			
42	TP-01	Hiro-o Hamaguchi	From Time-resolved Raman Spectroscopy to Time/Space-resolved Raman Spectroscopy
45	TP-02	W. Werncke, V. Kozich, and J. Dreyer	Vibrational Excitation after Ultrafast Intramolecular Proton Transfer of TINUVIN: A Picosecond Resonance Raman Study of Highly Vibrationally Excited Molecules
48	TP-03	Praveen D. Chowdary and S. Umapathy	Ultrafast Nonadiabatic Dynamics at Conical Intersections: A Resonance Raman Study
51	TP-04	M. Cather Simpson, J. Reddy Challa, and T. Gunaratne	Direct Study of Vibrational Dynamics in Hemes using Ultrafast Time-resolved Stokes and Anti-Stokes Raman Scattering and Transient Absorption Spectroscopy
54	TP-05	Teizo Kitagawa, Yu-Jun Mo, Dong–Lin Jiang, Makoto Uyemura, and Takuzo Aida	Anti-Stokes Resonance Raman Evidence for Energy Funneling of IR Photons Captured by Dendritic Antennae on Iron(III)-Porphyrin Complexes with a Poly(aryl ether) Dendrimer Framework
57	TP-06	Guy Buntinx, Olivier Poizat, and Christine Lapouge	Resonance Raman Characterization of the Lowest Excited $\pi\pi^*$ State of Methyl Viologen
60	TP-07	David Lee Phillips, Chensheng Ma, Wai Ming Kwok, Wing Sum Chan, and Peng Zou	Time-Resolved Spectroscopic Investigation of P-Hydroxyphenacyl Caged Phototrigger Compounds
61	TP-08	P. Matousek, M. D. Morris, N. Everall, I. P. Clark, M. Towrie, and A. W. Parker	Non-invasive Probing of Deep Layers of Turbid Media using Raman Spectroscopy
64	TP-09	Tahei Tahara, Misao Mizuno and Shoichi Yamaguchi	Picosecond/Femtosecond Time-Resolved Resonance Raman Study of Hydrated Electron

TRANSIENT INFRARED			
Page	*Talk Number*	*Authors*	*Title*
67	WA-01	Yung Sam Kim and Robin M. Hochstrasser	Multidimensional Infrared Spectroscopy Dynamics and Chemical Exchange
69	WA-02	Peter Hamm, Virgiliu Botan, and Roland Schanz	Femtochemistry in the Electronic Groundstate? IR-Driven *Cis-Trans* Isomerization of HONO
70	WA-03	Adam W. Smith, Hoi Sung Chung, Ziad Ganim, and Andrei Tokmakoff	The Thermal Denaturation of a Stable β-Hairpin
71	WA-04	T. Elsaesser, N. Huse , S. Ashihara, J. Dreyer, E.T.J. Nibbering,M.L. Cowan, B.D. Bruner, J.R. Dwyer, and R.J.D. Miller	Two-dimensional Infrared Spectroscopy of Coupled Hydrogen Bonds in Liquids
74	WA-05	Gerhard Seifert, Toralf Patzlaff, and Heinrich Graener	Comprehensive Study of the Vibrational Energy Relaxation of Monomeric Water Molecules in Nonpolar Organic Solvents
77	WA-06	Y. L. A. Rezus and H. J. Bakker	On the Orientational Relaxation of HDO in Liquid Water
80	WA-07	Prabuddha Mukherjee, Itamar Kass, Isaiah Arkin, and Martin T. Zanni	Vibrational Dynamics of the CD3ζ Membrane Peptide Studied with 2D IR Spectroscopy
81	WA-08	H. Iglev, M. Schmeisser, A. Thaller, and A. Laubereau	Ultrafast Vibrational Heating of Ice I_h: A Novel Transient State of Overheated Ice

TRVS THEORY			
82	RA-01	Tomoyuki Hayashi, Wei Zhuang, and Shaul Mukamel	Nonlinear Vibrational Response of the Amide I, II, III and A Bands of NMA: Simulation Study Based on an Electrostatic DFT Map
85	RA-02	James Skinner	Time- and Frequency-Domain Vibrational Spectroscopy of Water
87	RA-03	Sighart F. Fischer and Wolfgang Dietz	On the Time Evolution of Vibronic Spectra Coupled to an Electronic Solvation Process in Water
92	RA-04	Tim M. Watson and Jonathan D. Hirst	Theoretical Studies of the Amide I Vibrational Frequencies of Peptides and Proteins
95	RA-05	Vladimir Chernyak	Semiclassical Theory for Femtosecond Nonadiabatic Molecular Dynamics
96	RA-06	Ellen H.G. Backus and Mischa Bonn	Direct Observation of Ultrafast Hopping of Surface Molecules
97	RA-07	Motohiro Banno, Shin Sato, Koichi Iwata, and Hiro-o Hamaguchi	Solvent Dependent Ultrafast Vibrational Dynamics in Tungsten Complexes $W(CO)_{(6-n)}(CH_3CH)_n$(n=0,1) Probed with Sub-picosecond Time-resolved Infrared Spectroscopy
100	RA-08	Manuela Lima, Victor Volkov, Paolo Foggi, Riccardo Chelli, and Roberto Righini	Two-dimensional Infrared Spectroscopy and Molecular Dynamics of Liquid Formamide

PROTEIN DYNAMICS			
Page	*Talk Number*	*Authors*	*Title*
101	RP-01	Tom Spiro	Protein Dynamics from Time-Resolved Raman Spectroscopy
104	RP-02	J. Guijarro, F. Siebert, and M. Engelhard	What Causes Larger Protein Changes in Halorhodopsin: Retinal Isomerization or Anion Binding?
107	RP-03	Deborah Stoner-Ma, Andrew A. Jaye, Pavel Matousek, Michael Towrie, Peter Tonge and Stephen R. Meech	Ultrafast Dynamics in the Green Fluorescent Protein (GFP): Proton Transfer and Time Resolved Fluorescence Spectroscopy
110	RP-04	W. Zinth, F. O. Koller, R. Rehoa, T. Schrader, W. J. Schreier, C. Renner, L. Moroder, and J. Wachtveitl	Structural Dynamics in a Chromopeptide – Infrared Absorption Dynamics from Picoseconds to Minutes
113	RP-05	J. Timothy Sage, Georgi Y. Georgiev, Jasper van Thor, and Michael Towrie	Electrostatically Steered Photophysical Pathways in Green Fluorescent Protein
114	RP-06	Jens Bredenbeck, Jan Helbing, G. Andrew Woolley, Janet R. Kumita, and Peter Hamm	A Pico- to Microsecond Study of the Folding of a Photo-Switchable α-Helix
115	RP-07	Yasuhisa Mizutani and Akira Sato	Picosecond Protein Dynamics of Myoglobin Upon Ligand Dissociation Studied by Ultraviolet Resonance Raman Spectroscopy
118	RP-08	Paul Donaldson, Laura Barter, Jason Palmer, and David Klug	DOVE 2D-IR Spectroscopy as a Tool for Studying Protein Composition, Structure and Function
119	RP-09	J. Peng, T. Castonguay, D. F. Coker and L. D. Ziegler	Rotational Raman Responses of H_2 in Supercritical CO_2: A Probe of Local Ultrafast Anisotropic Solvent Dynamics

FUTURE DIRECTIONS			
122	FA-01	Takayoshi Kobayashi and Yoshiharu Yuasa	Real-time Molecular Vibrational Frequency and Amplitude Probing to Resolve Instantaneous Structure
123	FA-02	S. Laimgruber, W. Schreier, and P. Gilch	Mechanism of a Photo-Rearrangement Revealed by Combining Femtosecond Visible, Raman, and IR-Techniques
126	FA-03	Andrey N.Bordenyuk and Alexander V. Benderski	Hydrogen Bonding Dynamics of Interfacial Water by Spectrally- and Time-Resolved Sum Frequency Generation (STiR-SFG)
129	FA-04	Koichi Iwata	Progress Report from a Neighbor of Infrared - Tracing "Loose Electrons" with Femtosecond Time-Resolved Near-Infrared Spectroscopy
131	FA-05	T.W. Kee and M.T. Cicerone	Broadband CARS Microscopy
132	FA-06	Omer Nahmias, Oshrat Bismuth, O. Shoshana and Sanford Ruhman	Tracking Excited State Dynamics with Coherent Control: Automated Limiting of Population Transfer in LDS750
135	FA-07	Leonid Sheps, Andrew C. Crowther, and F. Fleming Crim	Towards Vibrationally Mediated Chemistry in Solution
138	FA-08	Klaas Wynne	A New Ultrafast Technique for Measuring the Terahertz Dynamics of Chiral Molecules: The Theory of Optical Heterodyne-Detected Raman-Induced Kerr Optical Activity (OHD-RIKOA)

POSTER PRESENTATIONS			
Page	*Poster Number*	*Authors*	*Title*
141	P-01	Andrey N. Bordenyuk,Himali Jayathilake, and AlexanderV. Benderski	Coherent Vibrational Quantum Beats as a Probe of Langmuir-Blodgett Monolayers
144	P-02	Gurusamy Balakrishnan, Ying Hu, Thomas G. Spiro, Gretchen M. Bender, Zelleka Getahun, and William F. DeGrado	Nanosecond T-jump Induced Unfolding Kinetics of α-Helical Peptide: A UV Resonance Raman Study
147	P-03	Gotard Burdzinski, Terry L. Gustafson, Christophe Lefumeux, Guy Buntinx and Olivier Poizat	Vibrational Cooling in the Excited State: A Comparison of Femtosecond Transient Absorption and Picosecond Raman Spectroscopies
150	P-04	Sohshi Yabumoto, Shin Sato, and Hiro-o Hamaguchi	Vibrational and Electronic Infrared Absorption Spectra of Benzophenone in the Lowest Excited Triplet State
153	P-05	Jagannadha R. Challa, Tissa C. Gunaratne, and M. Cather Simpson	Time-Resolved Resonance Raman Observations of Vibrational Dynamics in Heme Model Compounds
156	P-06	Kenan Gundogdu, Jigar Bandaria, and Christopher M. Cheatum	The Dynamics of Enzyme-Inhibitor Interactions
157	P-07	Feng Ding, Eric C. Fulmer, and Martin T. Zanni	Characterizing Coupled Vibrators Using Fifth-Roder Two Dimensional Infrared Spectra
160	P-8	Catherine C. Cooksey, Kevin J. Johnson, and Philip J. Reid	Time-Resolved Studies of Nitrosyl Halide Photoreaction Dynamics
163	P-09	David Gelman and Ronnie Kosloff	Dissipative Dynamics of a System Passing Through a Conical Intersection: Ultrafast Pump-probe Observables
166	P-10	Paul M. Donaldson, Laura M.C. Barter, Elizabeth M. Gardner, Jason D. Palmer and David R. Klug	Spectra/Structure Correlations and Temporal Behaviour of DOVE 2D-IR Spectra.
169	P-11	Tissa C. Gunaratne, J. Reddy Challa and M. Cather Simpson	Vibrational Energy Flow in Push-Pull Chromophores: A Time Resolved *anti*-Stokes Resonance Raman Study
172	P-12	Okan Esenturk and Edwin J. Heilweil	Terahertz Pump-Probe Spectroscopy of Trans-Azobenzene
174	P-13	Neil T. Hunt, Andrew R. Turner and Klaas Wynne	Inter- and Intra-Molecular Hydrogen Bonding in Phenol Derivatives: A Model System for Polypeptides
177	P-14	Peter Hamm, Jens Bredenbeck, and Jan Helbing	Nonlinear Solvation Dynamics: Beyond the Two-Point Frequency Fluctuation Correlation Function
178	P-15	Andrew A. Jaye, Deborah Stoner-Ma, Pavel Matousek, Michael Towrie, Stephen R. Meech and Peter J. Tonge	Evidence of Excited State Proton Transfer in the Green Fluorescent Protein from Picosecond IR Spectroscopy
181	P-16	Kunihiko Ishii, Satoshi Takeuchi, and Tahei Tahara	Ultrafast Pump-Probe Absorption Study of Reactive Excited State of *cis*-Stilbene: Wavelength-Dispersed Measurement of Quantum Beat
183	P-17	Renee D. JiJi, Ying Hu, Gurusamy Balakrishnan and Thomas G. Spiro	Early Events in β-sheet Formation: Nanosecond Temperature-jump Time-Resolved UV Resonance Raman Studies
186	P-18	Anwar Usman, Omar F. Mohammed, Jian Dong, Kyryl M. Solntsev, Laren M. Tolbert, and Erik T. J. Nibbering	Determination of the Excited State Twisting Angle of the Chromophore of Green Fluorescent Protein

POSTER PRESENTATIONS (continued)			
Page	*Poster Number*	*Authors*	*Title*
187	P-19	Anwar Usman, Omar F. Mohammed, Karsten Heyne, Jens Dreyer, Erik T. J. Nibbering, and Michael A. Cusanovich	Excited State Dynamics of PYP Chromophore Model Systems Explored with Ultrafast Infrared Spectroscopy
188	P-20	K.L. Ronayne, K. Bowes, M. Towrie, P. Raithby, and A. W. Parker	Photoexcited State Studies on Re(bipy)$(CO)_3$ in the Solid State by ps-TRIR
189	P-21	Yuta Takada, Koichi Iwata, and Hiro-o Hamaguchi	Observation of Vibrational Relaxation Processes of S_1 trans-Stilbene in Ionic-liquids
192	P-22	Gerald M Sando, Kevin Dahl, and Jeffrey C. Owrutsky	Vibrational Relaxation of Anions in Ionic Liquids
195	P-23	Costas Varotsis and Costas Koutsoupakis	Probing the Q-Proton Pathway and Docking Site Dynamics of ba_3-Oxidorereductase by Time-Resolved Step-scan Fourier Transform Infrared Spectroscopy
198	P-24	Tomohisa Takaya, Hiro-o Hamaguchi, and Koichi Iwata	Anisotropy-Resolved Near-IR Absorption Study of Photoinduced Electron Transfer Reaction in 9,9'-Bianthryl
200	P-25	Anne Colonna, Jean-Christophe Lambry, Géza I. Groma, Manuel Joffre, Jean-Louis Martin and Marten H. Vos	Ultrafast Polarization and Coherent Charge Motions in Bacteriorhodopsin Observed by Infrared Emission Interferometry
201	P-26	Tung To, Jake Yeston, Edwin Heilweil and Theodore Burkey	Ultrafast TRIR Chelation Studies Help Design Ultrafast Molecular Switches
203	P-27	David A. Turton, Neil T. Hunt, Andrew R. Turner, and Klaas Wynne	Polarisation Spectroscopy of Chiral Molecules: First Attempts at OHD-RIKOA on Phenylethanol and Quartz
206	P-28	Sangwoon Yoon, Philipp Kukura and Richard A. Mathies	Direct Observation of the Ultrafast Intersystem Crossing in Tris(2,2'-bipyridine) ruthenium(II) using Femtosecond Stimulated Raman Spectroscopy
210	P-29	Joshua C. Bolinger, Teresa J. Bixby, and Philip J. Reid	Time-Resolved Infrared Absorption Studies of the Solvent Dependent Vibrational Relaxation Dynamics of Chlorine Dioxide

TRVS XII

NIST National Institute of Standards and Technology

Washington, D.C.

May 23-27, 2005

Organic Spectroscopy

Observing Reaction Intermediates in Nanoporous Solids by Time-Resolved FT-IR Spectroscopy

Heinz Frei
Physical Biosciences Division, Lawrence Berkeley National Laboratory
Berkeley, CA 94720

Nanoporous solids offer unique environments for exploring thermal or photo-catalytic reactions for the synthesis of organic building blocks, industrial intermediates, or for making fuels from abundant sources like water and carbon dioxide using light as energy source. Insight into the mechanism of reactions in the pores and channels of zeolites and mesoporous inorganic oxides greatly facilitates progress in the use of these structured environments for accomplishing demanding chemical transformations. The behavior of short-lived species such as mobile radicals or transient complexes in pore systems, or of surface intermediates on catalytic metal nanoparticles occluded in the channels often determines the selectivity of the reactions. Time-resolved FT-IR spectroscopy from nanoseconds to milliseconds has proven as a very useful method for determining mechanisms by the detection of small transient intermediates, and for the understanding of diffusion and reactive behavior in the porous environment. Three recent examples from the areas of photocatalysis, heterogeneous thermal catalysis and artificial photosynthesis are presented.

Selective Hydrocarbon Photooxidation by O_2 in Zeolites

We have recently found that small alkanes, alkenes, or alkyl benzenes, when loaded from the gas phase into cation-exchanged zeolites, are partially oxidized by O_2 to corresponding carbonyl products with very high selectivity. The reactions are mediated by the extremely high electrostatic fields inside zeolite cages that stabilize the hydrocarbon-O_2 contact charge-transfer states of the collisional pairs, which can be accessed either by visible light or thermally by mild heating. Interestingly, the proposed hydrocarbon radical and HOO radical intermediates are also produced in the thermal autoxidation in gas or liquid phase, yet the processes in these homogenous media have low selectivity even at very low conversion. Hence, the nanoporous zeolite environment plays a decisive role whose understanding requires the direct observation of radical intermediates under reaction conditions.

Formyl and acetyl radicals were generated in ambient temperature zeolites in order to learn about the lifetime and behavior of very small radicals in the porous environment. Formyl radicals were generated by photodissociation of glycolaldehyde or acetaldehyde precursor in the cation-exchanged zeolite (NaY). Upon excitation of the precursor with a nanosecond laser pulse, HCO was detected by the C=O stretch mode at 1847 cm^{-1} ($H^{13}CO$, 1807 cm^{-1}). The initial intensity of the absorption revealed that the majority of the radicals survive on the microsecond time scale, which is 3-4 orders of magnitude longer than the residence time estimated for HCO in a zeolite NaY supercage. This implies that the geminate HCO and CH_2OH radicals (or HCO and CH_3 radicals) separate quantitatively after photolysis and explore many cages before they react, indicating that the interactions of the radicals with the zeolite environment and the many escape routes dictate their behavior. Interestingly, the decay exhibits biphasic behavior: a 24 microsecond initial decay, which is dominant, followed by a long tail extending to 500 microseconds. Since the observed final products indicate that HCO and CH_2OH decay exclusively by reacting with each other, the biphasic behavior is attributed to a heterogeneity of

the environment that influences the rate of reaction of HCO with CH_2OH, such as geminate and nongeminate radical encounters. We have used the random walk model to explore this possibility and found excellent agreement of the predicted geminate and nongeminate rate constants with the observed decay constant of the initial decay and the bimolecular rate constant determined by a kinetic fit of the long tail, respectively. While the geminate radical reaction dominates in the case of HCO but still is accompanied by nongeminate reaction, it is the only process observed in the case of the slightly larger acetyl radical (produced from pinacolone or naphthyl acetate precursor). Estimates of the diffusion rates of acetyl radical which take into account the presence of the much less mobile but far more abundant precursor molecules show that the precursor molecules obstruct the diffusion path of the rapidly hopping acetyl radicals. The result is that the radicals are confined to subspaces of the zeolite crystallite which do not intersect with those of neighboring geminate radical pairs, thus preventing nongeminate, radical scrambling reactions from occurring.

These results from the time resolved acyl radical studies suggest that the selectivity of hydrocarbon oxidation reactions in cation-exchanged zeolites is very likely not due to lack of radical mobility, but due to confinement of the rapid, random hopping radicals to subspaces by the less mobile and more abundant reactant and final product molecules. As a result, nongeminate encounters are prevented that otherwise would lead to radical scrambling products.

Ethylene Hydrogenation over Supported Pt Catalyst

Understanding of elementary reaction steps over supported metal catalysts is an important vehicle for optimizing the design of 3-D catalyst supports and metal nanoparticle arrangement for achieving high product selectivity in heterogeneous catalysis. In particular, detecting transient surface intermediates and learning how they relate kinetically to final product formation under reaction conditions will furnish crucial insights on the catalyst properties that steer the intermediates to the desired products.

Using the prototype ethylene hydrogenation as an example, we have directly observed the conversion of transient surface ethyl intermediate to gas phase ethane on Pt particles under reaction conditions (323 K, 1 atm, 9 L min^{-1} H_2/N_2 flow). Catalysts used were Pt nanoparticles supported on a mesoporous silica (SBA-15, 2.7% (wt) loading), or an industrial catalyst with finely divided Pt particles on amorphous Al_2O_3 support (Exxon). Twenty-five millisecond (ms) time-resolution of the catalysis was achieved by synchronizing the forward motion of the interferometer mirror with the opening of a fast mechanical valve for release of a millisecond pulse of ethylene gas. Surface ethyl species (2870 and 1200 cm^{-1}) were detected along with the gas phase ethane product (2954 and 2893 cm^{-1}). The CH_3CH_2Pt growth was instantaneous on the time scale of 25 ms under all experimental conditions. At 323 K, the decay time of surface ethyl (122 ± 10 ms) coincides with the rise time of C_2H_6 (144 ± 14 ms). This establishes direct kinetic evidence for surface ethyl as the relevant reaction intermediate. Such a link between the temporal behavior of an unstable surface intermediate and the final product in a heterogeneous catalytic system has not been demonstrated before. The ethane growth kinetics was identical for Pt/SBA-15 and Pt/Al_2O_3 catalyst, which implies that ethylene uptake into the silica mesopores or release of the ethane product from the pores are not rate limiting. A fraction (10 percent) of the asymptotic ethane growth at 323 K is prompt, indicating that there are surface ethyl species that react much faster than the majority of the CH_3CH_2Pt intermediates. The dispersive kinetics is attributed to the varying strength of interaction of the ethyl species with the Pt surface caused by heterogeneity of the surface environment.

The results demonstrated that time-resolved FT-IR spectroscopy allows the identification of the kinetically relevant surface intermediates of thermal catalysis under reaction conditions. The main technical challenge is the triggering of the catalysis by a fast reactant pulse. The success of the technique at higher time resolution will depend on the ability to generate reactant pulses of microsecond duration that deliver a sufficient number of molecules for detection by step-scan FT-IR spectroscopy.

Photochemical CO_2 Splitting in Transition Metal Molecular Sieves

The compartmentalized nature of mesoporous oxides and possibilities for framework incorporation or covalent anchoring of single metal centers of polynuclear moieties on pore surfaces offer opportunities to precisely arrange and couple photoactive components for accomplishing difficult photosynthetic transformations. An important example is the reduction of carbon dioxide to a liquid fuel like methanol. Here, the principal challenge is to achieve activation of CO_2 by H_2O under visible light. Our approach consists of engaging the visible light-absorbing metal-to-metal charge-transfer transition (MMCT) of binuclear units covalently anchored on the pore surface of MCM-41 silica sieves (featuring 30A channels separated by 10A walls). The colored redox sites consist of Ti or Zr centers oxo-bridged to a second metal that donates an electron upon visible light absorption, thereby generating transient Ti^{III} or Zr^{III} capable of reducing CO_2. We have recently found that the mesoporous silica MCM-41 featuring $ZrOCu^{I}$ sites is capable of reducing CO_2 to CO upon excitation of the $Zr^{IV}OCu^{I} \rightarrow Zr^{III}OCu^{II}$ MMCT transition.

In order to understand the mechanism of CO_2 reduction at excited group IVB metal centers, we have conducted an in-situ FT-IR and mass spectrometric study of UV light-induced CO_2 reduction by H_2O at isolated Ti centers of framework substituted TiMCM-41 sieve. Such porous Ti silica materials are known from work by Anpo et al. to afford reduction of CO_2 by H_2O to methanol and methane upon prolonged UV irradiation of the TiO ligand-to-metal charge-transfer absorption. Our in-situ spectroscopic study showed gas phase CO and O_2 as the only products. The yield dependence of CO was linear in photolysis light intensity, thus revealing CO as a single photon, 2-electron reduction product. The yield depended linearly on the H_2O concentration, confirming that water is the stoichiometric electron donor. This strongly suggest that the mechanism of CO_2 activation at transiently reduced group IVB metals is splitting to CO. The leaving group may be an O^- that is subsequently protonated by surface silanol groups to OH radical, or OH if protonation occurs simultaneously with the reduction of CO_2. Time-resolved monitoring of CO in MCM-41 using photolabile precursors (cyclopropenones) by nanosecond step-scan FT-IR revealed details of the behavior of the CO product inside the mesopores. The absorption of CO inside the pores of the room temperature sieve is very broad (FWHM 120 cm^{-1}) due to interaction with the many different sites on the silica pore surface, with two sites (2156 and 2107 cm^{-1}) showing much longer lifetimes (up to a milliseconds) than the average site (300 microseconds).

Acknowledgments

This work was supported by the Director, Office of Science, Office of Basic Energy Sciences, Division of Chemical Sciences of the U.S. Department of Energy under contract No. DE-AC03-76SF00098. We thank Prof. Gabor Somorjai and Mr. Robert Rioux for samples of Pt/SBA-15.

Sequential proton transfer through water bridges in acid-base reactions

Omar F. Mohammed[1], Dina Pines[2], Jens Dreyer[1], Ehud Pines[2], Erik T. J. Nibbering[1,*]

[1]: *Max Born Institut für Nichtlineare Optik und Kurzzeitspektroskopie,*

Max Born Strasse 2A, D-12489 Berlin, Germany

[2]: *Department of Chemistry, Ben-Gurion University of the Negev,*

P.O.B. 653, Beer-Sheva 84125, Israel

*: Corresponding Author E-mail: nibberin@mbi-berlin.de

Aqueous proton transfer is one of the most fundamental chemical reactions. For instance, water mediates the transfer of a proton in membrane protein proton channels. These proton channels function by a sequential hopping of protons through proton wires consisting of amino acid side groups and water molecules. A sequential proton transfer is also at the heart of the von Grotthuss mechanism of anomalous high proton mobility in water. Water is considered to play a key role in aqueous acid-base neutralization reactions, where a proton is exchanged between an acid and a base, forming the conjugated base and conjugated acid respectively. Theoretical considerations have shown that water facilitates an efficient charge separation when the proton leaves the acid. In this work we show compelling experimental evidence that water in addition functions as a bridge between an acid and a base, by both providing and stabilizing the proton transfer pathway. For optical triggering the proton tramsfer reaction we use a photoacid [1,2]. In particular we detect the transient behaviour of the IR-active marker mode of the hydrated proton to be correlated with the transient reactant and product bands. The hydrated proton in our acid-base neutralization experiment turns out to be similar to the Eigen cation – and not the Zundel cation – for solvated protons in water.

[1]. M. Rini, B.-Z. Magnes, E. Pines, E. T. J. Nibbering, *Science* **301**, 349 (2003).

[2]. M. Rini, D. Pines, B. Z. Magnes, E. Pines, E. T. J. Nibbering, *J. Chem. Phys.* **121**, 9593 (2004).

Organometallic Reactions in Conventional and Supercritical Fluids: Intermediates, Mechanisms and Spin

Mike George
School of Chemistry, University of Nottingham, University Park, Nottingham, NG7 2RD UK
Phone: 0115 951 3512; Fax: 0115 951 3563; e-mail: mike.george@nottingham.ac.uk

Supercritical Fluids are curious hybrids of gases and liquids which offer intriguing possibilities for transient vibrational spectroscopy. A fluid is said to be "supercritical" when its pressure and temperature exceed the pressure and temperature at the critical point (P_C and T_C). This lecture will present recent applications of nanosecond TRIR to examine inorganic reactions in conventional and supercritical fluids. Examples will be given including:

Organometallic Alkane Complexes and Noble Gas Complexes: A key intermediate in catalytic C-H Activation by organometallic complexes reaction is formation of organometallic alkane complexes.[1] We have performed systematic studies which has generated long-lived Re alkanes complexes which has subsequently allowed the characterisation of these complexes NMR.[2] We have also and examined the activation methane and ethane by $CpRh(CO)_2$ (Cp' = η^5- C_5H_5 or η^5- C_5Me_5) in supercritical fluids at room temperature. TRIR experiments in supercritical noble gas solvents allowed the characterisation of organometallic and Re-Xe complexes were again found to be long-lived at room temperature.[1] This has recently allowed the characterisation of organometallic Xe by NMR spectroscopy in liquefied xenon at low temperature.[3]

Monitoring Spin Changes in the Photochemistry of $Fe(CO)_5$: How spin states affect organometallic reactivity is a fundamental question, which is key to many areas of inorganic chemistry and this has been the subject of interest for more than 30 years.[4] A protypical molecule is $Fe(CO)_4$, generated photochemically from $Fe(CO)_5$, where low temperature matrix isolation experiments demonstrated that $^3Fe(CO)_4$ could be converted to $^1Fe(CO)_4$. The transition from $^3Fe(CO)_4$ to $^1Fe(CO)_4$ was highlighted as a great photochemical challenge in Angewante Chemie. Picosecond IR experiments on $Fe(CO)_5$ in *n*-hexane, and supercritical argon (scAr) and xenon (scXe) have allowed the dynamics of the solvation of organometallic intermediates to be understood by monitoring the conversion of $^3Fe(CO)_4$ to $^1Fe(CO)_4$(solvent).[5]

Understanding Real Advantages of Supercritical fluids for Green Chemistry: The high concentration of gases such as H_2 and N_2 that are possible in supercritical fluids is often given as a signification advantage over conventional solvents for reactions such as hydrogenation and preparative chemistry and are becoming increasingly attractive as environmentally acceptable replacement for organic solvents in chemical reactions and material processing.. We will show that reactions of organometallic complexes in $scCO_2$ are more complex and careful consideration of the role of the solvent is required.

1. X-Z. Sun, S. M. Nikiforov, D. C. Grills, M. Poliakoff and M. W. George, *J. Am. Chem. Soc*., **1997**, *119*, 7521.
2. D. J. Lawes, S. Geftakis, G. E. Ball, *J. Am. Chem. Soc.* **2005**, *127,* 4134 *and refs therein*
3. G. E. Ball, T. A. Darwish, S. Geftakis, M. W. George, D. J**.** Lawes, P. Portius, J. P. Rourke, *P. Nat. Acad. Sci.,* **2005**, *102,* 1853.
4. M. Poliakoff and J. J. Turner, *Angew*. *Chem*. **2001,** *40*, 2809 *and refs therein.*
5. P. Portius, J. Yang, X. Z. Sun, D. C. Grills, P. Matousek, A. W. Parker, M. Towrie, M. W. George**,** *J. Am. Chem. Soc.*, **2004**, *126*, 10713.

Detection of the Hofmann Intermediate By Time Resolved Infra Red Spectroscopy

Sarah M. Mandel, George Holinga, Matthew S. Platz
The Ohio State University
Columbus OH, 43210

Abstract:
The Hofmann reaction is a widely used reaction that allows primary amides to be converted to isocyanates in the presence of base and bromine. One of the important intermediates of the reaction is the N-Haloamide Anion (NXA-). In this research we are pleased to report the first detection of this intermediate by nanosecond time resolved infrared spectroscopy. The NXA- species was generated by trapping singlet benzoyl nitrene with a halide anion in solution. A variety of NXA- species have been observed and characterized, and their reactivity studied.

Discussion and Results:

The Hofmann reaction is a commonly used synthetic route to isocyanates and primary amines from primary amides (Figure 1).

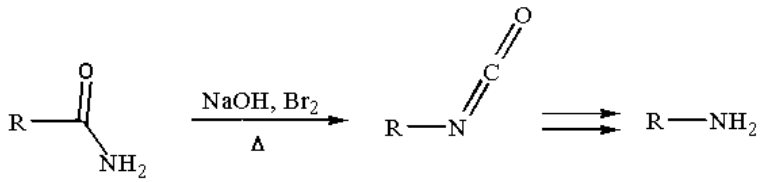

Figure 1. Overview of the Hofmann Reaction

The reaction was discovered and researched by a German chemist, August Hofmann at the University of Berlin in the 1800's and is still widely used today.

The reaction begins via deprotonation of the amide hydrogen atom, yielding an amide anion. This amine anion then reacts with bromine to give a N-bromoamide. Further deprotonation yields the N-bromo-amide anion (NXA-). Loss of the bromine atom yields an acyl nitrene, which will undergo the Curtius reaction to form an isocyanate. Hydrolysis gives a primary amine (Figure 2).

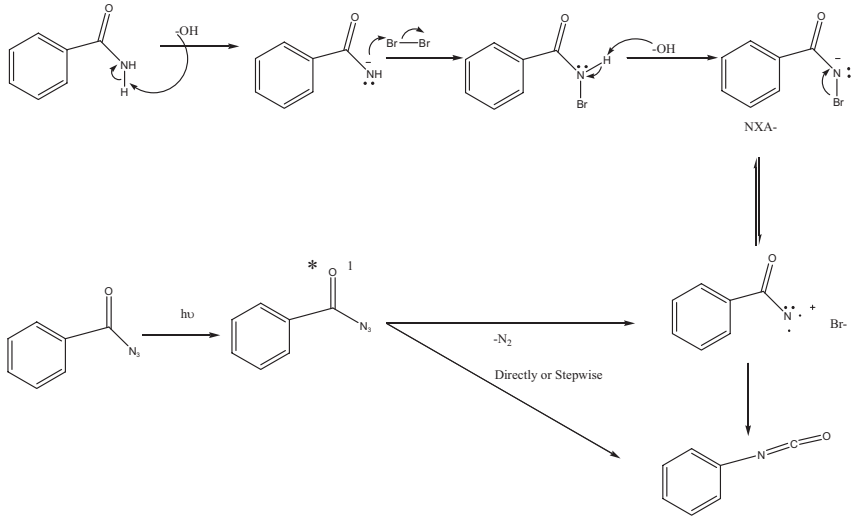

Figure 2. Reaction Mechanisms of the Hofmann Reaction and Benzoyl Azide.

This research focuses on attempting to observe the NXA- species created from bromine anion attack of the singlet benzoyl nitrene. Photolysis of benzoyl azide is another well-known method for creating acyl nitrenes. Singlet benzoyl nitrene is an excellent candidate for study by time resolved infrared spectroscopy because it exhibits a number of intense IR bands, most notably a 1635 cm^{-1} peak attributed to the nitrene acetonitrile ylide (Figure 3).[1] This ylide has been found to have a lifetime of approximately 40 μs in CD_3CN solution, (266 nm excitation 5 mM azide in CD_3CN).

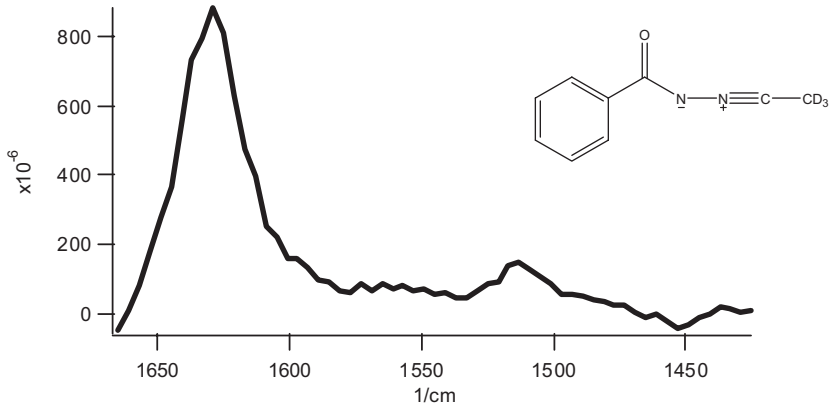

Figure 3. Time Resolved Infra Red Spectra of Benzoyl azide (5 mM) in CD_3CN after 266 nm photolysis. Spectra collected 1.2 μs after the pulse. The band at 1635 cm^{-1} is attributed the nitrene acetonitrile ylide.

Addition of 0.01M LiBr, NEt_4Br, LiCl, NEt_4Cl all were found to completely quench the signal at 1635 cm^{-1}. This was confirmed by direct quenching of singlet benzoyl nitrene by a variety of organic and inorganic salts, including LiBr, NEt_4Br (LFP, 266 nm excitation, 320 nm detection in acetonitrile). When IR detection was employed intense bands were observed at 1470 cm^{-1} for bromine salts and 1520 cm^{-1} for chlorine salts (Figure 4). The new intermediates were found to have lifetimes of 25-40 μs in CD_3CN solution.

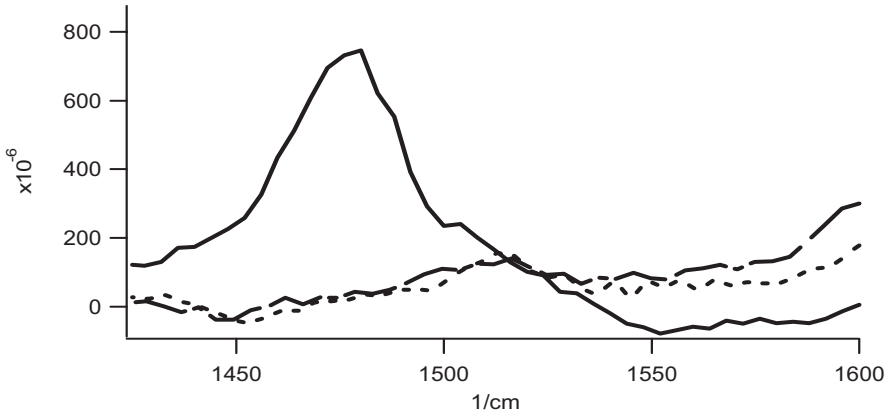

Figure 4. Transient IR spectrum observed after 1.2 μs photolysis (266 nm in CD_3CN) of BA (7 mM) -----, BA (7 mM) with $LiBF_4$ (0.01 M)— — and BA (7mM) with NEt_4Br (0.01M) ——

The fact that large counter ions, such as NEt_4Br were able to quench the benzoyl nitrene signal (320 nm) and the ylide signal (1635 cm^{-1}) indicates that the cation is not involved in intermediate formation observed by TRIR. Supporting this, addition of $LiBF_4$ did not create any new IR bands (Figure 4). This would indicate that the only the halide anion is responsible for the intermediate observed.

To confirm that the intermediate being studied was in fact the NXA- species, and not a nitrenoid, calculations at the B3LYP 6-31G* level of theory using the polarizable continuum model of acetonitrile were undertaken. Optimized geometries were found for both the nitrenoid and the NXA- species, and predicted IR spectra were calculated. Agreement between experimental results and predict results were only observed with NXA- (predicted 1471 cm^{-1}, observed 1470 cm^{-1})

The reactivity of NXA- species reactivity was probed via quenching experiments. Water was found to quench all of the NXA- species studied with an average rate of 1.9 x 10^4 $M^{-1}s^{-1}$. This is much slower than the rate of quenching of singlet benzoyl nitrene with water, 3.8 x 10^6 M^{-1} s^{-1}.[2] NXA- intermediates created with lithium salts were found to be quenched by the addition of 12-crown –4 ether, and the rate of formation of the NXA- species was increased, indicating that sequestering the lithium atom increased the nucleophilicity of the Br- atom, which in turn increased the rate of NXA- formation.

Conclusions:

In conclusion, the N- halo amide anion, NXA- was observed via time resolved infrared spectroscopy. Proof of this assignment includes that when a large cation (such as NEt_4^+), which cannot bind efficiently to the nitrene, are present in solution the NXA- is observed at 1470 cm^{-1} (Br^-) or 1520 cm^{-1} (Cl^-), identical to the intermediate observed with lithium salts. When a large anion (such as BF_4^-) is present, which cannot bind efficiently with the nitrene, with the nitrene the no new features in the IR are observed. Addition of 12-crown-4, (a Li+ specific crown) at constant [LiBr] increased the rate of NXA- formation. All of this leads to the conclusion that the intermediate observed is the Hofmann N-Halo Amide Anion (NXA-).

---

[1] Pritchina, E. A.; Gritsan, N. P.; Maltsev, A.; Bally, T.; Autrey, T.; Liu, Y.; Wang, Y.; Toscano, J. P. *Phys. Chem. Chem. Phys.* **2003**, *5*, 1010.

[2] Liu, J.; Mandel, S.; Hadad, C. M.; Platz, M. S.; *J. Org. Chem.*, **2004**, *69*, 8583.

New Pulse Sequence Developments in Two-Dimensional Infrared Spectroscopy

Eric C. Fulmer*, Feng Ding, and Martin T. Zanni
Department of Chemistry, University of Wisconsin – Madison, Madison WI 53706

Understanding the effects of dynamic solvent interactions on the potential energy surfaces of molecules is a central goal of condensed phase research. Solvent interactions alter the curvature of the potential energy surface, changing the molecular modes and their relaxation times. To study these effects, pulsed infrared spectroscopies are being developed with ultrafast time-resolutions to capture solvent structural dynamics. Using infrared pulses to manipulate vibrational coherences, integrated 3rd-order pulse sequences were first used by Fayer and coworkers,[1] and later extended by Hochstrasser and coworkers,[2] to measure the frequency fluctuations of solute modes in glasses, liquids, and proteins. These experiments revealed the magnitude and the timescales that the solvent environment alters the fundamental frequency of these modes. More recently, the time-dependence of the emitted 3rd-order electric field was measured, giving rise to heterodyned two-dimensional infrared (2D-IR) spectroscopy.[3, 4] A 2D-IR spectrum contains diagonal peaks for each molecular vibration and cross peaks between coupled modes. Third-order 2D-IR spectroscopy is proving to be a powerful advance over integrated methods because it can be used to measure vibrational couplings, correlate frequency fluctuations, line-narrow spectra, and monitor picosecond structural dynamics.[3-5] Both the integrated and heterodyned approaches for manipulating vibrational coherences in pulsed infrared spectroscopies make use of ideas originally developed for 2D NMR spectroscopy.[6] Again borrowing from NMR, higher-order pulse sequences have been proposed that more extensively manipulate vibrational coherences to further enhance infrared spectroscopy for studying condensed phase molecular dynamics.[7]

In this presentation, we demonstrate a heterodyned infrared 5th-order pulse sequence for the first time, which we have used to line-narrow and correlate the energy fluctuations of the first three anti-symmetric stretch vibrational levels of the azide ion, N_3^-, in the ionic glass $3KNO_3{:}2Ca(NO_3)_2$. The azide ion has become a model system for studying solvent/solute interactions. In water, the fundamental frequency of the anti-symmetric stretch exhibits non-Markovian vibrational dynamics due to the time-evolution of the distribution of water structures on femtosecond and picosecond timescales.[2] In comparison, the vibrational dynamics of solutes in molecular glasses at low temperature are described very well with a static inhomogeneous distribution of frequencies because the glass structure evolves little during the vibrational lifetime.[8] In this work, the glass consists of small atomic and molecular ions that create extremely strong

*Corresponding Author: fulmer@chem.wisc.edu

solvent/solute interactions. Linear infrared spectra show that the solvent interactions increase the azide anti-symmetric stretch frequency in the glass (ω_{10}=2096 cm^{-1}) compared to D_2O (2043 cm^{-1}) and in the gas-phase (1987 cm^{-1}). The FWHM of azide in glass is 41 cm^{-1} compared to 25 cm^{-1} in D_2O. To measure solvent effects on the anharmonicities and to ascertain the broadening mechanisms, non-linear techniques are required. The 5th-order 2D-IR spectrum presented here gives the anharmonicities of the molecular potential by revealing the frequencies distributions and the correlations of the υ=1, 2 and 3 anti-symmetric stretch vibrational levels. Surprisingly, we find that the solvent affects each vibrational level differently.

Third-order 2D-IR uses three femtosecond infrared pulses to manipulate vibrational coherences and populations while 5th-order requires five interactions. The 5th-order pulse sequence used here builds on a 3rd-order pulse sequence we have recently reported that correlates the two-quanta (2Q) overtone and combination bands to the one-quantum (1Q) fundamental frequencies.[9] We call this 2Q-2D-IR spectroscopy. The 2Q correlation is especially useful for measuring the diagonal and off-diagonal anharmonicities of molecules that lead to couplings and ultimately the molecular structure,[10] but the resolution is not optimal because a free-induction decay is generated. If an echo were generated instead, the 2Q-2D-IR features would be line narrowed and the resolution improved. Third-order pulse sequences exist that rephase 1Q coherences to line-narrow 2D-IR spectra of correlated 1Q states,[3] but there is no 3rd-order pulse sequence that can rephase a 2Q coherence. A minimum of five interactions with the pulses are needed to accomplish this. To this end, the 5th-order pulse sequence reported here is chosen to rephase a 2Q coherence and generate a line-narrowed spectrum. The narrowed lines reveal the anharmonicities and the correlations in the frequency fluctuations caused by the solvent.

The 5th-order signal is generated by five laser field interactions. For five laser pulses that each interact with the sample once and have unique wavevectors k_n, the rephased 2Q 5th-order signal is emitted in the $k_s= -k_1-k_2+k_3+k_4+k_5$ phase matching direction for five pulses following in the order they are written. Alternatively, three pulses can be used by measuring the signal in the $k_s= -2k_1+k_2+2k_3$ phase matching direction which requires that pulses k_1 and k_3 interact with the sample twice. We use the latter approach, which is equivalent to a five pulse experiment with $t_1=t_4=0$ and is analogous to the common practice of measuring 3rd-order photon echoes with only two pulses.[8] Using a laser system described elsewhere,[9] the femtosecond infrared pulses (~500 nJ each, 150 cm^{-1} bandwidth) are tuned to ~2100 cm^{-1} and intersect the sample in an equilateral triangle configuration. With this setup, we generate 3rd-order 2Q-2D-IR and 5th-order rephasing 2Q-2D-IR spectra. The former has very broad peaks that are severely overlapped with each other, distorting their lineshapes. The latter has three peaks with minimal interference due to the rephasing of the inhomogeneous distribution along the antidiagonal, and this allows extraction of detailed information about the azide in glass system that would not otherwise be available from the 3rd-order 2Q-2D-IR spectrum.

To quantify this detailed information, the 2D-IR spectrum is fit by simulating the electric field $E_R^{(5)}$ emitted by the system responding to the five pulse interactions.[11] In the rotating wave approximation there are seven response functions that contribute to the 5th-order signal of a single oscillator system for the phase matching direction and time delays used here. The responses can be derived using approaches developed previously,[12] and it is constructive to consider $E_R^{(5)}$ in the limit of δ-function pulses. From these simulations, we can determine the frequencies, anharmonicities, dephasing rates, inhomogeneous distributions, and correlations of the three lowest vibrational energy states of the azide ion in the ionic glass.

We have also investigated whether cascaded 3rd-order processes contribute to the signal. Cascades are caused by the 3rd-order electric field of three pulses acting as an excitation pulse with the remaining two pulses to generate another 3rd-order signal in the same phase matching direction.[13] We have measured the concentration dependence of the 5th-order signal, simulated the spectral signatures of possible cascades, calculated their probable contributions, and estimated their contributions based on the 3rd and 5th-order signal strengths. We see no evidence for cascaded signals. A complete description of our work investigating possible IR cascades has been published elsewhere. [14]

In conclusion, we have used a 5th-order 2D-IR pulse sequence to rephase a 2Q coherence, extract the first and second anharmonicities of the molecular potential, and measure the correlation between the frequency fluctuations of the first three asymmetric stretch vibrational levels in azide. The use of five pulses to manipulate the populations and coherences of vibrational modes opens the opportunity to explore many more pulse sequences for better control of infrared spectra and more accurately measure vibrational couplings in condensed phase systems. An interesting new capability is the control of an additional coherence time that might be used to improve signal strengths, collect 3D spectra, and map connected vibrational modes in analogy to heteronuclear NMR pulse sequences.[7]

Bibliography

[1] D. Zimdars, et al., Phys. Rev. Lett. **70**, 2718 (1993).
[2] P. Hamm, M. Lim, and R. M. Hochstrasser, Phys. Rev. Lett. **81**, 5326 (1998).
[3] M. T. Zanni, et al., J. Phys. Chem. B. **105**, 6520 (2001).
[4] O. Golonzka, et al., Phys. Rev. Lett. **86**, 2154 (2001).
[5] J. Bredenbeck, et al., Proc. Natl. Acad. Sci. U.S.A. **100**, 6452 (2003).
[6] T. Peifang, et al., Science **300**, 1553 (2003).
[7] C. Scheurer and S. Mukamel, J. Chem. Phys. **116**, 6803 (2002).
[8] A. Tokmakoff and M. D. Fayer, J. Chem. Phys. **103**, 2810 (1995).
[9] E. C. Fulmer, et al., J. Chem. Phys. **120**, 8067 (2004).
[10] A. Moran and S. Mukamel, Proc. Natl. Acad. Sci. U.S.A. **101**, 506 (2004).
[11] S. Mukamel, *Principles of Nonlinear Optical Spectroscopy* (Oxford University Press, New York, 1995).
[12] N.-H. Ge, M. T. Zanni, and R. M. Hochstrasser, J. Phys. Chem. A. **106**, 962 (2002).
[13] D. A. Blank, L. J. Kaufman, and G. R. Fleming, J. Chem. Phys. **111**, 3105 (1999).
[14] E. C. Fulmer, F. Ding, and M. T. Zanni, J. Chem. Phys. (in press).

TRVS XII

NIST National Institute of Standards and Technology

Washington, D.C.
May 23-27, 2005

Biological TRVS

Femtosecond Broadband Stimulated Raman Spectroscopy: A New Approach for Time-Resolved Vibrational Structural Studies

Philipp Kukura, Sangwoon Yoon and Richard A. Mathies
Department of Chemistry
University of California
Berkeley, CA 94720

ABSTRACT: Femtosecond Stimulated Raman Spectroscopy (FSRS) is a unique new approach for obtaining high time resolution (<100-fs) vibrational spectra with an instrument response limited frequency resolution of <10 cm^{-1}. A Titanium:sapphire-based laser system produces the three different pulses needed for FSRS: (1) a femtosecond visible actinic pump that initiates the photochemistry, (2) a narrow bandwidth picosecond Raman pump that provides the energy reservoir for amplification of the probe, and (3) a femtosecond continuum probe that is amplified at Raman resonances shifted from the Raman pump. We present here a description of this novel spectroscopic technique and illustrate its capabilities by obtaining fs time-resolved Raman vibrational spectra of the excited S_2 state of β-carotene.

Time-resolved Raman spectroscopy is a valuable tool for revealing structural dynamics in ultrafast chemical and biological reactions. Spontaneous Raman scattering can be used to obtain spectra over a ~1500 cm^{-1} spectral window, but requires picosecond or longer duration pulses for adequate spectral resolution and often presents poor data quality and acquisition times. To overcome these problems of time-resolution and spectral quality, we have developed the technique of femtosecond stimulated Raman spectroscopy (FSRS)[1-3]. FSRS can obtain Raman spectra over a broad spectral window free from fluorescence background, with both high time and frequency resolution. The system we have developed is unique in its ability to obtain high signal-to-noise spectra in seconds with < 100-fs temporal resolution and <10-cm^{-1} spectral resolution, producing an instrument response product of < 1 cm^{-1}ps, more than an order of magnitude better than the transform limit of spontaneous Raman (15 cm^{-1}ps).

An overview of the FSRS experiment is presented in Figure 1. The first temporal step is the production of a transient or excited state with a fs actinic pump pulse (Figure 1b,c). This nonstationary population is then probed by stimulated Raman spectroscopy. The stimulated Raman event is initiated by the simultaneous application of a narrow band ps Raman pump pulse and a broad band fs Raman probe pulse that contains sufficient energy width to drive all relevant Raman resonances. This Raman probe pulse gates or triggers the stimulated Raman process with excellent <100 fs time precision. Figure 1a presents the spectra of the narrow bandwidth Raman pump and the dispersed spectrum of the Raman probe both without and in the presence of the Raman pump. The difference between these two spectra for cyclohexane illustrates the acquisition of high quality Raman spectra in only a few laser shots.

Here we use FSRS to explore the vibrational structure and structural dynamics of the S_2 state of β-carotene. The generally accepted energy level ordering of long polyenes such as β-carotene is comprised of a one-photon allowed S_2 state of B_u^+ symmetry and a lower-energy optically forbidden state of A_g^- symmetry. However, theoretical and experimental suggestions have been made for the presence of an additional lower lying excited state ($1B_u^-$) located between the traditional S_2 and S_1 states [4-6]. Ultrafast time-resolved vibrational spectroscopy using the FSRS approach is an excellent way to examine the internal conversion processes in β-carotene because the time-resolved vibrational structural features provide much more information about the presence and identity of transients than does traditional fs electronic spectroscopy.

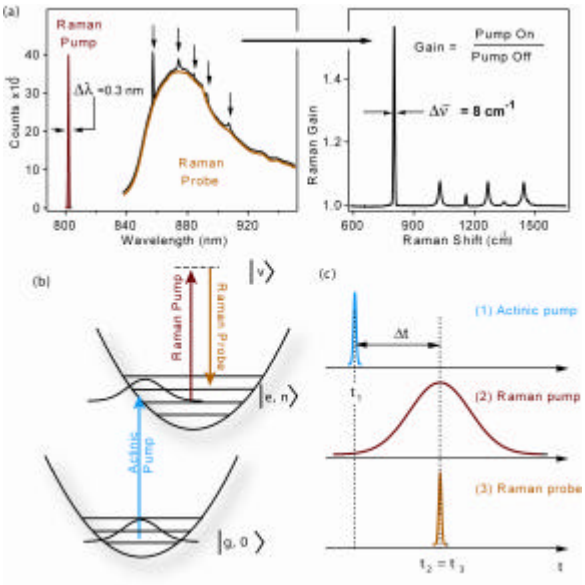

Figure 1. Femtosecond stimulated Raman spectroscopy (FSRS). (a) The spectra of the Raman pump and probe pulses for a typical FSRS experiment on cyclohexane. In the presence of the Raman pump pulse, the stimulated Raman effect amplifies the probe continuum at Raman frequencies (arrows) shifted from the Raman pump wavelength. The gain spectrum is obtained by dividing the *Raman-pump-on* probe spectrum by the *Raman-pump-off* probe spectrum. The frequency resolution of the spectrum is determined primarily by the bandwidth of the Raman pump pulse and is generally less than 16 cm^{-1}. (b) Energy level diagram showing the electronic and vibrational resonances of the three laser pulses. (c) Timing diagram for FSRS. Time resolution is obtained by optically delaying the femtosecond duration actinic pump pulse (1) relative to the Raman probe (3). The temporal instrument response is limited only by the cross-correlation of the actinic pump and Raman probe pulses and is typically < 100 fs.

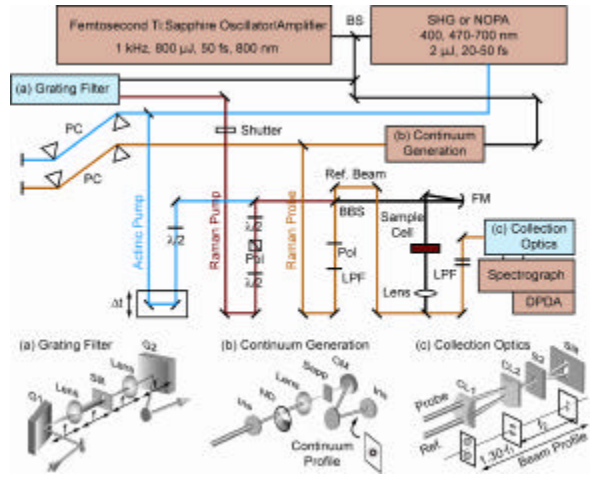

Figure 2. Laser and detection system for FSRS. The actinic pump (blue) is generated by second harmonic generation (SHG) or by the noncollinear optical parametric amplifier (NOPA). The Raman pump (red) is produced by spectrally filtering the output of the Ti:sapphire amplifier, as shown in (a). The Raman probe is produced by continuum generation in a sapphire plate (b) and split into a probe and reference beam for shot-to-shot normalization of the continuum intensity. The collection optics (c) image the probe and reference beams onto the slit as vertically displaced lines, before they are dispersed by the spectrograph and detected by a dual-photodiode array detector (DPDA).

The apparatus used to obtain FSRS spectra of β-carotene is presented in Figure 2. All three pulses for the experiment are produced by a single Ti:sapphire laser. The actinic pump is produced by pumping a non-collinear optical parametric oscillator to produce pulses from 470-700 nm with 20-50 fs duration and a power of 2 μJ. For this β-carotene work the 30 fs actinic pump pulses at 498 nm had a 12 nm fwhm and pulse energies of 50 nJ. The 50 nJ Raman pump pulse is produced by filtering the 800 nm fundamental with a narrow band-pass filter or a custom tunable spectral filter[2]. The Raman probe pulse is produced by focusing the fundamental on a sapphire plate producing a broad continuum that is filtered and compressed to a 20 fs duration and 5 nJ/pulse.

Figure 3 presents the transient FSRS spectra of β-carotene from 50 fs to 1 ps. The intense broad features in the 50 fs spectrum are assigned to the second $1B_u^+$ excited state of β-carotene due to their intense resonance enhancement as well as their decay within 350 fs. Comparison of the S_2 spectrum with that of the ground state indicates that the 1654-1739 cm^{-1} feature is the C=C stretch, the 1313-1400 cm^{-1} band is a mixture of C-C stretch and CCH rocking modes, and the methyl rocking modes are at 1067 and 1124 cm^{-1}. By 350 fs a new feature appears at ~1800 cm^{-1} that is characteristic for the up-shifted C=C stretch of the $2A_g^-$ state which subsequently decays back to the ground state in ~ 10 ps. The formation and decay of the S_1 state has been studied in detail in an earlier publication[1]. These features are also illustrated in the contour plot in Figure 3b. The superb S/N of FSRS combined with the high data acquisition rates makes it possible to record time-resolved vibrational spectra in 25 fs steps making this unique contour plot possible. The observed S_2 spectra exhibit a general up-shift in vibrational frequency compared with the ground state in agreement with theoretical predictions for octatetraene[7].

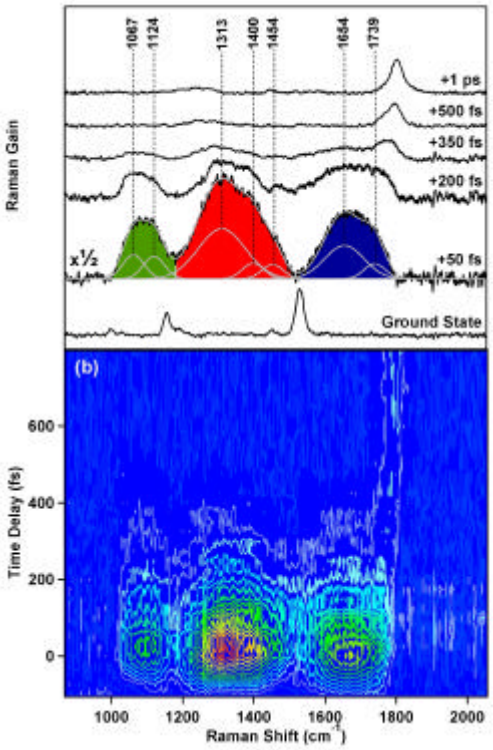

Figure 3. (a) Selected time-resolved femtosecond stimulated Raman spectra of β-carotene after photoexcitation at 500 nm. (b) Contour plot of all acquired spectra with time-delays between -200 and +1000 fs in 25 fs steps. Ground state, solvent and background features have been subtracted.

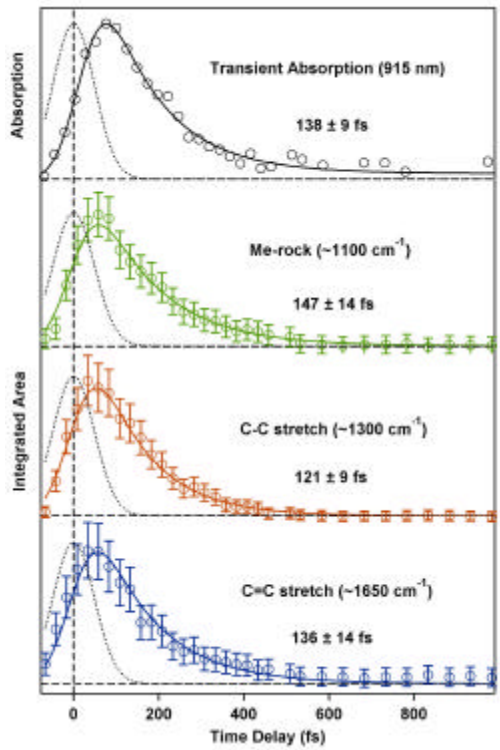

Figure 4. (a) Temporal evolution of the transient near-infrared absorption of the S_2 state of β-carotene. (b) – (d) Kinetics of the integrated areas of the three major Raman bands corresponding to the S_2 electronic state. Included are the instrument response (dotted lines), kinetic fits (solid lines) and lifetimes

The temporal dynamics of the vibrational and electronic transients of β-carotene are summarized in Figure 4. The transient absorption at 915 nm due to the S_2 state decays with a single exponential rate of 140 fs to the S_1 state. The C=C, C-C and methyl rocking features decay with similar time constants of 136, 121 and 147 fs, respectively. This excellent correspondence illustrates the superb time resolution of this new vibrational spectroscopy and demonstrates that the transient features we are observing are indeed due to the S_2 state which has a 140 fs lifetime.

This brief report has provided an introduction to the new time-resolved vibrational structural technique called femtosecond stimulated Raman spectroscopy and a demonstration of its capabilities through studies of β-carotene. The key advance in this experimental format is the use of a broadband compressed fs pulse to gate the stimulated Raman process at a very well defined point in time (~20 fs) relative to the actinic pump pulse. This approach gives simultaneously high time resolution, spectral resolution and high data quality and acquisition rates. The apparent paradox between the *instrumental* time resolution provided by our apparatus and the uncertainty principle, is resolved by realizing that the ultimate spectral resolution of the experiment is determined by the molecular properties especially the time scale for the vibrational free induction decay[3]. An additional advantage of FSRS is that the vibrational line positions and shapes are determined by the traditional Raman polarizability expressions and do not suffer from dispersive line shapes and background interference as in CARS. Furthermore, since this is a stimulated Raman experiment, the signals are much less sensitive to background fluorescence interference than traditional time-resolved spontaneous Raman experiments[8].

The experimental and theoretical advantages outlined above have been used here to examine the state ordering and internal conversion processes in β-carotene. In addition to providing the first vibrational spectrum of the S_2 state of β-carotene[9], these kinetic spectra show a smooth transition from the S_2 to the S_1 vibrational spectra without any indication of an intermediate electronic state in either the contour plots

of Figure 3 or in the kinetic traces in Figure 4. We can thus find no evidence in our time resolved vibrational structural data for an additional state lying between the S_2 and the S_1 states. It seems likely that the suggestions for this intermediate based on transient electronic spectroscopy by Cerullo and coworkers [6] are due to vibrational dephasing and cooling processes rather than new electronic states.

In summary, FSRS is a new time-resolved vibrational technique that dramatically enhances the capabilities of time-resolved Raman vibrational spectroscopy compared with conventional spontaneous ps Raman, CARS etc. The ability to rapidly obtain high quality spectra with the highest possible time-resolution and high spectral resolution, opens up a wide variety of time-resolved structural studies of chemical and biochemical reaction dynamics. We anticipate that with the construction and use of FSRS systems by more researchers interested in chemical reaction dynamics[2], FSRS will become the dominant method for obtaining time-resolved Raman spectra in the future.

References

[1] D. W. McCamant, P. Kukura, R. A. Mathies, *J. Phys. Chem. A* 107, 8208 (2003).
[2] D. W. McCamant, P. Kukura, S. Yoon, R. A. Mathies, *Rev. Sci. Instrum.* 75, 4971 (2004).
[3] S.-Y. Lee, D. Zhang, D. W. McCamant, P. Kukura, R. A. Mathies, *J. Chem. Phys.* 121, 3632 (2004).
[4] P. Tavan, K. Schulten, *J. Chem. Phys.* 85, 6602 (1986).
[5] T. Sashima, Y. Koyama, T. Yamada, H. Hashimoto, *J. Phys. Chem. B* 104, 5011 (2000).
[6] G. Cerullo, D. Polli, G. Lanzani, S. De Silvestri, H. Hashimoto, R. J. Cogdell, *Science* 298, 2395 (2002).
[7] F. Zerbetto, M. Z. Zgierski, F. Negri, G. Orlandi, *J. Chem. Phys.* 89, 3681 (1988).
[8] D. W. McCamant, P. Kukura, R. A. Mathies, *Appl. Spectrosc.* 57, 1317 (2003).
[9] P. Kukura, D. W. McCamant, R. A. Mathies, *J. Phys. Chem. A* 108, 5921 (2004).

Detection of a tryptophan neutral radical in DNA photolyase by resonance Raman spectroscopy

Ullas Gurudas and Johannes P. M. Schelvis

Department of Chemistry, New York University, 100 Washington Square East, New York, NY 10003

Introduction

Amino acid radicals play important roles in enzyme catalytic reactions [1]. Although other amino acids radicals have been detected or proposed in enzymatic reactions, tyrosine (Tyr) and tryptophan (Trp) radicals are of particular interest. Tyr radicals have been observed in and/or postulated to play important roles in systems such as RNR [2], photosystem II [3], and cytochrome *c* oxidase [4], while Trp radicals have been detected in cytochrome *c* peroxidase [5], DNA photolyase [6], RNR [2], catalase-peroxidase [7], and modified azurin [8]. The role of the Tyr and Trp radical intermediates in (proton-coupled) electron transfer [(PC)ET] is of great interest [2]. It has been recognized that intraprotein ET can occur over large distances (> 20 Å) and that long-range ET can be accelerated by positioning redox cofactors within short distances (< 14 Å) of one another even with one or more endergonic steps [16,17]. Nature seems to use this strategy often, and, in RNR and DNA photolyase, tyrosine and tryptophan neutral and cationic radical intermediates have been proposed for PCET and ET over distances of 35 Å and 15 Å, respectively [2,11].

In DNA photolyase, which is a flavoenzyme that repairs cyclobutane pyrimidine dimers of DNA by means of a light-induced, ET mechanism, Trp residues have been implied as ET mediators or true intermediates [11,12]. The *E. coli* enzyme binds two cofactors: flavin adenine dinucleotide (FAD), which forms the active site and is fully reduced ($FADH^-$) in the catalytically active enzyme, and 5,10-methenyltetrahydrofolate polyglutamate (MTHF), which functions as a light-harvesting pigment (Figure 1) [12]. The isolated enzyme contains the neutral radical semiquinone, FADH•, which is catalytically inactive [12,13]. The isolated enzyme can be photoreduced to its catalytically active form upon excitation of FADH• to form $FADH^-$ and $Trp\bullet^+$, which deprotonates to Trp• within 1 μs, though no evidence has yet been found that this process plays a role *in vivo* [12]. The neutral Trp radical resides on Trp_{306} [14]. In the absence of exogenous electron donors, pH-dependent charge-recombination occurs on the millisecond timescale in *E. coli* photolyase [11,13].

Photolyase provides an ideal model system to study the migration of tryptophan radicals through a protein, and recently, we have used nanosecond resonance Raman spectroscopy to determine the vibrational spectrum of the neutral radical of Trp_{306} in DNA photolyase [15].

Results

We used a Nd:YLF laser with 150 ns pulses at 527 nm to excite FADH• in photolyase and to initiate electron transfer to produce the charge separated state FADH- - Trp306•. The results are shown in Figure 1. At 0.5 kHz repetition rate we observe the regular resonance Raman spectrum of FADH• in photolyase (trace b) [16], but at 1.5 kHz repetition rate new vibrations of a possible intermediate are observed (trace a). After subtraction of the normalized spectra and removal of buffer contributions, the difference spectrum (trace c) shows vibrations that are completely different from the FADH• spectrum (trace a). This difference spectrum may

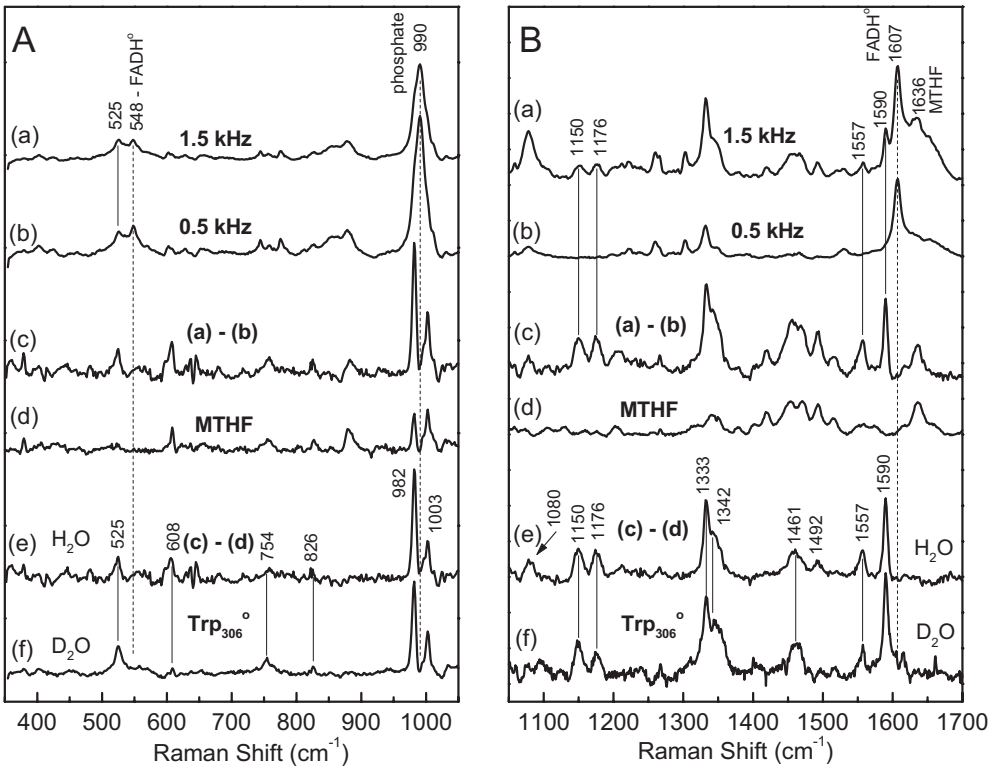

Figure 1. High (B) and low (A) frequency resonance Raman spectra of DNA photolyase. (a) At 1.5 kHz repetition rate. (b) At 0.5 kHz repetition rate. (c) Difference spectrum (a)-(b) after subtraction of buffer contributions. (d) Spectrum of reduced photolyase. (e) Difference spectrum (c)-(d). (f) The final difference spectrum in D_2O buffer.

contain yet contributions from $FADH^-$ and the MTHF cofactor. These contributions were removed by recording the spectrum of reduced photolyase, which contains $FADH^-$ and MTHF (trace d), to give the difference spectrum. The final difference spectrum (trace e in H_2O and trace f in D_2O) shows distinct vibrations that we have assigned to the neutral radical of Trp_{306}•. This assignment is supported by the absence of any significant change in the spectrum in the D_2O containing buffer because of loss of the N1 hydrogen upon formation of the neutral radical. See Figure 2 for the structure and atomic numbering of Trp.

In Table 1, we compare frequencies of Trp_{306}• to those of Trp and to the frequencies of indole and its neutral radical that have been predicted by DFT calculations. By comparing the DFT predicted frequency shifts to those observed for the vibrations of Trp_{306}• and of Trp, we can make tentative mode assignments. The agreement between predicted frequency differences and the observed ones is very good and provides further support for the assignment of the intermediate in our spectrum to Trp_{306}•.

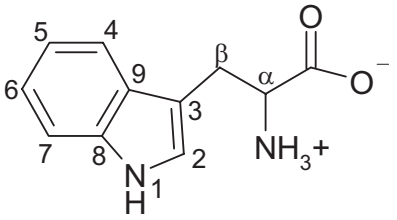

Figure 2. Structure and atomic numbering of tryptophan.

Our results show that it is possible to obtain resonance Raman spectra of tryptophan radicals and indicate that time-resolved resonance Raman spectroscopy can be employed to study (proton-coupled) electron-transfer processes that involve tryptophan radicals as intermediates.

Table 1. Comparison of experimental data to DFT calcuclations.

Trp[A]	Trp_{306}•	Δ	Indole[B]	Indole•[B]	Δ	Assignment[C]
1622	1590	-32	1613	1583	-30	W1, Φ8a; N1-C8ν
1575	1557	-18	1572	1560	-12	W2, Φ8b
1555	982	-573	1514	961	-553	W3, C2-C3ν
1496	1461	-35	1492	1457	-35	W5, Φ19a
1461	1492	+31	1450	1434	-16	W4, Φ19b
1127	1080	-47	1119	1063	-56	W13
1016	1003	-13	1012	1003	-9	W16
880	826	-54	882	831	-51	W17
762	754	-8	753	747	-6	W18
1622	1590	-32	1613	1583	-30	W1, Φ8a; N1-C8ν

A: Data taken from [17,18]; B: Data taken from [19]; C: Assignments following [17,20,21].

Acknowledgments

We thank Prof. Yvonne Gindt, Ms. Meghan Ramsey, and Ms. Katie Thoren at Lafayette College for providing purified *E. coli* photolyase.

References

1. Stubbe, J., and van der Donk, W.A., Chem. Rev. 98, 705-762, 1998.
2. Stubbe, J., Nocera, D.G., Yee, C. S., and Chang, M. C. Y., Chem. Rev. 103, 2167-2201, 2003.
3. Barry, B.A., Meth. Enzym. 258, 303-319, 1995.
4. Proshlyakov, D.A., Pressler, M.A., DeMaso, C., Leykam, J.F., Dewitt, D.L., and Babcock, G.T., Science 290, 1588-1591, 2000.
5. Sivaraja, M., Goodin, D.B., Smith, M., and Hoffman, B.M., Science 245, 738-740, 1989.
6. Kim, S.T., Sancar, A., Essenmacher, C., and Babcock, G.T., Proc. Natl. Acad. Sci. USA 90, 8023-8027, 1993.
7. Ivancich, A., Jakopitsch, C., Auer, M., Un, S., and Obinger, C., J. Am. Chem. Soc. 125, 14093-14102, 2003.
8. Miller, J.E., Gradinaru, C., Crane, B.R., Di Bilio, A.J., Wehbi, W.A., Un, S., Winkler, J.R., and Gray, H.B., J. Am. Chem. Soc. 125, 14220-14221, 2003.
9. Gray, H.B., and Winkler, J.R. in Electron Transfer in Chemistry, Balzani, V., Ed., Weinheim, New York, 3-23, 2001.
10. Page, C.C., Moser, C C., Chen, X., and Dutton, P.L., Nature 402, 47-52, 1999.
11. Aubert, C., Vos, M.H., Mathis, P., Eker, A.P.M., Brettel, K., Nature 405, 586-590, 2000.
12. Sancar, A., Chem. Rev. 103, 2203-2238, 2003.
13. Gindt, Y.M., Vollenbroek, E., Westphal, K., Sackett, H., Sancar, A., and Babcock, G.T., Biochemistry 38, 3857-3866, 1999.
14. Li, Y.F., Heelis, P.F., and Sancar, A.,, Biochemistry 30, 6322-6329, 1991.
15. Gurudas, U, and Schelvis, J.P.M., J. Am. Chem. Soc. 126, 12788-12789, 2004.
16. Schelvis, J.P.M., Ramsey, M., Sokolova, O., Tavares, C., Cecala, C., Connell, K., Wagner, S., and Gindt, Y.M., J. Phys. Chem. B 107, 12352-12362, 2003.
17. Miura, T., Takeuchi, H., and Harada, I., J. Raman Spectrosc. 20, 667-671, 1989.
18. Su, C., Wang, Y., and Spiro, T.G., J. Raman Spectrosc. 21, 435-440, 1990.
19. Walden, S.E., and Wheeler, R.A., J. Chem. Soc., Perkin Trans. 2, 2663-2672, 1996.
20. Harada, I., Miura, T., and Takeuchi, H., Spectrochim. Acta. 42A, 307-312, 1986.
21. Takeuchi, H., Biopolymers 72, 305-317, 2003.

Excited State and Photoionisation of DNA – A Time-resolved Vibrational Spectroscopy Study

Anthony W. Parker *(a.w.parker@rl.ac.uk)*

The photochemistry and the photophysics of nucleic acid bases and DNA continues to be of fundamental interest. We have recently used ultrafast time-resolved infrared spectroscopy to characterise the excited state reactivity[1] and photoionisation processes of nucleic acid bases and DNA.

When exciting the individual nucleic acid bases using 266 nm we observed the rapid formation and decay of vibrationally hot (S0, $\nu \geq 1$) ground state nucleic acid bases. The kinetics can be fitted to a single exponential process. Lifetimes of between 2.2 to 4.7 ps for the bases are measured. However, with synthetic polynucleotides we observe more complex kinetics and biexponentail decays are displayed. For poly(dG-dC)•poly(dG-dC) lifetimes of 12 (±2) ps and 50 (±10) ps are observed and for poly(dA-dT)•poly(dA-dT) lifetimes of 4 (±1) and 140 (±13) ps. The longer lifetimes correlate with fluorescence studies.[2]

Using 200 nm radiation direct ionisation of the nucleic acid bases occurs. This represents a primary step for genetic mutation. Under normal conditions the ease with which each individual base is ionised to produce the corresponding base radical cation is determined by its ionisation potential, the order being $G < A < C \approx T$. Thus, within a randomly photo-ionised DNA strand through hole transfer from one base to the next damage tends to localise onto G bases with the guanine radical cation ($G^{+\bullet}$) being produced.[3] Understanding the fundamental chemical mechanism whereby the guanine radical cation leads to mutation is therefore of primary importance in developing our understanding of this life threatening process and spectroscopic detection of this important species has been the subject of much international research effort. We have used picosecond-TRIR spectra, within the 1600 to 1750 cm^{-1} region, and have been able to identify the initially formed ($G^{+\bullet}$). These studies have now been extended to poly(dGdC)•poly(dGdC) and DNA and the results will be presented.

This work demonstrates how ultrafast time-resolved infrared absorption can be used to follow the rapid relaxation processes DNA and its constituent nucleobases as well as how ultrafast TRIR can be used to monitor base products generated by photoionisation of DNA.

---

[1] M. K. Kuimova, J. Dyer, M. W. George, D. C. Grills, J. M. Kelly, P. Matousek, A. W. Parker, X. Z. Sun, M. Towrie and A. M. Whelan. Chem. Comm., Accepted November 2004

[2] C. E.Crespo Hernandez, B. Cohen, P. M. Hare and B. Kohler, *Chem. Rev.*, 2004, **104**, 1977

[3] T. Melvin, M. A. Plumb, S. W. Botchway, P. O'Neill and A. W. Parker, *Photochemistry and Photobiology*, 1995, **61**, 584; T. Melvin, S. Botchway, A. W. Parker and P. O'Neill, *Journal of the Chemical Society-Chemical Communications*, 1995, 653.

Ultrafast heme structural changes upon ligand dissociation from the heme-based bacterial oxygen sensor FixL

Sergei Kruglik, Audrius Jasaitis, Latifa Bouzhir-Sima, Jean-Louis Martin, Ursula Liebl, and Marten H. Vos

Laboratory for Optical Biosciences, INSERM U696, CNRS UMR 7645, Ecole Polytechnique, 91128 Palaiseau cédex, France
email: Marten.Vos@polytechnique.fr
web: www.lob.polytechnique.fr

FixL is a sensor protein that contains a hemodomain of known structure, undergoing structural changes upon binding of small ligands (O_2, NO, CO) to the heme. These changes affect the (autophosphorylation) activity of an associated enzyme domain drastically (O_2) to moderately (NO, CO). This provides in principle an excellent system to follow the intra-protein signalling pathway in real time by time-resolved optical spectroscopy. Femtosecond absorption experiments indicated indeed strong perturbations of the heme upon ligand dissociation, especially for O_2, pointing at the formation of intermediates (*1*). Such perturbations are absent for oxygen-storage proteins with no signalling role as myoglobin.

To get insight in the nature of these primary intermediates at the heme level, we initiated a set of Time Resolved Resonance Raman experiments. We used a recently developed instrument for which the time/spectral resolution compromise was chosen to be biased towards the former (0.7 ps fwhm), and that has been employed to study ultrafast heme dynamics in cytochrome *c* (*2*). The accessible spectral range extends down to ~160 cm^{-1}, fully encompassing the important Fe-His stretching mode region, and special efforts were made to keep this zone accessible during pump-probe temporal overlap.

The first complexes of the hemodomain of FixL (FixLH) studied include FixLH-CO, FixLH-O_2 and comparison of the latter with Mb-O_2. Marked heme distortions were observed upon dissociation of CO from FixLH. Also the response to photoexciation of the oxycomplex appears unexpectedly small, a result which suggests, along with other observations, strain on the Fe-His bond induced by a single arginine residu that is H-bonded to heme-bound oxygen. These results are compared with those of myoglobin, for which the *static* structures of the heme are very similar, but the transient states are not. We will discuss routes to mapping out the initial dynamics of the distortional wave through the protein, by combining TRRR spectroscopy with absorption spectroscopy, site-directed mutagenesis, and molecular dynamics simulations.

1. Liebl, U., Bouzhir-Sima, L., Négrerie, M., Martin, J.-L., and Vos, M. H. (2002) Ultrafast ligand rebinding in the heme domain of the oxygen sensors FixL and Dos: general regulatory implications for heme-based sensors, *Proc. Natl. Acad. Sci. U.S.A. 99*, 12771-12776.
2. Cianetti, S., Négrerie, M., Vos, M. H., Martin, J.-L., and Kruglik, S. G. (2004) Photodissociation of heme distal methionine in ferrous cytochrome *c* revealed by sub-picosecond time-resolved resonance Raman spectroscopy, *J. Am. Chem. Soc. 126*, 13932 - 13933.

Time-Resolved Resonance Raman and Time-Resolved Step-Scan FTIR Studies of Nitric Oxide Reductase from *Paracoccus denitrificans*: Comparison of the Heme b_3-Fe_B Site to that of the Heme-Cu_B in Oxidases

Effie Pinakoulaki and Costas Varotsis*

University of Crete, Department of Chemistry, 71409 Heraklion, Crete, Greece

Time-resolved resonance Raman (TR^3) and time-resolved step-scan (TRS^2) FTIR spectroscopies have been used to probe the structural dynamics at the heme b_3 proximal and distal sites subsequent to carbon monoxide photolysis from fully reduced CO-bound nitric oxide reductase(Nor) and heme-copper oxidases (CcO). The TR^3 spectra of Nor exhibit structural differences relative to the equilibrium geometry of heme b_3. We suggest that relaxation along the tilt angle of the proximal histidine with respect to the heme plane and the out-of-plane displacement of the Fe (q) are coupled, and ligand binding and dissociation are accompanied by significant changes in the angular orientation of the His ligand. The results are compared to those obtained for CcO. The TR^3 and TRS^2-FTIR data demonstrate significant alterations in the nature of the heme-protein dynamics between Nor and CcO resulting from specific structural differences in their respective hemepockets.

References:1. E. Pinakoulaki and C. Varotsis *Biochemistry 42*, 14856-14861 **(2003).2**. E. Pinakoulaki *et al.* Raman Spectrosc. *in press* **(2005).**

Experimental Studies of Structure, Function, and Coherent Oscillations in Biomolecules

P.M. Champion, D. Ionascu, F. Gruia , A. Yu and X. Ye

Department of Physics and Center for Interdisciplinary Research on Complex Systems, Northeastern University, Boston, MA 02115 USA; E-Mail: champ@neu.edu

Femtosecond coherence spectroscopy (FCS) can be used to prepare and monitor coherent states of biological samples such as heme proteins. Following laser pulse induced ligand photolysis, the (initially planar) heme group is left far from its final product state equilibrium geometry. This leads to coherent oscillations of those modes composing the reaction coordinate for ligand binding and dissociation. Coherence studies, along with "white light" continuum measurements of the spectral dynamics, probe both the timescale for ligand dissociation as well as its rebinding. Investigations of the effect of temperature and sample condition on the coherent motions of the heme, and on the ultrafast geminate rebinding of the diatomic (NO and O_2) ligands, are described. FCS studies of various heme model compounds, which have the protein material removed, show that the spectrum of low frequency heme modes is softened in the absence of the axial ligand. The combined kinetic studies on myoglobin and the heme models allow the free energy barrier, associated with diatomic ligand binding, to be separated into "proximal" and "distal" contributions that can be separately determined.

NONINVASIVE REMOTE MONITORING OF TISSUE OXYGEN SATURATION

J. Terner, I.P. Torres-Filho, K.R. Ward, R.W. Barbee, M.A. Tiba, R. Pittman, L. Torres; Dept. of Chemistry and Virginia Commonwealth University Reanimation Engineering Shock Center, Virginia Commonwealth University, Richmond, VA 23284-2006
Support is acknowledged from NIH grant GM57042

Intravascular measurements of hemoglobin oxygen saturation of blood in the microcirculation have been primarily obtained by means of absorption spectrophotometry of hemoglobin (1). The procedure is based on measurements of light absorption at an isosbestic wavelength, and an additional wavelength where there is a substantial difference between the absorptions of oxy- and deoxyhemoglobin (2). This method yields reliable measurements when secondary absorptions from other portions of the tissue can be accounted for or effectively shielded. The technique has been primarily restricted to the measurement of hemoglobin oxygen saturation in relatively thin tissue where transillumination is possible (3,4). The procedure becomes more complex if hemoglobin oxygen saturation needs to be determined in capillaries, as well as in larger microvessels such as arterioles and venules (5,6).

To implement a means for determination of oxygen saturation without transillumination, we used Raman excitation within the hemoglobin Soret absorption band providing strong resonance enhancement. This is suitable for the detection of signals from strongly absorbing samples. Early studies indicated that hemoglobin resonance Raman spectra from red blood cells did not differ from purified hemoglobin resonance Raman spectra (7), allowing chemical characteristics of descriptions obtained from the previous studies of hemoglobin to be carried over to *in vivo* studies. The hemoglobin resonance Raman peaks observed in flowing blood using intravital microscopy (8) were essentially identical to those reported in previous *in vitro* studies (9).

Resonance Raman investigations have been performed on single red blood cells (10-12). In some studies, the cells were immobilized by methanol fixation on a glass slide in air (13) and adsorbed on polylysine-coated glass surfaces (14). In addition, Raman spectra have been obtained from individual optically trapped cells using different excitation lines (15). Those studies demonstrated the potential for Raman spectroscopy to study red blood cell disorders such as thalassemia, sickle-cell disease and malaria. Our own approach was directed to an in vivo evaluation of blood oxygenation states in microvessels (8).

In order to obtain a range of hemoglobin oxygen saturation levels; arterioles, capillaries and venules were evaluated *in situ* under controlled conditions after a rat was subjected to stepwise hemorrhage by withdrawing blood from the carotid artery. Blood pressure was recorded simultaneously. The method used for microvascular hemoglobin oxygen saturation measurements, as an *in vivo* reference, was the microspectrophotometric hemoglobin absorption method (also known as the 3-wavelength method) of Pittman and Duling (16,17). We compared the values of hemoglobin oxygen saturation obtained using resonance Raman (8) with those obtained using the 3-wavelength method in arterioles and venules. A digital video-based version of the 3-wavelength method using a high-resolution digital CCD camera was used to calculate hemoglobin oxygen saturation by digital video image analysis. For each microvessel, Raman spectra and snap shots for 3-wavelength evaluation were recorded sequentially, in random order, such that during hemoglobin oxygen saturation measurements, the tissue was exposed to only one light source at a time. The tested laser excitation spot sizes were in the range of 10 to 100 μm in diameter, but the resonance Raman data were obtained using an epi-illuminated area of approximately 30 μm in diameter that was placed in the interstitium (close to the vessel wall) or in the center of the vessel under study.

Raman spectra obtained with hemoglobin solutions, as well as with blood, showed two clearly defined hemoglobin peaks known as ν_4 bands in the range of 1350-1400 cm^{-1}. One peak (1358 cm^{-1}) is at maximum when hemoglobin is fully deoxygenated. The other (1376 cm^{-1}) is at maximum when hemoglobin is fully oxygenated. At intermediate oxygenation states, we made the assumption that the relative peak heights were proportional to the relative concentrations of deoxy-hemoglobin and oxy-hemoglobin, respectively. The assumptions were tested in the ranges of 5-13 g/dL of hemoglobin concentration and of 5-99 % in hemoglobin oxygen saturation. We found that the technique can be employed over a wide range of physiologically relevant hemoglobin concentrations, microvessel diameters and hemoglobin oxygen saturations. *In vitro* calibration showed excellent correlations between hemoglobin oxygen saturation values measured with a blood gas oximeter, and those obtained from resonance Raman spectra. The O_2 saturation of a sample was related to the ratio of peak heights, using both peaks as internal references. Hemoglobin oxygen saturation determination was not affected by changes in the overall intensity of the Raman signals since the correlations were self referencing.

Raman spectra were obtained with rat Hb solutions, as well as with rat and pig blood, equilibrated with known O_2 tensions. When the hemoglobin oxygen saturation (measured by the blood gas oximeter) was lower than 1% or above 98%, a single ν_4 resonance Raman peak was observed. For intermediate levels of hemoglobin oxygen saturation, the spectra showed two clearly defined ν_4 peaks in the 1350-1400 cm-1 range. Keeping the hemoglobin oxygen saturation constant, similar Raman spectra were obtained from solutions using glass capillary tubes with different diameters (50-800 μm) as well as with different laser excitation areas (15-150 μm).

Intravascular hemoglobin oxygen saturation was estimated from resonance Raman spectra in mesenteric arterioles and venules from anesthetized rats breathing 100 % O_2 following hemorrhage and before. Under control conditions, arteriolar (mean diameter 20.3 ± 7.1 μm, range = 11-31 μm) and venular (mean diameter 28.3 ± 9.8 μm, range = 19-60 μm) hemoglobin oxygen saturation averaged 83.4 ± 7.1 % and 70.0 ± 12.8 %, respectively (8). Under these conditions, a substantial reduction in perfusion was observed throughout the mesenteric network. Similar recordings were obtained from venules located in the mesentery and the serosal surface of the exposed ileum.

When hemoglobin oxygen saturation values estimated from resonance Raman spectra were compared to hemoglobin oxygen saturation values measured using the 3-wavelength method in the same microvessels, quite good correlations were found. The mean differences between hemoglobin oxygen saturation values estimated from resonance Raman spectra and the values measured using the 3-wavelength method for arterioles and venules were 0.2 ± 11.5 % and 0.4 ± 10.1 %. The fraction of methemoglobin was always below 2%.

Intravascular hemoglobin oxygen saturation measured in mesenteric arterioles and venules from anesthetized rats under baseline conditions and after hemorrhage were comparable to those reported in the same species, using the three wavelength method. Good correlation was found when hemoglobin oxygen saturation values estimated from Raman spectra were compared to hemoglobin oxygen saturation values measured using the 3-wavelength method in the same microvessels. An excitation laser spot size of 30 μm diameter gave adequate signal to noise ratios allowing measurement of hemoglobin oxygen saturation in

the whole range, of microvessels *in vivo*. The measurement of all physiological hemoglobin oxygen saturation levels was possible.

Since extravascular signals did not seem to interfere with resonance Raman signals from intravascular hemoglobin, it was not critical to keep the laser excitation exclusively over the vessel under study. The same estimated hemoglobin oxygen saturation was obtained when a 30 μm diameter laser spot was centered over a 15 μm diameter vessel, and when the laser spot was reduced to 15 μm. It was possible to observe the tissue (using transillumination) during the period of measurement, in order to check for movements of the preparation as potential sources of error. The position of the laser excitation spot was checked before and after each measurement. The laser was the only light source to which the tissue was exposed during the hemoglobin oxygen saturation measurements obtained from resonance Raman signals. The use of transillumination, concomitantly with the laser excitation and signal collection, increased the background noise level, but did not alter the hemoglobin resonance Raman peaks to any significant extent.

Our results showed the applicability of resonance Raman spectroscopy fort the evaluation of dynamic changes in oxygenation of individual microvessels under physiological conditions (8). The system was implemented to allow the acquisition of resonance Raman spectra and other microcirculatory variables in vivo while systemic parameters (such as blood pressure) are simultaneously recorded. While several Raman microscope systems are available commercially, they do not allow comprehensive evaluation of other physiological parameters *in vivo*. Our system is integrated and versatile, allowing digital imaging at a wide range of sensitivity levels, and measurements of several microcirculatory parameters. Phosphorescence quenching for pO_2 determinations (18) can be added to the system. *In vitro* calibration was performed using blood with different Hb concentrations equilibrated with known O_2 tensions. Approaches used to calculate peak intensity, average intensity and area resulted in significant correlations between hemoglobin oxygen saturation values measured with the blood gas oximeter (the standard of reference) and hemoglobin oxygen saturation values estimated from Raman spectra. Successive determinations of hemoglobin oxygen saturation in a given area of constant oxygen level provided results varying ± 1-4 %. The detection of all physiological hemoglobin oxygen saturation levels was possible. The fraction of methemoglobin was always below 3%.

In summary, we have employed resonance Raman spectroscopy to accurately measure intravascular hemoglobin oxygen saturation in the flowing blood of microvessels noninvasively *in vivo*. The system was implemented in the same optical system used for red blood cell velocity and microvessel diameter measurements, providing noninvasive measurements from all vessels in the microvascular network. This methodology can be used to study hemoglobin oxygen saturation in thin tissues (such as mesentery and small skeletal muscles), as well as in solid organs and tissues such as liver, brain and tumors, which are unsuitable for techniques that require transillumination.

1. Pittman, R. N. (1986) in *Microcirculatory Technology* (Baker, C. H., and Nastuk, W. L., eds), pp. 367-389, Academic Press
2. Pittman, R. N. (1986) *Ann Biomed Eng* **14**, 119-137
3. Ellsworth, M. L., and Pittman, R. N. (1986) *Am J Physiol* **251**, H869-879
4. Ellsworth, M. L., Popel, A. S., and Pittman, R. N. (1988) *Microvasc Res* **35**, 341-362.
5. Ellis, C. G., Ellsworth, M. L., and Pittman, R. N. (1990) *Am J Physiol* **258**, H1216-1223
6. Ellsworth, M. L., Pittman, R. N., and Ellis, C. G. (1987) *Am J Physiol* **252**, H1031-1040
7. Brunner, H., and Sussner, H. (1973) *Biochim Biophys Acta* **310**, 20-31.
8. Torres Filho, I. P., Terner, J., Pittman, R. N., Somera, L. G., 3rd, and Ward, K. R. (2005) *Am J Physiol Heart Circ Physiol* **289**, H488-495
9. Brunner, H., Mayer, A., and Sussner, H. (1972) *J Mol Biol* **70**, 153-156.
10. Wood, B. R., and McNaughton, D. (2002) *Biopolymers* **67**, 259-262
11. Wood, B. R., Tait, B., and McNaughton, D. (2001) *Biochim Biophys Acta* **1539**, 58-70
12. Wood, B. R., and McNaughton, D. (2002) *Journal of Raman Spectroscopy* **33**, 517-523
13. Ong, C. W., Shen, Z. X., Ang, K. K. H., Kara, U. A. K., and Tang, S. H. (1999) *Applied Spectroscopy* **53**, 1097-1101
14. Ramser, K., Bjerneld, E. J., Fant, C., and Kall, M. (2003) *J Biomed Opt* **8**, 173-178
15. Ramser, K., Logg, K., Goksor, M., Enger, J., Kall, M., and Hanstorp, D. (2004) *J Biomed Opt* **9**, 593-600
16. Pittman, R. N., and Duling, B. R. (1975) *J Appl Physiol* **38**, 371-388
17. Pittman, R. N., and Duling, B. R. (1975) *J Appl Physiol* **38**, 315-320
18. Torres Filho, I. P., and Intaglietta, M. (1993) *Am J Physiol* **265**, H1434-1438

Reverse proton transfer reaction dynamics of 2-aminopyridine-acetic acid complex with nanosecond time-resolved infrared spectroscopy

Shin Sato(shin@chem.s.u-tokyo.ac.jp), Chikako Kudo and
Hiro-o Hamaguchi(hhama@chem.s.u-tokyo.ac.jp)

Department of Chemistry, School of Science, The University of Tokyo
7-3-1 Hongo, Bunkyo-ku, Tokyo 113-0033, JAPAN

The excited-state double proton transfer reaction (ESPT) of the 2-aminopyridine (2AP)/acetic acid (AcOH) system was studied with picosecond time-resolved fluorescence spectroscopy by Ishikawa *et al.*[1] The photoexcited double hydrogen-bonded complex of 2AP and AcOH undergoes a stepwise double proton-transfer reaction within 5 ps in the excited state (Figure 1). We here study the overall reaction dynamics including the reverse proton transfer of the imio tautomer in the ground state with nanosecond time-resolved infrared spectroscopy.

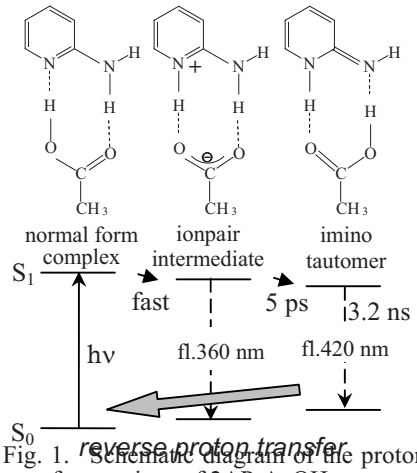

Fig. 1. Schematic diagram of the proton transfer reactions of 2AP-AcOH .

We have made a couple of modifications to the nanosecond time-resolved spectrometeter[2)] that is shown in figure 2 for doing experiment with the hydrogen bonded complex. The forth harmonic generation of a Nd:YAG laser is replaced by the second harmonic of the output of a Nd:YAG laser pumped dye laser for tuning the pumping wavelength to the exact peak wavelength of the complex absorption that slightly shifts from monomer peak. It is quite important to produce sufficient amount of the excited complex for observing the reverse proton transfer process in a good signal to noise ratio. We previously obtained an artificial temporal decay signal that originated from some photoproduct of the sample burned on inside surfaces of sample cell windows. A jet nozzle for dye laser is now used as a substitution for a conventional infrared sample cell for preventing the sample from being deposited on the cell windows.

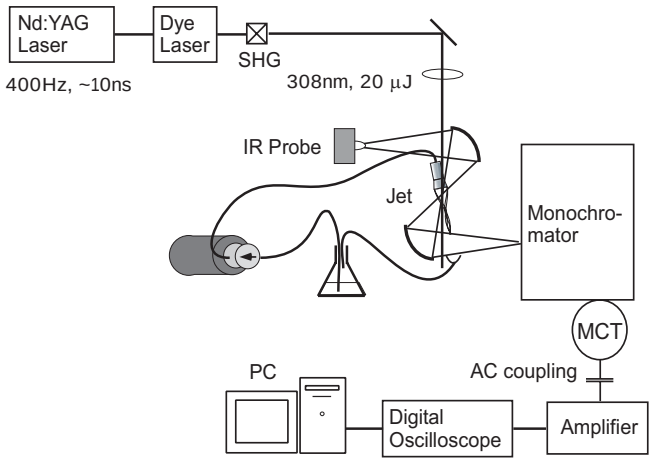

Fig. 2. Experimental setup of the nanosecond time-resolved spectrometer.

Figure 3 shows the steady-state infrared absorption spectra and the time-resolved infrared spectra of the 2AP/AcOH system and the 2AP monomer in dodecane solutions. The band at 1612 cm^{-1} is assigned to an overlap of the NH bend of 2AP monomer and the non-hydrogen bonded NH bend of the complex. We ascribe the 1636 cm^{-1} band, which newly appears by adding acetic acid, to the N-H bend involved in the hydrogen bonding. In the time resolved spectra of the complex (fig.3 (a)), both of the NH bend bands exhibit bleach and recovery corresponding to the photoexcitation and the recovery of the amino form complex. On the other hand, the time resolved spectra of the 2AP monomer (fig.3 (b)) shows the recovery of the bleaching at 1612 cm^{-1} and transient absorption in higher vibrational frequency region above 1625 cm^{-1}. The TRIR spectra of the monomer consists of two temporal components, a step function and an exponential decay with the time constant of 2.5 microsecond by SVD analysis. The step function is due to the population loss of the monomer in the ground state and some photoproduct of the 2AP monomer or its homodimer. The time constant of the transient absorption and the bleaching recovery derived from SVD analysis is much larger than the reported fluorescence lifetime of the 2AP monomer (1.4 ns)[3] even under the oxygen-rich condition. Therefore we tentatively assign the decay component with the time constant of 2.5 microsecond to the decay via its triplet state. The transient absorption of the triplet monomer appears also in the TRIR spectra of the mixture solvent (Fig. 3(a)) over 1625 cm^{-1} region and is overlapped with the bleaching signal of the two NH-bending vibrations of the complex. Consequently, the bleaching recoveries of the two bands of the complex that are shown in

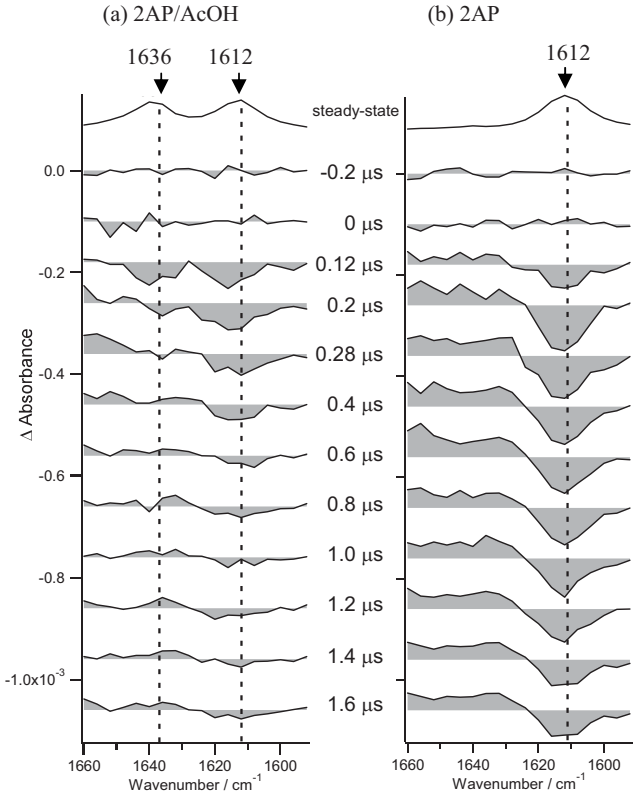

Fig. 3. Steady-state and transient infrared spectra. (a) 2AP/AcOH (b) 2AP in dodecane.

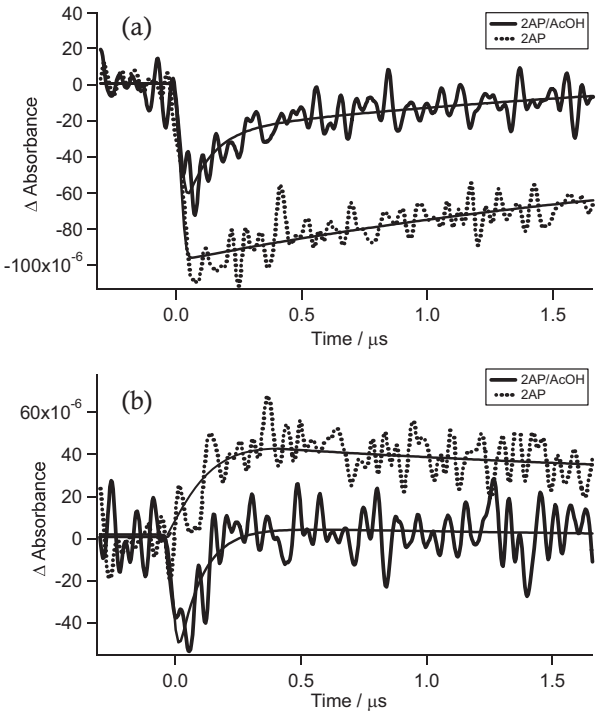

Fig. 4. Time dependence of NH-bending vibration. (a) 1612 cm^{-1} (b) 1636 cm^{-1}

figure 4 in solid line are not identical with each other. Even though there is a little difference in temporal change of the decay curves, the recovery of the bleaching of the complex shows much faster decay, which is superimposed on the slower decay of the monomer. We think that this fast recovery with a 200 ns time constant at 1612 cm^{-1} corresponds to the reverse proton transfer reaction in the electronic ground state of the complex. The time constant includes the double proton transfer in the excited state and the relaxation processes to the ground state. However, the former is much faster than the latter. Therefore, the 200 ns time constant is fully ascribed to the back double proton transfer in the ground electronic state.

We have thus observed the reverse proton transfer of the 2-aminopyridine-acetic acid complex as the recovery of bleaching with nanosecond time-resolved spectroscopy.

References

[1] H. Ishikawa, K. Iwata, H. Hamaguchi, *J. Phys. Chem. A*, **106**, 2305 (2002).

[2] T. Yuzawa, C. Kato, M.W. George, H. Hamaguchi, *Appl. Spectrosc*., **48,** 684 (1994).

[3] J. Konijnenberg, A. H. Ekelmans, C. A. G. O. Varma, *J. Chem. oc.*, *Faraday Trans. 2*, **85,** 1539 (1989).

TRVS XII

NIST National Institute of Standards and Technology

Washington, D.C.
May 23-27, 2005

Nanoparticles

COHERENT EXCITATION OF VIBRATIONAL MODES IN METALLIC NANOPARTICLES BY LASER-INDUCED HEATING

Gregory V. Hartland*

Department of Chemistry and Biochemistry, University of Notre Dame, Notre Dame, Indiana 46556-5670, USA; email: hartland.1@nd.edu, webpage: http://www.nd.edu/~ghartlan

Metal nanoparticles have intense optical absorption and scattering spectra due to the surface plasmon mode – which is a collective oscillation of the conduction electrons [1]. The position of the plasmon band depends on the size, shape and environment of the particles – properties which have made metal particles useful for sensing applications [2]. My group is interested in the fundamental photophysics of metal particles. Excitation of metal nanoparticles with sub-picosecond laser pulses deposits energy into the electron distribution, which causes a rapid increase in the electronic temperature [3]. The electronic temperatures created are extremely high — many thousands of Kelvin. The excited electrons subsequently equilibrate with the phonon modes of the particle via electron-phonon (*e-ph*) coupling. This gives rise to an increase in lattice temperature of tens to hundreds of degrees Kelvin. The increase in electronic temperature gives a strong bleach at the plasmon resonance, and transient bleach experiments performed at the maximum of the plasmon band can provide information about the time-scale for *e-ph* coupling, which is on-the-order of picoseconds for most metals [4].

The fast lattice heating induced by laser excitation can impulsively excite the phonon modes of the particle that correlate with the expansion co-ordinates [3]. The periods of these modes depend on the size, shape and elastic constants of the particles. Thus, time-resolved spectroscopy can be used to examine the material properties of nanometer-sized objects. Representative transient absorption data for spherical gold particles in aqueous solution is presented in Figure 1 [3]. The trace recorded at 525 nm (near the maximum of the plasmon band) shows a fast decay due to *e-ph* coupling, following by a slower decay that corresponds to heat dissipation to the environment. The trace recorded at 547 nm shows an additional feature: modulations that arise from the coherently excited breathing mode. The period of the mode is given by [5]

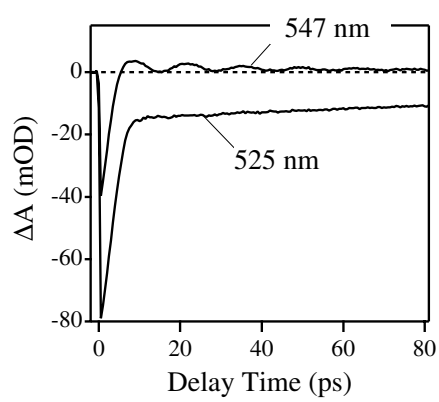

Fig. 1: Transient absorption data for gold particles in aqueous solution.

$$T_{br}^{(n)} = \frac{2\pi R}{\chi_n c_l} \tag{1}$$

where χ_n is an eigenvalue that is obtained from $\chi_n \cot \chi_n = 1 - (\chi_n c_l / 2c_t)^2$, and c_l and c_t are the longitudinal and transverse speeds of sound in the particles, respectively. Measurement for different sized particles show an almost perfect match with Equation

*This work was supported by the National Science Foundation (Grant Number CHE02-36279), and the donors of the American Chemical Society Petroleum Research Fund (Grant Number PRF-39761AC).

(1), which demonstrates that the elastic properties of small gold particles in aqueous solution are the same as bulk gold [6].

We have also performed these experiments for gold nanorods [7]. Nanorods show a transverse and a longitudinal plasmon resonance, corresponding to oscillation of the conduction electrons along the short and the long axis of the rod, respectively [8]. Figure 2 shows transient absorption data collected by exciting at 400 nm and probing the longitudinal plasmon band — which occurs in the near-IR for this sample. The two traces are for probe wavelengths on the red and the blue sides of the longitudinal plasmon resonance. The modulations have the same period, but are 180º out-of-phase, which shows that the signal arises from a periodic shift in the position of the plasmon resonance. The modulations are assigned to the extensional mode of the rods, and the period is given by [7,9]:

$$T_{ext}^{(n)} = \frac{2L}{(2n+1)\sqrt{E/\rho}} \qquad (2)$$

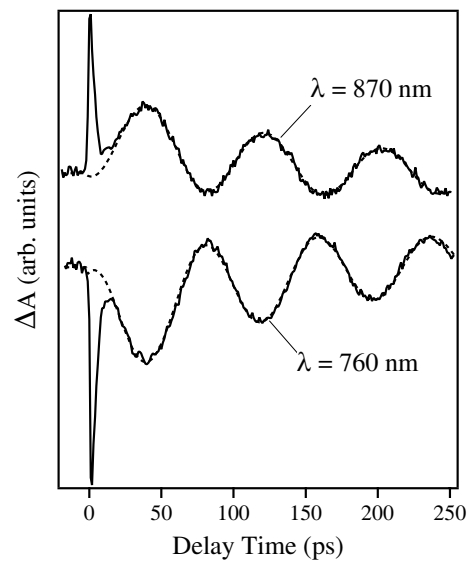

Figure 2: Transient absorption data for a gold nanorods sample with an average length of 75 ± 6 nm.

where L is the length of the rod, E is Young's modulus and ρ is the density. The extensional mode changes the length of the rods, which changes their aspect ratio and gives rise to a modulation in the position of the longitudinal resonance.

We have performed these experiments for several samples, and a plot of the measured periods versus the average length is presented in Figure 3 [7]. The solid line shows the period calculated for the fundamental extensional mode (n = 0 in Equation (2)) using values of E and ρ for bulk gold [10]. There is reasonable agreement with the experimental data, which confirms that observed modulations are due to the extensional mode. The dashed line shows a fit to the data where E was allowed to vary. The value obtained is E = 64 ± 8 GPa, which is ~19 % *smaller* than the room temperature value for bulk gold of 79 ± 1 GPa [7,11]. This is an unusual result: usually nanomaterials have superior mechanical properties than the bulk materials. For example, the value of Young's modulus for multi-walled [12] and single-walled carbon nanotubes [13] is up to 30 % *larger* than that for bulk graphite. This is because nanomaterials typically have less defects that the corresponding bulk [14]. The reason for the reduced value of Young's modulus for the nanorods is probably because of their unusual crystal structure (rather

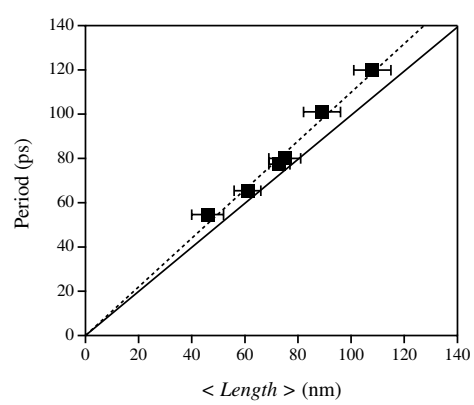

Figure 3: Period versus length for the gold nanorods

than just surface energy effects). Nanowires and nanorods of *fcc* metals have a 5-fold twinned structure with growth along the [110] axis [15,16,17]. This structure is not space filling: there is a 1.5º angular deficit at each of the twin planes. This will introduce edge dislocations that run along the length of the rod — we estimate a minimum of one edge dislocation per twin plane [11,18].

Both the growth direction and the presence of edge dislocations can affect the value of Young's modulus. However, calculations of *E* for different crystal directions show that the value of E for the [110] direction is essentially the same as the value for bulk gold (too high) [11]. Likewise, even though edge dislocations have a significant effect on the mechanical properties of metals, dislocations that run along the length of the rod should not affect extension and contraction along this axis [18]. Thus, the symmetry of the rods does not provide a simple explanation for the reduced value of Young' modulus. Clearly more experiments are needed here, but one possible explanation for our results is that the rods are much more defective than our estimate of one edge dislocation per twin plane. At very small grain sizes a reduction in Young's modulus has been predicted by simulation [19].

In conclusion, time resolved spectroscopy can be used to examine the low frequency vibrational modes of nanoparticles. Comparing the periods measured in these experiments to the results of continuum mechanics calculations yields information about the size of the particles if the shape and elastic constants are known or, alternatively, information about the elastic constants if the size and shape are known. The second application is the more scientifically interesting, as there are very few techniques available for accurately measuring the elastic constants of nanometer sized objects.

---

1 Kreibig U, Vollmer M 1995. *Optical Properties of Metal Clusters*, Berlin: Springer.
2 Haes AJ, Van Duyne RP. 2004. *Anal. Bioanal. Chem.* 379 (7-8): 920-930
3 Hartland GV. 2004. *Phys. Chem. Chem. Phys.* 6 (23): 5263-5274.
4 Arbouet A, Voisin C, Christofilos D, Langot P, Del Fatti N, Vallee F, Lerme J, Celep G, Cottancin E, Gaudry M, Pellarin M, Broyer M, Maillard M, Pileni MP, Treguer M, 2003, *Phys. Rev. Lett.* 90, 177401.
5 Lamb H. 1882. *Proc. London Math. Soc*., 13: 189-212.
6 Hodak JH, Henglein A, Hartland GV. 1999. *J. Chem. Phys.* 111 (18): 8613-8621
7 Hu M, Wang X, Hartland GV, Mulvaney P, Juste JP, Sader JE. 2003. *J. Am. Chem. Soc*. 125 (48): 14925-14933
8 Link S, Mohamed MB, El-Sayed MA. 1999. *J. Phys. Chem. B* 103 (16): 3073-3077
9 Landau LD, Lifshitz EM. 1970. *Theory of Elasticity; 2nd Edition,* Oxford: Pergamon Press
10 Simmons G, Wang H. 1971. *Single Crystal Elastic Constants and Calculated Aggregate Properties: A Handbook,* Cambridge: The MIT Press
11 Hu M, Hillyard P, Hartland GV, Kosel T, Perez-Juste J, Mulvaney P. 2004. *Nano Letters* 4 (12): 2493-2497
12 Treacy MMJ, Ebbesen TW, Gibson JM. 1996. *Nature* 381 (6584): 678-680
13 Krishnan A, Dujardin E, Ebbesen TW, Yianilos PN, Treacy MMJ. 1998. *Phys. Rev. B* 58 (20): 14013-14019
14 Wong EW, Sheehan PE, Lieber CM 1997. *Science* 277 (5334): 1971-1975
15 Johnson CJ, Dujardin E, Davis SA, Murphy CJ, Mann S. 2002. *J. Mat. Chem.* 12 (6): 1765-1770
16 Sun YG, Mayers B, Herricks T, Xia YN. 2003. *Nano Letters* 3 (7): 955-960
17 Lisiecki I, Filankembo A, Sack-Kongehl H, Weiss K, Pileni MP, Urban J. 2000. *Phys. Rev. B* 61 (7): 4968-4974
18 Hull D, Bacon DJ. 1984. *Introduction to Dislocations, 3rd Edition,* Oxford: Pergamon Press
19 Schiotz J, Di Tolla FD, Jacobsen KW. 1998. *Nature* 391 (6667): 561-563

Exciton spin flip dynamics in colloidal quantum dots

Gregory D. Scholes, Vanessa M. Huxter, Karolina Fritz, Jeongho Kim, and Cathy Wong
Department of Chemistry, University of Toronto, 80 St. George Street, Toronto, Ontario Canada M5S 3H6

Optical pumping of quantum dots (QDs) transfers photon angular momentum to excitons through its projection onto the wavevector direction in the crystal lattice. Thus, in oriented QDs, circularly polarized light can be used to select exciton total angular momentum. That means that exciton spin states can be established and followed spectroscopically in semiconductor quantum dots. This turns out to be interesting because the dynamics following excitation of the fine structure of a QD exciton state have not been previously observed because of inhomogeneous line broadening and degeneracy of levels in the absence of an applied magnetic field. We will describe how the fine structure of exciton states can be probed in isotropic QD ensembles using nonlinear optical spectroscopies. Thus we show that a variant on the transient grating method can be used to measure directly the dynamics of interconversion between the degenerate exciton states of QDs. We have found the dynamics of exciton spin flips to be strongly dependent on quantum size effects; with spin flip times varying from 100 fs to greater than 1 ps. These experimental results, for CdSe dots and rods, will be reported together with a discussion of the mechanism that promotes the spin flips. The relevant coupling matrix element acts in addition to the exchange interaction and usual spin orbit coupling that determines the fine structure we are probing.

Ultrafast THz studies of carrier cooling in CdSe Nanocrystals

M. Bonn[1, 2], E. Hendry[1,2 *], M. Koeberg[1,2], C. de Mello Donega[3], D. Vanmaekelbergh[3], F. Wang[4] and T.F. Heinz[4]

[1] *FOM Institute for Atomic and Molecular Physics, Kruislaan 407, 1098 SJ, Amsterdam, NL.*
[2] *Leiden Institute of Chemistry, Leiden University,Leiden, NL.*
[3] *Debye Institute, Utrecht University, NL.*
[4]*Departments of Physics and Electrical Engineering, Columbia University*
538 West 120th St., New York, NY 10027, USA.

We have applied Terahertz time-domain spectroscopy to probe the response of CdSe nanoparticles containing a single electron-hole pair. The dielectric response is found to be purely real at THz frequencies, and is determined by the large DC polarizability of the exciton, amounting to ~10^4 Å^3. The strength of the induced dipole moment varies strongly with particle radius R, approximating the R^4 variation predicted by simple models of quantum-confined systems. The response is dominated by the polarizability of the hole, owing to its relatively large mass and small energy level spacings.

Accordingly, the time scale on which the polarizability reaches its steady state value following exciton photogeneration is a direct measure of the hole cooling rate. The exponential hole cooling time is found to be ~400 fs, slightly increasing with R. Complementary time-resolved fluorescence experiments provide information about the timescale of combined electron and hole cooling, as the on-gap fluorescence is monitored. The unprecedented combination of time-resolved terahertz spectroscopy *and* time-resolved photoluminescence spectroscopy allows us to unambiguously determine the cooling rate for holes *and* electrons independently (see Fig. 1). We conclude that cooling proceeds without a phonon bottleneck for *both* holes and electrons, and present strong evidence of the involvement of Auger processes in the cooling mechanism.

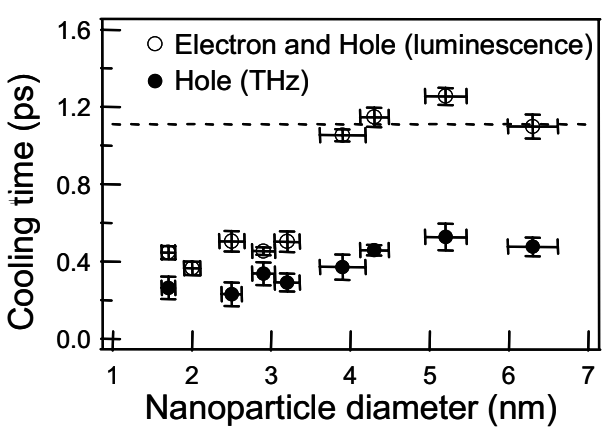

Fig. 1. The cooling time of holes (obtained from THz measurements, solid circles) and the combined hole and electron cooling time (from luminescence measurements, open circles). Above R=3.5 nm, a clear increase in electron cooling time is observed for the electrons, due to the apparently slower relaxation of higher electron levels that can be populated for larger particles with the 400 nm excitation wavelength.The dashed line shows the electron and hole cooling in near-bulk CdSe, measured by the rise in luminescence in large (20 nm) particles.

Some Interesting Properties and Application of Plasmonic Nanopartices of Different Shapes

Mostafa A. El-Sayed
Laser Dynamic Lab
Georgia Institute of Technology
Atlanta, Georgia

Abstract

The strong absorption, scattering and ultrafast relaxation properties of the surface plasmon oscillation in gold and silver nanoparticles are studied as a function of shape. These properties are further used to study the rapid coherent lattice oscillations of these particles[1], the enhanced surface Raman scattering processes[2], as well as for medical diagonostics[3] and treatment of cancer.

---

1. *Wenyu Huang; Wei Qian; Mostafa A. El-Sayed, "Coherent Vibrational Oscillation in Gold Prismatic Monolayer Periodic Nanoparticle Arrays", Nano Lett,* ***4****, (9), 1741-1747, (2004).*
2. *Babak Nikoobakht, Mostafa A. El-Sayed, "Surface-Enhanced Raman Scattering Studies on Aggregated Gold Nanorods," J. Phys. Chem A,* ***107(18)****, 3372-3378, (2003).*
3. *El-Sayed, Ivan; Huang, Xiaohua; El-Sayed, Mostafa A., "Surface Plasmon Resonance Scattering and Absorption of anti-EGFR Antibody Conjugated Gold Nanoparticles in Cancer Diagnostics; Applications in Oral Cancer," Nano Letters, in press, (2005).*

Ultrafast infrared spectroscopy of anions in reverse micelles

Jeffrey C. Owrutsky, Gerald M. Sando, and Kevin Dahl,
Chemistry Division, Naval Research Laboratory, Code 6111, Washington, DC 20375

Abstract:
Steady state and ultrafast infrared spectroscopy of anions dissolved in the water pools of reverse micelles (RM) have been used to characterize confinement effects in RMs. The spectra and vibrational energy relaxation (VER) times for both azide and cyanoferrate anions in RMs depend similarly on the surfactant charge in a manner that is explained in terms of the charge-mediated anion location in the RM.

Reverse micelles are composed of nanometer size water droplets stabilized in bulk organic phase by surfactants in which the droplet size increases with the water content (ω = [H_2O]/[surfactant]). Previous studies [1,2] have established that water inside RMs has less hydrogen bonding and lower polarity than bulk water, partially due to water molecules being occupied hydrating the surfactant headgroups. Solute probes are effective for investigating properties of the water core in RMs, but knowledge of the solute location is important for interpreting the results but is often challenging to determine. Small molecular ions are very hydrophilic so they are convenient solutes for probing the RM water interior via infrared spectroscopy. Confinement effects in RMs are determined from spectra and dynamics in RMs compared to those in bulk solvents for linear triatomic anions, especially azide, and cyanoferrate anions. For the antisymmetric stretching (ν_3) band of azide, the solvent shift of the band and its vibrational energy relaxation (VER) rate have been shown to increase in bulk solvents with increasing solute-solvent interaction, i.e, in those with higher polarity and more hydrogen bonding. [3] The shifts and rates increase in the order DMSO<MeOH<H_2O. Vibrational spectra and VER dynamics have also been measured for ferrocyanide and ferricyanide (CN stretches), and nitroprusside (SNP: CN, and NO stretches) in water and several other bulk solvents, [4] as a basis for determining the effects of confining these solutes in RMs. Their VER times exhibit similar solvent dependences as those for the triatomic molecular ions. Since the azide band is sensitive to the interaction strength in the solvation environment, it was used to probe the water pool of RMs composed of differently charged surfactants based on its solvent shift [5] and vibrational dynamics.[6,7] Similar studies were carried out for cyanoferrate anions.[8] All these results for aqueous RMs support the idea that the relative effects of confinement in the water core and interfacial effects near the surfactant headgroup region depend on the location as determined by the relative charge between the RM and the anion probe molecule. Studies have also been carried out for azide in formamide AOT RMs, in which the effects are more pronounced than in aqueous AOT.

Polarization-resolved infrared pump-probe transient absorption measurements are performed on static solutions of ions dissolved in RMs composed of different surfactants. Infrared pulses near 2000 cm^{-1} (FWHM of ~250 fs and 150 cm^{-1}) are generated with a 1 kHz Ti:Sapphire regenerative amplifier/OPA difference frequency generation scheme and split into pump and probe beams. Pump-induced transmission changes are measured on the probe beam, which is frequency and polarization resolved after the sample. T_1 times are measured at the magic angle (54.7º).

Figure 1 shows the dependence of the azide band vibrational frequency (left hand side) and VER times (right hand side) on ω for RMs composed of anionic (AOT), nonionic (NP and Brij-30), and cationic (CTAB) surfactants. The vibrational frequency in the smallest RMs is blue-shifted in AOT RMs and red-shifted in the others with the largest shift observed for CTAB. The red shifts, which are toward the gas phase value, are consistent with the previously established trend of water in the RMs being less polar and having reduced hydrogen bonding. The frequency approaches the bulk water value (2049 cm^{-1}) as ω increases, consistent with the water in the RM becoming more similar to bulk water as the water pool size increases with ω. The blue shift in AOT is more difficult to explain but may reflect ion pairing. The VER decay times (T_1) for azide in the RMs shown in Figure 1 follow a similar trend as the vibrational frequencies. The T_1 times are about three times longer (2.5 ps) than in bulk water for the smallest RMs studied in CTAB and NP; there is much less of an effect in AOT. The times also become shorter and approach the bulk water value with increasing RM water content. In CTAB and the nonionic RMs, the VER times are longer and become more bulklike with increasing ω, which is similar to the vibrational frequency behavior and is consistent with the previously established trend of solvation-dependent properties in RMs.

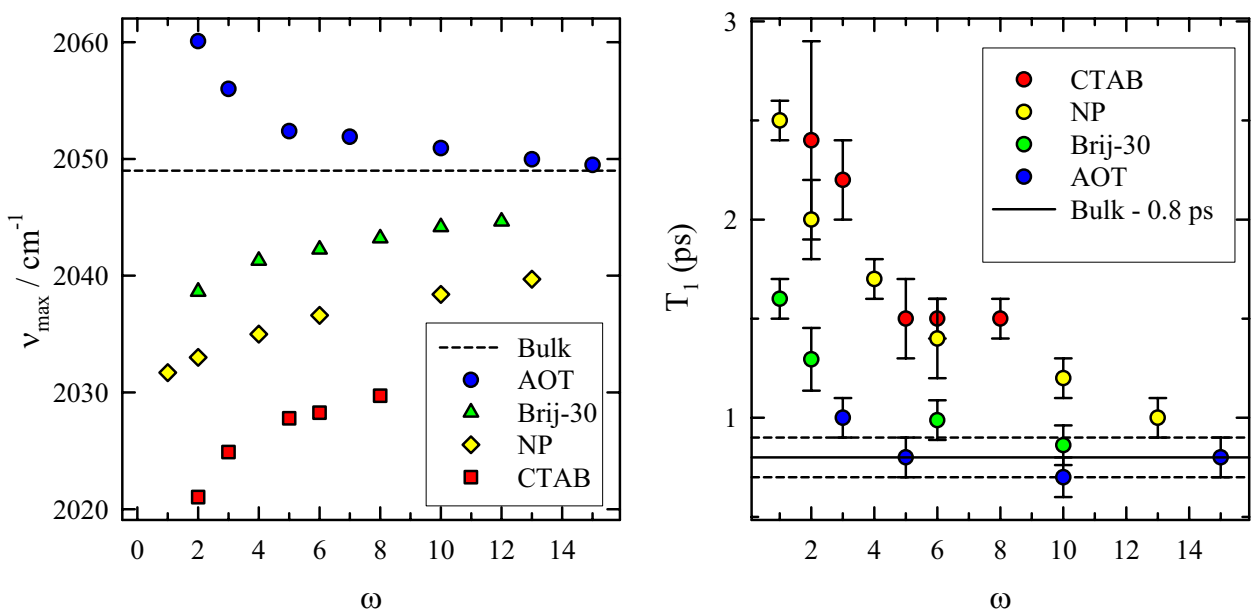

Fig. 1. Vibrational band centers (left, ν_{max}) and vibrational energy relaxation times (right, T_1) for azide in reverse micelles composed of anionic (AOT), nonionic (NP and Brij-30), and cationic (CTAB) surfactant as a function of water-to-surfactant molar ratio (ω).

The results demonstrate that both the vibrational frequency and VER rate of the antisymmetric stretching band of azide in RMs depend on the surfactant charge. The charge dependence of the spectra and dynamics are attributed to its determining the anion probe location in the RM due to Coulombic interactions. Of the RMs studied, in AOT the spectra and dynamics of azide are most similar to those in bulk water, suggesting that the anion is repelled by the negatively charged headgroups into the water core region where the water is most like bulk water. For cationic CTAB, the VER rate is about three times slower than bulk water for the

smallest RM, similar to nonionic NP RMs, but the VER rate for CTAB RMs levels off at $\omega = 5$ and the vibrational frequency is more shifted. This is consistent with the anion being attached to or strongly interacting with the CTAB RM interface. The results for nonionic Brij-30 RMs are similar to those for NP RMs. For CTAB and AOT RMs, the relative rates and spectral shifts are similar in D_2O and H_2O. Measurements were also performed in mixtures of water and tri(ethyleneglycol) monomethyl ether (TGE), in which the latter resembles the hydrophilic portion of the nonionic surfactants. The results for the spectra and VER times as a function of water content strongly resemble those for the nonionic RMs. Water and azide appear to interact with the polyethyleneoxide chains for small ω, especially for the longer chained NP surfactant. As ω increases and the water pool becomes better defined, azide begins to prefer a location within the water pool, allowing bulk-like behavior to be approached for large RMs. The similar results for nonionic RMs and TGE/water suggest that water penetrates into and hydrates the polyethyleneoxide chains before a water pool is formed. The interfacial region in nonionic RMs include the polyethyleneoxide chains, which appear to be hydrated, so that the boundary between the interface and the water core is less clearly defined than for the ionic RMs.

Bulk solution results for cyanoferrates indicate that the VER times are relatively short (<10 ps for all except the CN band of SNP, which is much longer) and depend on solvent interaction strength in a manner similar to azide. Studies of the NO band of SNP in the RMs of AOT, CTAB, and nonionic surfactants yielded results similar to those in azide in terms of the relative effects depending on the RM charge. These observations are again attributed to the anion probe location that depends on the anion – surfactant relative charge as for azide.

In addition, vibrational spectra and dynamics were measured for azide in nonaqueous, formamide AOT RMs. Although previous studies suggest that nonaqueous solvents are less affected than water in RMs, the azide vibrational band is more blue-shifted and the energy relaxation times are longer in formamide compared to aqueous AOT RMs.

Acknowledgements. This work was supported by the Office of Naval Research at the Naval Research Laboratory. G.M.S. acknowledges the NRL-ASEE Postdoctoral Fellowship program. K.D. acknowledges the NRL-NRC Postdoctoral Fellowship program.

References

1. N. E. Levinger, Current Opinion in Colloid and Interface Science **5**, 118 (2000).
2. N. Nandi, K. Bhattacharyya, and B. Bagchi, Chem. Rev. **100,** 2013 (2000).
3. M. Li, J. Owrutsky, M. Sarisky, J. P. Culver, A. Yodh, and R. M. Hochstrasser, J. Chem. Phys. **98**, 5499 (1993).
4. G. M. Sando, Q. Zhong, J. C. Owrutsky, J. Chem. Phys. **121**, 2158 (2004).
5. Q. Zhong, D. A. Steinhurst, E. E. Carpenter, and J. C. Owrutsky, Lang. **18**, 7401 (2002).
6. Q. Zhong, A. P. Baronavski, and J. C. Owrutsky, J. Chem. Phys. **118**, 7074 (2003).
7. Q. Zhong, A.P. Baronavski, and J. C. Owrutsky, J. Chem. Phys. **119**, 9171 (2003).
8. G. M. Sando, K. Dahl, J. C. Owrutsky, J. Phys. Chem. B **109**, 4084 (2005)

Vibrational energy transfer in reverse micelle molecular nanostructures

Yoonsoo Pang,[1] Zhaohui Wang,[1] John C. Deàk,[2] and Dana D. Dlott[1]
[1]School of Chemical Sciences, University of Illinois at Urbana-Champaign, Urbana, IL
[2]Deaprtment of Chemistry, University of Scranton, Scranton, PA

An IR-Raman technique with mid-IR pump and Stokes and anti-Stokes Raman probe is used to investigate energy transfer in reverse micelle molecular nanostructures and vibrational relaxation of confined water nanodroplet. Fast energy transfer between two liquid phase separated by a surfactant layer has been found and explained by the specific vibrational relaxation. Vibrational relaxation decay of "interfacial" water stretch is twice slower than bulk water due to confinement.

The micelles, consisting of nanodroplets of water surrounded by a monolayer of Aerosol OT (AOT), are suspended in carbon tetrachloride.[1,2] Water molecules confined in nanometer-scale reverse micelle have very different properties from bulk water including differences in the vibrational dynamics. The size of the reverse micelle is directly proportional to the surfactant-to-water molar ratio, w = [water] / [surfactant]. The structure and dynamics of the reverse micelles have been studied by various experiments such as light scattering, small-angle neutron scattering, FT-IR/Raman and NMR spectroscopy.[1] These "nanopools" of water, isolated and coated by surfactant molecules, can be a good model system for confined water in biological systems since their interior dimensions are similar to those of water cavities in protein, lipid bilayers, etc.[2] In this study we have shown that vibrational energy from water is transferred to the head and tail groups of surfactant molecules and further to carbon tetrachloride using ultrafast IR-Raman pump and probe experiments.[3]

Simulations and light scattering measurements of AOT/water/CCl_4 reverse micelles[1,4,5] confirm that AOT reverse micelles (w = 2) is about 35Å in mean diameter with an AOT mean aggregation number of 17 to 18, enclosing water droplets of ~35 molecules. We analyzed IR spectra of the concentration-dependent ν_{OH} line shape and found that most of the confined water was "interfacial" water bound or trapped near the AOT SO_3^- (sulfonate) head groups with w = 2 micelle, which is well explained by simulation results.[5] Interior or "bulklike" water dominates in reverse micelles with bigger w ratio.

Vibrational energy transfer

Fig. 1 shows a series of anti-Stokes Raman spectra acquired with increasing delay after 3500 cm^{-1} ν_{OH} pumping of confined water in w = 2 micelle. About 5% of the water molecules are excited[6] and IR pulse also excited the carbonyl stretching overtone $2\delta_{CO}$. The amount of $2\delta_{CO}$ excitation was small compared to the amount of ν_{OH} excitation and variation of the amount of $2\delta_{CO}$ had little effect on the vibrational energy transfer. The case of AOT ν_{CH} alkyl tail excitation is shown in the series of anti-Stokes Raman spectra in Fig. 2.

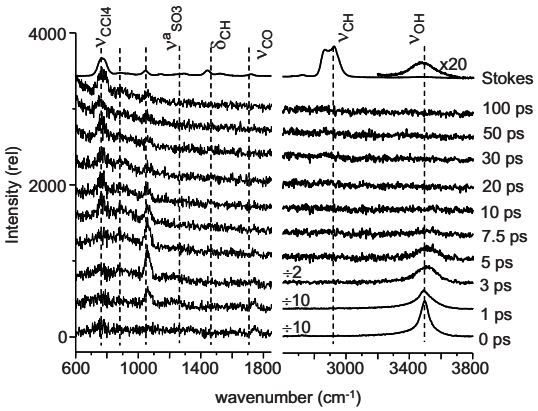

Fig. 1. Top trace: Stokes Raman spectrum of AOT micelle suspension (w =2). Lower traces: A time series of transient anti-Stokes spectra at each time delay after ν_{OH} pumping of confined water at 3500 cm^{-1}.

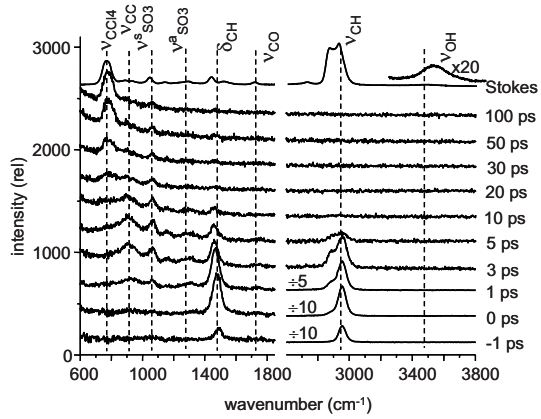

Fig. 2. Top traces: Stokes Raman spectrum of AOT micelle suspension (w = 2). Lower traces: A series of transient anti-Stokes spectra (as in Fig. 1) acquired at successively longer delay times after ν_{CH} pumping of AOT at 2950 cm^{-1}.

The ν_{OH} decays with 1.8 (±0.1) ps time constant with confined water pumping (shown in Fig. 1), more than twice the 0.75-ps lifetime of bulk water pumped at 3500 cm^{-1}.[6] This lifetime increase is due to reduced anharmonic coupling to the bath resulting from anion-induced weakening of the hydrogen bonding, that is confinement effect.[1,5,7] As energy leaves the ν_{OH} vibration, a substantial portion passes into the sym. and asym. ν_{SO3} of head group and then is transferred to ν_{CCl4} in ~10 ps.

With ν_{CH} pumping (shown in Fig. 2) the parent ν_{CH} excitations decay with 2.3 (±0.1) ps time constant. The δ_{CH} and ν_{CC} tail excitations plus just a small amount of head group stretch modes are generated with the decay of ν_{CH}. Pumping ν_{CH} of AOT leads to less head group excitation but much more AOT tail excitation than we observed after pumping the water. Pumped energy is transferred in 20-40 ps to ν_{CCl4}. This energy transfer across the surfactant layer should be understood by the specific vibrational energy relaxation pathway, where excitation of sulfonate head group of AOT is important.

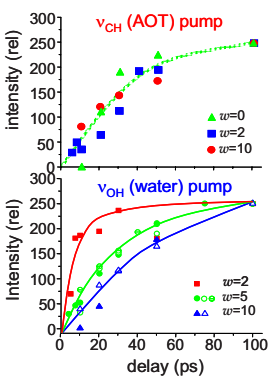

Fig. 3. Dynamics extracted from Figs. 1-2 and more micelle experiments results. Rise of the CCl_4 molecular thermometer after CH pumping of confined water and OH pumping of AOT at different micelle size. Both CCl_4 signals were normalized to the same final temperature. The lines through the data are guides to the eye.

Fig. 3 shows the energy transfer rate from water core or AOT tail to surrounding CCl_4 at different micelle size. With AOT pumping, this micelle cooling rate is almost constant upon micelle size variation. But energy transfer from confined water to CCl_4 with water pumping can be slowed down (up to 30-40 ps) by enlarging the size of reverse micelle. The fact that micelle cooling from a hot water nanodroplet is faster than that with AOT tail excitation is the direct evidence that the fast energy transfer between two liquid phases separated by a surfactant layer must be understood in terms of specific vibrational couplings, rather than ordinary heat conduction. In large micelles like w = 10, the fast energy transfer between two phases becomes inefficient so ordinary heat transfer dominates.

Seifert et al.[8] measured cooling of the confined water in AOT reverse micelle over hundreds of ps with much bigger micelles with w = 10 to 55. The dependence of heat transfer rate on micelle diameter could be explained with ordinary heat conduction theory. We here have shown that energy transfer between nanodroplet water confined reverse micelle and surrounding solvent can occur by fast vibrational energy relaxation or by ordinary heat transfer and that the micelle size is the most important factor in determining the energy transfer rate.

Vibrational relaxation of confined water

Fig. 4 shows anti-Stokes Raman spectra of two different micelles with 3600 cm^{-1} pumping. At this pump-frequency, "interfacial" water ν_{OH} is mainly excited with minor pumping of "bulklike" water stretch. With small reverse micelle where most of the water molecules are "interfacial" (w = 2 in Fig. 2(a)), only "interfacial" water stretch gets excited by pump and decays with very slow 3.4 (±0.3) ps time constant. Symmetric stretch (1050 cm^{-1}) of sulfonate group is excited with the decay of "interfacial" ν_{OH}. With a little bigger micelle (w = 5 in Fig. 2(b)), "interfacial" and "bulklike" water stretch get excited simultaneously and then decay with similar 1.5 (±0.2) ps time constant for "bulklike", and 1.7 (±0.1) ps for "interfacial". Whenever "bulklike" water stretch gets some excitation, asymmetric ν_{SO3} (1250 cm^{-1}) is excited as well as symmetric one with the decay of ν_{OH}.

"Bulklike" water can also be selectively pumped with 3300 cm^{-1} pulse but "interfacial" water stretch gets excited as well due to fast energy transfer from "bulklike" to "interfacial" water (not shown here).

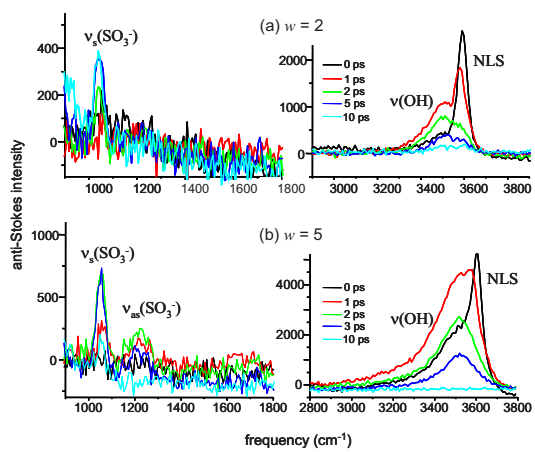

Fig. 4. Anti-Stokes spectra of (a) w = 2 and (b) w = 5 AOT reverse micelle with 3600 cm^{-1} pump at different time delays. The ν_{OH} of confined water (right) and sym./asym. ν_{SO3} of AOT (left) shows that "interface" and "bulklike" water molecules in the micelles have clearly different vibrational relaxation mechanism.

Decay of "interfacial" stretch (1.3 - 1.6 ps) is much slower than that of "bulklike" stretch at this pumping frequency. At lower frequency than 3200 cm^{-1} fast transfer from "bulklike" ν_{OH} to ν_{CH} of AOT layer also occurs, where T_1 of "bulklike" stretch is ~0.5 ps. Vibrational relaxation of confined water in this case is very complicated.

Vibrational relaxation of water molecules confined in AOT reverse micelles has been investigated by adopting pump frequencies and reverse micelle sizes. Vibrational relaxation time of "interfacial" ν_{OH} is about two times slower than that of bulk water due to confinement, but T_1 of "bulklike" water is about the same as bulk.[6] Confinement effect on vibrational relaxation time was seen only with "interfacial" stretch of water.

Conclusion

Vibrational energy transfer and vibrational relaxation of confined water in Aerosol OT reverse micelle have been studied using ultrafast IR-Raman pump-probe experiments. Vibrational energy from nanodroplet water can be transferred over the surfactant layer into surrounding solvent in 10 - 20 ps, but transfer from AOT tail to solvent takes longer (30 - 40 ps). This is due to the specific vibrational relaxation pathway of confined water in reverse micelle and cannot be explained with the ordinary heat conduction. Vibrational relaxation of confined water has been studied by changing micelle size and pumping frequency. Vibrational decay of "interfacial" ν_{OH}, bound to sulfonate head group of the surfactant, is about twice slower than that of bulk water. But decay of "bulklike" ν_{OH}, in the core of micelle, is not affected by confinement.

Acknowledgement

This work is supported by the U.S. Department of Energy, Division of Materials Sciences, under Award No. DEFG02-91ER45439, through the Frederick Seitz Materials Research Laboratory at the University of Illinois at Urbana-Champaign, by the Air Force Office of Scientific Research under contract F49620-03-1-0032, and the National Science Foundation under award number DMR-0096466.

References

[1] T. K. De and A. Maitra, Adv. Colloid Interface Sci. **59**, 95 (1995).
[2] N. E. Levinger, Science **298** (5599), 1722 (2002).
[3] J. C. Deak, Y. S. Pang, T. D. Sechler, Z. H. Wang, and D. D. Dlott, Science **306** (5695), 473 (2004).
[4] B. Derecskei, A. Derecskei-Kovacs, and Z. A. Schelly, Langmuir **15** (6), 1981 (1999).
[5] J. Faeder and B. M. Ladanyi, J. Phys. Chem. B **104** (5), 1033 (2000).
[6] A. Pakoulev, Z. H. Wang, Y. S. Pang, and D. D. Dlott, Chemical Physics Letters **380** (3-4), 404 (2003).
[7] D. S. Venables, K. Huang, and C. A. Schmuttenmaer, J. Phys. Chem. B **105** (38), 9132 (2001).
[8] T. Patzlaff, M. Janich, G. Seifert, and H. Graener, Chem. Phys. **261** (3), 381 (2000); G. Seifert, T. Patzlaff, and H. Graener, Phys. Rev. Lett. **88** (14) (2002).

TRVS XII

NIST National Institute of Standards and Technology

Washington, D.C.
May 23-27, 2005

Transient Raman

From Time-resolved Raman Spectroscopy to Time- and Space-resolved Raman Spectroscopy

Hiro-o Hamaguchi

Department of Chemistry, School of Science, The University of Tokyo, Tokyo 113-0033, Japan
Email: hhama@chem.s.u-tokyo.ac.jp

In the last two decades, time-resolved Raman spectroscopy has been developed and established. It provides us with a reliable basis for elucidating ultrafast elementary processes taking place at the molecular level. Future time-resolved Raman studies will certainly be directed to more complex molecular systems and ensembles (the left-to-right arrow in Fig. 1). It would also be interesting, however, to go directly to the extreme of large biological systems and come down to smaller systems (the right-to-left arrow in Fig. 1). We thus started Raman spectroscopy of living cells. In these studies, only modest time-resolution of second or decasecond is needed but high spatial resolution is indispensable so as to obtain non-space averaged meaningful dynamical information (termed time- and space-resolved Raman spectroscopy).

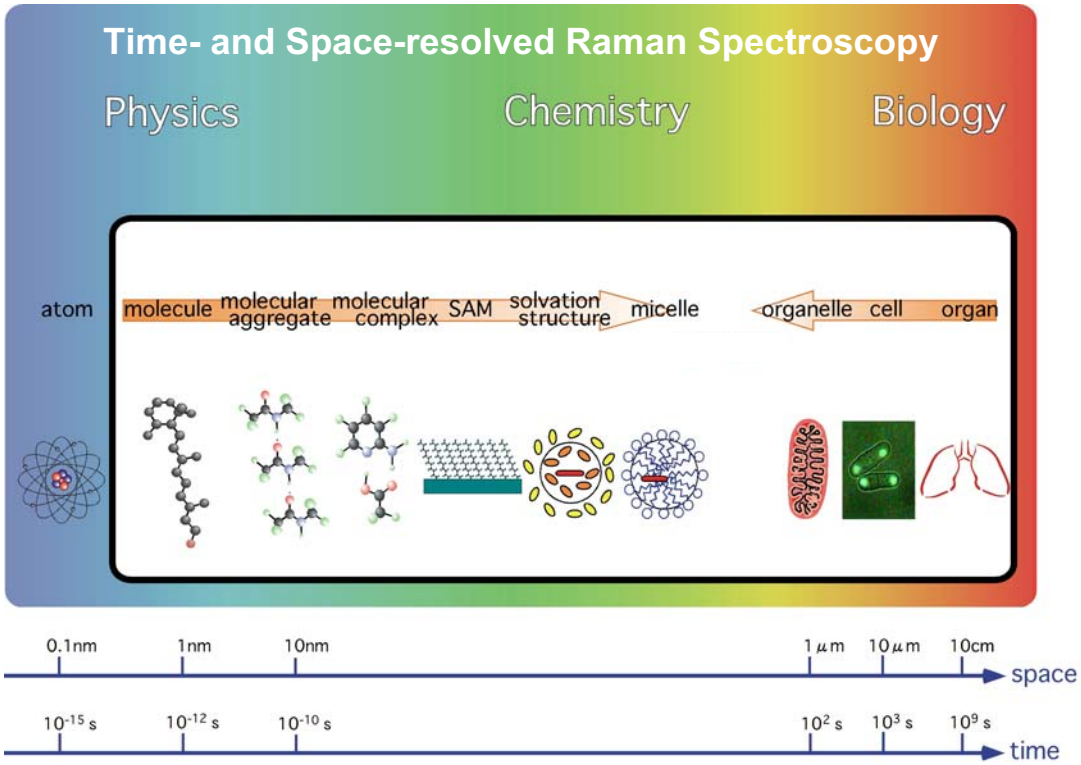

Figure 1. Time- and space-resolved Raman spectroscopy looks at molecular systems from a molecule to a living cell and a human organ.

As an example, the time- and space-resolved Raman spectra of the central part of a living cell of fission yeast, Schizosaccharomyces pombe (S. pombe) are shown in Figure 2.[1] The measurement starts from the early M phase of cell division, when the Raman spectrum is dominated by the well known protein peaks. After 9 min, the nucleus is separating and moving symmetrically toward the perimeter of the cell. At 1 hr and 13 min, strong peaks assignable to phospholipids of mitochondria appear with an unidentified strong band at 1602 cm^{-1}. At 2 hr and 19 min a primary septum forms and the spectrum is dominated by oligosaccharides peaks, which eventually change into those of polysaccharides when the septum is matured (5 hr and 54 min). As mitosis progresses, the Raman spectrum changes drastically reflecting the changes of molecular compositions of the organelle exiting at the central part of the cell. It is of interest that the band at 1602 cm^{-1}, which, as shown in the following, is a sensitive marker of the metabolic activity of mitochondria, becomes very strong during the M/G1/S periods when the cell needs a lot of chemical energy to synthesize materials for division.

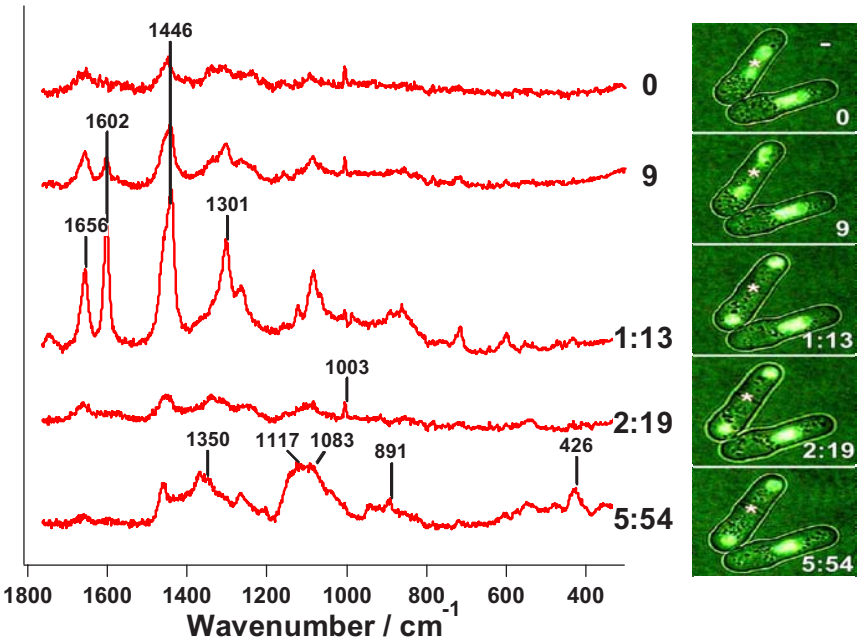

Figure 2. Time- and space-resolved Raman spectra of a dividing *S. pombe* cell.

The relationship of the 1602 cm^{-1} band with the metabolic activity of mitochondria has been examined by a respiration inhibiting experiment using KCN.[2,3] The results are shown in fig. 3. Before adding KCN, the intensity of the 1602 cm^{-1} band is comparable with that of the 1655 cm^{-1} band of phospholipids. At 3 min after adding KCN, the 1602 cm^{-1} band becomes weaker, while the other phospholipid bands remain unchanged. At 11 min and later, the 1602 cm^{-1} band becomes further weaker and, in addition, the band shapes of the 1655 cm^{-1}, 1446 cm^{-1} and 1300 cm^{-1} bands change gradually. We suspect that the intensity of the 1602 cm^{-1} band is a

measure of the respiratory activity in a mitochondrion. The gradual changes of the shapes of the phospholipid bands are thought to arise from the structural degradation of the mitochondrial membranes. The Raman spectral changes in fig.3 most probably correspond to the *early dying process* of a living yeast cell and, in this regard, we call the 1602 cm^{-1} band as "the Raman spectroscopic signature of life"

.

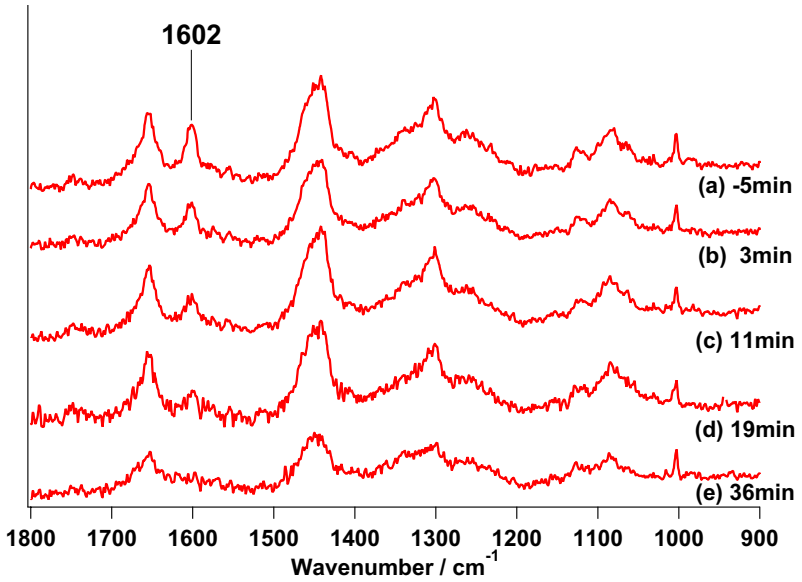

Figure 3. Time-resolved Raman spectra showing the effect of a respiration inhibitor KCN on a living *S. pombe* cell and "the Raman spectroscopic signature of life at 1602 cm^{-1}.

Thus, time- and space-resolved Raman spectroscopy has been successfully used to trace the growing and dying process of a single living cell at the molecular level.

References:

1. Y. -S. Huang, T. Karashima, M. Yamamoto and H. Hamaguchi, J. Raman Spectrosc., **34**, 1-3 (2003).
2. Y. -S. Huang, T. Karashima, M. Yamamoto, T. Ogura and H. Hamaguchi, J. Raman Spectrosc., **35**, 525-526 (2004).
3. Y. -S. Huang, T. Karashima, M. Yamamoto and H. Hamaguchi, Biochemistry, in press.

Vibrational Excitation after Ultrafast Intramolecular Proton Transfer of TINUVIN: A Picosecond Resonance Raman Study of Highly Vibrationally Excited Molecules

W. Werncke, V. Kozich, and J. Dreyer

Max-Born-Institut, Max-Born-Strasse 2A, D-12489 Berlin, Germany

werncke@mbi-berlin.de

2-(2'-hydroxy-5'-methyl-phenyl)benzotriazole (TINUVIN) is a prototypical example undergoing a complete reaction cycle of intramolecular photo-induced proton transfer within about 1 ps [1]. A prominent role of a low-frequency mode at 469 cm^{-1} in the reaction is indicated by coherent oscillations during and after the reaction cycle as well as by resonance Raman data. This mode containing a coordinate changing the O…N separation in the intramolecular hydrogen bond has been identified as a proton transfer promoting mode [1].

Femtosecond absorption measurements [1] of the enol gound state absorption line shape indicate non-equilibrium vibrational populations after the reaction up to about 10 ps followed by vibrational cooling of the thermalized molecule on a 30 ps time scale, however information about excitation and energy redistribution of distinct modes is still missing.

To get mode-specific information about vibrational excitation and energy redistribution of TINUVIN we applied time-resolved resonance Raman spectroscopy after initiating the proton transfer cycle by a picosecond UV laser pulse. For time-resolved resonance Raman spectroscopy we used a two-color 1 kHz Ti-sapphire laser system delivering picosecond pulses at 310-325 and 340-360 nm [2]. After frequency doubling of the fundamental radiation at 790 nm these pulses were generated using an optical parametic generator/amplifier followed either by frequency doubling or sum frequency generation with the 790 nm radiation. A typical cross correlation width of the near UV pulses was 1.5 ps. Pulses around 350 nm, i.e. near to the 0-0 electronic transition of TINUVIN were applied for electronic excitation, whereas the pulses around 320 nm served for anti-Stokes and Stokes resonance Raman probing, respectively.

In this study we demonstrate that for highly vibrationally excited molecules mode population can not simply be derived from anti-Stokes resonance Raman intensities because of the time-dependence of the absorption line shape resulting in dramatic changes of the resonance Raman line shape function [3,4]. Instead, avoiding its influence, information for distinct modes is derived from their time-dependent anti-Stokes to Stokes resonance Raman intensity ratios.

The kinetics of measured resonance Raman intensities of three prominent Raman lines (469, 685 and the spectrally unresolved doublet at 1435 cm^{-1}) after UV-excitation is shown below (right hand side). For the Stokes Raman intensities we observed an 5-fold decrease followed by a slow recovery within about 30 ps. Time-resolved anti-Stokes resonance Raman intensities of the three modes (plotted as differences of the intensities before and after UV-excitation) show different rise and decay times. The 1435 cm^{-1} doublet shows a fast rise of intensities close to our temporal resolution whereas the 469 and 685 cm^{-1} modes approach their maxima much slower within about 7 and 10 ps, respectively. The anti-Stokes Raman intensity of the 360 cm^{-1} mode is even decreased after excitation approaching its room temperature intensity level within about 15 ps.

Calculated

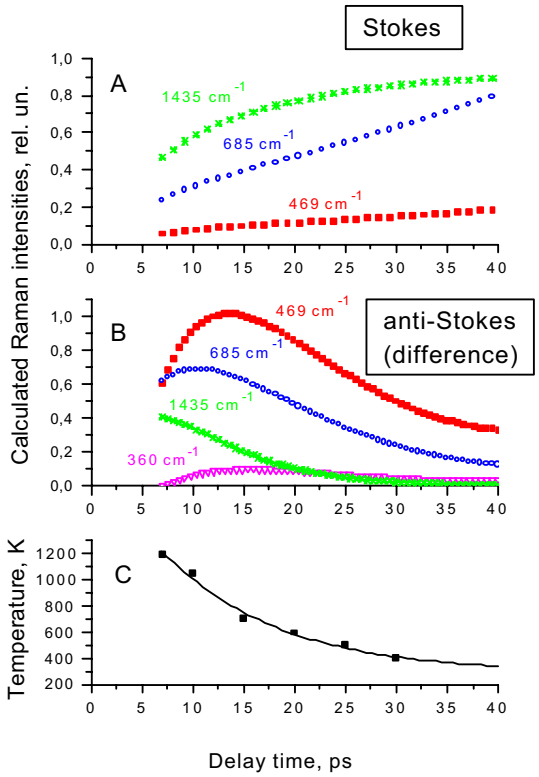

Experimental

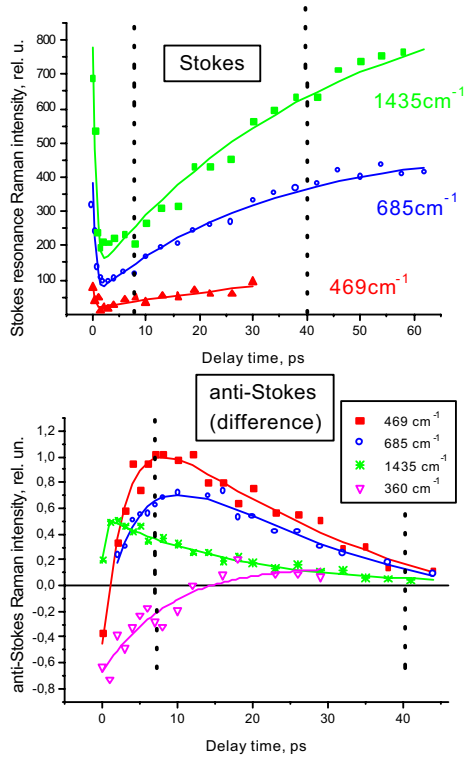

The proton transfer cycle is completed after 3 ps. The much slower recovery of Stokes resonance Raman intensities occurs on a time scale typical for vibrational cooling. Tentatively, assuming thermal equilibrium in the molecule and applying transform theory we calculated the Stokes and anti-Stokes resonance Raman kinetics from the temperature-dependence which has been determined from the measured time-dependence of the absorption band after the proton transfer cycle (left hand side) [1]. The comparison between the calculated and experimental kinetics kinetics (within the temporal range indicated by the dotted vertical lines) demonstrates that main features of the experimental curves are reproduced by these calculations [4]. These calculations show that the time-dependence of the Stokes resonance Raman intesities are mainly due to the time-dependence of the line-shape function whereas anti-Stokes resonance Raman intensities are due to the competing contributions from the line-shape function and population factor of the mode. These competing contributions lead to maxima in the anti-Stokes intensities (different for each mode) which do not coincide with the maximum of vibrational populations for the highest temperature at 7 ps. The influence of the line-shape function is more severe for low-frequency than for high-frequency modes.

To avoid the influence of the time-dependent resonance Raman line shape function, and to determine even non-thermal vibrational populations instead of using anti-Stokes Raman intensities, we characterized vibrational populations by the ratios of time-dependent anti-Stokes and Stokes resonance Raman intensities [5]. They are presented below. Excitations of the modes are expressed by "mode

temperatures" which follow from the ratios. At earlier times the ratios indicate pronounced non-thermal vibrational population distributions. For instance, 5 ps after excitation the anti-Stokes intensity ratios of the 1435 and 685 cm^{-1} modes may still correspond to the same temperature of about 1050 K. In contrast, the "mode temperature" of 2300 K of the 469 cm^{-1} mode is significantly higher than the highest possible equilibrium temperature of TINUVIN of 1200 K [1]. These findings indicate a strong excess population of the 469 cm^{-1} mode, i.e. this mode acts as an accepting mode. It modulates the O…N separation in the intramolecular hydrogen bond. Also the mode at 1435 cm^{-1} representing combined phenyl stretching and OH bending motions primarily accepts excess energy above the equilibrium level. Thermal equilibrium among the vibrations occurs on a 10-15 ps time scale.

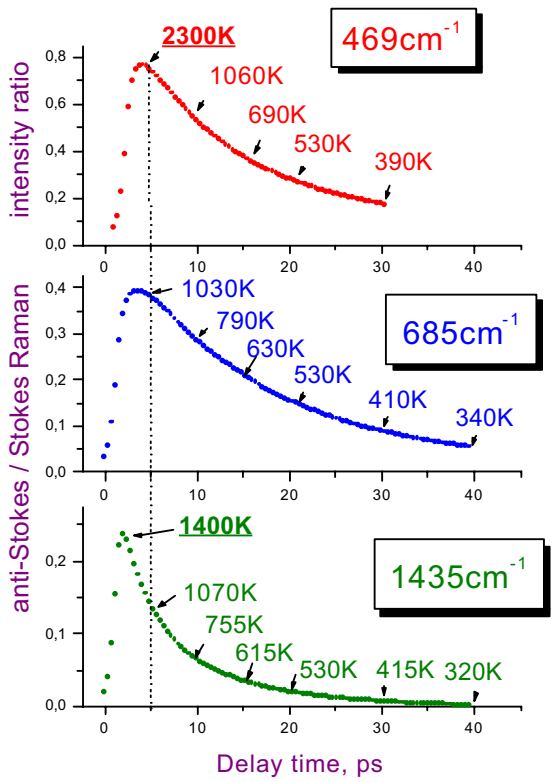

In conclusion evidence of a strong influence of the time-dependent line-shape function on the time-dependence of Stokes resonance Raman intensities after the ultrafast proton transfer cycle of TINUVIN has been obtained. It originates from the time-dependence of populations of the manifold of Franck-Condon active modes being excited due to the reaction. Their influence has to be taken into account, e.g. in deriving data of formation kinetics of "hot" products by time-resolved resonance Raman spectroscopy.

Furthermore, this influence prevents from extracting valid mode specific kinetic data directly from time-resolved anti-Stokes resonance Raman measurements of highly vibrationally excited molecules. We demonstrate, that information on vibrational temperatures or more in general, vibrational excess populations can be derived from combined anti-Stokes and Stokes resonance Raman intensity measurements.

For TINUVIN after the intramolecular proton transfer cycle we show that a low-frequency mode being coherently excited on a femtosecond time scale acts as a major accepting mode of the process.

Acknowledgements. This research was supported by the Deutsche Forschungsgemeinschaft.

References

[1] T. Elsaesser, in *Ultrafast Hydrogen Bonding Dynamics and Proton Transfer Processes in the Condensed Phase,* Edited by T. Elsaesser and H. Bakker, Kluwer Academic Publishers, Dordrecht, 119, 2002.

[2] V. Kozich, W. Werncke, A.I. Vodchits, and J. Dreyer, J. Chem. Phys. **118**, 1808, 2003.

[3] X. Ye, A. Demidov, F. Rosca, W. Wang, A. Kumar, D. Ionascu, L. Zhu, D. Barrick, d. Wharton, and P.M. Champion, J. Phys. Chem. A **107**, 8157, 2003.

[4] V. Kozich and W. Werncke, J. Mol. Struct. **735-736**, 145, 2005.

[5] V. Kozich, J. Dreyer and W. Werncke, Chem. Phys. Lett. **399**, 484, 2004.

Ultrafast nonadiabatic dynamics at conical intersections: A Resonance Raman study

Praveen D. Chowdary and S. Umapathy

Department of Inorganic & Physical Chemistry, Indian Institute of Science, Bangalore 560012, India

Conical intersections (CI's),[1] a generic class of degeneracies of adiabatic potential energy surfaces, are now being considered as the microscopic bases for ultrafast nonadiabatic (photophysical/photochemical) processes in polyatomic molecules. From a theoretical point of view, significant progress has been made of late in the location and characterization of potential energy surfaces in the vicinity of intersections. *Ab initio* calculations are increasingly being used for qualitative discussion of various photochemical pathways and calculation of optical spectra. Not surprisingly however, given the multidimensional nature of molecular potential energy surfaces, experimental probes of these intersections have been limited so far. We observe here that the Raman excitation profiles (REP's), being highly sensitive to vibronic coupling,[3] are potential tools to probe the ultrafast nonadiabatic dynamics induced by CI's of excited states.

We studied the manifestations of CI's in the REP's by extensive calculations on the prototype two state-two mode model based on harmonic diabatic potentials and linear coupling.[4] Two excited states, one bright and one dark, of different spatial symmetry are coupled by a non-totally symmetric mode while the energy gap between them is tuned by a totally symmetric mode. The Hamiltonian, describing the dynamics on coupled surfaces, is given in diabatic representation by

$$H_d = (T_N)1 + V_d = (T_N)1 + \begin{bmatrix} V_{11} & V_{12} \\ V_{21} & V_{22} \end{bmatrix} \qquad \text{Where } V_{12} = V_{21} = \lambda Q_a$$

$$T_N = -\frac{1}{2}\hbar\omega_s \frac{\partial^2}{\partial Q_s^2} - \frac{1}{2}\hbar\omega_a \frac{\partial^2}{\partial Q_a^2}$$ is the diagonal nuclear kinetic energy operator and λ is the coupling strength. Since the question being addressed here is the observability of conical intersection in the REP's, an optically bright state coupled to a dark state with well-separated vertical excitation energy is chosen, where this is not obvious. For a fixed displacement of state 2 the displacement of state 1 is varied along with coupling strength to get intersections of varied accessibility and topography. Time dependent theory for vibronically coupled states is used for calculation and analysis of REP's and the wave packet dynamics on coupled surfaces is tracked by the split operator technique modified accordingly. Exact REP's, of relevant quantum transitions of the two modes, are compared with those calculated within adiabatic approximation and with those of uncoupled diabatic states to identify the nonadiabtic effects.

Model I: Intersection at the classical turning point opposite to Franck-Condon zone

Notable of the spectral features in the REP of tuning mode, caused by coupling, are the loss of intensity and splitting of peaks. The splitting however cannot be resolved when the damping factor is large but the intensity loss can be observed. The strength of

these effects depends crucially on λ. Increasing values of λ perturb the profiles to such an extent that identification in terms of uncoupled states becomes difficult. Similar effects are seen in the absorption spectrum but a significant difference is that while the peaks near and above the intersection in absorption spectrum are split and broadened, there occurs a loss in intensity for the same energies in the excitation profile. The REP calculated within adiabatic approximation matches well with the exact REP at lower energies but fails to explain the energy dependent peak splitting and loss of intensity (near and above the energy of intersection), which evidently are due to profound non-adiabatic effects. The coupling induced damping of autocorrelation function broadens absorption spectra but by virtue of appearing at amplitude level for the Raman process, causes the reduction of Raman intensities.

A variety of other models have been studied with varying topography and accessibility of intersections and the REP's, depending on the value of λ, are highly sensitive to the nonadiabatic effects.[5] Simulations on pyrazine and trans-azobenzene (TAB) ascertain the practical feasibility of extending this study to polyatomic systems. REP's of pyrazine (fig 1), with an intersection at the minimum of upper diabatic sate, are calculated using the well-studied two state-three mode model.[6] The extreme sensitivity of the profiles to the coupling is obvious. In this case the coupling affects the REP's at all energies because of the location of intersection at the minimum of state 2.

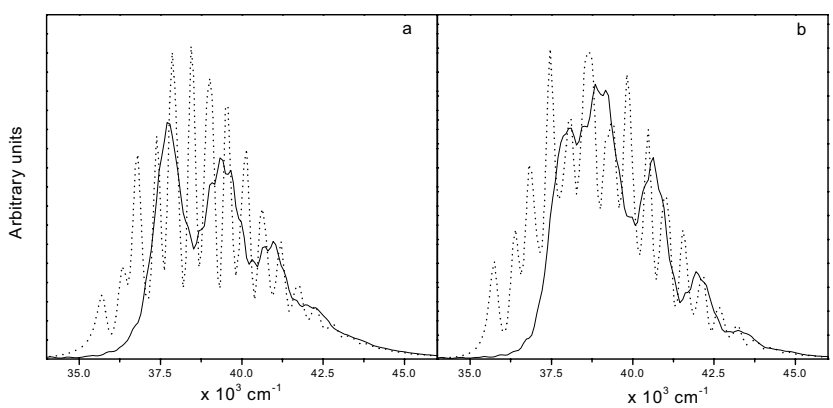

Fig 1: Exact and diabatic (λ = 0) excitation profiles of the tuning modes of pyrazine, which has a conical intersection at the minimum of state 2, calculated by the three mode model with parameters from ref 6. (a) fundamental (597 cm^{-1} mode) (b) Combination profile of the fundamentals of the tuning modes. Exact profiles are shown in solid and diabatic profiles in dots.

S_1-S_2 conical intersection in trans-azobenzene (TAB):

The purpose of studying TAB has been twofold where in lies our other objective which is to understand the ultrafast dynamics and photochemistry of π-π* excited TAB. While this serves as a case study demonstrating the applicability of REP analysis to the modeling of CI's, it also specifically addresses the suspected involvement of a CI in the relaxation of π-π* excited TAB.[7] The excited state structure and dynamics of TAB are extracted by modeling the Raman excitation profiles (REP's) of the S_1 and S_2 states and the absorption spectrum of TAB by Heller's time dependent formalism. Based on the

potential parameters in S_1 two extremes of coupling are identified, a strong coupling extreme with an accessible intersection (model I) and a weak coupling extreme with a remote intersection. Using a three mode-two state model with two tuning modes and an effective coupling coordinate[8] we fit the vibronically borrowed intensity of S_1 absorption to estimate λ. The potential parameters of S_2 are varied to give the best fit to experimental REP's of S_2 (fig 2). The results indicate that the intersection is remote and not directly accessible within electronic dephasing time to cause significant population decay from S_2. A detailed discussion of the modeling is to be published elsewhere.[9]

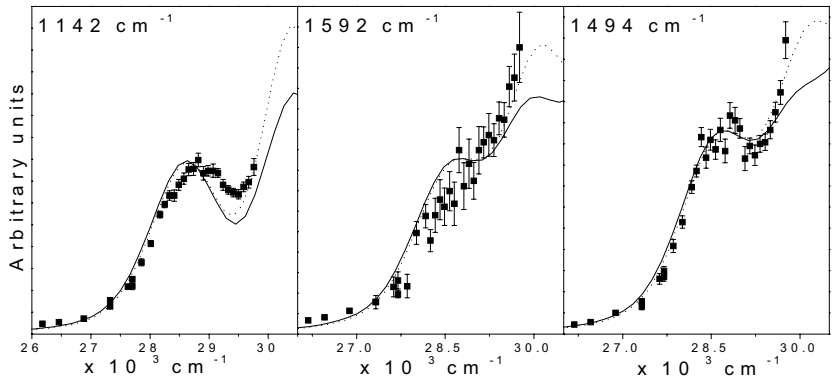

Fig 2: Raman excitation profiles on resonance with S_2 state of TAB for remote (dotted) and accessible (solid) intersections.

Conclusions:

This study demonstrates that the analysis of REP's provides a crucial test of parameters in the theoretical modeling of nonadiabatic dynamics. Many of the ultrafast processes ascribed to conical intersections that occur within electronic dephasing times are amenable to such an analysis.

References:

1. D. R. Yarkony, Acc. Chem. Res. **31**, 511 (1998)
2. H. Köppel, W. Domcke and L.S. Cederbaum, Adv. Chem. Phys. **57**, 59 (1984).
3. W. Siebrand and M. Z. Zgierski, in Excited states, vol **4**, ed. E.C. Lim (Academic, NY, 1979), p.1.
4. W. Domcke and G. Stock, Adv. Chem. Phys. **100**, 1 (1997).
5. P. D. Chowdary and S. Umapathy, *to be published.*
6. R. Schneider and W. Domcke, Chem. Phys. Lett. **150**, 235 (1988).
7. T. Schultz, J. Quenneville, B. Levine, A. Toniolo, T.J. Martinez, S. Lochbrunner, M. Schmitt, J.P. Shaffer, M.Z. Zgierski, and A. Stolow, J. Am. Chem. Soc. **125**, 8098 (2003).
8. P. Cattaneo and M. Persico, J. Phys. Chem. A. **101**, 3454 (1997).
9. P. D. Chowdary and S. Umapathy, *to be published.*

Direct Study of Vibrational Dynamics in Hemes using Ultrafast Time-resolved Stokes and Anti-Stokes Raman Scattering and Transient Absorption Spectroscopy.

M. Cather Simpson, J. Reddy Challa, T. Gunaratne

Center for Chemical Dynamics
Department of Chemistry
Case Western Reserve University
Cleveland, OH 44106-7078
mcs9@case.edu
http://www.cwru.edu/artsci/chem/faculty/simpson/

The prevalence of hemes in biological systems and their increasing potential in practical applications makes understanding heme photodynamics essential. Despite active research by a number of groups, a picture of the electronic and vibrational behavior of photoexcited hemes has still not converged to a single model, though there is some consensus. Photoexcitation into the Soret (π-π^*) transition leads to rapid internal conversion (IC) through the singlet manifold that deposits a large excess of vibrational energy in the ground state. The vibrational tiers of these electronic states, both ground and excited, are important contributors to the fast behavior observed. Our studies are designed to develop hitherto unknown answers to important questions surrounding these electronic and vibrational dynamics, and their potential impact upon molecular function. The new ultrafast vibrational dynamics reported here for 5-coordinate, Fe^{II} heme explore the interplay between temporally overlapping intramolecular vibrational energy redistribution (IVR) and intermolecular vibrational energy relaxation (VER), and examine the effects of the details of the excited state preparation process upon subsequent dynamical heme behavior.

The studies discussed here focus upon Fe^{II} octaethylporphyrin – 2-methyl imidazole (FeOEP-2MeIm). This model system is ideal for this purpose; it undergoes the appropriate fast electronic dynamics, is soluble in a range of solvents, is hardy in the laser beam, and fast dynamical studies of this system have direct biological and technological value. Sub-picosecond, time-resolved, resonance Raman spectroscopy (Stokes and anti-Stokes) and transient absorption (TA) [1] spectroscopy have been used to probe both the electronic and vibrational dynamics. In addition to the heme photophysical findings, these studies confirm that in order to truly understand the dynamics of complex systems, one must perform such complementary methods in tandem.

The TA measurements used a 50 fs pump at 400 nm and white-light continuum probe. Figure 1 shows a selected kinetic trace for λ = 426 nm, the peak value for the intense Soret ground state spectrum, chosen in an attempt to highlight electronic dynamics by minimizing the contribution from broadening that is traditionally associated with vibrational dynamics. The bleach recovery fits two time constants, 550 fs and 2.2 ps. The fast component dominates (86%) and is assigned to the recovery of the ground electronic state, consistent with recent findings from other groups.[2, 3] The 2.2 ps decay is assigned to IVR and VER associated with the ground state.

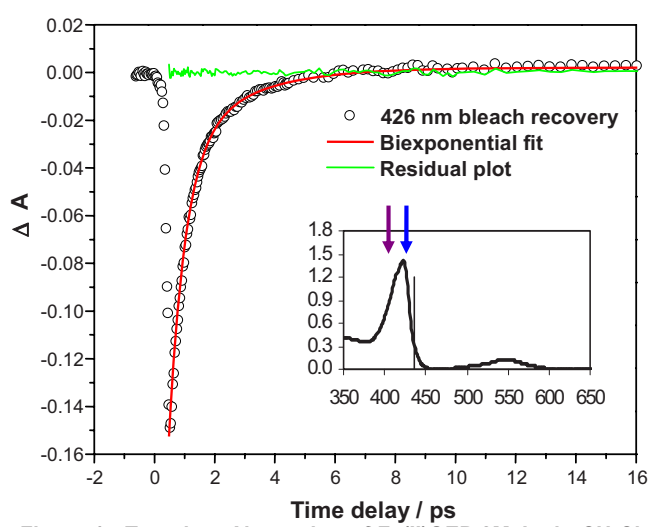

Figure 1. Transient Absorption of Fe(II)OEP-2MeIm in CH_2Cl_2. Inset = UV/Vis absorption spectrum. Purple arrow = excitation wavelength (405 nm); Blue arrow = probe wavelength (426 nm). Bi-exponential fit: A_1 = 0.86, τ_1 = 550 fs; A_2 = 0.14, τ_2 = 2.2 ps.

One-color time-resolved resonance Raman Stokes (TR^3_S) and anti-Stokes (TR^3_{AS}) spectra are consistent with the TA findings (Figure 2, Figure 3). Sub-picosecond IC, observed in the rise-time of the TR^3_{AS} spectra, generates a vibrationally excited ground state whose decay can be observed in both the Stokes bleach recovery and the anti-Stokes excited vibrational state decay. In Figure 2, the behavior of the ν_4 and ν_7 modes, at 1360 and 670 cm^{-1} respectively, shows a 1-2 ps component and a longer lived 8.5 ps component. At this point, a tentative assignment of fast IVR and somewhat slower VER is consistent with all

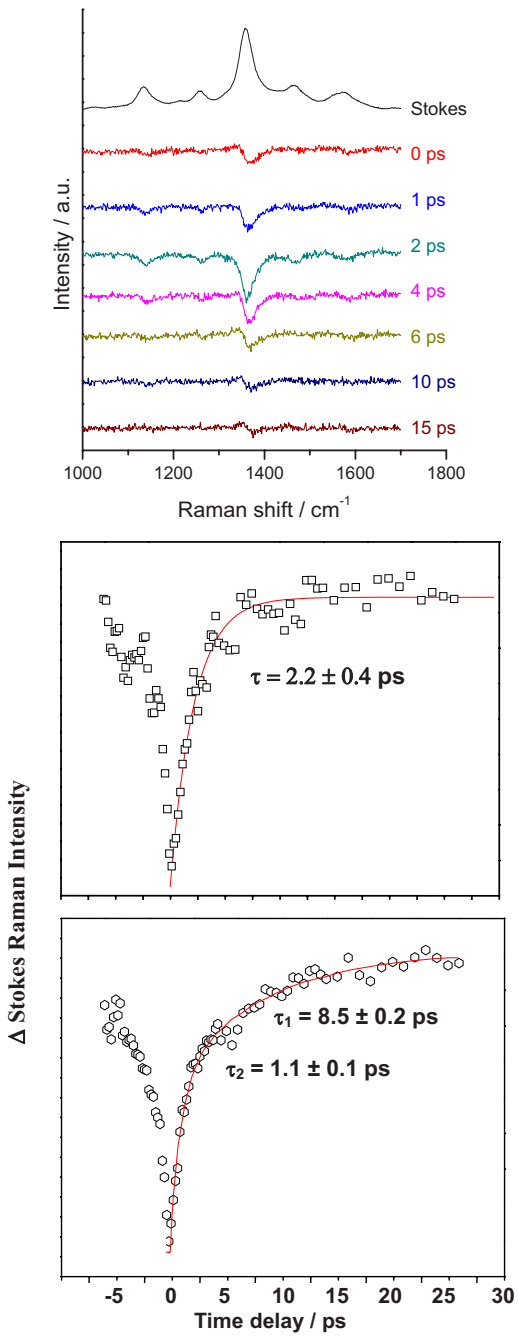

Figure 2. TR^3_S Spectroscopy. $\lambda_{pump} = \lambda_{probe} = 405$ nm; 600 fs pulses. Top panel: difference Stokes spectra = pump + probe – (pump only + probe only). Middle panel: ν_4 dynamics (1360 cm^{-1}); Bottom panel: ν_7 dynamics (670 cm^{-1}).

of the data. In particular, previous ns transient resonance Raman spectroscopy indicated that ν_4 has a longer lifetime than does ν_7, and that ν_7 appears to communicate effectively with the bath [4 and refs therein].

The TR^3_{AS} spectra (Figure 3) show several modes that appear and decay with characteristic time constants: ν_4 (1360 cm^{-1}), ν_2 (1565 cm^{-1}), and ν_5 (1135 cm^{-1}). Under the excitation conditions employed, ν_7 (670 cm^{-1}) is obscured by the solvent anti-Stokes band. The ν_4 and ν_5 modes decayed with lifetimes of 2.6 and 2.8 ± 0.2 ps, respectively; ν_2 decayed more rapidly (1.6 ± 0.2 ps). The rise-times of these anti-Stokes signals (650-750 fs) agrees with the TA dynamics (550 fs) assigned to electronic decay. Intuitively, anti-Stokes scattering in resonance with the Soret π-π^* transition should not be observed until repopulation of the ground state occurs, and this is what is observed. However, one puzzling feature of the TR^3_S spectra is the absence of a ~550 fs component associated with ground electronic state recovery observed in the TA experiments. Current efforts focus upon untangling the fairly complex influence of the evolving UV/Vis absorption intensity and lineshape upon the resonance Raman Stokes and anti-Stokes intensities. The complementary findings are summarized in Figure 4.

In order to examine the dependence of the vibrational dynamics upon the nature of the initial electronic excited state, and the dynamics thereon, these FeOEP-2MeIm results can be compared to studies in which the vibrationally excited, five-coordinate, ground electronic state is generated by photolysis from a six-coordinate heme. The fast phase of the photoresponse of chemically prepared, five-coordinate, high-spin hemes should differ significantly from that of six-coordinate, low-spin hemes, even though the latter experiments probe the transient, vibrationally excited, five-coordinate, high-spin heme created by the photolysis event. In particular, photolysis must be followed by a rapid iron spin-state change and movement of the iron out of the heme plane; this does not occur in chemically prepared five-coordinate systems. This difference should be reflected in the normal coordinates that facilitate IC and/or accept excitation energy to appear in the anti-Stokes spectra.

Indeed, our initial studies reported here seem to have successfully probed this difference. In particular, CO-photolysis from CO-myoglobin deposits significant excess vibrational energy in the ν_3 band [5, 6] but not in the ν_2 vibration. In contrast, the ν_2 mode is significantly excited in the five-coordinate studies reported here, in which ν_3 is silent. This difference agrees quite well with physical intuition. The ν_2 mode is comprised largely of C_β-C_β stretching motion at the back of the pyrrole rings while ν_3 is a C_α-C_m mode. Movement of the iron from in-plane to out-of-plane will have a major impact upon the bridging carbon network (C_α-C_m bonds), but should have little effect upon the relatively isolated bonds within the pyrrole rings. In the FeOEP-2MeIm experiment, the macrocycle does

not need to contract via the bridging network, as the iron starts in a domed-position. In this molecule, the excess energy apparently localizes in the pyrrole rings more effectively. One interesting observation is that the intense breathing mode ν_4 appears in both types of experiments. Further investigation of the mode-selective behavior is underway. In particular, what we are learning about heme photophysical dynamics is being applied to the development of new, potentially very powerful phototherapeutic systems that rely upon the rapid conversion of energy from a visible photon into focused vibrational energy – molecular scale heat – flow.

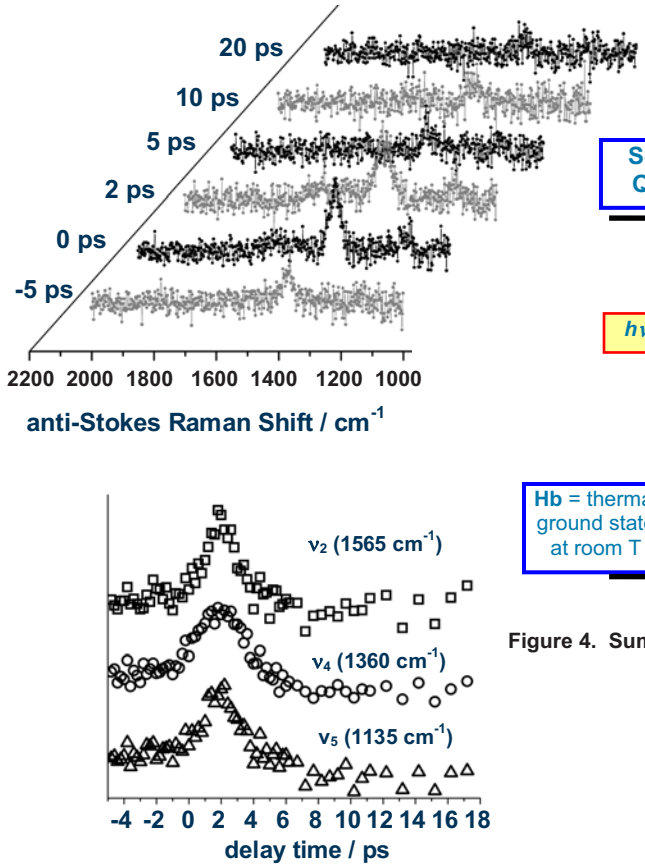

Figure 3. TR^3_{AS} Spectroscopy. $\lambda_{pump} = \lambda_{probe}$ = 413 nm; 750 fs pulses. Top panel. difference anti-Stokes spectra = pump + probe – (pump only + probe only). Bottom panel: dynamic traces for ν_2 (1565 cm^{-1}), ν_4 (1360 cm^{-1}) and ν_5 (1135 cm^{-1}) from top to bottom. Data deconvolutions using a Gaussian pulse envelope of 750 fs and a bi-exponential function yielded rise times of 650 fs (ν_2) and 750 fs (ν_4 and ν_5) and decay times of 1.6 ± 0.2 ps (ν_2), 2.6 ± 0.2 ps (ν_4) and 2.8 ± 0.2 ps (ν_5).

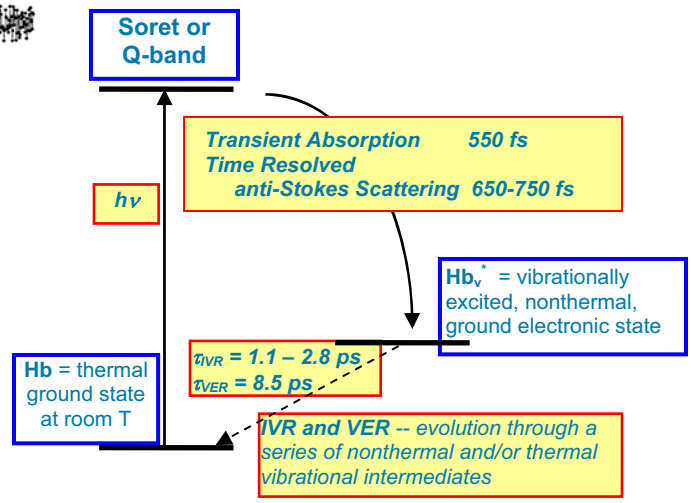

Figure 4. Summary of Heme Photophysics. see text for details.

References cited.

1. Performed at the Ohio Laboratory for Kinetic Spectrometry, Bowling Green State U. (www.bgsu.edu/departments/chem/cks/labprofile.htm)
2. X. Ye, A. Demidov, F. Rosca, W. Wang, A. Kumar, D. Ionascu, L. Zhu, D. Barrick, D. Wharton and P. M. Champion, "Investigations of Heme Protein Absorption Line Shapes, Vibrational Relaxation, and Resonance Raman Scattering on Ultrafast Time Scales." J. Phys. Chem. A **107**, 8156-8165 (2003).
3. Y. Kholodenko, M. Volk, E. Gooding and R. M. Hochstrasser, "Energy Dissipation and Relaxation Processes in deoxy Myoglobin after Photoexcitation in the Soret Region." Chem. Phys. **259**, 71-87 (2000).
4. J. J. Loparo, C. M. Cheatum, M. R. Ondrias and M. C. Simpson, "Transient Raman observations of heme vibrational dynamics in five-coordinate iron porphyrins." Chemical Physics **286**, 353-374 (2003).
5. Y. Mizutani and T. Kitagawa, "Direct Observation of Cooling of Heme Upon Photodissociation of Carbonmonoxy Myoglobin." Science **278**, 443-446 (1997).
6. Y. Mizutani and T. Kitagawa, "Ultrafast Dynamics of Myoglobin Probed by Time-Resolved Resonance Raman Spectroscopy." Chemical Record **1**, 258-275 (2001).

Anti-Stokes Resonance Raman Evidence for Energy Funneling of IR Photons Captured by Dendritic Antennae on Iron(III)-Porphyrin Complexes with a Poly(aryl ether) Dendrimer Framework

Teizo Kitagawa,[1*] Yu-Jun Mo,[1,†] Dong–Lin Jiang,[2] Makoto Uyemura,[2] and Takuzo Aida[2]

[1]*Okazaki Institute for Integrative Bioscience, National Institutes of Natural Sciences, Myodaiji, Okazaki 444-8787, Japan.* e-mail: teizo@ims.ac.jp

[2]*Department of Chemistry and Biotechnology, School of Engineering, The University of Tokyo, Hongo, Bunkyo-ku, Tokyo 113-8656, Japan.*

[†]Present address: Physics Department, Henan University, Kaifeng 475001, China. e-mail: yujunmo@henu.edu.cn

Abstract: A series of poly(aryl ether) dendrimer chloro-iron(III)porphyrin complexes (L_nTPP)Fe(III)Cl (number of aryl layers [*n*] = 3 to 5) were synthesized and their Boltzman temperatures under IR irradiation were evaluated by ratios of Stokes to anti-Stokes intensities of resonance Raman bands. While the Boltzman temperature of neat solvent was unaltered by IR irradiation, (L_nTPP)Fe(III)Cl (*n*= 3-5) all showed a temperature rise that was larger than that of the solvent and greater as the dendrimer framework was larger. Among vibrational modes of the metalloporphyrin core, the temperature rise of an axial Fe–Cl stretching mode at 355 cm^{-1} was larger than that for a porphyrin in–plane mode at 390 cm^{-1}. Although the most of IR energy is captured by the phenyl ν_8 mode at 1597 cm^{-1} of the antenna, an anti-Stokes Raman band of the phenyl ν_8 mode was not detected, suggesting the extremely fast vibrational relaxation of the phenyl vibrations. From these observations, it is proposed that the energy of IR photons captured by the aryl dendrimer framework is transferred to the axial Fe-Cl bond of ironporphyrin core and then relaxed to the porphyrin macrocycle. Details of the results will be published, separately (Mo, et al., J. Am. Chem. Soc. in press, 2005).

Experiments The resonance Raman spectra of (L_nTPP)Fe(III)Cl were observed for dioxane solution using a spinning cell and CW excitation at 413.1 nm. The IR illumination intensity was varied by changing the input voltage to IR source. The Fe-Cl stretching band was assigned on the basis of comparison of the spectra of (TPP)FeCl and (TPP)FeBr prepared separately. Raman intensities were determined with Grams/32 Version 4.14' (Galactic Industries Corp.) for the Fe-Cl stretching band at 355 cm^{-1}, a porphyrin in-plane band at 390 cm^{-1} and a solvent band at 835 cm^{-1} for the Stokes and anti-Stokes simultaneously measured spectra.

Method of analysis The ratio of Stokes (I_S) to anti-Stokes (I_{AS}) Raman intensities for a nondegenerate vibrational mode (ν_i) in a thermal equilibrium at a particular absolute temperature (T), can be represented by the following equation:[13]

$$I_S/I_{AS} = [(\nu_0 - \nu_i)/(\nu_0 + \nu_i)]^3 \exp(h\nu_i/kT) \qquad (1)$$

where ν_0 is the frequency of Raman excitation light, $\nu_0 - \nu_i$ and $\nu_0 + \nu_i$ are the absolute frequencies of Stokes and anti-Stokes Raman bands, respectively, and *h* and *k* are Planck's and Boltzmann's constants, respectively. In the physical sense, the intensity ratio of Stokes to anti-Stokes Raman bands depends only on the population ratio of the vibrationally excited to the ground levels. If thermal

equilibrium has not been established, vibrational populations among different modes cannot be determined with this equation. However, even in such a case, the vibrational temperature of a given mode can be defined by Eq.(1), and, therefore, we estimated the cooling of photoexcited metalloporphyrin successfully from the temporal dependence of the anti-Stokes Raman intensities. For the sake of convenience, we call such a temperature the Boltzmann temperature, because it may differ from the macroscopic temperature. Accordingly, the Boltzmann temperature (T_w) is defined for each vibrational mode, where w denotes a vibrational frequency (ν_i) and can be obtained experimentally from the I_S/I_{AS} measurement as follows:

$$T_w = (h\nu_i/k)/\ln[(\nu_0 + \nu_i)^3 I_S/(\nu_0 - \nu_i)^3 I_{AS}] \qquad (2)$$

Although the vibrational mode dependence would not be large in the measurements using a continuous wave (CW) laser due to rapid vibrational relaxation, some trends are expected to appear if the Fe–Cl bond is specifically heated.

In the case of nonresonance Raman scattering, absorption for scattered light is negligible and accordingly, the observed intensities would correspond to true intensities. In the case of resonance Raman scattering, however, the absorption of scattered light by the solution is different at $\nu_0 + \nu$ and $\nu_0 - \nu$ in the envelope of absorption band of the solution. This effect is larger as the separation between $\nu_0 + \nu$ and $\nu_0 - \nu$ becomes larger and thus depends on vibrational frequency ν. Furthermore, the scattering cross sections under resonance conditions at an excitation frequency ν_0 for Stokes and anti-Stokes Raman scattering are, strictly speaking, different (difference in E_i in the denominaor of the scattering cross section). To reduce such effects, we selected smaller values of ν among many Raman bands and two different modes whose ν were close to each other. Since amounts of real absorption for the excitation light and the scattered light by the sample solution depend on the optical pass length through the solution (a distance between the cell surface and scattering point) in each measurement and thus on the geometrical arrangement of the cell, quantitative estimation of these terms is difficult. However, to precisely determine the Boltzmann temperature from the I_S/I_{AS} ratio, such effects should be corrected experimentally as much as possible.

These effects would be same at different temperatures for a given optical setting of the sample and for a given vibrational mode. To circumvent these problems, we tried to incorporate these effects into I_S/I_{AS} using a correction factor. The basic assumption is that the experimental I_S/I_{AS} can be represented by the true $(I_S/I_{AS})_{true}$ multiplied with a correction factor, $C_i \times (I_S/I_{AS})_{true}$. The value of C_i depends on vibrational mode and scattering geometry but not on temperature (applied voltage for IR irradiation). In other words, C_i is specific to a given experimental geometry and concentrations of sample, and therefore can be used for all temperatures under the same scattering geometry when once C_i is determined at a certain temperature. The true value, $(I_S/I_{AS})_{true}$ would be obtainable for ideal experimental values of I_S and I_{AS} and therefore should be same as the value obtained from Eq. (1) when $T = T_0$ and $\nu = \nu_i$.

We determined the value of C_i using the experimental value of I_S/I_{AS} [$= (I_S/I_{AS})_0$] obtained from each Raman measurement of (L_nTPP)Fe(III)Cl at room temperature without IR irradiation and the ideal true value, $(I_S/I_{AS})_{true}$, calculated from Eq. (1) with ν_i and T_0. Accordingly, C_i was determined for each ν_i:

$$C_i = (I_S/I_{AS})_0/(I_S/I_{AS})_{true} \qquad (3)$$

In the practical measurements under IR irradiation, we represent that the true value of I_S/I_{AS} is $(I_S/I_{AS})_T$ and experimentally obtained value of I_S/I_{AS} is $(I_S/I_{AS})_{obs}$. Then, $(I_S/I_{AS})_T$ was obtained from $(I_S/I_{AS})_{obs}$ using the following equation for three kinds of ν_i.

$$(I_S/I_{AS})_T = (I_S/I_{AS})_{obs}/C_i \qquad (4)$$

Results

The temperature of solvent is represented as T_{835}, and the temperatures of solute are represented as difference with regard to that of solvent; the temperatures of the Fe-Cl stretching and porphyrin in-plane

modes are represented as ΔT_{355} (= $T_{355} - T_{835}$) and ΔT_{390} (= $T_{390} - T_{835}$), respectively. The experimental results are summarized in the following way;

1) All of the ΔT_{355} and ΔT_{390} values are positive, suggesting that the Boltzmann temperatures of the solute (T_{390} and T_{355}) are higher than that of the solvent (T_{835}).
2) The ΔT_{355} and ΔT_{390} values show a weak but clear tendency to increase with the voltage applied to the IR source.
3) At a designated voltage applied to the IR source, the ΔT_{355} and ΔT_{390} values increase with the number of the aryl ether layers (*n*) of the dendrimer framework.
4) For each dendrimer chloroiron(III) porphyrin complex, the temperature rise for the Fe–Cl stretching mode is always higher than that for the porphyrin ν_8 mode ($\Delta T_{355} > \Delta T_{390}$), regardless of whether it is measured in the presence or absence of the IR band-pass filter.
5) The difference between ΔT_{355} and ΔT_{390} enlarges when the generation of the dendrimer framework is increased.
6) The ΔT_{355} and ΔT_{390} values in the presence of the band-pass filter are smaller than those evaluated in the absence of the filter. However, the proportion of reduction is compatible with the idea that IR energy is primarily captured by the aryl ν_8 vibration of the dendrimer framework as discussed below quantitatively.

Interestingly, both ΔT_{355} and ΔT_{390} are positive, meaning that the observed temperature changes are caused by some systematic process, and the ΔT_{355} thus obtained is still larger than ΔT_{390} (7.5 *vs.* 3.8 K in the presence of the IR filter and 11.5 *vs.* 5.7 K in the absence of the IR filter). The proportion of reduction of ΔT by the IR filter is 65% (= 7.5/11.5) and 67% (= 3.8/5.7) for the 355 and 390 cm^{-1} bands, respectively. These values happen to be very close to the value of transmittance of the IR filter at 1597 cm^{-1} (70.05%). Since the ν_8 IR absorption of the dendrimer framework has some width and the transmittance of the filter changes with the frequency, the precise estimation of the expected value is not straightforward. However, it can be concluded that other dendrimer modes (such as CH_2-O str. at 1155 cm^{-1}) do not play a larger role in the heating. If the CH_2-O mode were involved, the measurements with the filter should include the contribution of removing this large absorber, and thus the ΔT change should be much greater than 65%. Consequently, the present observations strongly suggest that IR energy contributing to temperature rise of the core porphyrin are mainly captured by the ν_8 mode of the dendrimer faramework. Such a trend is observed for all members of the (L_nTPP)Fe(III)Cl family.

Acknowledgments

The authors wish to thank Prof. Hiroshi Fujii of the Okazaki Institute for Integrative Bioscience, Japan for his help in the preparation of (TPP)Fe(III)Br, and Dr. Hirotsugu Hiramatsu of this laboratory for determination of transmittance spectrum of the IR filter. This work was supported by a Grant-in-Aid for Specifically Promoted Research from the Ministry of Education, Culture, Sports, Science, and Technology, Japan to T.K. (14001004).

Resonance Raman characterization of the lowest excited ππ* state of methyl viologen

Guy buntinx, Olivier Poizat, Christine Lapouge

Laboratoire de Spectrochimie Infrarouge et Raman (LASIR), UMR 8516 CNRS/USTL, Centre d'Etudes et de Recherches Lasers et Applications, FR 2416 CNRS, Bâtiment C5, Université des Sciences et Technologies de Lille, 59655 Villeneuve d'Ascq cedex, France.
Phone : 33 3 20 43 40 85, Fax : 33 3 20 33 63 54, buntinx@univ-lille1.fr.

The reaction of photoreduction of the methyl viologen dication (MV^{2+}) into its radical cation ($MV^{+\cdot}$) is of considerable interest because the strong reductant character of this radical allows attractive applications in domains such as herbicinal activity and solar energy conversion. This reaction can occur by direct excitation within charge transfer transitions in MV^{2+}/X^- and $MV^{2+}/(X^-)_2$ complexes pre-existing in solution in the presence of an excess of halide ions X^- [1, 2]. It can also arise by diffusional quenching of the ππ* S_1 state of MV^{2+} by methanol or halide ions via electron transfer [3, 4]. The S_1 state of MV^{2+} is efficiently quenched by water as well but this nonradiative decay process does not yield the $MV^{+\cdot}$ product and is still unexplained [4]. Accordingly, much shorter S_1 lifetime are observed in water (3.1 ps) and methanol (<180 fs) than in acetonitrile (1 ns). The quenching mechanism in solution is thus complex and highly solvent-dependent and remains unclear in many aspects. The structural, electronic and optical characteristics of the $MV^{+\cdot}$ radical have been extensively studied by UV-visible absorption, ESR, Raman and surface enhanced Raman spectroscopy. However, almost nothing is known about the precursor S_1 (ππ*) state. Recently, Kohler and co-workers characterized the S_1 state absorption and emission spectra and dynamics of MV^{2+} in polar solvents [4]. The $S_1 \rightarrow S_n$ absorption spectrum of MV^{2+} appears quite similar to that of $MV^{+\cdot}$, with two bands around 390 and 630 nm.

We present here a first vibrational identification of the S_1 (ππ*) state of MV^{2+} by picosecond time-resolved Raman spectroscopy. The excited state was probed at two different wavelengths, 380 and 752 nm (i.e., in resonance with the two $S_1 \rightarrow S_n$ absorption bands), 1 ps following excitation at 253 and 250.7 nm, respectively, of the dichloride MV^{2+} salt (10^{-3} M) in water (this solvent was chosen to minimize the fluorescence emission). The salt being entirely dissociated in water, diffusional quenching by the chloride ions cannot occur during the 3.1 ps lifetime of S_1. Three isotopomers were investigated, the fully hydrogenated (MV^{2+}-*h*), ring deuterated (MV^{2+}-d_8), and methyl-deuterated (MV^{2+}-d_6) species. For a more comprehensive vibrational analysis, the S_1 state spectra of the isoelectronic 4,4'-bipyridinium analogues (fully hydrogenated $44BPYH_2^{2+}$-*h*, ring-deuterated $44BPYH_2^{2+}$-d_8, and N-deuterated $44BPYD_2^{2+}$ species) produced upon excitation of 4,4'-bipyridine in acidic aqueous solution (pH 1), were also recorded. The pump and probe pulses (magic angle polarization arrangement) were provided by a 1 kHz Ti-Sapphire laser system (Coherent MIRA 900D oscillator + BM Industries ALFA 1000 regenerative amplifier) set in a picosecond configuration.

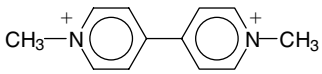

MV^{2+}

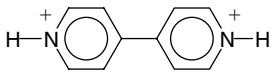

$44BPYH_2^{2+}$

Figure 1 presents the time-resolved resonance Raman spectra of the excited S_1 state of the MV^{2+} isotopomers probed in water at 752 nm. These spectra are entirely extinguished at a time delay of 10 ps, in agreement with the fast decay previously reported for S_1 from transient absorption measurements. All Raman peaks decay simultaneously and thus characterize the S_1 state species only. Similar spectra were obtained for the $44BPYH_2^{2+}$ species.

The vibrational assignment of the S_1 state Raman lines of MV^{2+} can be established without ambiguity by analogy with the reliable assignments performed for the MV^{2+} ground state and $MV^{+\cdot}$ species on the basis of DFT calculations [5]. The correlation is established by comparing the frequency shifts observed upon deuteration and on going from the MV^{2+} to the $44BPYH_2^{2+}$ species. For example, Figure 2 presents a comparison of the time-resolved Raman spectra of the S_1 state of MV^{2+}-*h* and of the radical cation $MV^{+\cdot}$ in resonance with their respective UV and visible electronic transitions. Examining these spectra lead to the following conclusions:

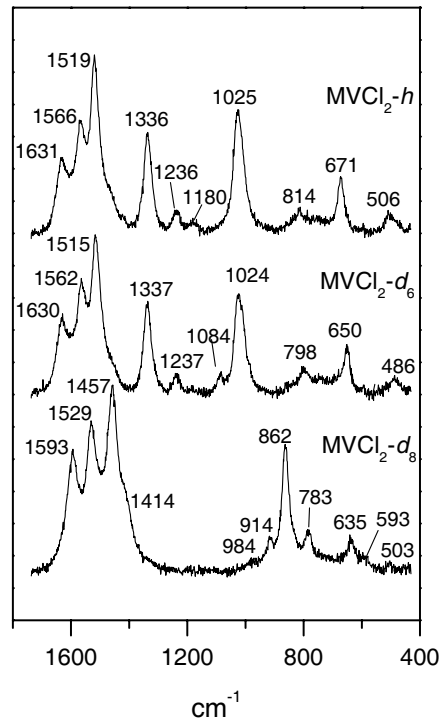

Figure 1. Time resolved resonance Raman spectra of the excited S_1 state of the MV^{2+} isotopomers probed in water at 752 nm at a time delay of 1 ps after 250.7 nm excitation (solvent bands are removed).

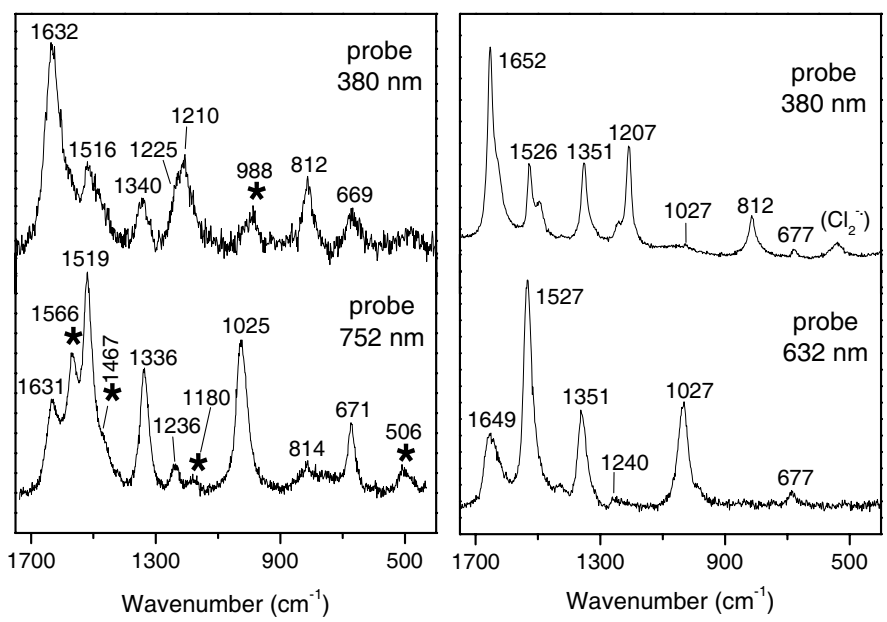

Figure 2. Time-resolved Raman spectra of the S_1 state of MV^{2+} (left) and of the radical cation $MV^{+\cdot}$ (right) probed in resonance with their respective UV and visible electronic transitions.

- The $MV^{+\cdot}$ resonance Raman activity is consistent with a coplanar (D_{2h}) molecular symmetry (all the expected totally symmetric modes are observed) [5, 6]. The frequency changes on going from MV^{2+} to $MV^{+\cdot}$ have been shown to result from the appearance of a quinoidal distorsion [5, 6].

- Most of the S_1 state resonance Raman active modes correlate clearly with those observed for $MV^{+\cdot}$ and show similar relative resonance Raman intensity enhancements. On the other hand, comparable frequency shifts are found for these modes on going from the ground state spectrum of MV^{2+} to the S_1 state and $MV^{+\cdot}$ spectra. This undeniable analogy points out a certain resemblance of the $MV^{+\cdot}$ and S_1 state species concerning the structure and electronic configuration. In particular, it can be concluded that the S_1 state presents, as $MV^{+\cdot}$, a quinoidal distortion with a notable double-bond character of the interring CC bond (the mode having a dominant contribution from the interring stretching coordinate shifts from 1299 cm^{-1} in S_0 to 1336 in S_1 and 1351 cm^{-1} in $MV^{+\cdot}$).

- However, 5 additional Raman bands are active in the S_1 state spectra compared to the $MV^{+\cdot}$ spectra (those noted by symbols * in Figure 2). By analogy with the B3LYP description of the MV^{2+} modes [5], these 5 bands can be confidently correlated to 5 B_{3u} modes of MV^{2+}, i.e., to the analogues of 5 totally symmetric modes for which the vibrations of the two pyridinium rings are *out-of-phase* instead of being *in-phase*. In the hypothesis of pure Franck-Condon origin of the resonance Raman effect (all active mode are totally symmetric), this activity strongly suggests that the S_1 state structure presents an asymmetry along the main molecular axis, which leads to the surprising conclusion that the two pyridinium rings are structurally non-equivalent.

[1] T. W. Ebbesen, G. Levey, L. K. Patterson, Nature 298, 545-548 (1982).
[2] W. Jarzeba, S. Pommeret, J.-C. Mialocq, Chem. Phys. Lett. 333, 419-426 (2001).
[3] T. W. Ebbesen, G. Ferraudi, J. Phys. Chem. 87, 3717-3721 (1983).
[4] J. Peon, X. Tan J. D. Hoerner, C. Xia, Y. F. Luk, B. Kohler, J. Phys. Chem. A 105, 5768-5777 (2001).
[5] C. Lapouge, G. Buntinx, O. Poizat, unpublished results.
[6] S. Ghoshal, T. Lu, Q. Feng, T. M. Cotton, Spectrochim. Acta 44A, 651-660 (1988).

Time-Resolved Spectroscopic Investigation of *P*-Hydroxyphenacyl Caged Phototrigger Compounds

David Lee Phillips*, Chensheng Ma, Wai Ming Kwok, Wing Sum Chan, Peng Zou
Department of Chemistry, The University of Hong Kong,
Pokfulam Road, Hong Kong S.A.R., P. R. China
Email: phillips@hkucc.hku.hk

Efficient phototrigger compounds are needed for the fast and localized release of biological stimulants for real-time monitoring of physiological responses in biological systems. The *p*-hydroxyphenacyl (*p*HP) caged class of phototrigger compounds was recently discovered to undergo a favorable photodeprotection reaction in aqueous solutions that leads to the fast and efficient release of various biological stimulants and the concurrent release of a biologically benign rearrangement product. An investigation of the photorelease reaction of *p*HP phototriggers containing acetate (*p*HPA) and diethyl phophate (*p*HPDP) leaving groups in acetonitrile *vs* water/acetonitrile mixed solvent systems is presented. The goal of this study is to better understand the mechanism for the photodeprotection reaction that occurs in aqueous environments. Femtosecond Kerr gated time-resolved fluorescence (KTRF), transient absorption (TA) and picosecond Kerr gated time-resolved resonance Raman (ps-KTR^3) spectroscopies were utilized to examine the structure and dynamics of the photophysical and photochemical processes involved in the photodeprotection reactions. The KTRF spectra show that there is a rapid ISC that is fairly independent of the solvent and the type of leaving group. The ps-TR^3 and TA experiments show the triplet decay kinetics is highly solvent and leaving group dependent. These experiments found a substantially faster decay of the triplet in water mixed solvent compared to neat acetonitrile. A comparison of results from DFT calculations with the TR^3 spectra acquired in neat acetonitrile *vs* mixed water/acetonitrile solvents found there is significant perturbation of the triplet structure. This perturbation of the triplet structure appears to be caused by multi-site solute-solvent H-bonding interactions. These strong excited solute- solvent water coupling may act as a driving force for the photocleavage reaction. The TR^3 technique was used to monitor the product formation dynamics and the cleavage rate for *p*HPDP has been determined explicitly for the first time and this indicates the cleavage and product formation occur in a step wise manner. Our results lead to a substantially improved understanding of the *p*HP photorelease mechanism and an overall reaction mechanism is proposed that is consistent with both the experimental and computational results.

References

[1] C. Ma, W. S. Chan, W. M. Kwok, P. Zuo and D. L. Phillips, J. Phys. Chem. B **108**, 9264-9276 (2004).
[2] C. Ma, P. Zuo, W. M. Kwok, W. S. Chan, J. T. W. Kan, P. H. Toy and D. L. Phillips, J. Org. Chem. **69**, 6641-6657 (2004).
[3] C. Ma, W. M. Kwok, W. S. Chan, P. Zuo, J. T. W. Kan, P. H. Toy and D. L. Phillips, J. Am. Chem. Soc. **127**, 1463-1472 (2005).
[4] W. S. Chan, C. Ma, W. M. Kwok, and D. L. Phillips, J. Phys. Chem. A **109**, 3454-3469 (2005).
[5] P. Zuo, C. Ma, W. M. Kwok, W. S. Chan and D. L. Phillips, J. Org. Chem. submitted.

Non-invasive Probing of Deep Layers of Turbid Media using Raman Spectroscopy

P. Matousek[1)], M. D. Morris[2)], N. Everall[3)], I. P. Clark[1)], M. Towrie[1)] and A. W. Parker[1)]

1) Central Laser Facility, CCLRC Rutherford Appleton Laboratory, Didcot, Oxfordshire, OX11 0QX, UK
2) Department of Chemistry, University of Michigan, Ann Arbor, MI 48109, USA
3) ICI PLC, Wilton Research Centre, Wilton, Redcar, Cleveland, TS10 4RF, UK

Introduction

Diffusely scattering media are frequently encountered in many analytical applications: examples include monitoring of food products, colloids, polymers, catalysts, powders in general, coating technology, dermatology applications involving the probing of tissue, and biochemical identification for medical studies and treatments. Such samples are often highly heterogeneous and can be composed of various layers each having a different chemical make-up. A major goal for analytical sciences in this area is to provide a method capable of determining the chemical composition of these layers in a non-destructive way. Here we present two such approaches enabling the retrieval of deep-layer Raman signals and their separation from those of the overlaying matrix in the temporal and spatial domains. The proposed techniques are akin to optical tomography using NIR absorbance[1] or fluorescence spectroscopy[2].

Temporal Approach

The temporal method[3] separates Raman components in the time domain using a fast shutter based on a 4 ps optical Kerr shutter described in detail earlier[4]. In a test experiment we used a two-layer sample consisting of a 1 mm optical path cuvette of 1 cm width and ~ 4 cm height, with 300 μm custom made fused silica windows, filled with PMMA (poly(methyl methacrylate)) spheres of ~20 μm diameter. A 4 mm thick tablet of *trans*-stilbene powder was placed immediately behind the back wall. The probe wavelength was 400 nm, the pulse duration 1 ps, the pulse energy ~5 μJ and the repetition rate 1 kHz. The beam was weakly focused onto the sample surface to a ~500 μm diameter spot size. The laser beam was generated using a regenerative amplifier providing 800 nm, ~1 ps, 2 mJ pulses at 1 kHz. Raman scattered light was collected in the backscattering geometry.

Figure 1a shows Raman spectra measured from the PMMA/stilbene two-layer system as a function of the Kerr gate time delay. The top spectrum is that measured without the Kerr gate and consequently contains contributions from both the layers. The early time delay spectra are dominated by the Raman spectrum of the top, PMMA layer. Only at 50 ps does one begin to discern a contribution from the stilbene layer with its characteristic doublet appearing at around 1600 cm^{-1}. The stilbene signal then continues to grow, peaking at around 200-300 ps from which point it gradually dies away. The PMMA signal on the other hand decays monotonically from 20 ps onwards and is largely absent at delay times above 100 ps. An experiment performed at longer acquisition time (1200 s) established that the contrast of the bottom layer the ratio of PMMA/stilbene signal was at least 5-times lower in the spectra with the Kerr gate than that in the spectrum with no gate (this figure is noise limited).

The Raman Kerr shutter used in this study was originally developed to separate Raman signal from fluorescence backgrounds. This capacity is still retained in diffusely scattering media although this performance can be compromised by large temporal spread of Raman signals that can become comparable to the lifetime of fluorescing species.

Spatial Approach – SORS

The spatial methodology[5] is based on the collection of Raman spectra from regions spatially offset, by different amounts, from the point of incidence of the probe laser beam on the surface of a diffusely scattering sample. Crucially, such an array of spectra contains different relative Raman contributions from the surface and sub-surface layers. In a test experiment we used a probe wavelength of 514 nm. The laser power was 12 mW at the sample and the beam was focused to a diameter of 300 μm. The test sample was identical to that used in the temporal approach.

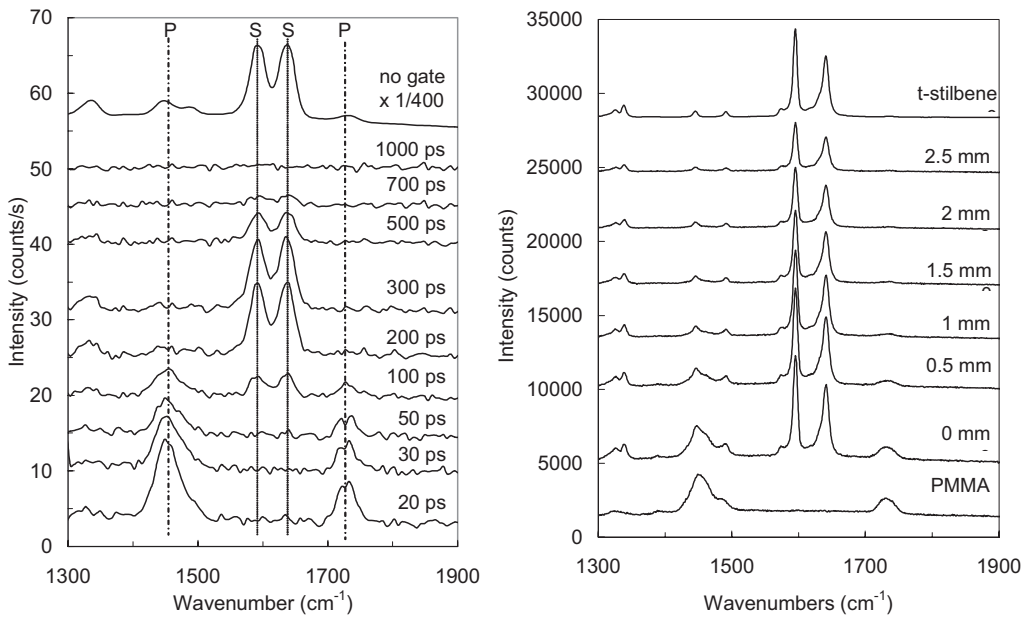

a) b)

Figure 1. a) Temporal Approach: The Kerr gated Raman spectra of a two-layer system consisting of PMMA spheres (P) followed by trans-stilbene powder (S). The top spectrum is obtained with no Kerr gating. The acquisition time was 200 s for each spectrum. b) Spatial Approach: A set of spatially offset Raman spectra collected from a two-layer system identical to that used in the temporal approach. The top and bottom spectra are those of pure trans-stilbene and pure PMMA layers, respectively. The acquisition time was

A set of Raman spectra measured with a varying degree of spatial offset is shown in Figure 1b with the spatial offset indicated next to the spectra. For comparison, the Raman spectra of the pure layers measured in separate experiments are also displayed. The spectrum measured with zero offset represents the Raman spectrum one would typically obtain using a conventional Raman instrument. It is evident that it contains an appreciable contribution from the both layers. The gradual separation of the PMMA and trans-stilbene signals is accomplished using the SORS (Spatially Offset Raman Spectroscopy) approach as one keeps increasing the lateral offset between the Raman collection point and the point of probe beam incidence. At distances of >2 mm one reaches around an order of magnitude improvement in the ratio of the lower layer to the top layer Raman signals.

To quantify the contrast improvement achievable on this sample by this approach, we have acquired a Raman spectrum with a longer acquisition time (1000 s) at an offset of 3.5 mm.

The contrast of the lower layer was improved by a factor of 19 by rejecting the top layer spectral component. This result compares very favourably with the contrast improvement obtained using the temporal Kerr gating approach. Another striking observation is that the signal-to-noise obtained using the much more simple spatially offset method was substantially higher than that observed with the temporal gating approach. This is understandable as the spatial gating technique integrates all Raman components spread in the temporal domain, unlike in the temporal approach. A downside of the SORS approach is, however, the fact that it does not have simultaneous fluorescence suppression capability as the Kerr gated approach.

Spectra collected by SORS are amenable to multivariate data analysis. This reduction techniques provide an advantage when one desires a complete separation of the spectral features of the surface and sub-surface layers that that available from the raw spectra[5].

Conclusions

We have proposed and demonstrated two non-invasive methods for the extraction of Raman spectra from a deep layer within a diffusely scattering sample. The techniques can be used for the effective extraction of pure Raman spectra of top and underlying layers, without any prior knowledge of their chemical composition. The approaches hold great promise for biomedical applications, where monitoring sub-surface tissue layers normally would require sectioning the superficial tissues, or many analytical applications such as catalysts, food, polymer research and dermatology applications. Recently, the temporal approach was successfully used in the retrieval of bone spectra noninvasively through mouse skin (1.1 mm) and 'brittle bone disease' condition was recognised[6].

References

1. H. Koizumi, Y. Yamashita, A. Maki, T. Yamamoto, Y. Ito, H. Itagaki and R. Kennan, J. Biomed. Opt. **4** (1999) 403.
2. T. J. Pfefer, K. T. Schomacker, M. N. Ediger and N. S. Nishioka, Appl. Opt. **41** (2002) 4712.
3. P. Matousek, N. Everall, M. Towrie and A. W. Parker, Appl. Spectrosc. 59 (2005) 200.
4. P Matousek, M Towrie, C Ma, W M Kwok, D Phillips, W T Toner and A W Parker, J. Raman Spectrosc. **32** (2001) 983.
5. P. Matousek, I. P. Clark, E. R. C. Draper, M. D. Morris, A. E. Goodship, N. Everall, M. Towrie, W. F. Finney and A. W. Parker, Appl. Spectrosc. **59** (2005) 393.
6. E. R. C. Draper, M. D. Morris, N. P. Camacho, P. Matousek, M. Towrie, A. W. Parker and A. E. Goodship, 'A Novel Assessment of Bone: Time-Resolved Transcutaneous Raman Spectroscopy of Bone', Journal of Bone and Mineral Research, 2005, submitted.

Picosecond/Femtosecond Time-Resolved Resonance Raman Study of the Hydrated Electron

Tahei Tahara*, Misao Mizuno and Shoichi Yamaguchi
Molecular Spectroscopy Laboratory, RIKEN
2-1 Hirosawa, Wako 351-0198, Japan

1. Introduction

When an electron is injected into water, the electron is solvated and forms the hydrated electron. This hydrated electron is the most fundamental anionic species in solution and it has been attracting much interest for decades. The hydrated electron exhibits a strong broad absorption peaked around 720 nm. Recently, Raman spectra were measured under the resonance condition with the electronic transition of the hydrated electron, and it was found that Raman scattering from the water molecules that solvate the electron gains high resonance enhancement.[1,2] This result implies that the electronic state of the electron is strongly coupled with the vibrational state of the solvating water molecules and that we should treat the hydrated electron as a "quasi-molecule" or "negative ion cluster in the condensed phase" when we consider its vibronic states. Here, we report our picosecond and femtosecond Raman study of the hydrated electron, which shed a new light on this fundamental transient species from a viewpoint of vibrational spectroscopy.

2. Resonance Raman spectra of the hydrated electron

Figure 1 shows the resonance Raman spectrum of the hydrated electron measured by picosecond time-resolved Raman spectroscopy. The pump and probe wavelengths are 273 and 620 nm, respectively, and the delay time was 20 ps. The electron was produced by the photoionization of $[Fe(CN)_6]^{4-}$ that was added to water for efficient generation of the electron. The Raman spectrum of bulk water is also shown for comparison. The spectrum of water shows strong Raman bands around 3300 cm^{-1} and a weak band around 1640 cm^{-1}, which are attributed to the OH stretch and HOH bend vibrations, respectively. The spectrum of the hydrated electron shows corresponding two prominent Raman bands in the OH stretch and HOH bend region. This similarity indicates that the spectrum of the hydrated electron is basically the spectrum of water. Thus, it was concluded that the resonance Raman spectrum of the hydrated electron provides vibrational spectra of the water molecules that solvate the electron. The vibrational frequencies

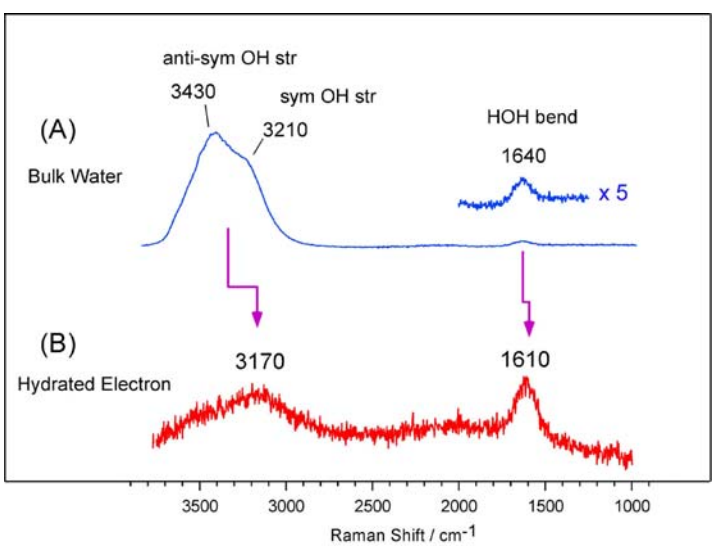

Fig. 1. The non-resonance Raman spectrum of water (A; 600 nm excitation) and the resonance Raman spectrum of the hydrated electron (B; 620 nm excitation).

* Corresponding author. E-mail: tahei@riken.jp

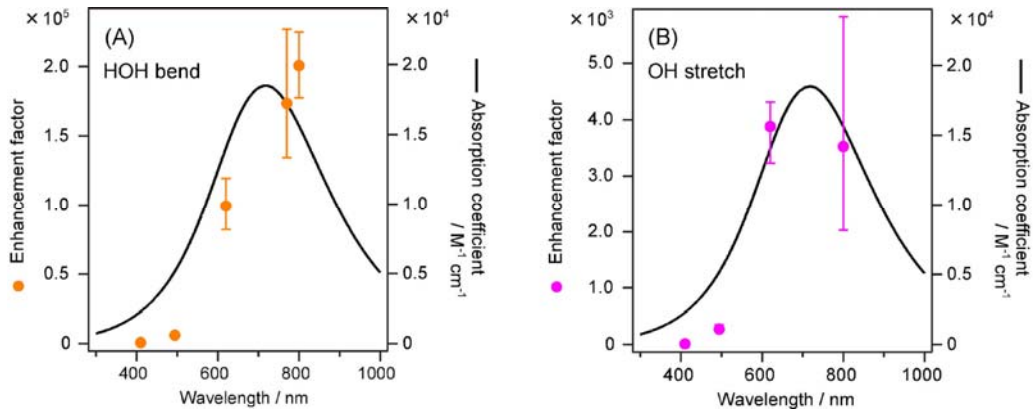

Fig. 2. Excitation profiles of the HOH bend (A) and OH stretch (B) bands.

of the spectrum of the hydrated electron are downshifted by ~150 cm^{-1} (OH stretch) and ~30 cm^{-1} (HOH bend) compared to those of the bulk water, indicating strong interaction between the electron and the solvating water molecules. A theoretical calculation of the hydrated-hydronium cluster, which is a finite-size model of the hydrated electron, gave results consistent with the observed Raman frequencies.[3]

3. Excitation profiles and resonance enhancement

To quantitatively discuss the resonance enhancement of the solvating water molecules, we evaluated the magnitude of the resonance enhancement (the enhancement factor) of the OH stretch and HOH bend bands at five different probe wavelengths. The obtained excitation profiles are compared with the absorption spectrum of the hydrated electron in Figure 2. The enhancement factors of both bands are maximized around the intensity maximum of the absorption and they become as large as ~2×10^5 (HOH bend) and ~4×10^3 (OH stretch). The excitation profiles also show that the enhancement factors sharply decrease in the blue side of the absorption band and, especially, they become very small around 400 nm. The very small resonance enhancement in the blue side of the absorption is ascribable to the difference in the nature of the electronic transition in resonance. A theoretical calculation showed that the major part of the absorption is attributable to the s → p transition whereas the blue side of the absorption band has a nature of the s → conduction band (CB) transition.[4] Therefore, the excitation profiles indicate that Raman scattering from the solvating water molecules are enhanced when the probe wavelength is resonant with the s → p transition, but not with the s → CB transition.

4. Femtosecond time-resolved Raman measurements and the formation/relaxation dynamics

It is known that the electron injected to water is fully relaxed within ~1 ps and forms the "equilibrated" hydrated electron that was studied by picosecond Raman spectroscopy. With the formation/relaxation process of the hydrated electron, a broad absorption appears in the near infrared region and it subsequently shifts to the higher energy side until it becomes identical to the spectrum of the equilibrated hydrated electron centered at 720 nm. The precursor that gives the initial red-shifted absorption as well as the femtosecond evolution of the transient absorption has been intensively studied and discussed. To examine this femtosecond process by vibrational spectroscopy, we carried out femtosecond time-resolved resonance Raman measurements [5]. It is noted that femtosecond time-resolved spontaneous Raman measurements are not usually performed because the broad bandwidth of femtosecond pulses makes the observed Raman bands broad and prevents observation of well-resolved vibrational spectra. In the case of water, however, femtosecond pulse longer than a few hundred femtoseconds can still provide reasonable Raman spectra because the water Raman bands are isolated and intrinsically broad.

Figure 3 shows femtosecond time-resolved resonance Raman spectra of the hydrated electron in the delay time range from -1.9 ps to 5.1 ps. In this femtosecond experiment, the electron was produced by two-photon ionization of water itself. The pump and probe wavelengths are 267 nm and 800 nm, respectively, and the time resolution (FWHM of the cross correlation) was ~250 fs. The probe wavelength of 800 nm was adopted because it can be resonant not only with the electronic transition of the equilibrated

hydrated electron but also with the red-shifted absorption due to the precursor. As clearly seen in this figure, the rise of Raman bands due to the HOH bend vibration and libration of the solvating water molecules was successfully time-resolved. In Figure 4, the temporal intensity change of the HOH bend transient Raman band was compared with the time evolution of the transient absorption signal monitored at 800 nm. In addition, the transient absorption trace was decomposed into the contributions of the precursor state and the equilibrated hydrated electron.[5] It is clear that the rise of the transient Raman band is faster than the appearance of the equilibrated hydrated electron, indicating that the precursor state also gives rise to resonance Raman scattering. This means that the precursor state is the non-equilibrated s-state electron because the resonance Raman enhancement arises from the resonance with the s → p transition. Figure 4 also shows that the rise of the Raman signal is slower than the rise of the transient absorption at 800 nm. This delayed rise was explained in terms of the temporal change of the resonance condition. In very early time when the absorption is largely red-shifted, the probe at 800 nm is resonant with the high energy part of the absorption that provides little resonance Raman enhancement because of the s → CB character. This temporal change of the resonance condition due to the spectral shift of the absorption is a manifestation of the temporal increase of the transition energy between the s and CB and that between the s and p states in the femtosecond region.

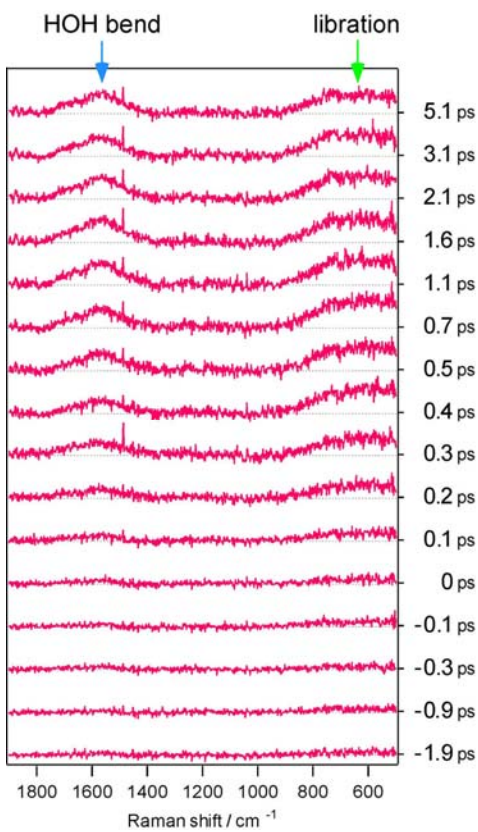

Fig. 3. Femtosecond time-resolved resonance Raman spectra of the hydrated electron.

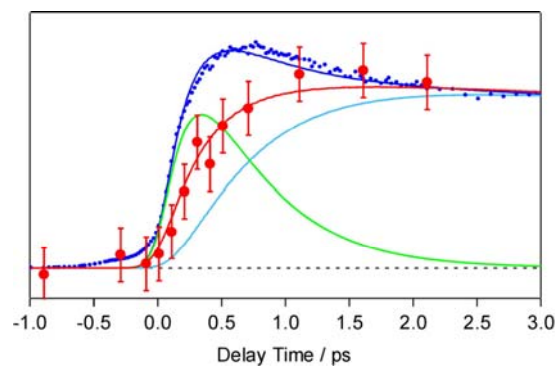

Fig. 4. Comparison of the temporal intensity change between the transient Raman band due to the HOH bend vibration (red) and the transient absorption monitored at 800 nm (blue). The transient absorption is decomposed into the contributions of the precursor state (green) and the equilibrated hydrated electron (light blue).

References

1. M. Mizuno and T. Tahara, *J. Phys. Chem. A,* **105**, 8823 (2001); *J. Phys. Chem. A,* **107**, 2421 (2003).
2. M. Tauber and R. Mathies, *J. Phys. Chem. A,* **105**, 10952 (2001); *J. Am. Chem. Soc*., **125**, 1394 (2003).
3. S. Neumann, W. Eisfeld, A. Sobolewski, and W. Domcke, *Phys. Chem. Chem. Phys*. **6**, 5297 (2004).
4. J. Schnitker, K. Motakabbir, P. Rossky, R. Friesner, *Phy. Rev. Lett.*, **60**, 456 (1988).
5. M. Mizuno, S. Yamaguchi and T. Tahara, *J. Phys. Chem. A*, **109**, 5257 (2005).

TRVS XII

NIST National Institute of Standards and Technology

Washington, D.C.
May 23-27, 2005

Transient Infrared

Multidimensional Infrared Spectroscopy Dynamics and Chemical Exchange

Yung Sam Kim and Robin M. Hochstrasser*
Department of Chemistry, University of Pennsylvania
Philadelphia, Pennsylvania 19104-6323, USA.

Vibrational spectroscopy provides important experimental access to the microscopic aspects of hydrogen bonds in complex systems. The OH stretching vibrational modes in water or alcohol, the vibrations of molecular aqueous ions, and the N-H stretching modes in peptides or proteins are very sensitive to and correlated with the structural and dynamical properties of hydrogen bonds. In principle, the shape of the conventional IR absorption spectrum provides information on the equilibrium dynamics of a hydrogen bonded system. However, in many cases the line shapes are determined by population lifetimes and spectral diffusion processes that usually cannot be reduced to the unique set of parameters needed to describe the frequencies and amplititudes of coupled solvent nuclear motions. With the help of multidimensional nonlinear spectroscopic techniques in the IR, it has become possible to probe these dynamics and extract more details on the structures with high time resolution. Dynamical information on the O-H, O-D, and N-H stretching modes of intermolecular hydrogen bonded systems such as alcohols, water and amides has been obtained in the form of vibrational lifetimes, energy transfer, hydrogen bond breaking and reforming rates, and the time dependence of spectral diffusion. In protein secondary structures the amide carbonyl group is very often involved in hydrogen bonding either to water or to N-H groups or to both. Too little is known from experiments about the dynamics of these hydrogen bonds for a wide range of environments. The 2D IR experiments generally measure the vibrational frequency correlation function which reflects the solvent or internal motions that couple to the mode.

The vibrational population and coherent vibrational dynamics of hydrogen bonded systems have been examined by a wide variety of nonlinear IR techniques thas have analogies in NMR. As part of this presentation we introduce a new approach : chemical exchange 2D IR which is again analogous to a well-known NMR method.

Chemical exchange processes in equilibrium dynamics have been studied since the earliest days of NMR and one of the most important common uses of one and two dimensional NMR methods has been in the determination of rate constants. The same general concepts should be applicable to 2D IR with the time scales shifted into the picosecond/femtosecond regime, because the most accurate exchange data are obtained if the reaction rate is fast compared with the population relaxation time but slow compared with the spectral parameters affected by the exchange. In the presence of chemical exchange the usual fluctuating frequency in the nonlinear response function must incorporate deterministic transitions between the exchanging states. In this paper we report results on internal hydrogen bonded structures and on an alcohol OH---NC-Me hydrogen bond exchange, which will be examined through the fluctuations in the CN frequency at around 2250 cm^{-1}. This is a case where the CN vibrational frequency fluctuates on the few ps time scale between that found in a free and an H-bonded structure.

The 2D IR is a three pulse experiment. After a vibrational coherence time, τ , the system enters a population period for time T after which it is driven into a new coherent state from

which a signal field is detected at time *t*. In a chemical exchange experiment the coherence, initially associated with one chemical state, may be transferred to another chemical species after the time *T*. The presence of deterministic processes in the vibrational dynamics requires that the third order responses due to the various Liouville pathways involved in 2D IR be modified. The essential difference with the picture in the absence of exchange is that the phase evolutions of the vibrational coherences, which are represented by the integrated frequency fluctuations $\delta\omega(\tau)$ caused by the interactions of the vibrator with the medium, contain deterministic components where the system jumps back and forth stochastically between a small number of identifiable chemical states. In the vibrational response functions that are used in conventional nonlinear spectroscopy the number of these states may become very large and the phase evolution characterizes the dynamics of a nearly continous inhomogeneous distributions of frequencies. One of the advantages of 2D IR in exchange studies of spectrally isolated, uncoupled vibrators is that the existence of chemical exchange can be firmly established from the existence of the cross peaks.

The 2D IR heterodyne echo spectroscopy was successfully used to obtain the analogue of chemical exchange 2D NMR. The 2D IR spectra show cross peaks caused by the H-bond exchange. The exchange dynamics of hydrogen bond exchange is observed clearly on the hydrogen bond potential surfaces associated with both the v=0 and v=1 states of the CN stretching mode. The existence of the strong cross peaks between two different chemical states is firm evidence of the hydrogen exchange between them. The relative magnitudes of the cross peaks and the diagonal peaks at various intervals is used to obtain rate coefficients for H- bond transfer that are in the few picoseconds regime, while the temperature dependences indicate that the energy of activation for the exchange from the H-bonded to free state is ~7.9 kJ/mol. The results expose the hydrogen bond dynamics in both the v=0 and the v=1 vibrational states and they indicate that the CN stretching mode is not strongly coupled to the hydrogen bond reaction coordinate.

Femtochemistry in the Electronic Groundstate? IR-Driven *Cis-Trans* Isomerization of HONO

Peter Hamm, Virgiliu Botan, Roland Schanz

Physical Chemistry Institute, University of Zurich, Switzerland

The *cis-trans* isomerization of nitrous acid (HONO) in rare gas matrices is one of the few known photoreactions that can be triggered by IR excitation of a single vibrational quantum [1, 2]. The molecule is well suited as a model system to study the dynamics of chemical reactions on electronic ground state potential surfaces. High level quantum dynamic calculations indicate that the reaction could not take place in the gas phase [3]. Hence, HONO furthermore appears to be a good candidate to examine how the condensed phase environment allows chemical reactions to occur.

Femtosecond pump-probe techniques have been applied to excite the OH stretching mode of the molecule and to track the progress of the photoreaction [4]. Depletion of the *cis*-isomer and simultaneous creation of the *trans*-isomer is observed on a 20 picosecond time-scale. The *cis-trans* quantum yield is about 10-20%, while the *trans-cis* quantum yield is significantly lower. Cooling of the molecule occurs on a 100 ns timescale. In order to interpret and understand these observations on a qualitative level, quantum dynamical calculations have been performed. A model Hamiltonian is introduced that illustrates how the rare gas matrix couples the excited (OH-stretching) mode to the reactive (OH-torsional) mode.

[1] R. Hall, G. Pimentel, J. Chem. Phys., 1963, 38, 1889.

[2] L. Khriachtchev, J. Lundell, E. Isoniemi, M. Räsänen, J. Chem. Phys., 2000, 113, 4265.

[3] F. Richter, M. Hochlaf, P. Rosmus, F. Gatti, H.-D. Meyer, J. Chem. Phys., 2004,120,1306.

[4] R. Schanz, V. Botan, P. Hamm, J. Chem. Phys., 122, 044509 (2005)

The thermal denaturation of a stable β-hairpin

Adam W. Smith, Hoi Sung Chung, Ziad Ganim, and Andrei Tokmakoff

Department of Chemistry, Massachusetts Institute of Technology, Cambridge, Massachusetts 02139

We have recently used 2D IR spectroscopy to follow the thermal denaturation of a β-hairpin forming peptide, trpzip2. Peptides that form stable secondary structural elements are commonly used as minimalist models to study protein folding. Trpzip2 has received considerable attention as such a model because it is monomeric and very stable in aqueous solutions at neutral pH. The low temperature 2D IR spectrum of trpzip2 shows two diagonal peaks, with a ridge forming in the cross peak region of spectrum. These features are consistent with previous studies of β-sheet systems, where the amide I oscillator strength is carried primarily by two modes whose transition moments are oriented roughly perpendicular or parallel to the strands ($\nu_{\perp}$ and $\nu_{\parallel}$). The cross-peak ridge further demonstrates the two-mode structure and is consistent with strong inter-strand interactions of a hairpin in antiparallel registry. With increasing temperature, the diagonal peaks shift toward band center, and some of the ridge structure is lost. However, at 82°C there remain two distinct maxima in the positive diagonal region and significant intensity in the cross peak region of the 2D spectrum. Earlier work using traditional spectroscopic probes followed the thermal denaturing of trpzip2, and the results were interpreted in terms of loss of the native anti-parallel hydrogen bonding contacts between strands. In contrast, the sensitivity of cross peaks in 2D IR spectroscopy to the amide I vibrational coupling between strands leads us to conclude that there is residual antiparallel structure and considerable native hydrogen-bonding in the partially disordered, thermally denatured state of trpzip2.

Two-dimensional infrared spectroscopy of coupled hydrogen bonds in liquids

T. Elsaesser[1], N. Huse[1] , S. Ashihara[1], J. Dreyer[1], E.T.J. Nibbering[1],
M.L. Cowan[2], B.D. Bruner[2], J.R. Dwyer[2], R.J.D. Miller[2]

[1]*Max-Born-Institut für Nichtlineare Optik und Kurzzeitspektroskopie,*
Max-Born-Str. 2 A, D-12489 Berlin, Germany
[2]*Departments of Chemistry and Physics, University of Toronto,*
80 St. George St., Toronto, Ontario, Canada M5S3H6

Vibrational dynamics of hydrogen bonds occur mainly in the ultrafast time domain and, thus, femtosecond nonlinear vibrational spectroscopy has developed into a major tool for studying their basic structural and functional properties. In this paper, we present new results on two types of hydrogen-bonded systems, (i) dimers of acetic acid, a model system with a well-defined geometry of two coupled O-H...O hydrogen bonds [1,2], and (ii) the fluctuating network of intermolecular hydrogen bonds in neat liquid water [3,4].

We apply a diffractive optic (DO) technique [5] to measure both the absorptive and dispersive components of the two-dimensional vibrational spectra. This technique uses a DO to generate two passively phase-locked beam pairs, the two pump pulses ($\mathbf{k}_1$, $\mathbf{k}_2$) and the probe and local oscillator ($\mathbf{k}_3$, $\mathbf{k}_{LO}$), delayed with respect to each other by a time t_{13}. After the DO, the coherence time τ is generated by delaying pulse $\mathbf{k}_2$ with respect to pulse $\mathbf{k}_1$, and the local oscillator with respect to pulse $\mathbf{k}_3$. Since the same retroreflective delay line is used to produce both delays, the phase noise correlations set up by the DO are preserved. Locking of the relative phases of the beams was better than $\lambda/150$. Furthermore, the local oscillator generated by the DO is automatically spatially overlapped with the echo signal for heterodyne detection, which we implement using spectral interferometry [6]. The spectral fringes are detected using a monochromator and a HgCdTe detector array, directly giving the echo as a function of the detection frequency ν_3. The coherence time τ is then scanned at constant population time T, and the signal is Fourier transformed along the τ dimension to produce the excitation frequency dimension ν_1.

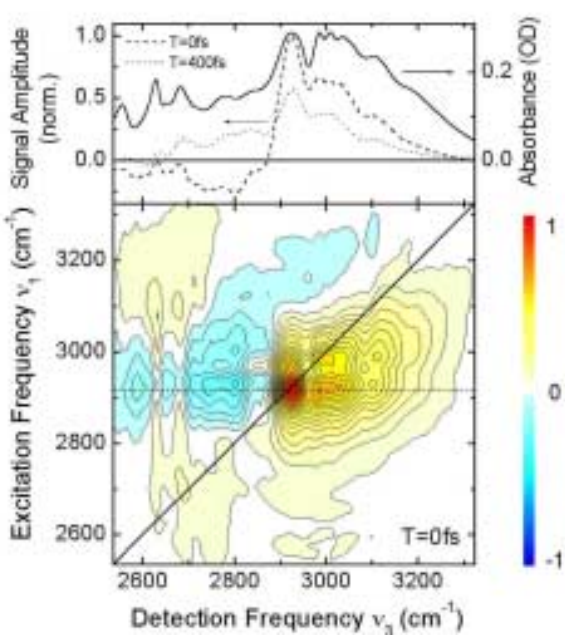

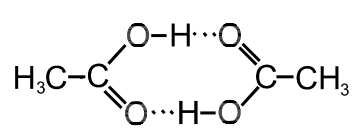

Fig. 1
2D vibrational spectrum (real part of photon echo signal) of cyclic acetic acid dimers in CCl_4 (concentration 0.2 M) for a population time T=0 (bottom) and cross section at an excitation frequency ν_1=2920 cm^{-1} for population times T=0 (top, dashed line) and T=400 fs (dotted line). The solid line in the top panel represents the linear O-H stretching absorption.

Two-dimensional (2D) photon-echo spectroscopy of acetic acid dimers allows for a separation of different vibrational couplings, i.e., Fermi resonances in the range of the O-H stretching fundamental and anharmonic couplings to low-frequency modes of the dimers. In Fig. 1, a 2D spectrum, i.e. the real part of the photon echo signal recorded for a population time T=0 (bottom), is presented together with cross sections for a fixed excitation frequency ν_1=2920 cm^{-1} and the linear O-H stretching absorption band. The 2D spectrum displays a number of off-diagonal peaks at spectral positions which are independent from T and coincide with peaks in the linear spectrum. A theoretical analysis of the 2D spectrum demonstrates that such cross peaks originate from Fermi resonances between the O-H stretching mode and over- and combination tones of fingerprint modes [7,8]. The Fermi resonance lines dominate the envelope of the linear O-H stretching absorption band. Anharmonic coupling to underdamped low-frequency modes of the intermolecular hydrogen bonds gives rise to multilevel quantum beats in the homodyne-detected photon echo [2] and weak progressions in the linear O-H stretching absorption. Both types of anharmonic couplings have absolute values of the order of 100 cm^{-1}.

Neat liquid water represents a highly disordered fluctuating network of coupled intermolecular hydrogen bonds, resulting in fast vibrational dephasing, resonant energy transfer between O-H stretching oscillators and a pronounced inhomogeneous broadening of the O-H stretching absorption band. In Fig. 2, we present 2D infrared spectra for population times T=0 and T=50 fs (real part of the photon echo signal) [3]. At T=0, the positive peak due to the v=0 to 1 transition of the O-H stretching mode is elongated along the diagonal, giving evidence of inhomogeneous broadening. This behavior is absent in the spectrum for T=50 fs, pointing to an extremely fast sweep of O-H stretching frequencies on a 50 fs timescale and a concomitant decay of the initial inhomogeneous distribution of sites, i.e., loss of structural memory. Such ultrafast frequency sweeps are also observed in the spectrally resolved transient grating signal [3]. In addition, one finds a decay of the anisotropy of the transient grating signal with a 100 fs time constant, reflecting the resonant transfer of energy between O-H stretching oscillators. We attribute the ultrafast decay of inhomogeneity to librational

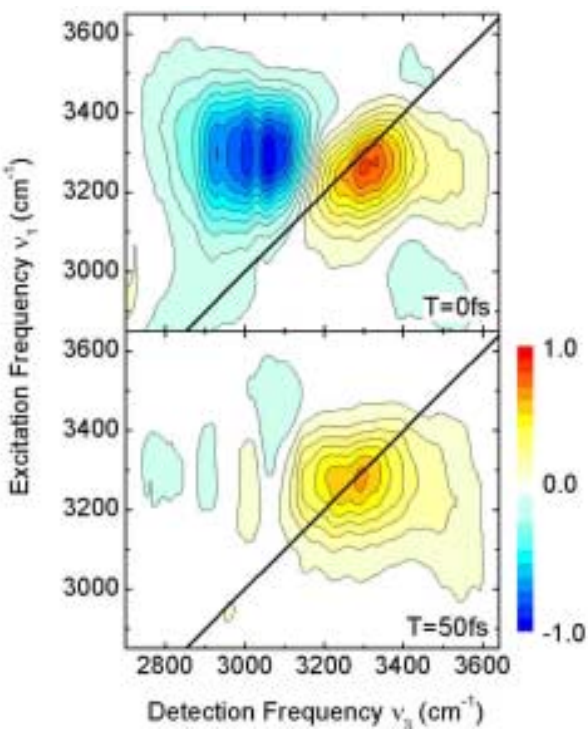

Fig. 2
2D vibrational spectra of O-H stretching excitations in neat liquid water for population times T=0 and T=50 fs. The spectra reveal ultrafast spectral diffusion on the v=0 to 1 transition of the stretching oscillators.

excitations resulting in a high-frequency component of the fluctuating force exerted on the O-H stretching oscillator. On a somewhat slower time scale, energy transfer contributes to spectral diffusion. Population relaxation of the O-H stretching and O-H bending vibrations of neat water occurs with respective lifetimes of 190 and 170 fs [3,4]. First two-color pump-probe experiments on high-frequency librations in the range between 1000 and 1600 cm^{-1} reveal an initial sub-100 fs decay followed by slower energy redistribution processes which result in a macroscopic heating of the liquid.

In conclusion, the two systems studied here represent two markedly different model cases for the behavior of intermolecular hydrogen bonds. In acetic acid dimers, there is negligible structural disorder resulting in a homogeneously broadened O-H stretching band which consists of a superposition of lines due to Fermi resonances and - to lesser extent - due to progressions of anharmonically coupled low-frequency modes. The fluctuating force exerted by the surrounding solvent results in a dephasing of O-H stretching excitations on a 200 fs time scale, whereas low-frequency coherences persist for picoseconds. In contrast, water represents an extended fluctuating network of hydrogen bonds making a distinction of solute and solvent impossible. Fluctuations and structural changes occur in a broad temporal range and result in a pronounced inhomogeneous broadening of the O-H stretching absorption. O-H stretching oscillators embedded in this network display dephasing and spectral diffusion on a 50 fs time scale and resonant energy transfer in the 100 fs time domain, leading to an ultrafast loss of structural memory.

References

[1] K. Heyne, N. Huse, J. Dreyer, E. T. J. Nibbering, T. Elsaesser, S. Mukamel, J. Chem. Phys. **121**, 902 (2004).

[2] N. Huse, K. Heyne, J. Dreyer, E. T. J. Nibbering, T. Elsaesser, Phys. Rev. Lett. **91,** 197401 (2003).

[3] M.L. Cowan, B.D. Bruner, N. Huse, J.R. Dwyer, B. Chugh, E.T.J. Nibbering, T. Elsaesser, R.J.D. Miller, Nature **434**, 199 (2005).

[4] N. Huse, S. Ashihara, E.T.J. Nibbering, T. Elsaesser, Chem. Phys. Lett. **404**, 389 (2005).

[5] M.L. Cowan, J.P. Ogilvie, R.J.D. Miller, Chem. Phys. Lett. **386**, 184 (2004).

[6] J.-P. Likforman, M. Joffre, V. Thierry-Mieg, Opt. Lett. **22**, 1104 (1997).

[7] N. Huse, B.D. Bruner, M.L. Cowan, J. Dreyer, E.T.J. Nibbering, R.J.D. Miller, and T. Elsaesser, unpublished.

[8] J. Dreyer, Int. J. Quant. Chem., in press.

Comprehensive study of the vibrational energy relaxation of monomeric water molecules in nonpolar organic solvents

Gerhard Seifert, Toralf Patzlaff, and Heinrich Graener

Martin-Luther-University Halle, Physics Institute, Hoher Weg 8, D-06099 Halle, Germany
E-mail: g.seifert@physik.uni-halle.de

We have studied comprehensively the dynamics of vibrational excess energy of monomeric water molecules in relatively nonpolar solvents by help of an infrared pump-probe spectroscopy with ≈ 2.5 ps pulses. Since both frequencies can be independently varied from 1500 to 4000 cm^{-1}, all three fundamental vibrations are accessible for both excitation and probing of transient population changes. With this approach, which can be understood as populational 2D IR spectroscopy, it is possible to monitor the dynamics of vibrational population either (i) directly as bleaching of an excited fundamental or as induced absorption due to overtone transitions, or (ii) indirectly at different spectral positions utilizing the anharmonic shift of combination modes.

Water molecules provide a unique opportunity to study the vibrational relaxation of a high-frequency "gate mode", because the bending vibration ν_2 is their lowest vibrational mode, but has a frequency of $E_{vib} \approx 1600$ cm^{-1} being approximately a factor of 8 larger than thermal energy at ambient temperature (k_BT corresponds to 208 cm^{-1} at 300 K). So, looking at binary mixtures of water in organic solvents, it is very improbable that the OH bending vibration transfers its energy directly into non-vibrational, low-frequency modes of the surrounding liquid. Instead, an intermolecular process populating suitable vibrations of the solvent molecules can be assumed as the main relaxation process, which in turn lets one expect a considerable dependence of the water OH bend relaxation on the resonance structure of the solvent molecules. The situation is different in neat liquid water, the relaxation dynamics of which was studied extensively in the last years by different methods with fs time resolution: in neat water (or isotopic mixtures) the complex hydrogen bond network provides a large density of states of low-frequency modes, which can accept the relaxed energy, giving rise to population lifetimes of the order of a picosecond or faster [1,2]. It is generally accepted in this context that the relaxation of OH stretching quanta involves the bending mode ν_2, as was concluded previously from experiments on neat water [2], monomeric water molecules in non-polar solvents [3] and theoretical calculations [4].

Here we report a series of experiments on the OH bending relaxation of (monomeric) H_2O molecules in various halogenated and/or deuterated methane and ethane derivates, where the water molecules are dissolved dominatingly in monomeric form, often accompanied by a quite low total solubility. With the experimental setup used, excess vibrational population can be created on both OH stretching and bending modes of H_2O; the following redistribution of vibrational energy within the molecule and to the solvent is then monitored by the delayed probe pulses via transient absorbance changes, which are directly proportional to population differences between two vibrational levels [5]. A previous study showed that the intermolecular energy transfer process from the OH bending mode of H_2O in $CHCl_3$ and $CDCl_3$ to the respective solvent occurs with very different relaxation rate constants (decay times of 28 and 8.5 ps, respectively) despite the obvious similarity of the solvent molecules [6]. This result already showed clearly that the vibrational resonance structure of the acceptor molecules plays a decisive role for the energy transfer. However, a close inspection of the acceptor modes with low total number of vibrational quanta (which is a prerequisite for considerable transition probability) gave no unambiguous hint for a simple assignment of, e.g., one dominating accepting mode.

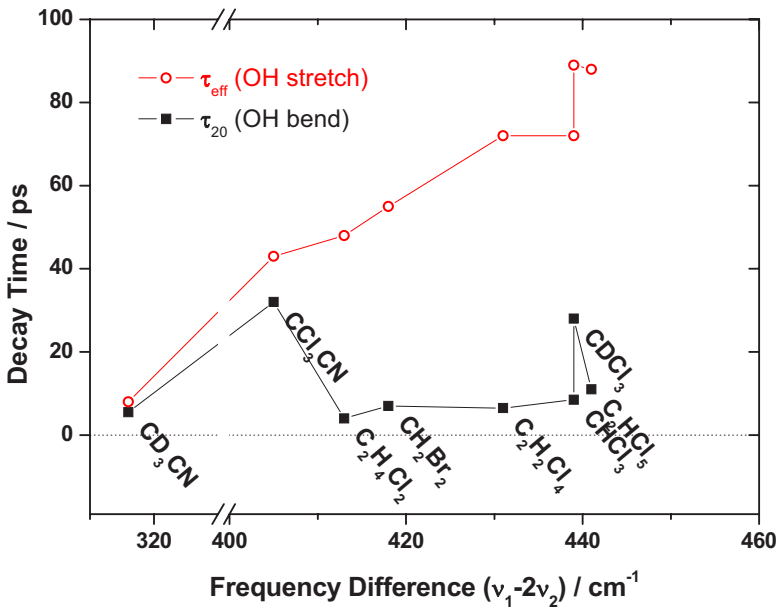

Fig. 1: Measured vibrational lifetimes of the OH stretch ensemble (circles) and the OH bending mode (square) of H_2O in various solvents, plotted as a function of the frequency difference $\nu_1 - 2\nu_2$; see text for explanation.

The whole series of experiments on the OH bending relaxation times (τ_{20}) of various binary mixtures of H_2O in organic liquids, as shown in Fig. 1 (solid squares), confirms that the intermolecular relaxation rate of the bending mode is governed by the individual situation: The values are ordered along the frequency difference $\Delta\nu = \nu_1 - 2\nu_2$ between the water symmetric stretching vibration and the overtone of the bending mode. $\Delta\nu$ is a very reliable and sensitive probe for the interaction strength between solute and solvent [3], as can be seen looking at the vibrational effective lifetimes of the OH stretch ensemble (given as open circles in Fig. 1), which exhibit a very clear, nearly monotonous decrease with decreasing $\Delta\nu$ (increasing interaction strength). In contrast to that, the relaxation rate of the OH bending mode shows no correlation at all with $\Delta\nu$, but varies significantly from solvent to solvent including the already mentioned, quite unexpected difference of a factor of 3 between the chloroform isotopes $CHCl_3$ and $CDCl_3$. We are planning a series of comparable experiments on the D_2O and HDO bending modes, which should allow us to gain more insight into the accepting modes most probably involved in this particular intermolecular energy transfer, and to promote the theoretical understanding of the process in general.

Apart from the problem that a detailed understanding of the characteristic solvent dependence observed is still lacking, the results of our study can be used to explain comprehensively the vibrational energy relaxation scheme of monomeric H_2O molecules. The picture used previously for both neat and monomeric water after OH stretch excitation (relaxation via bending overtone and fundamental) is strongly supported: looking, e.g., at "cross-region" data like the ones shown in Fig. 2, it comes clear that the red-shifted induced absorption observed in the bending spectral region can be due to bending population (lower panel), but also due to population on the OH stretching modes being observed via the transition to a combination mode ($\nu_{bend} + \nu_{stretch}$); from the latter spectral data (upper panel of Fig. 2) and the complementary ones (population on bending mode probed in stretching spectral region) anharmonic constants of $x_{12} = -20\pm1$ cm^{-1} and $x_{23} = -24\pm1$ cm^{-1} were obtained for H_2O in dichloroethane. In general the values for the anharmonic constants turn out to be very close to the values known from the gas phase in all of

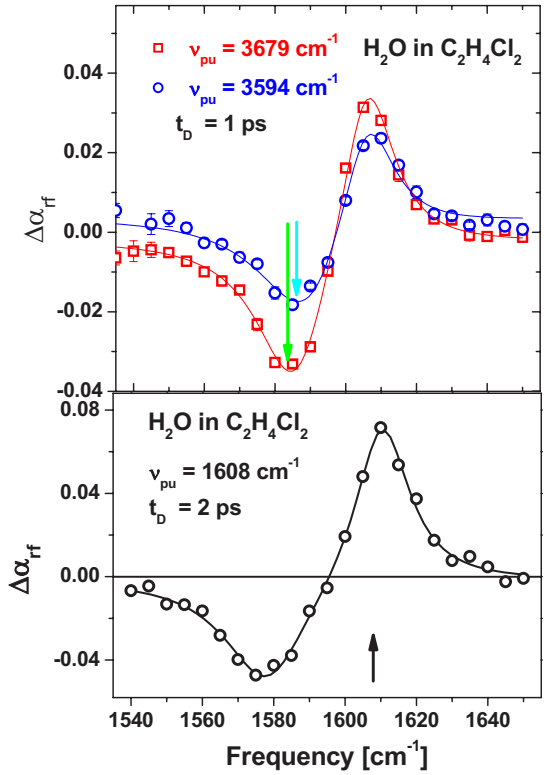

Fig.2: transient spectral data on H_2O in $C_2H_4Cl_2$, after OH stretch excitation (upper panel) and OH bend Excitation (lower panel)

our solvents On the basis of these spectral assignments derived directly from transient data, it finally becomes possible to analyze transient data in detail and prove experimentally [7] that in fact after OH stretch excitation there is population on the water bending mode in the course of relaxation.

So the widely accepted model for the vibrational energy relaxation scheme of water molecules could be proven for monomeric H_2O in the liquid phase. Additionally our approach of populational 2D IR spectroscopy not only provides anharmonic constants, but in particular reveals that the knowledge of the comprehensive relaxation scheme is crucial for the critical evaluation of transient IR spectroscopy, because hot band transitions from populated levels to combination modes may influence strongly the transient signals in quite different spectral regions. The results will be presented in detail in a forthcoming publication [7]. The 2D-IR-spectroscopy using vibrational population will be of particular interest for future structural studies on larger (biological) molecules.

References

1. A. J. Lock, S. Woutersen, and H. J. Bakker, J. Phys. Chem. A **105**, 1238, 2001.
2. A. Pakoulev, Z. Wang, Y. Pang, and D. D. Dlott, Chem. Phys. Lett. **380**, 404, 2003.
3. H. Graener, G. Seifert, and A. Laubereau, Chem. Phys. **175**, 193, 1993.
4. R. Rey and J. T. Hynes, J. Chem. Phys. **104**, 2356, 1996.
5. G. Seifert, T. Patzlaff, and H. Graener, Phys. Rev. Lett. **88**, 147402, 2002.
6. G. Seifert, T. Patzlaff, and H. Graener, J. Chem. Phys. **120**, 8866, 2004.
7. G. Seifert, T. Patzlaff, and H. Graener, to be published.

On the orientational relaxation of HDO in liquid water

Y. L. A. Rezus and H. J. Bakker
FOM institute for Atomic and Molecular Physics,
Kruislaan 407, 1098 SJ Amsterdam, The Netherlands

Introduction

Liquid water plays an important role in many biological and chemical processes, varying from simple acid-base reactions to the folding of complex proteins. It is generally believed that many of the special properties of water arise as a consequence of its unique structure that comprises a three-dimensional network of molecules, held together by hydrogen bonds. This network is highly dynamic: hydrogen bonds continuously stretch, contract, break and reform, all on a subpicosecond to picosecond timescale.

The dynamical properties of the hydrogen-bond network can be elegantly studied by polarization-resolved pump-probe spectroscopy of the OH-stretch vibration. This method allows one to monitor the orientational motion of individual water molecules. Because of the strong correlation between the OH-stretch frequency and the hydrogen-bond strength of a hydrogen-bonded molecule (figure 1), we can selectively study water molecules that have a particular hydrogen-bond strength, e.g. those molecules that are tightly bound or those that are weakly bound. This allows us to investigate an important question, namely whether the structural relaxation of water depends on the local properties of the hydrogen-bond network or only on its global properties.

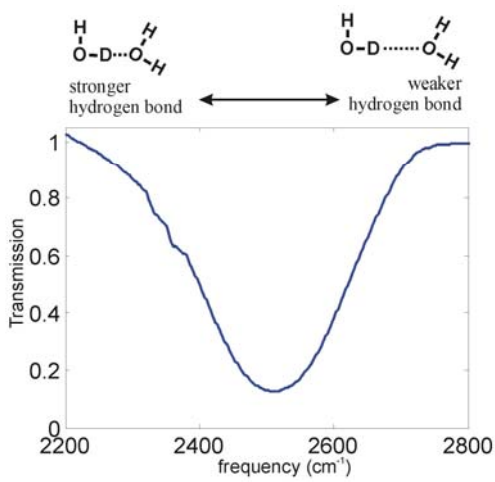

Figure 1. Infrared transmission spectrum of the OD vibration of HDO in H_2O. The band shows strong inhomogeneous broadening, the absorption frequency of a particular HDO molecule depending strongly on the strength of its hydrogen bond. By probing at different frequencies in the spectrum we can selectively monitor HDO molecules with a particular hydrogen-bond strength.

Here we report on the measurement of the reorientation rate of HDO molecules dissolved in H_2O as a function of the OD-stretch frequency.

Results and discussion

Figure 2 shows the anistropy decay of the bleach of the OD vibration of HDO dissolved in H_2O. The anisotropy decays monoexponentially with a time-constant of 2.5 ps, which corresponds to the second order rotational correlation time of the HDO molecule.

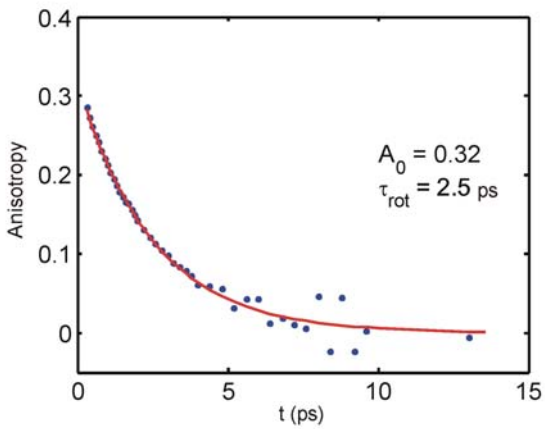

Figure 2. Anisotropy decay of the bleach of the OD vibration of HDO in H_2O. The solid line is a monoexponential fit with a time-constant of 2.5 ps. The initial value of the anisotropy deviates significantly from the maximum value of 0.4 that is expected for an electric dipole transition.

The initial value of the anisotropy deviates significantly from the theoretically expected value of 0.4. This indicates the possible presence of an unresolved fast component in the orientational dynamics of water, which may correspond to the inertial motion of water molecules. In order to estimate the amplitude of this motion we assume that it leads to a scrambling of the orientation of an OD dipole over a cone with semi-angle θ_0. It can be shown that this process leads to a decrease of the initial value of the anisotropy from 0.4 to[1]

$$A_0 = \frac{2}{5}\left[\frac{1}{2}\cos\theta_0(1+\cos\theta_0)\right]^2$$

From the observed initial value of 0.32 we thus deduce a cone semi-angle of approximately 20º.

Comparison with HDO in D_2O

It is interesting to compare the time-constant of 2.5 ps with the time-constant that was previously reported for the reorientation of the OH vibration of HDO in D_2O (3 ps), which is a system that can be regarded to be complementary to the system we studied.[2] At first sight it may seem surprising that the OD vibration reorients faster than the OH vibration, as its moment of inertia is almost twice as large. However, one should realize that in the diffusive limit the rotational brownian motion of a molecule is fully determined by collisions with the solvent molecules. This is expressed by the Debye-Stokes-Einstein relation, which relates the (first order) rotational correlation time τ_1 of a molecule to the solvent viscosity η

$$\tau_1 \propto \frac{\eta}{T}$$

where T is the absolute temperature. From the viscosities of H_2O and D_2O (0.9 mPa s and 1.1 mPa s, respectively) one expects a ratio of 0.8 for the reorientation times of the OH and OD vibrations, which is identical to the measured ratio. This agreement indicates that the orientational relaxation of water molecules is diffusive.

---

[1] G. Lipari and A. Szabo, Biophys. J. 30, 489 (1980)
[2] Nienhuys et al. J. Chem. Phys. 112, 8487 (2000)

Frequency dependence

Figure 3 shows the reorientation time constant as a function of the OD-stretch frequency. Apparently there is no marked frequency-dependence: weakly bound HDO molecules reorient with the same time-constant as strongly bound molecules.

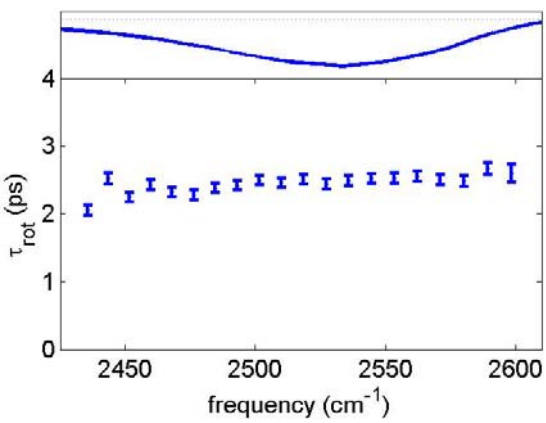

Figure 3. Reorientation time-constant of HDO in H_2O vs. the frequency of the OD-stretch vibration. The top panel shows the transient spectrum.

This behavior contrasts with that previously reported for the HDO/D_2O system. For this system the anisotropy was found to decay faster on the blue side of the spectrum than on the red side. We offer a tentative explanation that accounts for these observations. We assume that the barrier for reorientation is so high that even the most weakly bound hydroxyl groups cannot overcome this barrier by thermal activation alone. The majority of the hydroxyl groups can therefore only reorient if the entire network reorganizes. However, for the weakly bound OH groups we can envision an additional mechanism by which they can reorient, namely that of tunneling through the potential barrier. As the tunneling probability decreases exponentially with the effective mass of the hydroxyl group and the height of the energy barrier, this mechanism will only play a substantial role in the reorientation of the weakly bound OH groups and will not affect the reorientation of the OD groups. Recent calculations[3] indeed show that this quantum effect leads to a broader distribution of hydrogen-bond angles for H_2O than for D_2O.

Conclusion

We studied the orientational dynamics of HDO molecules dissolved in H_2O by probing the anisotropy of the excitation of the OD vibration, and found the reorientation of HDO molecules to occur with a time constant of 2.5 ps and not to depend on the frequency of the OD-stretch vibration. A comparison with studies on the complementary system of HDO in D_2O shows that the *picosecond* orientational dynamics of water are diffusive, in the sense that they follow the Debye-Stokes-Einstein relation. The *subpicosecond* dynamics, on the other hand, may very well involve inertial motion with a maximum rotation angle of 20º, as is suggested by the observed initial value of the anisotropy of 0.32. Whereas the orientational dynamics of HDO in D_2O are known to display a marked frequency dependence, those of HDO in H_2O show no frequency dependence whatsoever. We have provided a tentative explanation for this phenomenon, in which the reorientation of part of the OH groups is assisted by tunneling.

[3] L. H. de la Pena and P. G. Kusalik, J. Chem. Phys. 121, 5992 (2004)

Vibrational dynamics of the CD3ζ membrane peptide studied with 2D IR spectroscopy

Prabuddha Mukherjee,* Itamar Kass,† Isaiah Arkin,† and Martin T. Zanni*

*Department of Chemistry, University of Wisconsin, Madison, WI 53706
†Department of Biological Chemistry, Hebrew University, Givat-Ram, Jerusalem, 91904, Israel

Membrane peptides serve a variety of functions in cell biology including acting as antimicrobial drugs and as models for the transmembrane segments of proteins. In this talk, experiments will be presented using heterodyned 2D IR spectroscopy and $^{13}C{=}^{18}O$ isotope labeling to study the conformational and environmental heterogeneity of a 27-residue peptide in lipid vesicles that encompasses the transmembrane domain of the T-cell receptor CD3 . In membranes, this peptide forms a tetramer transmembrane helical bundle with the helices pointing 12° to the membrane normal. Using $^{13}C{=}^{18}O$ isotope labeling, the amide I modes of 10 different residues have been labeled along the length of the peptide spanning the width of the membrane. The $^{13}C{=}^{18}O$ label shifts the amide I band about 60 cm^{-1}, spectrally isolating it from the remaining residues. For each of the 10 residues, heterodyned 2D IR spectra have been collected using an echo pulse sequence and each spectrum has been fit to extract the inhomogeneous and homogeneous linewidths. We find that the homogeneous linewidths of all the labeled residues are the same to within our resolution, but that the inhomogeneous linewidth of residues near the center of the peptide are narrower than for residues at the ends. The data are interpreted based on a structural model of the bundle, the heterogeneous environment of the membrane itself, and with a force-force correlation function calculated from molecular dynamics simulations.

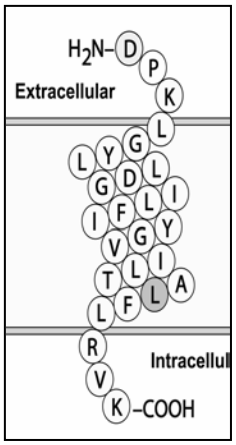

Fig. 1. Sequence of the CD3 peptide.

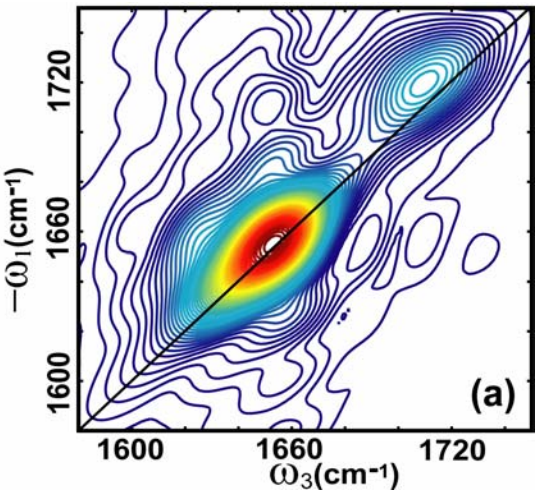

Fig. 2. 2D IR spectrum of the the CD3 peptide in lipid vesicle.

Ultrafast vibrational heating of ice I_h : a novel transient state of overheated ice

H. Iglev, M. Schmeisser, A. Thaller, and A. Laubereau

Physik-Department, Technische Universitaet Muenchen, Germany

Because of its profound role in nature, considerable experimental and theoretical efforts have been invested up to the present time to explain the anomalous properties of ice, water clusters and liquid water. Nevertheless, the comprehension of the phase transition processes, e.g. the melting of ice, is fragmentary. Towards the goal of a microscopic understanding we have performed for the first time ultrafast temperature jump measurements in hexagonal ice at ambient pressure. The isotopic mixture HDO : D_2O (15 M) is studied, pumping the hydroxilic stretching vibration, OH or OD, of a thin crystalline platelet (about 2 microns) with resonant subpicosecond pulses in the mid-infrared. The OH-and OD-stretching vibrations are monitored with polarization resolution as fast, highly sensitive spectral probes for the local temperature and structure. Calibration of this picosecond OH- and OD-thermometer is performed by comparison with careful stationary measurements under identical conditions (blocking the pump pulse) and conventional FTIR spectroscopy. Starting at 200 K, our probe spectra verify that the vibrational energy is quickly equilibrated with a time constant of 8.7 ps, leading to a long-lived (hundreds of picoseconds), isochoric temperature change of approximately 20 K (and corresponding pressure increase) for our pumping conditions.

Of special interest are the measurements for the same pumping conditions but initial temperature of 270 K. Transient breaking of hydrogen bonds is suggested by our polarization-resolved probe spectra, but no evidence for (partial) melting of the excitation volume is observed. In fact, simple energy arguments indicate that the deposited excitation energy covers only less than 10 percent of the required latent heat of melting, i.e. a bulk phase transition is not possible. Our time-resolved vibrational spectra, however, strongly suggest overheating of the crystalline HDO:D_2O sample to 290 K, approximately 15 K above the steady state melting point (274.7 K), not previously observed for ice. The simultaneous pressure increase accompanying the isochoric heating of is estimated to approximately 300 bar. The lifetime of the novel overheated ice state exceeds 200 ps.

TRVS XII

NIST National Institute of Standards and Technology

Washington, D.C.

May 23-27, 2005

TRVS Theory

Nonlinear Vibrational Response of the Amide I, II, III and A Bands of NMA: Simulation Study Based on an Electrostatic DFT Map

Tomoyuki Hayashi, Wei Zhuang, and Shaul Mukamel
Department of Chemistry, University of California, Irvine, California 92697, USA

Coherent multidimensional infrared spectroscopy provides a valuable tool for protein structure determination[1]. The amide infrared absorption bands originating from stretching and bending of the peptide bonds provide a useful probe for secondary-structure changes because of their sensitivity to hydrogen bonding, dipole-dipole interactions and geometry of the peptide backbone. Most effort has been focused on the Amide I band[2-4] and its cross peaks[5]. However, the cross peak pattern of other amide bands can provide additional structural information. In this paper we simulate the photon-echo signals of the amide I, II, III and A bands in N-methyl acetamide (NMA), which is the simplest model for the amide system.

MD simulations were performed using the CHARMM force field for NMA and TIP3 water at constant temperature (300 K) and volume (NVT) using the CHARMM package. One NMA and 1000 water molecules were held rigid using the SHAPE and SHAKE algorithms respectively.

The fluctuating vibrational Hamiltonian was constructed using an electrostatic model[6,7], which includes the fundamental and overtone frequencies of each of the four amide vibrations, their combination bands, and the transition dipole matrix. The fundamental frequency of each amide vibration is given by $\varepsilon(E) = \varepsilon_{gas} - \delta\varepsilon(E)$ where ε_{gas} is the experimental frequency of an isolated NMA in the gas phase. To calculate the fluctuation $\delta\varepsilon(E)$, we first carried out geometry optimization of an isolated NMA at the BPW91/6-31G(d,p) DFT level using Gaussian03. The middle point of the carbonyl oxygen and the amide Hydrogen of the optimized structure was chosen as a reference point. . A DFT map was constructed which relates $\delta\varepsilon(E)$ to a 19 component vector $\mathbf{C}^T \equiv (E_x, E_y, E_z, E_{xx}, \cdots, E_{xxx}, \cdots)$ representing all independent components of the electric field, its gradients and second derivatives at the reference point**:**

$$\delta\varepsilon(E) = \mathbf{O}_\alpha^{\nu(1)T}\mathbf{C} + \frac{1}{2}\mathbf{C}^T\mathbf{O}^{\nu(2)}\mathbf{C},$$

where $\mathbf{O}^{(1)}$ is a 19 component row vector and $\mathbf{O}^{(2)}$ is a 19x19 matrix, both obtained from the DFT calculations. For each configuration along the 1 fs timestep 1 ns trajectory, three electric field components at 67 points in space which span the transition charge density region of the amide modes [figure 2 in ref5] were calculated. The components of C^T were determined at each time point by a least-square fit to the electric field sampled at these 67 points. C^T calculated using this protocol represents the electric field distribution across the transition charge density region. A similar map was created for the diagonal anharmonicities and transition dipoles.

The resulting map provides the entire fluctuating Hamiltonian required for simulations of third order spectra (fundamental and overtone frequencies as well as the transition dipole magnitudes and directions) from first principles. It has several advantages over other empirical maps which predict the linewidth with comparable accuracy[7,8]. First, it gives a clear physical picture for the origin of the solvent shift of the amide bands; we found that the global sampling of the spatially nonuniform electrostatic field across the region of transition charge densities (TCDs) of amide modes is essential for the accurate prediction of solvent shifts[5].

Second, the map is not optimized to a particular solvent or solvent environment and is therefore transferable.

The third-order response functions were calculated using the cumulant expansion of Gaussian fluctuations model (CGF) [1]. The photon-echo signal $S(\omega_1, t_2 = 0, \omega_3)$ was obtained by 2-D Fourier transform with respect to the time delays t_1 and t_3 (shown in Fig. 1) by selecting the resonant transitions assuming rectangular frequency pulse shapes with bandwidth of 250 cm^{-1} within the rotating wave approximation. $|S(\omega_1, t_2 = 0, \omega_3)|$ in two frequency regions are displayed in Fig. 2. In the left panel the three incident pulses are tuned to 1500 cm^{-1}. The diagonal and off-diagonal peaks of amide I, II, and III are observed at $(\omega_1, \omega_3) = (-1670,1670), (-1515,1515), (-1293,1293), (-1515,1670), (-1293,1670), (-1293,1515)$. In the right panel where the third pulse is tuned to 3300 cm^{-1}, cross peaks of amide A with amide I, II and III modes are observed at $(\omega_1, \omega_3) = (-1670,3450), (-1515,3450), (-1293,3450)$. The amide A band is hidden underneath the broad O-H stretch band of water, nevertheless its cross-peaks with the amide I, II and III modes can be observed in the photon echo signal. The imaginary part of the diagonal amide I, II and III photon echo peaks and their cross peaks are displayed in Fig. 3. The elliptical elongated peak shapes indicate that the broadening is inhomogeneous. The negative and positive peaks along ω_3 come from stimulated emission and ground state bleach respectively. Anharmonic shifts of amide I, II and III defined as the frequency differences between the two peaks are 17 cm^{-1}, 13 cm^{-1} and 13 cm^{-1} respectively. The calculated diagonal and off-diagonal anharmonicities of amide modes of NMA in water are listed in Table. 1. The anharmonic shifts of amide I and III are larger than these anharmonicities due to interference between the two peaks. Only the amide I and II cross peak shows a positive peak at larger ω_3 due to its negative anharmonicity. The simulated linewidths of the amide I, III and A bands are in good agreement with experiment. The amide II liewidth is underestimated. One possible reason is that its highly delocalized transition charge density extends over regions of the amide and methyl groups which are not sampled in the present simulations.

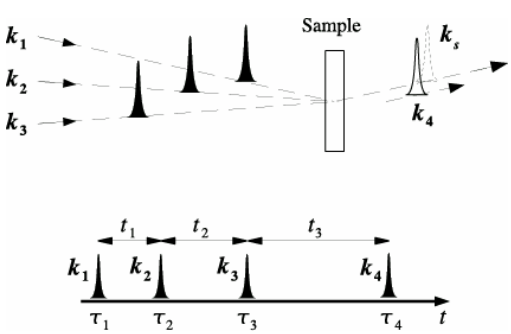

Fig. 1 Laser pulse sequence (upper panel), the peak ordering and time variables (lower panel) in the photon echo experiment. $\mathbf{k}_s = -\mathbf{k}_1 + \mathbf{k}_2 + \mathbf{k}_3$.

Table 1. Diagonal and off-diagonal anharmonicities (in cm^{-1})

	I	II	III
I	14.3	-3.1	19.7
II		13.0	11.0
III			10.7

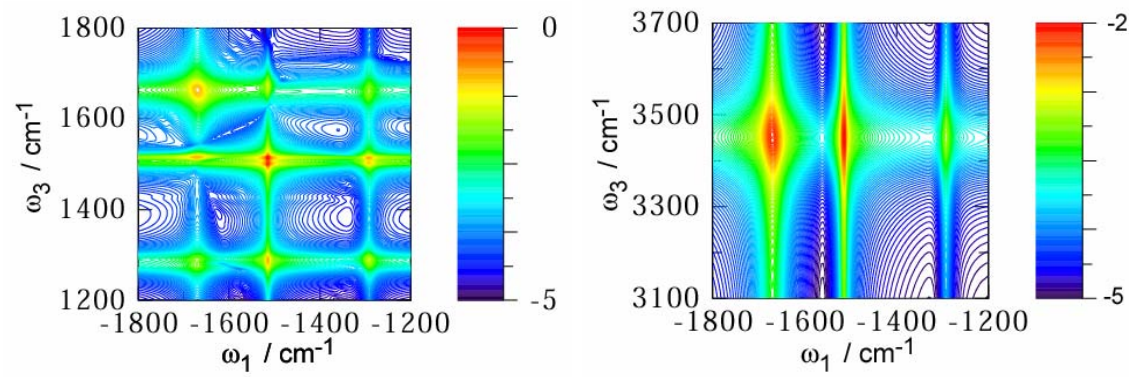

Fig. 2: Photon echo signals $\log|S(\omega_1, t_2 = 0, \omega_3)|$ of NMA. Left: The amide I, II, III frequency region; right: cross peaks between amide A (ω_3) and amide I, II, III(ω_1)

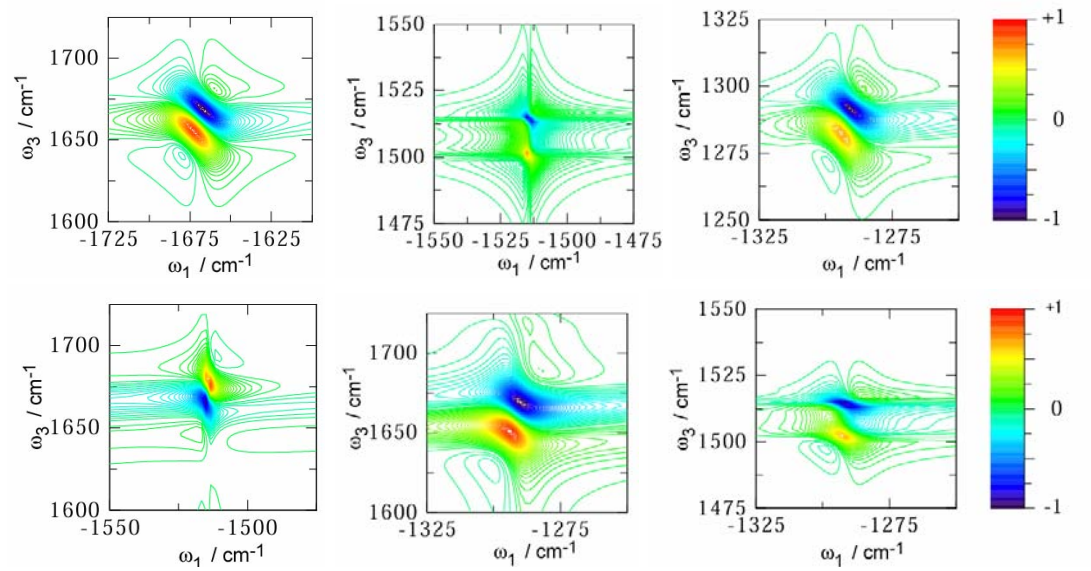

Fig. 3: Photon echo spectra $\mathrm{Im}[S(\omega_1, t_2 = 0, \omega_3)]$. Top: Diagonal peaks; amide I (left), II (center), III (right). Bottom: cross peaks; I-II (left), I-III (center), II-III (right).

The support of the National Institutes of Health grant no. (RO1GM59230-04) and the National Science Foundation grant no. (CHE-0446555) is gratefully acknowledged.

1. D. Abramavicius and S. Mukamel, *Chem. Rev.* **104**, 2073 (2004)
2. P. Hamm, M. Lim, W. F. DeGrado, and R. M. Hochstrasser, *PNAS,* **96**, 2036 (1999)
3. A. Moran, S. -M. Park, J. Dreyer, and S. Mukamel, *J. Chem. Phys*. **118**, 3651 (2003)
4. M. F. DeCamp, L. DeFlores, J. M. McCracken, A. Tokmakoff, K. Kwac, M. Cho, *J. Phys. Chem. B* **109**, 11016 (2005)
5. I. V. Rubtsov, K. Kumar, R. M. hochstrasser, *Chem. Phys. Lett*. **402**, 439 (2005)
6. T. Hayashi, W. Zhuang, and S. Mukamel, *J. Phys. Chem. A* (in press) "Electrostatic DFT Map for the Complete Vibrational Amide Band of NMA"
7. T. Hayashi, T. l. Jansen, W. Zhuang, and S. Mukamel, *J. Phys. Chem. A* **109**, 64 (2005)
8. S. A. Corcelli, C. P. Lawrence, and J. L. Skinner, *J. Chem. Phys*. **120**, 8107 (2004)

Time- and Frequency-Domain Vibrational Spectroscopy of Water

J. L. Skinner

Department of Chemistry

University of Wisconsin

Madison, WI 53706

A combined electronic structure/molecular dynamics approach was used to calculate infrared and isotropic Raman spectra for the OH or OD stretches of dilute HOD in D2O or H2O, respectively. The quantities needed to compute the infrared and Raman spectra were obtained from density functional theory calculations performed on clusters, generated from liquid-state configurations, containing an HOD molecule along with 4-9 solvent water molecules. The frequency, transition dipole, and isotropic transition polarizability were each empirically related to the electric field due to the solvent along the OH (or OD) bond, calculated on the H (or D) atom of interest. The frequency and transition dipole moment of the OH (or OD) stretch of the HOD molecule were found to be very sensitive to its instantaneous solvent environment, as opposed to the isotropic transition polarizability, which was found to be relatively insensitive to environment. Infrared and isotropic Raman spectra were computed within a molecular dynamics simulation by using the empirical relationships and semiclassical expressions for the line shapes. The line shapes agree well with experiment over a temperature range from 10 to 90 C.

In the context of vibrational spectroscopy in liquids, this dependence of the vibrational transition dipole moment of a particular molecule on the rotational and translational coordinates of all the molecules in the liquid is referred to as a non-Condon effect. For strongly hydrogen-bonded systems such as liquid water, these non-Condon effects are large. That is, the bond dipole derivative of an OH stretch depends strongly on its hydrogen-bonding environment. Previous calculations of non-linear vibrational spectroscopy in liquids have not included these non-Condon effects. We find that for water, inclusion of these effects is important for an accurate calculation of, for example, homodyned and heterodyned three-pulse echoes. Such echo experiments have been "inverted" to obtain the OH stretch frequency time-correlation function, but by necessity the Condon and other approximations are made in this inversion procedure. Our conclusion is that for water, primarily because of strong non-Condon effects, this inversion may not lead to the correct frequency time-correlation function. Nevertheless, one can still make comparison between theory and experiment by calculating the experimental echo observables themselves.

On the time evolution of vibronic spectra coupled to an electronic solvation process in water

By

Sighart F. Fischer and Wolfgang Dietz
Physik Department
Technical University of Munich
85747 Garching Germany

Abstract:

The s – p absorption spectrum for an electron is considered during the initial solvation process, where the transition energy is comparable to the O-H stretching vibrations of the water molecules.
The model considers the time evolution of the electronic state including the selfconsistent coupling to librational modes and the transition dipole – transition dipole couplings between the electronic and the randomly distributed O-H stretching vibrations. The properly averaged spectra have Fano type character and compare well to experimental data [R. Laenen, T. Roth and A. Laubereau, Phys.Rev.Letters **85** 50 (2000)].

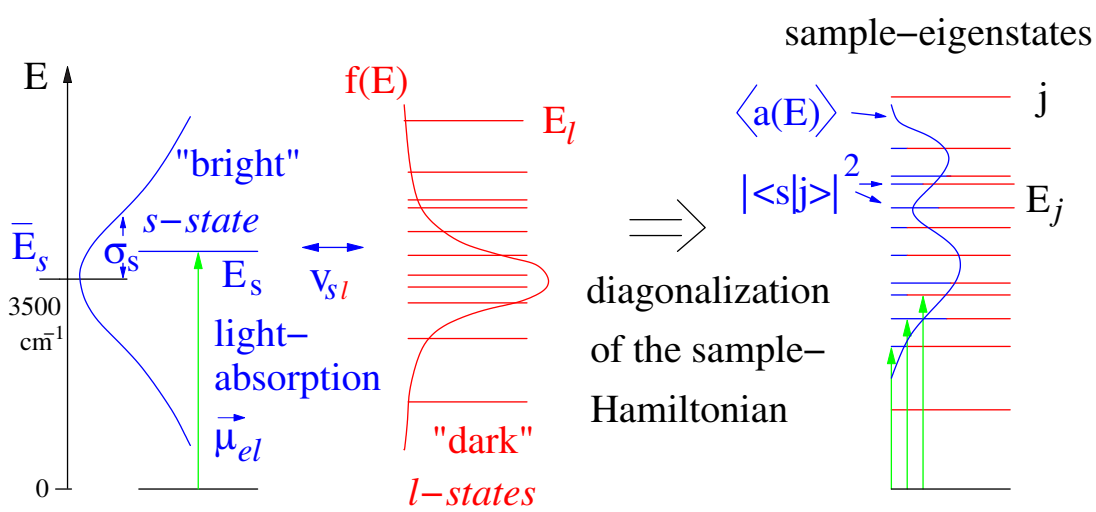

We consider a model system (Fig. 1) consisting of a bright state, which carries strong oscillator strength wth an energy E_s a width $2\sigma_s$, and a transition dipole $\vec{\mu}_{el}$. It couples with the matrix elements v_{sl} to a manifold of l-states with

energies E_l that carry little oscillator strength and are denoted as dark states. Their energies are distributed randomly with a distribution function $f(E)$. Also the couplings are random variables. The goal is to study the lineshape function $a(E)$ and its average $\langle a(E) \rangle$.

The application will be twofold. In the first part we consider the time dependent sovation process of an electron in a polar medium. Starting from the delocalized state, an s-type state will be formed, with a time dependent width and an increasing s – p transition energy denoted as E_s. As this energy passes through the energy regime of the spectrum of the 0-H stretching modes of the solution water molecules, the electronic transition couples to the vibrational modes via a Förster type mechanism and a complex time dependent spectrum evolves. This system can be studied in the so called mean coupling limit, which applies if the coupling moments of higher than second order are relatively small. In a second application we refer to a limit of a localized excitation where the couping has to be studied in detail. An example is the low temperature energy fluctuation in proteins, which is dominated by long range transition dipole couplings between two level systems. Its correlation function decays as $\exp\{-(t/\tau)^{1/2}$, which is observed in holeburning experiments by J.Schlichter, V.V.Ponkratov and J. Friedrich, Fizika Nizkih Temp 29, 1054 (2003).
. Our model hamiltonian reads

$$H = |s\rangle E_s \langle s| + \sum_{l=1}^{N} |l\rangle E_l \langle l| + \sum_{l=1}^{N} |s\rangle v_{sl} \langle l| + \sum_{l=1}^{N} |l\rangle v_{ls} \langle s| \quad . \tag{1}$$

The line shape function is

$$a(E) = \sum_{j=1}^{N+1} |\langle s|j\rangle|^2 \delta(E - E_j) \quad , \tag{2}$$

where j labels the eigenstates. Its ensemble average can be expressed by the integral,

$$\langle a(E) \rangle = \mathrm{Re}\{\int_0^\infty dk \exp\{ik(E - E_s) - ik\Delta(E,k) - k\Gamma(E,k)\} \tag{3}$$

with the ensemble levelshift-functions

$$\Delta(E,k) = -Nk^{-1}\left\langle \int_{-\infty}^{\infty} \sin\left(\frac{kv^2}{E_l - E}\right) f(E_l)\, dE_l \right\rangle_v \tag{4}$$

and

$$\Gamma(E,k) = Nk^{-1}\left\langle \int_{-\infty}^{\infty} \left[1 - \cos\left(\frac{kv^2}{E_l - E}\right)\right] f(E_l)\, dE_l \right\rangle \quad . \tag{5}$$

For the solvated electron we take for the coupling the form

$$v_{sl}(r) = \left\{ \begin{array}{l} v_0 \\ \alpha / r^3 \end{array} \; if \begin{array}{l} r \le r_0 \\ r > r_0 \end{array} \right. \quad , \tag{6}$$

Where r_0 is the radius of the solvating electron. It is about 6Å for the interesting coupling regime of strong overlap of the electronc and the vibrational spectra. At this point in time many water molecules fall in the regime of a sphere spanned by r_0 and the mean-coupling approximation can be justified, leading to the following averaged spectral line shape function

$$\langle a(E) \rangle = \frac{\Gamma(E)/(2\pi)}{[E - E_s - \Delta(E)]^2 + \Gamma(E)^2/4} \tag{7}$$

with level shift and damping parts

$$\Delta(E) = PV \int_{-\infty}^{\infty} \left\langle \frac{\sum_l f(E_l) v_{sl}{}^2}{E - E_l} \right\rangle_v dE_l \tag{8}$$

and

$$\Gamma(E) = 2\pi \left\langle \sum_l v_{sl}{}^2 \right\rangle_v f(E) \quad , \tag{9}$$

where PV denotes Cauchy's principle value and $\left\langle \sum_l v_{sl}^{\ 2} \right\rangle_v f(E)$ is the ensemble mean of the coupling-weighted density of states. Finally, via the convolution of $\langle a(E) \rangle$ with a gaussian electronic broadening of variance $\sigma_s^{\ 2}$ we get the absobance of the sovated electron. The results are shown together with the experimental ones by Laenen et. al. in the figure below.

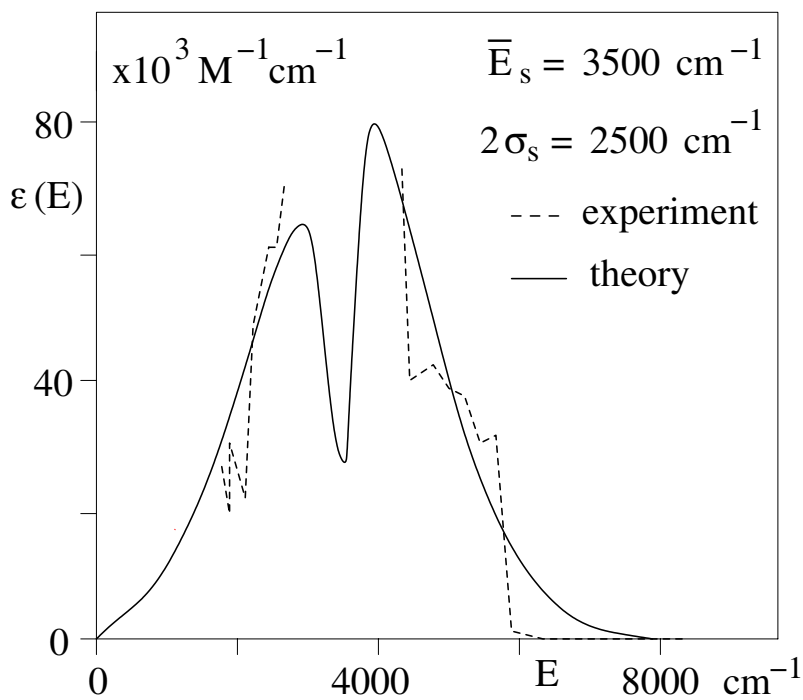

Next we consider the detailed-coupling limit, where all moments of the coupling have to be incorporated. For a coupling with a radial dipole dependence [Eq.(6) with $r_0 = 0$] the ensemble level shift functions (4) and (5) in this limit write

$$\Delta(E,k) - i\Gamma(E,k) = ik^{-1}\rho \left\langle \int_0^\infty 4\pi r^2 [\exp(-y^2) - 1] dr \right\rangle_{E_l} \tag{10}$$

where ρ is the mean density of the dipoles in space and

$$y = \frac{\alpha}{r^3}\left(\frac{ik}{E - E_l}\right)^{1/2} \quad . \tag{11}$$

For a suffiiciently smooth background energy distribution $f(E)$, which is also broad compared to the coupling at the mean of the next neighbour distance,
the ensemble line shape can be brought into the form

$$\langle a(E)\rangle = \pi^{-1}\,\mathrm{Im}\left\{\frac{\sqrt{\pi}\lambda\exp(\lambda^2)erfc(\lambda) - 1}{E - E_s}\right\} \tag{12}$$

with

$$\lambda = \frac{2i}{3}\pi^{3/2}\rho\alpha\frac{\left\langle (E_s - E_l)^{-1/2}\right\rangle_{E_l}}{(E - E_s)^{1/2}} \tag{13}$$

and the Fourier transform gives for the average decay of the s-state

$$\langle\langle s|s(t)\rangle\rangle = \exp[-(\frac{t}{\tau})^{1/2}] \tag{14}$$

This correlation function can explain the observed time dependence of a hole burnt in the excitation spectrum of a porphyrin-like molecule in a protein.

Theoretical studies of the amide I vibrational frequencies of peptides and proteins

Tim M. Watson & Jonathan D. Hirst

School of Chemistry, University of Nottingham, University Park,

Nottingham NG7 2RD, United Kingdom. Email: jonathan.hirst@nottingham.ac.uk

In this paper, we describe our recent theoretical studies of the amide I band of peptides and proteins. The amide I mode in peptides is primarily the stretching mode of the carbonyl bond. The band that arises from the interaction of many amide I vibrations in a polypeptide leads to a distinct profile in the infrared spectrum between 1600 cm^{-1} and 1700 cm^{-1}, which reflects the local, regular secondary structure in the protein. The spectroscopy of peptides in this region has attracted much attention recently, due to the time-resolution with which measurements can be made, and the information that these can provide on folding and unfolding conformational changes on nanosecond timescales, as demonstrated by the pioneering studies of Callender, Woodruff and Dyer and others [1]. Such timescales are increasingly accessible to classical molecular dynamics simulations, and there is growing interest in improving the realism of simulations of unfolding events, such as the acid induced unfolding of apomyoglobin [2]. Accurate calculations of the amide I band from first principles or indeed other spectroscopic properties would provide a direct link between experiment and simulation [3], allowing

new hypotheses regarding important conformational transitions in the folding process to be posed and tested.

Our earlier work focused on density functional theory (DFT) calculations on model hydrogen-bonded complexes [4]. However, such calculations will not be feasible for full proteins in the near future, especially when one is likely to need to consider an ensemble of structures, due to the conformational flexibility of these large biomolecules. Nevertheless, quantum chemical calculations can inform more approximate approaches and in this paper, we discuss recent DFT calculations on model hydrogen-bonded complexes and their use in the 'floating oscillator' model introduced by Krimm [5] for the calculation of protein vibrational spectra. Torii and Tasumi [6] applied this approach to proteins over a decade ago. We have re-visited their work [7], and codified some of the methodology, to make it more robust and applicable to larger data sets of proteins.

Most recently, we have examined how point charge environments can mimic features of proteins. DFT vibrational frequency calculations on conformers of *trans*-N-methylacetamide + D_2O clusters, and various dipeptides were used to parameterize a seven–site model [8] for predicting the diagonal force constants of the amide I mode of arbitrary polypeptides at the EDF1/6-31+G* level. The ultimate aim of the work is to improve the accuracy of the simple 'floating oscillator' method for calculating the amide I band profiles of proteins. To test the model, we determined the vibrational frequencies of the low energy conformers of the pentapeptide, [Leu]-enkephalin at the EDF1/6-31+G* level. The model reproduced the DFT diagonal force constants well [8]. We then develop a general automated strategy for applying the transition dipole coupling method for computing the IR spectra of proteins.

References

[1] Gilmanshin R, Williams S, Callender RH, Woodruff WH & Dyer RB (1997). Fast events in protein folding: Relaxation dynamics of secondary and tertiary structure in native apomyoglobin. *Proc Natl Acad Sci, USA*, **94**, 3709-3713.

[2] Onufriev A, Case DA & Bashford D (2003). Structural details, pathways, and energetics of unfolding apomyoglobin. *J Mol Biol*, **325**, 555-567.

[3] Hirst JD, Bhattacharjee S & Onufriev AV (2003). Theoretical studies of time-resolved spectroscopy of protein folding. *Faraday Discussions*, **122**, 253-267.

[4] Watson TM & Hirst JD (2002) DFT vibrational frequencies of amides and amide dimers. *J Phys Chem A*, **106**, 7858-7867; Watson TM & Hirst JD (2003). Influence of electrostatic environment on the vibrational frequencies of proteins. *ibid*, **107**, 6843-6849.

[5] Krimm S & Abe Y (1972) Intermolecular Interaction Effects in the Amide I Vibrations of β Polypeptides. *Proc Natl Acad Sci, USA*, **69**, 2788-2792.

[6] Torii H & Tasumi M (1992). Model calculations on the amide I infrared bands of globular proteins. *J Chem Phys*, **96**, 3379-3387.

[7] Watson TM & Hirst JD (2004). Calculating vibrational frequencies of amides: from formamide to concanavalin A. *Phys Chem Chem Phys*, **6**, 998-1005.

[8] Watson TM & Hirst JD (2005). Theoretical studies of the amide I vibrational frequencies of [Leu]-enkephalin. *Mol Phys*, **103**, 1531-1546.

Semiclassical Theory for Femtosecond Nonadiabatic Molecular Dynamics.

Vladimir Chernyak
Department of Chemistry, Wayne State University

Nonadiabatic vibrational dynamics in the vicinity of the electronic energy surface crossing is a key to understanding many fundamental processes in photophysics and photochemistry including radiativeless energy relaxation and photoisomerization in (bio) molecules, and conformational dynamics of Jahn-Teller centers. Nonadiabatic effects in vibrational dynamics being intrinsically quantum are traditionally addressed using quantum mechanical calculations which are numerically demanding (and often intractable), especially in the case of molecular dynamics in condensed phase.

We apply a semiclassical approach to the scattering problem of a vibrational wavepacket in the vicinity of a conical intersection of electronic energy surfaces and derive analytical expressions for scattering amplitudes. The latter are valid when the scattering length that scales as $\sqrt{\hbar}$ is small and the wavepacket passes the conical intersection balistically. The analytical results agree very well with direct numerical simulations for a realistic set of parameters.

Direct Observation of Ultrafast Hopping of Surface Molecules

Ellen H.G. Backus[1] and Mischa Bonn[1,2]
[1] *Leiden Institute of Chemistry, Leiden University, P.O. Box 9502, 2300 RA Leiden, The Netherlands*
[2] *FOM Institute for Atomic and Molecular Physics, Kruislaan 407, 1098 SJ Amsterdam, The Netherlands*

Diffusion of molecules on surfaces is a key step in surface (catalytic) reactions, as it provides the driving force for, for example, combining adsorbed reactants on the surface. Whereas in conventional catalysis diffusion is governed by thermal processes, non-thermal control of surface diffusion has received much attention, e.g. for the potential growth of novel materials. Recent Scanning Tunneling Microscope (STM) experiments have demonstrated controlled diffusion of molecules on a surface, induced by electrons, provided by either the STM tip or a femtosecond laser pulse[1]. Although this STM detection scheme provides excellent spatial resolution, information on the timescales of the hopping process, i.e. time resolution, is lacking.

Here, we report the real-time observation of the motion of carbonmonoxide (CO) molecules, initiated by a femtosecond laser pulse, on a single crystal platinum (Pt(533)) surface. Sub-200 fs temporal resolution is obtained by using femtosecond time-resolved vibrational sum-frequency generation, monitoring the internal C—O stretch vibration. Sub-nm spatial resolution is obtained indirectly, through the morphology of the surface: our platinum surface consists of 7 Ångstrom wide, flat terraces separated by monatomic steps. The differently bound CO molecules on the steps and terraces exhibit distinct vibrational frequencies, allowing us to quantitatively follow the time-dependent population of CO molecules on the terraces and the steps. Hopping of CO molecules from steps to terraces is induced by 800 nm pulsed excitation of the surface, with depopulation of step sites occurring on sub-picosecond timescales. At elevated temperatures diffusion from the terraces back onto the step sites can also be observed.

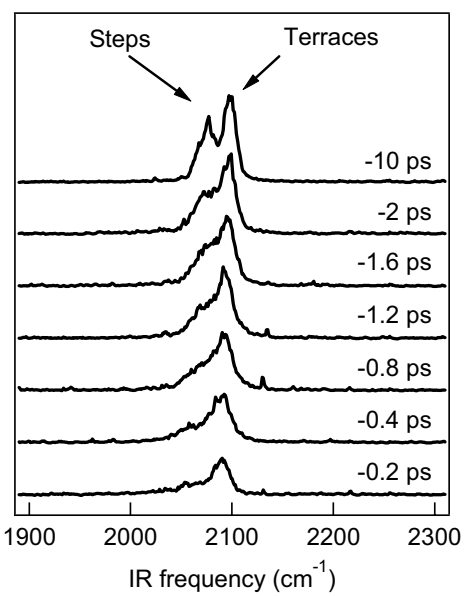

In conclusion, we have observed the ultrafast motion of CO molecules with spatial and time resolution using time-resolved vibrational sum-frequency generation on a stepped surface.

[1] T. Komeda, Y. Kim, B.N.J. Persson, and H. Ueba, Science **295**, 2055 (2002)
J.I. Pascual, N. Lorente, Z. Song, H. Conrad and H.-P. Rust, Nature **423**, 525 (2003)
L. Bartels, F. Wang, D. Möller, E. Knoesel, and T.F. Heinz, Science **305**, 648 (2004)

Solvent dependent ultrafast vibrational dynamics in tungsten complexes $W(CO)_{6-n}(CH_3CN)_n$ (n=0, 1) probed with sub-picosecond time-resolved infrared spectroscopy

Motohiro Banno (gen@chem.s.u-tokyo.ac.jp), Shin Sato (shin@chem.s.u-tokyo.ac.jp),
Koichi Iwata (iwata@chem.s.u-tokyo.ac.jp), and Hiro-o Hamaguchi (hhama@chem.s.u-tokyo.ac.jp)

Department of Chemistry and Research Centre for Spectrochemistry, School of Science,
The University of Tokyo, Hongo 7-3-1, Bunkyo-ku, Tokyo 113-0033, Japan

1. Introduction

To understand the mechanism of a chemical reaction in solution, it is essential to acquire the information on the molecular environment, which is determined by intermolecular interaction between the solute reactant molecule and the surrounding solvent molecules. Vibrational energy relaxation should be a good probe for the molecular environment because a vibraitonally excited molecule relaxes to the ground state by intra- and inter-molecular energy transfer. In this study, we observe a vibrational energy relaxation process and examine the relation between the molecular environment and the vibrational energy relaxation.

2. Experiment

We used sub-picosecond infrared pump-probe spectroscopy, in which both the pump and the probe pulses are resonant with a vibrational transition of the sample molecule. The pump pulse changes the vibrational population distribution and the probe pulse detects the absorbance change caused by the vibrational excitation. Time dependence of the bleaching of the ground state absorption indicates the vibrational energy relaxation from the first excited state v=1 to the ground state v=0. The estimated time resolution of our spectrometer is 200 fs, while the spectral width of the infrared laser pulse is 130 cm^{-1}.

We used normal alkane solutions (C_nH_{2n+2}; n=6 to 14) of two tungsten carbonyl complexes, $W(CO)_6$ and $W(CO)_5(CH_3CN)$, as the samples. We observed the vibrational energy relaxation of the triply degenerate CO stretch of $W(CO)_6$ and the doubly degenerate CO stretch of $W(CO)_5(CH_3CN)$. We studied the effect of the ligand and solvent on the relaxation rate systematically.

3. Results and discussion

The bleaching and its recovery of the ground state absorption of the triply degenerate CO stretch of $W(CO)_6$ are observed with the polarization relation of the pump light being parallel or perpendicular to the probe. The results in a heptane solution are shown in Fig. 1. The two recovery

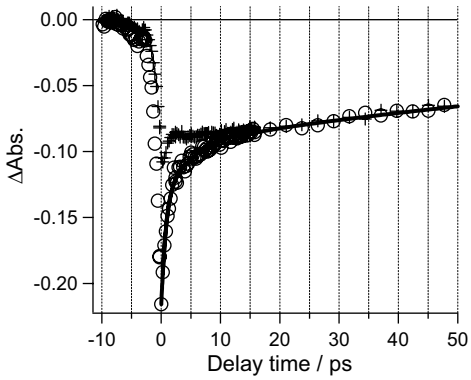

Fig. 1. Observed recovery curve of $W(CO)_6$, T_{1u} mode in heptzane. The polarization relation between pump and probe is parallel (open circle) and perpendicular (crossing).

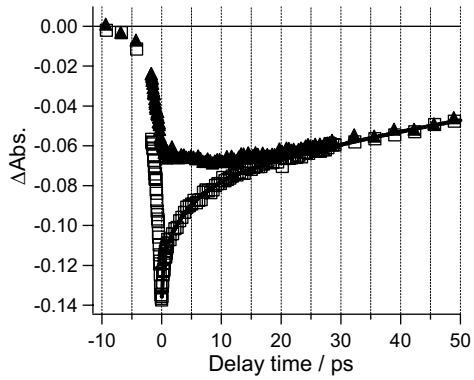

Fig. 2. Observed recovery curve of $W(CO)_5(CH_3CN)$, E mode in heptane. The polarization relation between pump and probe is parallel (open square) and perpendicular (filled triagle).

curves can be fitted well with the sum of three exponential functions with time constants τ_1 (0.7 ps), τ_2 (4.7 ps) and τ_3 (140 ps). The observed recovery curves of the doubly degenerate CO stretch of $W(CO)_5(CH_3CN)$ in heptane are shown in Fig. 2. The recovery curve is fitted with a triple exponential function with time constants τ_1 (0.7 ps), τ_2 (4.2 ps), and τ_3, (86 ps) for the parallel polarization measurement and with a double exponential function with time constants τ_2' (8.6 ps) and τ_3 (86 ps) for the perpendicular polarization.

The decaying component with the time constant τ_1 probably comes from fast intramolecular dynamics. The effect of perturbed free induction decay is also observed at negative time delays. Here, we do not discuss this fast component in details.

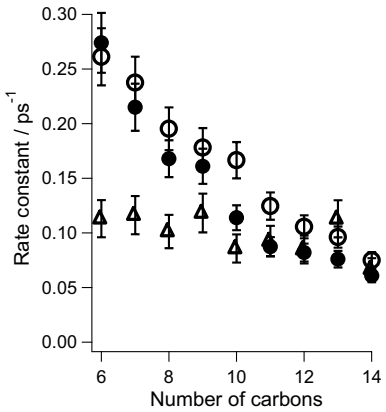

Fig. 3. Relation between the rate constants of anisotropic components, the inverse of $W(CO)_6$, τ_2 (filled circle), $W(CO)_5(CH_3CN)$, τ_2 (open circle), and $W(CO)_5(CH_3CN)$, τ_2' (open triangle), and the numbers of carbon atoms in a solvent alkane molecule.

In the time domain corresponding to τ_2, the absorbance difference (ΔAbs) values are different between the parallel and perpendicular polarizations. The absorption anisotropy disappears with the time constant τ_2. The alignment of the vibrational dipole moment induced by the pump light disappears with the randomization of the dipole moment. The relation between the inverse of τ_2 and τ_2' values, or rate constants, and the number of carbon atoms in the solvent alkane molecule is shown in Fig. 3. As shown in Fig. 3, the τ_2 values of the two complexes show large solvent dependence, while the τ_2' value does not depend on the solvent much. The τ_2 and τ_2' values and their solvent dependence should be determined by the rotation of the molecule and intramolecular energy transfer dynamics. We are trying to separate the contribution of these factors to the

τ_2 and τ_2' values from experimental results.

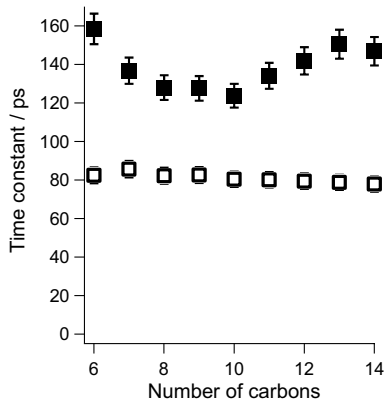

Fig. 4. Relation between the time constants τ_3, $W(CO)_6$, (filled square), $W(CO)_5(CH_3CN)$, (open square), and the numbers of carbon atoms in a solvent alkane molecule.

We observed the solvent dependence of the τ_3 value for each tungsten carbonyl complex. The relation between the τ_3 value and the number of carbon atoms in the solvent alkane molecule is shown in Fig. 4. The τ_3 value for $W(CO)_6$ shows its minimum in decane with the value of 120 ps. It increases as the chain length of the alkane either increases or decreases. The τ_3 value is 160 ps in hexane and 150 ps in tetradecane. This "V-shaped" solvent dependence cannot be explained by the macroscopic properties of the solvent, such as dielectric constant, viscosity, or density. These properties change monotonically as the number of carbons increases.

For $W(CO)_5(CH_3CN)$, τ_3 value ranges from 78 to 86 ps in the nine alkane solvents. These values are smaller than $W(CO)_6$ and show smaller solvent dependence. The difference between $W(CO)_6$ and $W(CO)_5(CH_3CN)$ strongly suggests that the acetonitrile ligand of $W(CO)_5(CH_3CN)$ accelerates the energy relaxation of the degenerate CO stretch vibration. The τ_3 process for $W(CO)_5(CH_3CN)$ is mainly controlled by the intramolecular energy transfer from the CO stretch to the vibrational modes of acetonitrile moiety.

4. Conclusion

We observed the vibrational energy relaxation of the degenerate CO stretch modes of two tungsten carbonyl complexes in nine alkane solutions. The vibrational energy relaxation process involves three steps. The fastest step probably reflects intra-molecular vibrational dynamics and coherent artifacts. The second fastest anisotropic components indicate the rotation of the transition dipole moment. The time constants of this rotation reflect the solvent induced rotation of the vibration within the degenerate CO stretches as well as the rotation of the molecule itself. The slowest component indicates the relaxation of vibrational population distribution. The time constant is determined by faster intramolecular process and slower intermolecular process and reflects sensitively the microscopic molecular environment which is not explained by macroscopic properties of the solvent. The vibrational relaxation is a sensitive measure of microscopic molecular environment.

Two-dimensional Infrared Spectroscopy and Molecular Dynamics of Liquid Formamide

Manuela Lima, Victor Volkov, Paolo Foggi, Riccardo Chelli, Roberto Righini
LENS, University of Florence

The structural and dynamical properties of liquid formamide have been investigated by means of pump-probe two-dimensional infrared (2DIR) spectroscopy in the C=O stretching region, and by Molecular Dynamics (MD) computer simulations. Both experiments and simulations were performed in a broad temperature range, from the supercooled liquid (T = 265 k) to high temperature liquid (T = 353 K). The 2DIR spectra give evidence the inhomogeneous origin of the spectral lineshape; the time resolved experiments allows determining the time scale for the spectral diffusion. A very fast decay of the spectral anisotropy is measured, and attributed to the strong dipole-dipole coupling responsible for the extended delocalization of the vibrational excitation. The picture of liquid formamide emerging from the MD simulations is that of a liquid characterized by a very extended hydrogen bond network. The excitonic model applied to the liquid molecular configurations obtained from the simulations reproduces very well the observed linear IR spectrum in the CO stretching region, and allows attributing its peculiar shape to the structural features of the liquid.

TRVS XII

NIST National Institute of Standards and Technology

Washington, D.C.
May 23-27, 2005

Protein Dynamics

Protein Dynamics from Time-Resolved Raman Spectroscopy

Thomas G. Spiro

Department of Chemistry, Princeton University, Princeton N.J. 08544.

Raman spectroscopy can provide unique information on the evolution of structure in proteins over a wide range of time-scales, using pump-probe techniques. The pump laser can initiate structure change via photolysis or via a temperature jump. Specific parts of the molecule can be interrogated by tuning the probe laser to a resonant electronic transition, including the UV transitions of aromatic residues and of the peptide bond. Allostery and folding are two broad categories of protein structure change that are of great current interest.

Time-resolved Raman spectroscopy makes it possible to monitor multiple structural features simultaneously on fast time scales. Thus the allosteric transition in hemoglobin (Hb) can be probed at the heme group, using visible excitation in resonance with the porphyrin π-π^* electronic transition[1], or at tryptophan and tyrosine residues strategically located throughout the protein, using UV excitation in resonance with the aromatic ring π-π^* transitions[2].

The heme resonant RR spectra reveal porphyrin ring vibrations which are markers of porphyrin core-size, and which relax in the earliest kinetic phase (~70 ns) following ligand photodissociation in Hb, as the protein allows the Fe atom to move fully out of the heme plane[2]. These spectra also reveal the stretching vibration of the Fe-histidine bond, which shows more complex relaxation kinetics, culminating in a wavenumber lowering at the final (~20 μs) locking in of the T quaternary structure, when tension is developed at this bond[3].

Both tryptophan and tyrosine residues can be probed with excitation at 229 nm, and their vibrations reveal a sequence of H-bond breaking and making, signaling helix displacements and subunit rearrangements along the allosteric reaction coordinate[2,4]. We have recently implemented a kilohertz Ti:sapphire laser whose output can be efficiently doubled and quadrupled, providing tunable excitation and high data throughput[5]. Two lasers are used in tandem, one for photolysis of HbCO, and the other providing the Raman probe, with adjustable electronic delay[6]. The improved signal/noise of this system permitted detection of previously unrecognized kinetic intermediates in the HbCO photocycle, and allowed elaboration of a working model for the allosteric pathway[7]. It also permitted studies of limited quantities of recombinant Hb, with site mutations designed to test specific features of the model[8]. In this way, we could test the hypothesis that the stereochemical trigger for the allosteric transition, namely the transition from low- to high-spin Fe as the ligand dissociates, is transduced by an intitial rotation of the E and F helices, which hold the heme like a clamshell[8,9]. This clamshell rotation breaks H-bonds that connect the E and F helices to the N- and C-terminal A and H helices, and initiates a conformational search that leads to subunit rearrangement and the formation of quaternary T-state contacts[4,7,8].

Fast folding events in proteins are conveniently studied in the nanosecond to millisecond regime by using an infrared laser pulse to heat the sample through absorption by a water vibrational overtone[10]. We have implemented a kilohertz OPO laser, tunable over the 1.8 μm water overtone, to provide high data rate T-jumps of up to 30^0C in aqueous solution of peptides and proteins[11]. Operation of the kilohertz Ti:sapphire probe laser has been extended to 193 nm (fourth harmonic)[12]. Excitation at this wavelength provides enhanced signals for amide vibrations (I, II, III and S), which are sensitive to secondary structure. A library of

secondary structure spectra has been constructed from a training set of crystallographically characterized proteins[13]. Time-resolved UVRR spectra can be used to characterize melting and folding dynamics of the polypeptide backbone (197 nm) and of aromatic sidechains (229 nm), thus providing separate dynamical probes of secondary and tertiary structure.

References.

1. S. Z. Hu, K. M. Smith, and T. G. Spiro, *J. Am. Chem. Soc.* **118**, 12638 (1996).
2. K. R. Rodgers, C. Su, S. Subramaniam, and T. G. Spiro, *J. Am. Chem. Soc*. **114**, 3697 (1992).
3. V. Jayaraman and T. G. Spiro, *Biospectroscopy* **2**, 311 (1996).
4. V. Jayaraman, K. R. Rodgers, I. Mukerji, and T. G. Spiro, *Science* **269**, 1843 (1995).
5. X. J. Zhao, R. P. Chen, C. Tengroth, and T. G. Spiro, *Appl. Spectrosc.* **53**, 1200 (1999).
6. X. J. Zhao, C. Tengroth, R. P. Chen, W. R. Simpson, and T. G. Spiro, *J. Raman Spectros.* **30**, 773 (1999).
7. G. Balakrishnan, M. A. Case, A. Pevsner, X. J. Zhao, C. Tengroth, G. L. McLendon, and T. G. Spiro, *J. Mol. Biol.* **340**, 843 (2004).
8. G. Balakrishnan, C. H. Tsai, Q. Wu, M. A. Case, A. Pevsner, G. L. McLendon, C. Ho, and T. G. Spiro, *J. Mol. Biol.* **340**, 857 (2004).
9. K. R. Rodgers and T. G. Spiro, *Science* **265**, 1697 (1994).
10. J. V. Beitz, G. W. Flynn, D. H. Turner, and N. Sutin, *J. Am. Chem. Soc.* **92**, 4130 (1970).
11. G. Balakrishnan, Y. Hu, and T. G. Spiro, (in prep.).
12. G. Balakrishnan, Y. Hu, S. B. Nielsen, and T. G. Spiro, *Appl. Spectrosc.* **59**, 776 (2005).
13. C. Y. Huang, G. Balakrishnan, and T. G. Spiro, *J. Raman Spectros.*, (submitted).

What Causes Larger Protein Changes in Halorhodopsin: Retinal Isomerization or Anion Binding?

J. Guijarro[1], F. Siebert[1], and M. Engelhard[2]

(1): Sektion Biophysik, Albert-Ludwigs-Universität, Hermann-Herderstr. 9, 79104 Freiburg, Germany
(2): Max-Planck-Institut für Molekulare Physiologie, Otto-Hahnstr. 11, 44227 Dortmund, Germany

The light-driven anion pump halorhodopsin belongs to the class of bacterial rhodopsins and shares many similarities with the well-known light-driven proton pump bacteriorhodopsin. In both systems, ion translocation is initiated by the light-induced all-*trans*→13-*cis* isomerization of the retinal chromophore. It has been shown that a single mutation converts bacteriorhodopsin into an anion pump (1). There are two main variants of halorhodopsin, from *Halobacterium salinarum* and from *Natronobacterium pharaonis.* Whereas the crystal structure of the former has been determined (2), the latter is more stable and does not need the presence of high salt concentration. Therefore, we used the latter in our studies on the molecular mechanism of the ion-translocating mechanism using static and time-resolved infrared difference spectroscopy. In previous studies, using the time-resolved step-scan FTIR technique, we could identify 3 intermediates of the photocycle which can be characterized with respect to chromophore geometry and anion location: 1. L1, with 13-*cis* chromophore and anion still at the uptake site; L2, with 13-*cis*-chromophore and anion at the release site; and O, with all-*trans*-chromophore and protein without anion (3). In this last intermediate, the spectrum is characterized by large protein distortions, as deduced from large amide-I changes. From these studies, it was not clear, whether the chromophore isomerization or the anion-depletion are the main cause for these distortions.

Pharaonis halorhodopsin offers the unique possibility to study an empty state separately, since it is stable in salt-free solution. This anion-depleted form has a red-shifted absorption maximum, due to the removal of the negative charge close to the protonated Schiff base (4). Using the ATR technique, the anion-uptake can be monitored by static FTIR difference spectroscopy, and the effect of different anions on the protein can be studied. Surprisingly, the difference spectra between the anion-depleted form and the anion-bound forms are not only very similar for the mono-atomic anions Cl^-, Br^-, and I^-, but also for NO_3^-, and N_3^-. Whereas NO_3^- is equally pumped as the mono-atomic anions, binding of N_3^- converts halorhodopsin into a proton pump (5). The binding-induced difference spectra are almost identical to the O difference spectrum. Especially, they all exhibit the large amide-I bands. These features are demonstrated in figures 1 and 2. In figure 1 the chloride binding spectrum (a) is compared to the bromide and iodide binding spectrum and to the negative of the O difference spectrum (c) (i.e. the transition from the putative anion-free O intermediate

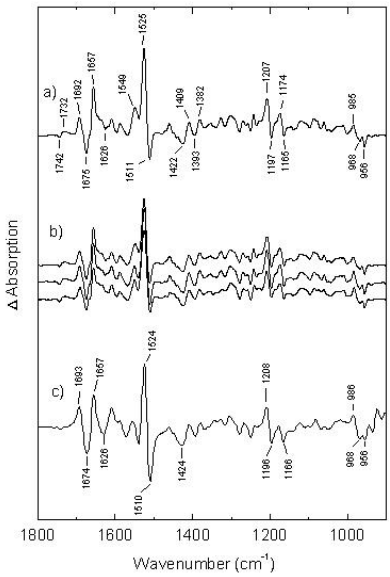

Figure 1

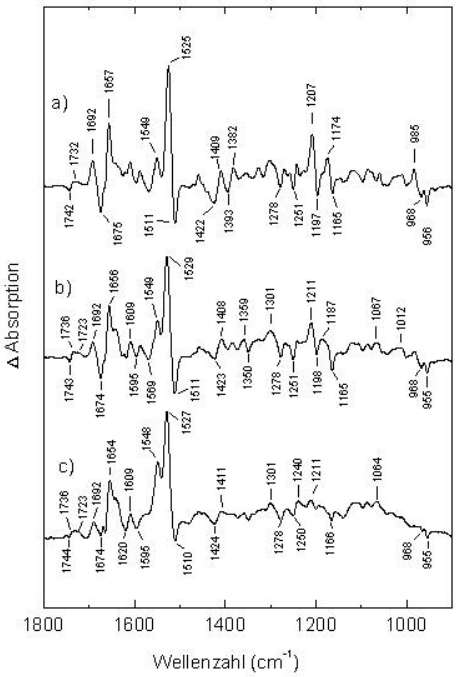

Figure 2

to the dark state). In Figure 2, the chloride binding spectrum (a) is compared to the nitrate (b) and azide binding spectrum (c). Although even here the general features are retained, some deviations have to be mentioned. The positive fingerprint band at 1174 cm^{-1} in (a) is missing in (b) and (c). Probably, this indicates that a small structural change takes place in the case of the non-spherical anions, causing a preference for the all-*trans* chromophore, whereas for the spherical anions about 15 % 13-*cis* are present in the dark state, which, however, do not take part in the photoreaction. Therefore, this positive band is equally not seen in the transition from O to the dark state. Further small deviations occur between 1300 and 1400 cm^{-1}. Probably they are caused by CH bending modes of aliphatic groups in the binding pocket, reflecting small alterations in the interaction. Finally, both non-spherical anions cause a blue-shifted absorption maximum, shifting the chromophore ethylenic mode from 1526 to 1529 cm^{-1}. Thus, one can conclude that the O-intermediate corresponds to the static anion-depleted form of halorhodopsin, and that its decay to the initial state merely reflects the anion-uptake. This is further supported by the anion concentration dependence of the decay of the O intermediate to the dark state. Furthermore, the shape of the anion has a minor influence on the spectra, excluding specific interactions involving a single amino acid side chain. Since the accompanying amide I changes are larger than those observed in the earlier intermediates K, L1 and L2 (3), one can conclude that the electrostatic changes within the protein induce larger protein changes as compared to chromophore isomerization.

This is corroborated by time-resolved FTIR studies of the photoreaction of the anion-depleted form. For this we used our step-scan FTIR set-up. Only two intermediates can be identified with our time resolution of 30 ns. The corresponding spectra are shown in figure 3, (a) and (b). The fingerprint bands of the chromophore clearly indicate that the usual all-*trans*→13-*cis* isomerization takes place and that the 13-*cis* geometry persists in the next intermediate. Thus, only with the decay to the initial state the backisomerization takes place. This step is approx. faster by a factor of 2 compared to the photocycle with anion, where the backisomerization occurs with the formation of the O intermediate (3). In total, the photocycle is accelerated by a factor of 5 to 10. In figure 3 we also show for comparison the spectrum of L2 (c), the amplitude spectrum of the L2→O transition (d), and the negative of the O difference spectrum (e), the latter also shown in figure 1 (c). These three spectra all pertain to the photocycle with anion. It is obvious that the L2 spectrum and the second spectrum of the anion-free reaction share many similarities. In both cases, the chromophore isomerization is the dominant molecular event. Furthermore, in agreement with earlier conclusions (3), we confirm that the transfer of the anion from the Schiff base region to the release site is not accompanied by larger protein conformational changes. As already discussed earlier, the larger protein changes take place with the anion release (formation of O) and the reverse changes with the anion

uptake (decay of O). Interestingly, these protein changes seem to determine the slowing-down of the kinetics of the corresponding transition. Taking together, the studies of the photocycle of the anion-depleted form of halorhodopsin from *Natronobacterium pharaonis* further provide evidence for the different roles of chromophore isomerization and anion uptake in directing protein conformational changes. The lack of distinct amino acids changing their interaction with the anion support an anion transporting model in which the anion is transferred by movement of some of the transmembrane helices (3, 6, and 7), squeezing the anion through the transmembrane protein.

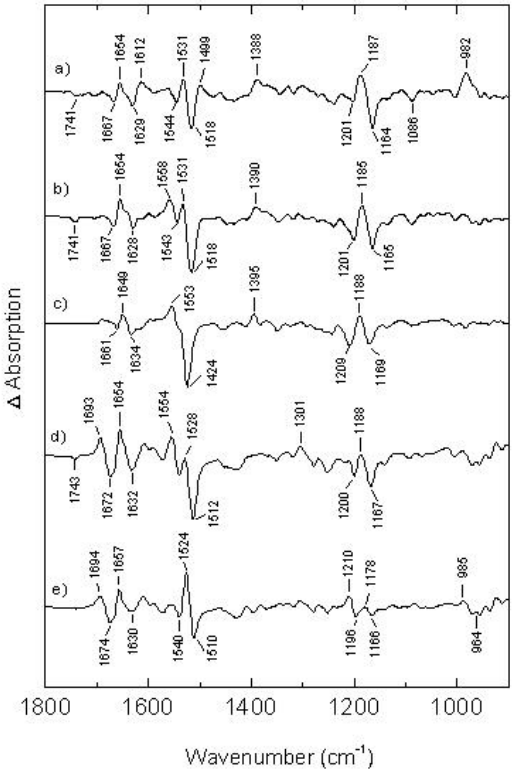

Figure 3

References

(1) Sasaki,J., Brown,L.S., Chon,Y.-S., Kandori,H., Maeda,A., Needleman,R., Lanyi,J.K.; (1995) Science 269: 73-75; Tittor,J., Haupts,U., Haupts,C., Oesterhelt,D., Becker,A., Bamberg,E.; (1997) J.Mol.Biol. 271: 405-416.
(2) Kolbe,M., Besir,H., Essen,L.O., Oesterhelt,D.; (2000) Science 288: 1390-1396.
(3) Hackmann,C., Guijarro,J., Chizhov,I., Engelhard,M., Rödig,C., Siebert,F.; (2001) Biophys.J. 81: 394-406.
(4) Scharff,B., Engelhard,M.; (1994) Biochemistry 33: 6387-6393.
(5)KulczárA., Groma,G., Lanyi,J.K., Váró,G.; (2000) Biophys.J. 79: 2705-2713;

Ultrafast Dynamics in the Green Fluorescent Protein (GFP): Proton Transfer and Time Resolved Fluorescence Spectroscopy

Deborah Stoner-Ma,[1] Andrew A. Jaye,[1,2] Pavel Matousek,[3] Michael Towrie,[3] Peter Tonge[1] and Stephen R. Meech[2]

[1] Department of Chemistry, Stony Brook University, Stony Brook, NY 11794-3400, USA
[2] School of Chemical Sciences & Pharmacy, University of East Anglia, Norwich, NR4 7TJ UK
[3] CCLRC Central Laser Facility, Rutherford Appleton Laboratory, Chilton, Didcot, Oxfordshire, OX11 0QX England

1. Introduction

Green fluorescent protein (GFP) has several properties which make it unique and of key importance in photobiology. It is an intrinsically fluorescent protein, the visible absorbing chromophore being formed in a cyclisation and oxidation reaction involving three amino acid residues. By combining the gene for GFP with that of a target protein, it is possible to irreversibly and non-perturbatively label a specific protein in a living cell. This has led to the very widespread use of GFP as a fluorescence marker.

The photophysics of GFP are dominated by an excited state proton transfer reaction, the rate of which is a strong function of mutation. Boxer and coworkers examined this reaction between the neutral (A) and anionic (B and I) forms of wtGFP using ultrafast fluorescence up-conversion spectroscopy.[1] They concluded that excited state proton transfer occurs upon excitation of the neutral (A) form of the chromophore, leading to the formation of the anion within an unrelaxed protein environment (I state). This unrelaxed anionic form of wtGFP, fluoresces strongly at 509 nm. The I form may also relax to a stabilized anionic ground state (B form) on a slower timescale.

We have employed ultrafast time resolved infra-red (TRIR) and fluorescence spectroscopy to investigate (1) the dynamics of the excited state proton transfer reaction with vibrational resolution and (2) the time resolved fluorescence spectrum of the emissive states (A and I). The TRIR data reveal for the first time conclusive evidence that the ultimate proton acceptor is the residue E222.[2] This is proven by studies of GFP mutants selected because either the proton transfer is blocked, or it has already occurred in the ground state. The time resolved (Kerr gated) fluorescence spectra are also interesting because they show that the emission spectrum of both A* and I* are independent of time, at least on the timescale of picoseconds.[3] This suggests that the protein environment does not relax to accommodate the increased dipole moment of the I* state (compared to A) despite the fact that the permanent dipole moment change accompanying this transition is appreciable.[4] One interpretation of this is that the protein environment is relatively rigid restricting orientational relaxation of polar residues.

2. Experimental

The experiments described here were performed at the Rutherford Appleton Laboratory. The TRIR experiments were performed at the PIRATE facility. The key feature of this facility from the point of view of ultrafast studies of proteins is its high signal to noise. This is important as the concentration of the protein is limited to millimolar at most, due to solubility considerations, which means that absorbance changes in region of 0.1 mOD must be accurately measured. The apparatus has been

described in detail elsewhere.[5] GFP samples were prepared at concentrations up to 2 mM in 50 μm pathlength cells. The excitation power was reduced to < 1 μJ per pulse to minimize sample damage and multiphoton absorption. For wtGFP the excitation wavelength was 400 nm. For excitation of the anionic mutant T203V/E222Q an excitation wavelength of 500 nm was used.

The time resolved fluorescence spectra were recorded using the Kerr gate method. The sample fluorescence was excited by a pulse at 400 nm. The fluorescence was collected and focused into a carbon disulfide Kerr gate. The Kerr gate is opened by irradiation with an intense 800 nm pulse, and remains open on the timescale of the relaxation time of the induced anisotropy. During this time (ca 2ps) the fluorescence is transmitted and measured in a multi channel detector. Time resolved spectra are obtained by delaying the gate pulse. The overall temporal resolution is about 4 ps, and the spectral resolution is 4 nm.

The samples studied were wtGFP and two mutants: S65T at low pH and T203V/E222Q. In S65T the proton acceptor is misaligned, disrupting the H bonding network so that no proton transfer is possible and only A* state emission is seen. In T203V/E222Q the chromophore has been deprotonated in the ground state, which has the structure of the I form.[6] Thus only I → I* absorption and I* emission are seen.

3. Results and Discussion

TRIR spectra between ca 1400 and 1750 cm^{-1} were measured for 4 samples. With 400 nm (A*) excitation we obtained data for the model chromophore, wtGFP and S65T. With 500 nm excitation (I* state) the transient IR spectra of T203V/E222Q were obtained. The data are shown in Figure 1.[2]

The study of the model chromophore is important as it allows the distinction of transients associated with chromophore modes from those associated with the surrounding protein. The model chromophore shows a simple bleaching and ground state recovery mechanism. The ground state recovery is on the picosecond timescale, as expected from earlier studies of the chromophore.[7] The bleaches around 1610

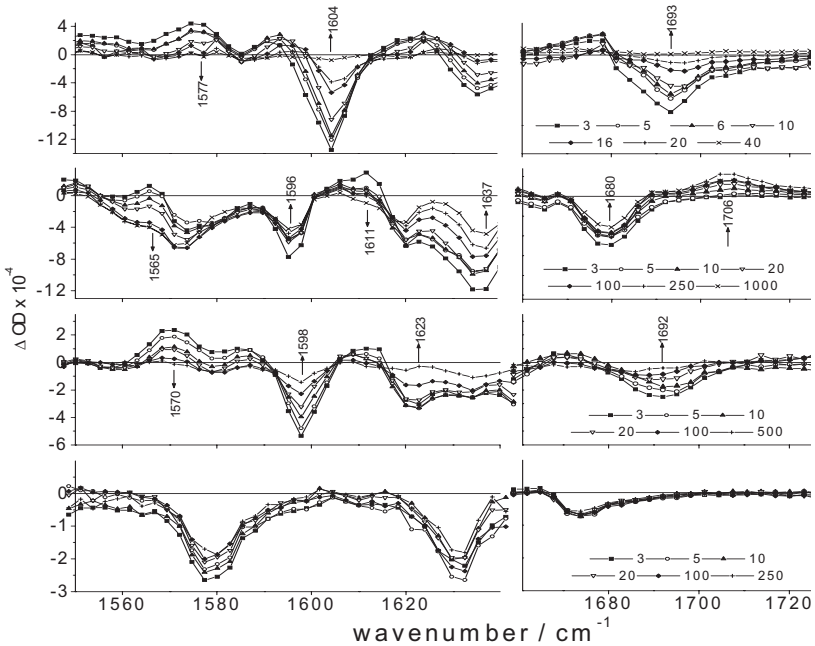

Figure 1. TIR data for: A HBDI in DMSO, B wt GFP, C S65T, all excited at 400 nm, and D T203V/E222Q excited at 500 nm. Arrows indicate the direction of absorbance with increasing time. All protein data were measured in D_20

and 1640 cm^{-1} can be assigned to phenolic and exocyclic C=C modes respectively, on the basis of earlier static and isotopic substitution measurements.[8] Transient absorption is also seen, which may be associated with excited state or hot ground state absorption. More detailed time domain measurements are required to differentiate between these possibilities. The TRIR data for wtGFP are clearly much more complex. The same chromophore modes are seen, but shifted and with an altered intensity distribution. Most important is the observation of two new bands: at 1570 cm^{-1} a bleach grows in on the tens of picoseconds time scale and at 1710 cm^{-1} a transient absorption grows with the same time constant. These are assigned to bleaching of a protein carboxylate (COO^-) group and concomitant formation of a protonated carboxyl (COOD) group, consistent with the assignment of E222 as the proton acceptor. This is supported by studies of the mutants. When proton transfer is blocked (S65T) neither band is observed, so the transients are associated with proton transfer. When the I form (T203V/E222Q) is directly excited, the 1710 cm^{-1} band is not observed, and thus this mode is not associated with I*. Further studies of these spectra and additional mutants are in progress.

We have also measured the time resolved fluorescence spectra of wtGFP following excitation into the A* state. The spectra for several times after excitation are shown in Figure 2. As expected from earlier single wavelength studies, the A* emission disappears rapidly, and I* emission appears with a corresponding rate constant. When the entire spectra are revealed, two new factors become apparent. First, there is an isoemissive point, which suggests that the proton transfer reaction can be thought of as a simple two state reaction. Second, the I* state does not shift with time after excitation. We have shown in a more detailed analysis of the spectra that this is also true of the A* emission.[3] This is surprising given the change of dipole moment between the A state and the I* state, which one would expect to lead to a strong interaction between I* and the polar and polarisable residues in the protein. Orientational relaxation would then lead to stabilisation of I*, accompanied by a spectral shift. The fact that this is not observed suggests orientational relaxation of these residues in the protein is highly restricted – i.e. the protein matrix surrounding the chromophore is rigid.

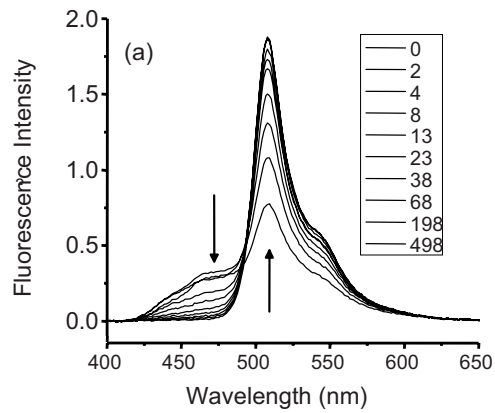

Figure 2 Time resolved emission of wtGFP (times shown in picoseconds)

References

[1] M. Chattoraj et al Proc. Natl. Acad. Sci. USA **1996**, *93*, 8362
[2] D. Stoner-Ma, et al J. Amer. Chem. Soc., **2005**, *127*, 2864 – 2865
[3] A. A. Jaye et al Photochem. Photobiol In Press
[4] Bublitz, et al. *J. Am. Chem. Soc.* **1998**, *120*, 9370
[5] M. Towrie et al. Appl. Spectrosc. **2003**, 57, 367
[6] J. Wiehler et al Chembiochem. **2003**, *4*, 1164
[7] (a) K. Litvinenko et al. J. Phys. Chem. A **2003**, *107*, 2616 (b) D. Mandal et al. J. Phys. Chem. B **2004**, *108*, 1102
[8] (a) A. F. Bell et al. Biochemistry, **2000**, 39, 4423 (b) X. A. He et al. J. Phys. Chem. B, **2001**, *105*, 5316 (c) A. F. Bell et al. J. Am. Chem. Soc., **2003**, *125*, 6919

Structural Dynamics in a Chromopeptide - Infrared Absorption Dynamics from Picoseconds to Minutes

W. Zinth[a], F. O. Koller[a], R. Reho[a], T. Schrader[a], W. J. Schreier[a], C. Renner[b], L. Moroder[b], J. Wachtveitl[c]
[a]BioMolekulare Optik, Department für Physik, Ludwig-Maximilians-Universität München, Oettingenstraße 67, 80538 München
[b]Max-Planck-Institut für Biochemie, Am Klopferspitz 18A, 82152 Martinsried, Germany
[c]Institut für Physikalische und Theoretische Chemie, Johann Wolfgang Goethe Universität, Marie-Curie-Str. 11, 60439 Frankfurt, Germany

Folding of an amino-acid chain into a functional protein is one of the key processes in biology. Unfortunately a molecular understanding of this important process is still missing. In an attempt to gain information on the initial processes in folding dynamics, we have recently developed light-switchable chromopeptides /1,2/. The incorporation of an azobenzene molecule into a peptide chain allows to induce structural changes of the peptide moiety with subpicosecond precision. Ultrafast visible spectroscopy yields information on the chromophore and on the back-action of the peptide on the chromophore. Transients on the time scale of picoseconds have been observed here /2-4/. Molecular dynamics simulations of the reaction dynamics show, that the initially stored energy is released to the surrounding on the same time scale /2/. Infrared spectroscopy can be used to monitor the dynamics of the chromophore and the peptide moiety and has the advantage to display in detail the structural changes of the peptides /5/.

Picosecond absorption dynamics recorded in the IR

In a first set of experiments we discuss data from light induced infrared absorption dynamics on the picosecond time-scale of two azobenzene peptides. For the bicyclic azobenzene peptide bc-AMPB (switched from the cis to the trans state) it was shown recently that the dominant part of the absorption transients occur on the time-scale of 20 ps /5/. Within that period, the absorption spectrum in the amide I range has reached large similarities to the cw spectrum. Only weak absorption changes are found on longer time-scales. Apparently the major part of the structural changes proceeds on the 10 ps time-scale. When we investigate the cyclic azobenzene peptides c-APB where we switch the molecule from the trans to the cis state (see Fig. 1) we observe intense fast absorption transients on the 10 ps time-scale. They are related to the decay of the S_1-state of the chromophore and to heat dissipation to the surrounding molecules. Subsequently we find absorption changes extending into the nanosecond range. The absorption difference spectrum recorded in the amide I band around 1660 cm^{-1} has acquired the shape of the stationary spectrum within ≈ 1 ns. However in the 1640 and 1600 cm^{-1} range the cw-shape is not reached, indicating, that the chromopeptide did not accomplish all structural changes within a few nanoseconds (see Fig. 1).

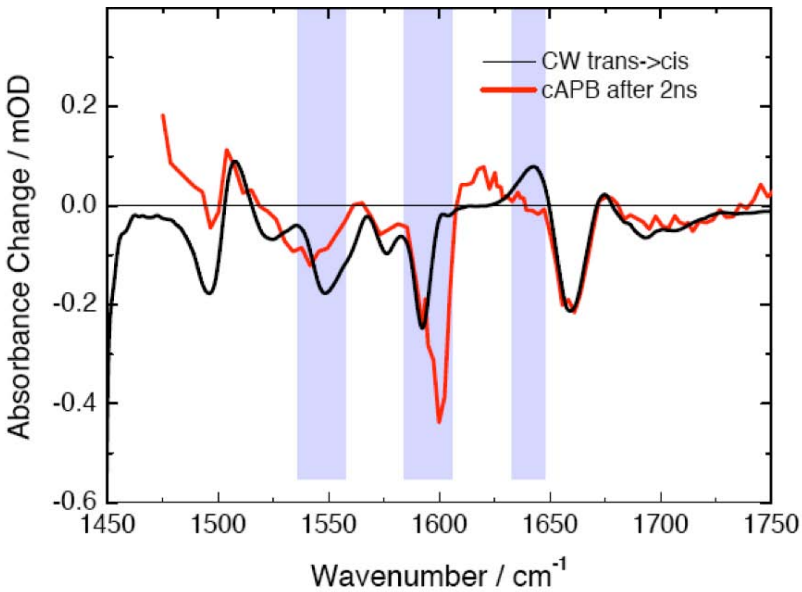

Fig. 1: Light induced absorption changes in c-APB recorded after 2 ns and in a cw-experiment. The data indicate, that not all structural transients are finished within 2 ns.

IR- Absorption Transients on the Time Scale of Minutes

In a second study we observed absorption transients induced in the bc-AMPB peptide after thermal treatment. Upon cooling the sample below the freezing temperature of the DMSO-solvent, we observed an interesting behavior. When the sample contains traces of water in the range of > 0.5% (by volume) cw-illumination induced absorption changes appear similar to the ones observed above the melting point. A different behavior resulted in a sample with reduced H_2O concentration of ≈ 0.1%. Here light induced absorption changes are much weaker. Only around 1635 cm^{-1} we find a pronounced absorption difference spectrum.

An absorption change also results without illumination in the same spectral range just induced by cooling the sample below the melting point. When the dry frozen sample of trans bc-AMPB-molecules is heated up to room temperature a slow absorption transient is seen (see Fig. 2): Measuring the IR-spectrum at different times after the thawing we find a pronounced absorption decrease at 1635 cm^{-1}. The original absorption of the bc-AMPB sample only recovers on the time scale of 10 min (see Fig. 2, upper part). Immediate restoration of the initial absorption spectrum is also obtained by an trans to cis / cis to trans illumination cycle (see Fig. 2, lower part). Since experiments performed on samples with elevated H_2O content did not lead to the observed long-lasting absorption transients, and since the transients are related predominantly to a band in the spectral range of ≈ 1630 cm^{-1}, where residues with strong hydrogen bonds absorb, one may tentatively assign the observation to molecular arrangements with special hydrogen bonding patterns.

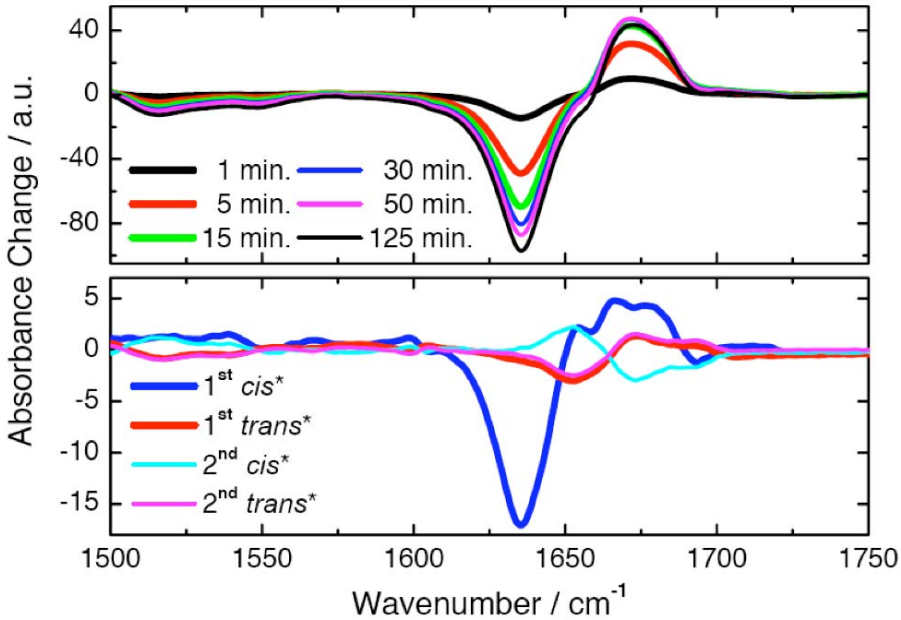

Fig. 2: Upper part: Absorption difference spectra recorded at different times after the thawing of the bc-AMPB sample. Lower Part: Light induced difference spectra obtained after thawing of the sample. The strong asymmetry in the first illumination cycle points to the light induced decay of a species present in the sample after passing the melting point.

In conclusion: time resolved experiments on azobenzene peptides show that ultrafast structural changes can be induced by optical trigger pulses in small cyclic azobenzene peptides. Depending on the specific properties of the chromopeptides one observes transients extending to longer time scales. While the IR-absorption transients in the bc-AMPB-peptide indicate, that the structural dynamics are essentially finished within a few 10 ps, we find transients on the twelve orders of magnitude longer time scale of minutes, when an initially frozen sample is heated to room temperature. The investigations show, that small chromopeptides not only form a group of molecules interesting for the study of fastest structural transients, but that these molecules may be understood as model systems for complex protein reactions on the various time scales relevant for protein folding.

References

1 Naegele T, Hoche R, Zinth W and Wachtveitl J (1997) Femtosecond photoisomerization of cis-azobenzene. Chem. Phys. Lett. 272: 489-495

2 Spoerlein S, Carstens H, Satzger H, Renner C, Behrendt R, Moroder L, Tavan P, Zinth W and Wachtveitl J (2002) Ultrafast spectroscopy reveals subnanosecond peptide conformational dynamics and validates molecular dynamics simulation. Proc. Natl. Acad. Sci. U. S. A. 99: 7998-8002

3 Satzger H, Root C, Renner C, Behrendt R, Moroder L, Wachtveitl J and Zinth W (2004) Picosecond dynamics in water-soluble azobenzene-peptides. Chem. Phys. Lett. 396: 191-197

4 Wachtveitl J, Spoerlein S, Satzger H, Fonrobert B, Renner C, Behrendt R, Oesterhelt D, Moroder L and Zinth W (2004) Ultrafast conformational dynamics in cyclic azobenzene peptides of increased flexibility. Biophys. J. 86: 2350-2362

5 Bredenbeck J, Helbing J, Sieg A, Schrader T, Zinth W, Renner C, Behrendt R, Moroder L, Wachtveitl J and Hamm P (2003) Picosecond conformational transition and equilibration of a cyclic peptide. Proc. Natl. Acad. Sci. U. S. A. 100: 6452-6457

Electrostatically Steered Photophysical Pathways in Green Fluorescent Protein

J. Timothy Sage, Georgi Y. Georgiev, Northeastern University
Jasper van Thor, Oxford University
Michael Towrie, Rutherford Appleton Laboratory

Green fluorescent protein (GFP) and its variants find a growing range of applications in proteomics and cell biology. Electronic spectroscopy has revealed important aspects of the complex chomophore photophysics, most notably the occurrence of excited state proton transfer (ESPT), but is not directly sensitive to the surrounding protein. Time-resolved infrared spectroscopy, on the other hand, reveals vibrational changes on picosecond time scales that reflect not only the photoionization of the chromophore but also the rapid response of nearby amino acids to this dramatic electrostatic event. These measurements confirm Glu 222 as the acceptor of the proton ejected from the chromophore and exclude alternative proposals. We interpret additional vibrational changes in the light of crystal structures of cryotrapped intermediates determined after irreversible chromophore photoionization at 100 K. The observation of common spectroscopic features at 100 K and in room temperature transient spectra supports the use of these structures to model the electrostatically driven conformational dynamics in the GFP photocycle. Both spectroscopic and crystallographic measurements identify conformational changes of Gln 69, Cys 70, and an associated H-bonded cluster of internal water molecules. Polarized infrared measurements on oriented single crystals establish the presence of a hydrogen bond from Cys 70 to the backbone carbonyl of Ala 68, which is weakened following chromophore ionization. The combined crystallographic and spectroscopic results paint a detailed picture of structural dynamics during the GFP photocycle. In particular, unexpectedly "fluid" structural changes take place on picosecond time scales and at cryogenic temperatures far below the ca. 200 K "dynamical transition" generally believed to enable functional protein motions. This contrasts with the prevailing view that the rigid interior of the GFP β-barrel inhibits nonradiative processes, such as the isomerization that quenches the fluorescence of the isolated chromophore. Instead, we propose that rapid rearrangements of the chromophore environment enhance the fluorescence quantum yield by stabilizing the charge distribution of the radiative state. We expect that improved understanding of the GFP photocycle will facilitate reengineering the protein to incorporate novel properties without sacrificing the desirable high fluorescence efficiency.

A Pico- to Microsecond Study of the Folding of a Photo-Switchable α-Helix

Jens Bredenbeck*, Jan Helbing*, G. Andrew Woolley[+], Janet R. Kumita[+], Peter Hamm*

** Physical Chemistry Institute, University of Zurich, Switzerland, and*

[+]Department of Chemistry, University of Toronto, Canada

We study the folding dynamics of a photo-switchable α-helix by time resolved IR spectroscopy. To this end, we have recently developed an apparatus based on two femtosecond laser systems, which allows us to continuously scan over seven orders of magnitudes in time from 2 ps to 50 μs [1]. With this setup we can, for the first time, resolve the complete folding transition without being affected by the time resolution and are sensitive to potential precursor steps in the otherwise relatively slow folding of the helix.

The system under study is a small hexadeca-peptide, in which two cysteine side chains are connected by a photo-isomerizible azobenzene linker. The linker controls the conformation of the peptide in such a way that it is preferentially unfolded when the azo-linker is in the *cis* configuration, while switching the azo-linker into *trans* favors a helical conformation of the peptide [2]. We observe helix folding to occur on a time scale of 270 ns to 2.3 μs, depending on temperature. The process is strongly thermally activated. However, the folding kinetics is non-exponential and different sites in the peptide respond in different ways [3]. Hence, helix formation clearly is not a two-state process. We discuss the non-exponentiality of the kinetics in the context of diffusion models on physically meaningful free energy surfaces [4].

[1] J. Bredenbeck, J. Helbing, P. Hamm, Rev. Sci. Instr., Rev. Sci. Instr. 75, 4462-4466 (2004)

[2] D. G. Flint, J. R. Kumita, O. S. Smart, G. A. Wooley, Chem. Biol. 9 (2002) 391-397

[3] J. Bredenbeck, J. Helbing, J. R. Kumita, G. A. Wooley, P. Hamm, Proc. Natl. Acad. Sci. USA, 102, 2379 (2005)

[4] P. Hamm, J. Bredenbeck, J. Helbing, Chem. Phys. submitted.

PICOSECOND PROTEIN DYNAMICS OF MYOGLOBIN UPON LIGAND DISSOCIATION STUDIED BY ULTRAVIOLET RESONANCE RAMAN SPECTROSCOPY

Yasuhisa Mizutani* and Akira Sato

Molecular Photoscience Research Center, Kobe University, 1-1 Rokkodai, Nada, Kobe 657-8501, Japan and Core Research for Evolutional Science and Technology, Japan Science and Technology Agency, Honmachi, Kawaguchi, 332-0012, Japan

Protein dynamics are intimately connected to the structure/function relationship of biological systems. In numerous biological processes, the ensuing protein structural changes accompanying a reaction at a specific site must spatially extend to mesoscopic dimensions to achieve a biological function. The molecular mechanism of cooperativity in oxygen binding of hemoglobin (Hb) is one of the classical problems in this aspect.[1] The binding of small molecular ligands to the hemes in Hb is a highly localized perturbation. Nonetheless, this localized perturbation initiates a sequence of propagating structural events that culminates in a change of quaternary structure. The large-amplitude motions at the quaternary level, which form a communication link at the subunit interface, are driven by changes of the tertiary structure upon ligation. In this respect, myoglobin (Mb), which is structurally very similar to a subunit of Hb serves as a model system for the tertiary relaxation processes.

Vibrational structural studies of biomolecules have greatly advanced since the introduction of UV resonance Raman (UVRR) spectroscopy.[2] When the excitation wavelength is tuned between ~195 and 260 nm, strong resonance Raman scattering from the peptide backbone and aromatic amino acids provides vibrational information on local protein structure and environmental changes. We have constructed a picosecond time-resolved UVRR spectrometer which consists of a tunable (204-243 nm) picosecond UV light source and a highly sensitive detection system. Here, we report a structural study of the protein conformational changes associated with ligand dissociation in Mb using the spectrometer.

Figure 1 demonstrates time-resolved UVRR difference spectra expanded the region of 650-1850 cm^{-1}. The top and bottom traces correspond to the contracted probe-only spectrum and equilibrium deoxyMb minus MbCO difference spectrum, respectively. Tryptophan (Trp) and tyrosine (Tyr) bands appeared in the UVRR spectra are labeled by W and Y. Negative difference features appeared at 763, 1012, 1553 and 1620 cm^{-1} at the delay time of 5 ps. Former three negative features can be ascribed to the intensity decrease of Trp bands of W18, W16, and W3 modes. The negative feature at 1620 cm^{-1} is attributable to the intensity drop of Tyr Y8a band, which is superimposed on a small contribution from the intensity decrease of W1 band. In delay times between 5 and 300 ps, negative difference bands of W18, W16, and W3 modes showed little

* e-mail: mizutani@kobe-u.ac.jp

intensity change, on the other hand, negative difference band at 1620 cm^{-1} appreciably decreased in intensity. The intensity of W1 band with 226-nm excitation is less than one third of that of W3 band and the intensity of Trp bands other than W1 is invariant, hence, the intensity change of difference signal at 1620 cm^{-1} observed at 5 to 300 ps can be attributed to the intensity restoration of Y8a band. At 2.5 ns time delay, the features in the difference spectrum are approaching those in the equilibrium deoxyMb minus MbCO spectrum. However, the transient difference spectrum does not coincide with the equilibrium difference spectrum. This means that the structural rearrangements toward the deoxy structure are not completed at 2.5 ns.

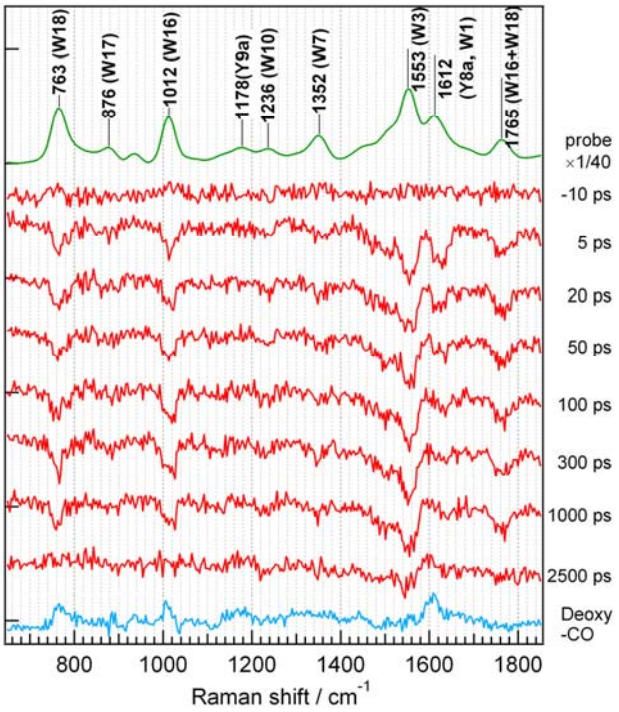

Figure 1. Picosecond time-resolved UVRR spectra of photodissociated MbCO in the 700 to 1800-cm^{-1} region. The equilibrium deoxyMb minus MbCO difference spectrum is depicted at the bottom for comparison.

Horse Mb has two Tyr residues: Tyr103 and Tyr146. X-ray crystallographic studies showed Tyr103 is exposed to the solvent in both deoxyMb and MbCO.[3, 4] Therefore, Tyr103 is not expected to show intensity changes upon CO dissociation. On the other hand, Tyr146 has a side chain which locates in the FG corner of Mb. It forms hydrogen bond to the backbone carbonyl of the proximal histidine (His93). Therefore, Tyr146 can be perturbed by the structural changes of the heme. We previously reported structural dynamics of Mb probed by visible resonance Raman spectroscopy.[5] The data showed that the structural changes of the heme completes within 2 picoseconds and that there is structural relaxation around the heme with the time constant of 100 ps based on the frequency shift of iron-histidine stretching mode. The present data on the Tyr band are consistent with the previous data on heme and iron-histidine stretching band. Because Tyr146 forms hydrogen bond to the backbone carbonyl of the proximal histidine, spectral changes on both sites can be ascribed to the common protein motion in the heme vicinity of Mb.

The Raman bands of Trp residues showed instantaneous intensity decrease and the intensity recovery in the nanosecond regime. In 100 ps region, there is no apparent intensity change for Trp bands in contrast to the change of Tyr Y8a band. Two Trp residues are involved in horse Mb: Trp7 and Trp14. Both residues are in the A helix and contact with the E helix. Although the A helix is far from the heme, intensity change of Trp bands occurs within 5 ps. It is hard to assume that the structural changes propagate from the heme group to the A helix in such a short time. More plausible idea is that upon CO dissociation the E helix moves and the movement perturbs the

environments of Trp residues. Because the E helix locates just above the heme and can respond quickly to the CO dissociation at the heme. Spectral changes in nanoseconds can be attributed to following motion of the A helix toward the heme group. As shown by the Tyr spectral changes, the F helix moves quickly upon the CO photodissociation. This means the E and F helices move within 5 ps as if they are single dynamical unit. For Hb, similar motion of the EF helices was also proposed from nanosecond time-resolved UVRR study by Spiro and coworkers.[6] But, in the case of Hb, the spectral changes occurred in tens of nanosecond. The motion of Mb is much faster than that of Hb. Such an ultrafast protein response of Mb was also reported by a transient grating study.[7] The motion of EF helical section would lead to the shape change of Mb within 5 ps.

In this study, we made the site-specific observation of protein dynamics in Mb with picosecond time-resolved UVRR spectroscopy. Our results demonstrated impulsively driven protein motion following the ligand dissociation and several phases of structural rearrangements towards the deoxy structure of Mb in subnanosecond to nanosecond.

References

1. Dickerson, R. E.; Geiss, I., *Hemoglobin: Structure, Function, Evolution, and Pathology*. ed.; Benjamin Cummings: Menlo Park, 1983.
2. Kitagawa, T. *Prog. Biophys. Mol. Biol.* **1992,** 58, 1-18.
3. Kuriyan, J.; Weis, W. I. *Proc Natl Acad Sci U S A* **1991,** 88, 2773-7.
4. Kachalova, G. S.; Pepov, A. N.; Bartunik, H. D. *Science* **1999,** 284, 473-476.
5. Mizutani, Y.; Kitagawa, T. *J. Phys. Chem. B* **2001,** 105, 10992-10999.
6. Jayaraman, V.; Rodgers, K. R.; Mukherji, I.; Spiro, T. G. *Science* **1995,** 269, 1843-1846.
7. Goodno, G. D.; Astinov, V.; Miller, R. J. D. *J. Phys. Chem. A* **1999,** 103, 10630-10643.

DOVE 2D-IR spectroscopy as a tool for studying protein composition, structure and function

Paul Donaldson, Laura Barter, Jason Palmer, David Klug

Department of Chemistry, Imperial College London, United Kingdom, SW7 2AZ

We report infrared spectra of proteins and peptides measured using a picosecond two dimensional infrared spectroscopy (DOVE 2D-IR). DOVE 2D-IR is a frequency domain 2D-IR technique which has particular advantages for the study of complex biomolecules.[1] It allows convenient investigation of combination bands in the near infrared spectral region. The resulting 2D spectra are sensitive to composition, chemical state and structure. In particular we demonstrate that 2D-IR methods have potential as tools for proteomic analysis.

1) Wright, J.C. International Reviews in Physical Chemistry, 2002, **21**(2), 185-255

Rotational Raman Responses of H_2 in Supercritical CO_2: A probe of local ultrafast anisotropic solvent dynamics

J. Peng, T. Castonguay, D. F. Coker and L. D. Ziegler, Department of Chemistry, Boston University, Boston MA 02215

Introduction. H_2 is a relatively free quantum rotor in solution as evidenced by the appearance of discrete well-resolved rotational transitions in condensed phase Raman spectra. However, band broadening and frequency shifts have been previously reported for H_2 dissolved in a variety of solvents.[1-3] In contrast to the gas phase, the solvent environment of a fluid creates a local instantaneous potential which is no longer isotropic. Thus, the 2J+1 M sublevels of a given J level split for a rotor in solution, creating a static contribution to the Raman linewidth. In addition, solvent motions cause the energies of these M-sublevels to fluctuate and nonadiabatically mix on the time scale of H_2 rotational motion. Thus, the Raman rotational bandshapes or equivalently the decay of the impulsively excited Raman response functions of H_2 in fluids are a sensitive probe of local dynamical intermolecular environments. The decay time of these responses are thus determined predominantly by orientational coupling. Since photon echo measurements, i.e. the ability to directly observed spectral diffusion, are not possible for this Raman active only solution, molecular level physical interpretation of the rotational Raman responses will be derived from nonadiabatic mixed quantum-classical simulations. Observations of these ultrafast responses in supercritical fluids allows the evolution of solvation from the uncorrelated isolated binary collision regime to the highly correlated motion regime of liquids at a given temperature to be studied. Thus, insight into a dynamic picture of the special solvation properties of SCFs and the evolution of liquid-like response characteristics may be obtained from the analysis of these responses.

Experimental. The impulsively excited (22 fs pulses at ~800 nm) S(0) (~354 cm^{-1}) and S(1) (~587 cm^{-1}) rotational responses of H_2 in CO_2 have been observed as a function of CO_2 density along an isotherm (T = 308 K) in the vicinity of the critical point spanning a CO_2 concentration range from 2.7M to 13.3M ($\rho^* = 0.25$ to 1.25) as shown in Fig. 1. These anisotropic pump-probe Raman responses are observed in an OKE configuration. Signals due to 0↔2 and 1↔3 H_2 rotational Raman responses and the much stronger intermolecular CO_2 (solvent) response are evident in these responses.

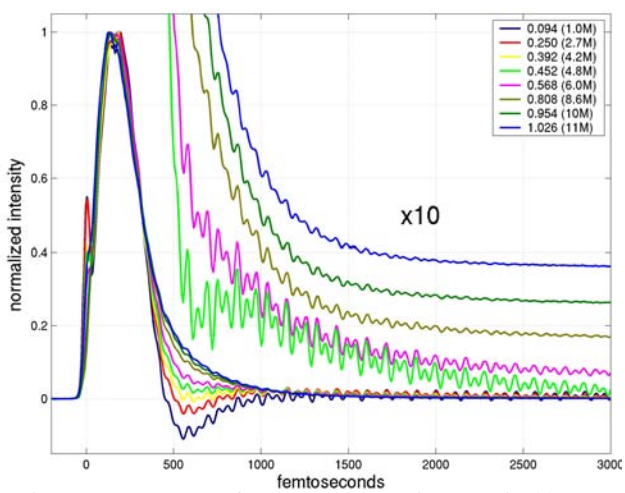

Figure 1. Responses of H_2 in CO_2 (18 mole %) excited by 22 fs pulses at 800nm in an OKE configuration.

The time-domain observations of these H_2 rotational Raman responses in solutions have several advantages as compared to frequency domain (i.e. spontaneous Raman) measures such as: better S/N and frequency accuracy, direct comparison with theoretically calculated correlation functions, better evidence of multiple time scale components and short time behavior, larger dynamic range for comparison with theory and simultaneous observation of intermolecular solvent response.

Data Analysis. The H_2 S(0) and S(1) rotational responses in CO_2 at 308 K at a given solvent density are separated from the observed time domain signals by Fourier filtering techniques, normalized for the finite pulse duration and are displayed in Fig. 2. These are essentially experimentally derived anisotropic rotational correlation functions which can be directly compared with the theoretical results. The effect of the increasing CO_2 density are evident in this figure. These coherences exhibit multiple timescales in their decays: nonexponential (inertial components at short times and exponential relaxation at long times. These decays do not decrease linearly with density, especially at the higher densities ($\rho^* \geq 0.8$). S(0) and S(1) exhibit the same exponential decay rates at long times but slightly different early (inertial) decays. This long time exponential component for the H_2 Raman relaxation scales proportionately with the rotational diffusive decay time of the CO_2 response as a function of density.

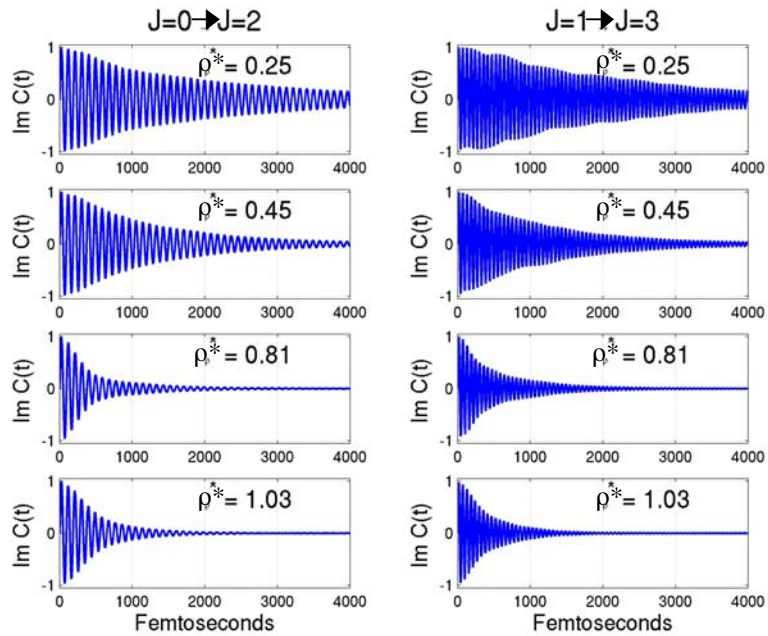

Fig. 2. Experimentally determined H_2 in CO_2 rotational correlation functions.

Mixed quantum-classical simulation of the H_2 Raman correlation function. The theoretical treatment applied here is analogous to that previously developed for calculation of the anisotropic Raman correlation function of H_2 in Ar and H_2O.[3-6] The motions of the CO_2 molecule and the H_2 center of Mass (COM) are treated classically using standard MD methods. H_2 rotational and orientational motion are the quantal degrees of freedom coupled to the classical bath. Trajectories are determined by classical dynamics. Then at each time step instantaneous adiabatic states of the H_2 rotor using the full anisotropic potential are found. The solvent driven mixing of these instantaneous adiabatic levels is then computed and the corresponding Raman correlation functions determined. The main approximation in this formulism is the so-called zero back reaction approximation, i.e. the solute-solvent interaction potential is independent of the rotational quantum state. This approximation is essential to make this calculation of the quantum correlation function coupled to classical degrees of freedom, even in this small system, tractable.

In contrast to previous theoretical investigations of the H_2 Raman spectrum in solution,[4-6] the main electrostatic solute-solvent interaction in this H_2/CO_2 system is electric quadrupole-electric quadrupole. Point-charge and point-quadrupole models for this interaction in mixed quantum-classical MD simulations were not successful in capturing the observed Raman responses. An *ab initio* generated H_2-CO_2 potential has been fit and have been implemented in our latest version of the MD simulation for of this system for the interpretation of these data.

The resulting calculated instantaneous adiabatic rotational energies of the S(0) transition levels are shown in Fig. 3 for ρ* = 0.8 and T = 308K. Anisotropy splittings as large as 300 cm^{-1} are

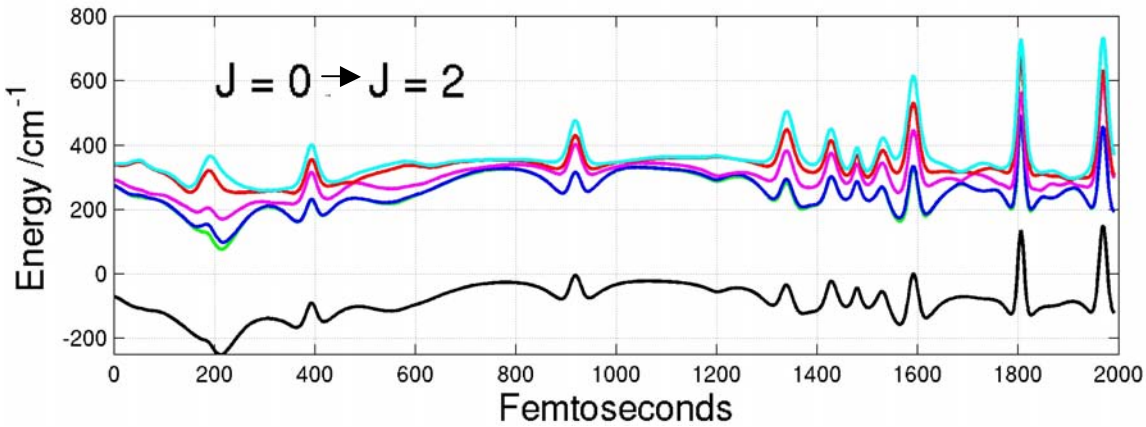

Fig. 3. Calculated instantaneous adiabatic rotational energies of the S(0) Raman transition of H_2 in CO_2 at T = 308 K and ρ* = 0.8.

observed but these are not big enough to mix different J levels in CO_2.

The corresponding adiabatic and nonadiabatic Raman S(0) and S(1) correlation functions are compared with the experimentally derived ones in Fig. 4 for ρ* = 0.8, T = 308K. As seen in this figure, agreement with theory can only be achieved when the nonadiabatic mixing is included. Theory captures the nonexponential character at early times. The agreement between theory and experiment with the current anisotropoic model is better for the S(0) transition probably due to the more anisotropic J = 1 initial level of the S(1) transition.

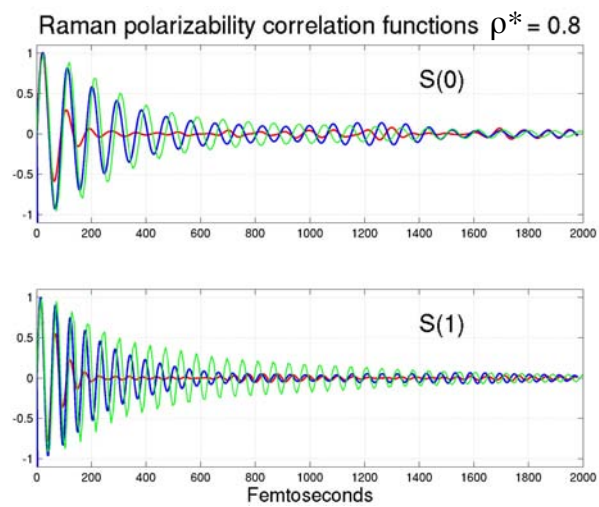

Fig. 4. Comparison of experimental and calculated adiabatic and nonadiabatic S(0) and S(1) Raman responses for ρ* = 0.8 and T = 308K.

Conclusions. Analysis of the time domain Raman coherence decays coupled with mixed classical/quantum MD simulations incorporating nonadiabatic effects can be a sensitive probe of solvent fluctuation dynamics, in general. In SCF's we hope to see dynamical structural effects associated with near critical solvation phenomena, such as clustering or longer range fluctuations manifested in these decays. Subsequent improvements to the model anisotropic potential will be implemented. Additional tests of this analysis are given by D_2/CO_2 Raman responses.

References

1. D. G. Taylor and H. L. Strauss, J Chem Phys **90** (2), 768 (1989).
2. D. G. Taylor and H. L. Strauss, J Chem Phys **96** (5), 3367 (1992).
3. S. M. Howdle and V. N. Bagratashvili, Chem. Phys. Lett. **214**, 215 (1993).
4. H. S. Mei, L. Xiao, and D. F. Coker, J Chem Phys **105**, 3938 (1996).
5. L. Xiao and D. F. Coker, J Chem Phys **100**, 8646 (1994).
6. L. Xiao and D. F. Coker, J Chem Phys **102**, 1107 (1995).

Future Directions

Real-time molecular vibrational frequency and amplitude probing to resolve instantaneous structure

Takayoshi Kobayashi and Yoshiharu Yuasa
Department of physics, Graduate School of Science, University of Tokyo, 7-3-1 Hongo, Bunkyo-ku, Tokyo, 113-0033, Japan
Tel. +81-3-5841-4228, Fax. +81-3-5841-4240, yuasa@femto.phys.s.u-tokyo.ac.jp

Optical and electrical properties of conjugated polymers have attracted enormous attention because of their unique properties as model compounds of one-dimensional electronic systems. Among conjugated polymers polydiacetylenes (PDA's) have special interests because of their large nonlinearity. The ultrafast optical responses in PDA's have been intensively investigated using femtosecond absorption spectroscopy. The mechanism was explained by the following model. First, photoexcited ^1B_u free exciton (FE) relaxes to the nonfluorescent ^1A_g state, which lies lower than the ^1B_u exciton. The nonthermal ^1A_g state relaxes to the bottom of potential curve of the self-trapped exciton (STE) state and then thermalizes and then relaxes to the ground state.

In the present paper, real time evolution of the energies and intensities of features in transmittance change spectra was investigated and real-time vibrational frequencies of several modes were found to provide important information of instantaneous structure of polymers.

In the normalized difference transmission ($\Delta T/T$) spectra, two components with different lifetimes were separated by the singular value decomposition (SVD) method. One is short-lived component of about 60 fs and the other is long-lived component of about 0.9 ps. In the separated spectrum of short-lived component, five positive peaks are found which are assigned to induced emission from the excited-state (ES) vibrational levels to the ground-state (GS) vibrational levels where no population exists because of much larger energies of the levels than the thermal energy of these peaks. Negative peaks in short-lived components could be due to induced absorption, but probe photon energy measured in this study is out of the range of two-photon absorption peaks from the ground state. Therefore only one-photon absorption is to be taken into account in the energy region from 1.68 to 2.28 eV and no induced absorption from 1^1B_u is appeared in short-lived component. The time trace of energy of a short-lived peak near 1.88 eV, which disappear within 100 fs, is shown in Fig. 1 with exponential fitting curves.

The transition energy from ES to GS is directly observed and it is found to shift to lower energy associated with the decay process from 1^1B_u FE to STE and geometrically relaxed 2^1A_g state after photo-excitation. The time constant of the Stokes shift agrees well with decay time (~50 fs) of the induced emission. This is quite reasonable if we consider the facts that the quantum efficiency of emission is smaller than 10^{-5}. Stokes shift has been estimated to be about 90 meV in PDA-3BCMU and 100 meV in red phase of PDA-4BCMU by stationary fluorescence spectra [4-6]. The binding energy of the STE in red-phase 3BCMU is smaller than that of blue-phase 3BCMU as known from the fact that zero phonon transition energy in the former is larger than that of the latter. Therefore, the configuration in the excited state of 4BCMU is considered to be unstable and hence Stokes shift is larger than in 3BCMU.

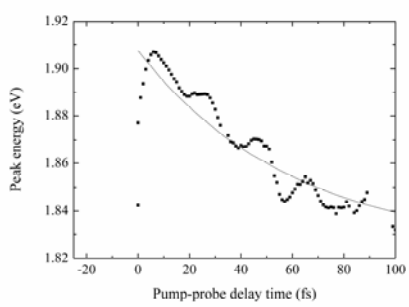

Fig. 1. Energy shifts of peaks due to geometrical relaxation from 1^1B_u FE to 2^1A_g STE.

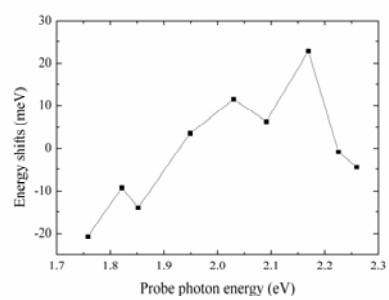

Fig. 2. Energy shifts due to thermalization in 2^1A_g STE during 1400 fs between 100 fs and 1500 fs

Mechanism of a Photo-Rearrangement Revealed by Combining Femtosecond Visible, Raman, and IR-Techniques

S. Laimgruber, W. Schreier, P. Gilch

Department für Physik, Ludwig-Maximilians-Universität München, Oettingenstr. 67, D-80538 München, Germany. Phone: +49-89-2180-9243, Fax: +49-89-2180-9243, e-Mail: peter.gilch@physik.uni-muenchen.de, Internet: www.bmo.physik.uni-muenchen.de

Most organic reactions involve substantial rearrangements of molecules. Identifying the intermediates of such rearrangements, i.e. formulating a reaction mechanism, often has to rely on theory since thermal chemical reaction usually proceed under quasi steady state conditions. Therefore, the concentrations of the intermediates might not surmount the detection threshold. For photochemical rearrangements this needs not to apply, and intermediates might be detected. Ideally, the knowledge gained by such studies may then be transferred to thermal chemical reactions. Tracing photochemical processes requires high temporal resolution, down to say 100 fs, and a detection technique that is sensitive to structural changes. Femtosecond vibrational spectroscopy fulfils these two conditions.

Aromatic nitro compounds will serve as an example to demonstrate the power of this approach. Their photochemistry lends to a number of application, for instance in protection group chemistry and in caged compound experiments. The particular reaction looked upon is the photo-induced transformation of *o*-nitrobenzaldehyde NBA to *o*-nitrosobenzoic acid or the corresponding ester.

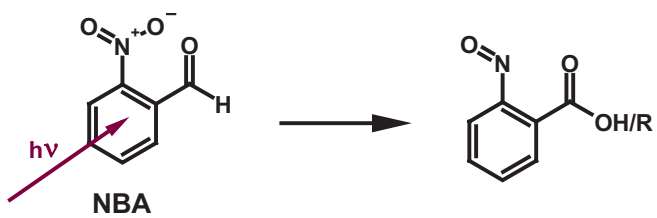

This reaction that has already been addressed by picosecond transient absorption experiments[1]. Here, we will present a comprehensive view on this process by employing femto-second visible, Raman, and IR techniques. The first technique is particularly useful to settle the time scales of the reaction. It is found that in < 1 ps an intermediate I is formed which is transformed to a second intermediate II in ~ 80 ps. That intermediate then forms the final product in ~ 2-3 ns (Figure 1, left). The decay time of intermediate I proves to be particular sensitive to the solvent properties. With increasing water content of the solvent the decay is accelerated – for a water content of 50 % the decay time is as low as 13 ps (Figure 1, right). Based on such solvent dependencies it has been argued[1] that intermediate I is a ketene (structure as given in Figure 2). In fact, a ketene intermediate of the NBA photoreaction has been trapped by matrix isolation in argon at 20 K[2]. A clear cut identification of the ketene was possible via IR spectroscopy. Ketenes feature highly characteristic IR resonances around 2100 cm^{-1} which are due to the anti-symmetric stretch vibration of the ketene function[3]. Probing the photoreaction of NBA with femtosecond IR spectroscopy proves unambiguously that a ketene intermediate is also formed at room temperature and in polar solution. Within the time resolution (~ 400 fs) of the set-up an IR band rises in the ketene stretch region around 2100 cm^{-1} (Figure 2). The signal persists for ~ 60 ps – in line with the decay time derived form the UV/Vis technique. This experiment not only proves the participation of a ketene intermediate in the NBA photo-chemistry but also gives information on the vibrational dynamics during the ketene formation.

---

[1] R.W. Yip, and D.K. Sharma, Research on Chemical Intermediates, **1989**, 11, 109-116
[2] S. Kuberski and J. Gebicki, J. Mol. Struct. **1992,** 275, 105-110
[3] J.L. Duncan , A.M. Fergusson, J. Harper, and K.H. Tonge, J. Mol. Spectr. **1987,** 125, 196-213

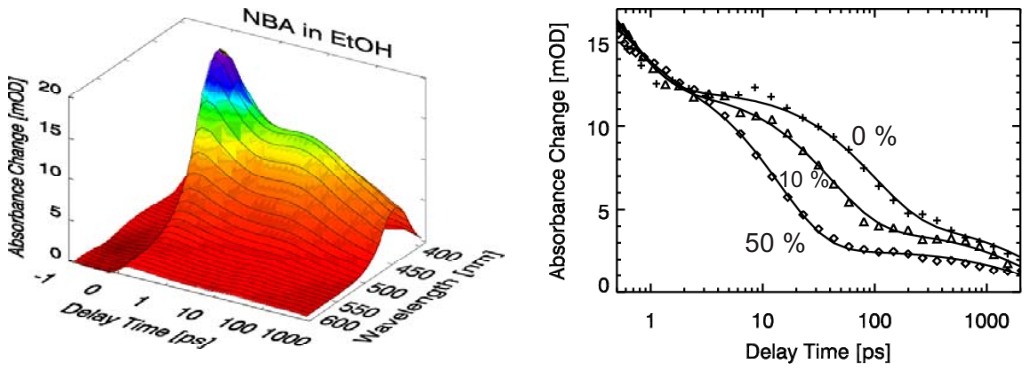

Figure 1. Femtosecond UV/Vis absorption changes of NBA in ethanol after 260 nm excitation. *Left*: Overview in neat ethanol. *Right*: Dependence of the time traces at 475 nm on the water content of ethanol.

The ketene formation goes along with a substantial reorganisation of the (former) aldehyde substituent. This translates into a strong excitation of the ketene vibration. In the IR experiment this excitation is expressed as an initial low frequency shift of the ketene resonance which relaxes as the vibration cools down.

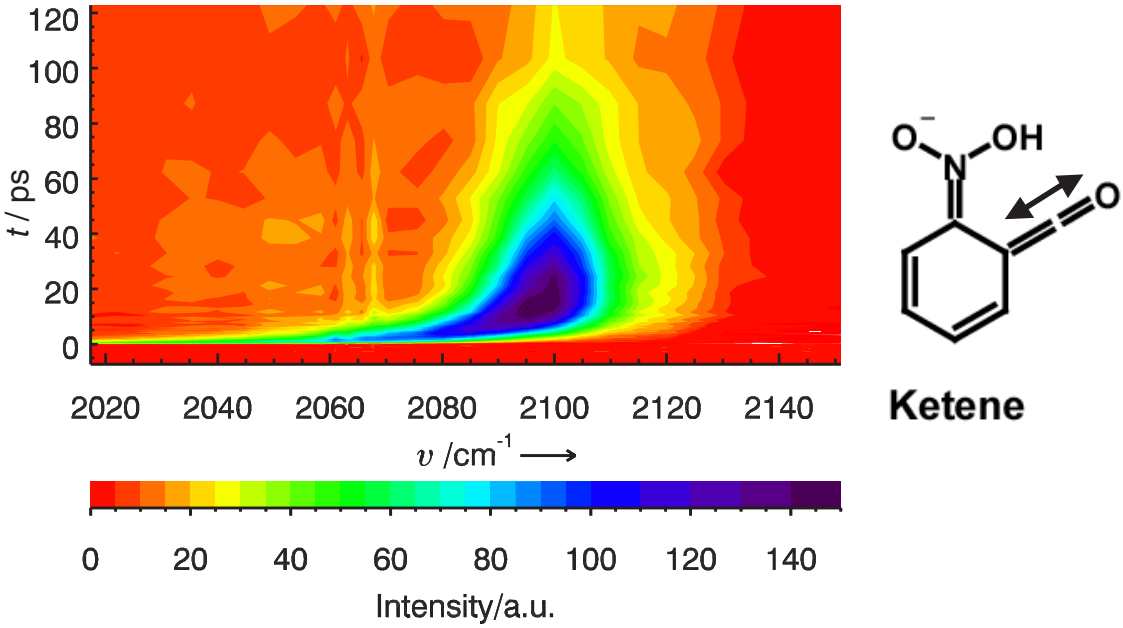

Figure 2. Femtosecond IR absorption changes of NBA in ethanol after 260 nm excitation. Blue coloring stands for strong induced absorption. The observed vibrational resonance is due to the asymmetric stretch vibration of the ketene function.

Vibrational spectroscopy also holds information of the product of the ketene decay (intermediate II). Based on the strong solvent dependence of the ketene decay time it was argued that the ketene reacts with a solvent molecule[1]. In the present case several tautomeric forms of a ketene-ethanol-adduct are conceivable (structures **A** – **C** in Figure 3). Alternatively, one could imagine that the ethanol solvent catalyses – via hydrogen bonding – an *intramolecular* ring closure reaction. This would result in structure **D** or tautomers of it. Femtosecond IR spectra in the carbonyl range (around 1700 cm^{-1}) exclude form **A.** These spectra (data not shown) demonstrate that the intermediate II carries a carbonyl function. To further constrict the structure time resolved Raman experiments were performed. These

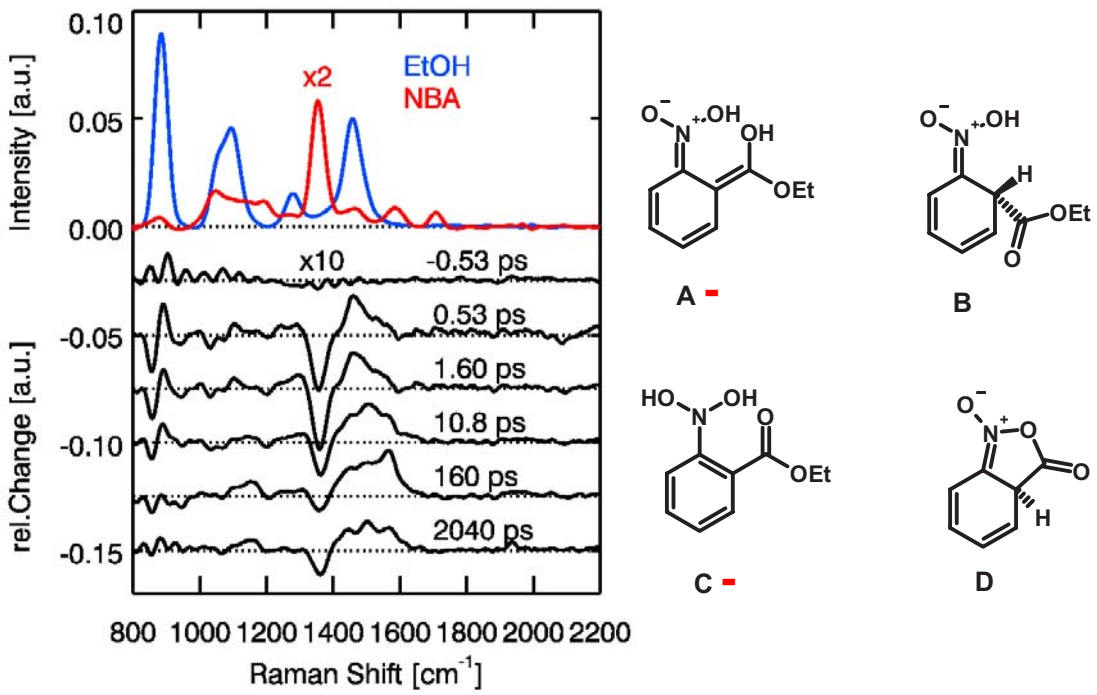

Figure 3. Femtosecond stimulated Raman spectra of NBA in ethanol after 260 nm excitation in comparison with cw spectra (upper part). Possible structures of intermediate II present at 160 ps are included. Those that can be ruled out spectroscopic grounds are marked with a "-".

experiments relied on femtosecond stimulated Raman scattering[4,5]. In contrast to other implementation of this technique, here a ~ 400 nm Raman pump pulse was used to resonantly enhance the solute signal. The time resolved difference spectra (Figure 3) feature a pronounced bleach at the location of symmetric NO_2 stretch of NBA (1360 cm^{-1}) and distinct new bands in between 1400 – 1600 cm^{-1} due to the Raman resonance of the intermediate. Let us focus on the 160 ps spectrum when the reaction is in the intermediate II stage. It bears a pronounced resonance around 1550 cm^{-1}. Such a resonance is indicative of a cyclohexadiene motif[6] as contained in the suggested structures **B** and **D**, most likely ruling out form **C** with its phenyl ring. This interpretation is underscored by DFT calculations. At present we cannot decide upon **B** and **D** since we are lacking spectroscopic data in OH stretch region. The respective experiments are currently undertaken. In either case, the intermediate II then is transformed to the final nitroso product.

In conclusion, modern femtosecond vibrational spectroscopy allows to identify short lived intermediates of photochemical transformation and thereby answer longstanding in mechanistic photochemistry. In that respect, the combination of IR and Raman spectroscopy proves to be particularly useful as both techniques have their particular sensitivity. In the present context, IR spectroscopy is unbeatable for the identification of the ketene intermediate. Raman spectroscopy demonstrates its strength when it comes to detecting molecules with distinct C=C double bond structures. Finally, with the present work we have enlarged the region of application of femtosecond stimulated Raman scattering to photochemistry.

---

[4] M. Yoshizawa, H. Aoki, M. Ue, H. Hashimoto, Physical Review B **2003**, 67, 174302-1-7
[5] D.W. McCamant, P. Kukura, S. Yoon, R. Mathies, Rev. Sci. Instrum. **2004** 75 4971-4980
[6] Raman/IR Atlas of Organic Compounds, B. Schrader and W. Meier, Verlag Chemie 1974

Hydrogen Bonding Dynamics of Interfacial Water by Spectrally- and Time-Resolved Sum Frequency Generation (STiR-SFG)

Andrey N. Bordenyuk and Alexander V. Benderskii
Department of Chemistry, Wayne State University, Detroit, MI 48202
alex@chem.wayne.edu

Abstract:
Spectrally- and Time-Resolved Sum Frequency Generation (STiR-SFG) is presented as the lowest-order nonlinear technique that is both surface-selective and capable of measuring spectral evolution of vibrational coherences. Ultrafast spectral dynamics of the OD-stretch of D_2O at the CaF_2 surface was measured to investigate how the dynamics of water H-bond network is affected by the interface. Tuning the IR pulse wavelength to the blue or red side of the OD-stretch transition, we selectively monitor the dynamics of different sub-ensembles in the distribution of the H-bond structures. A dynamical heterogeneity of the aqueous hydrogen bonding network at interfaces is discovered. The blue-side excitation (weaker H-bonding structures) shows monotonic decay and red-shift of ν(OD) frequency on a 100 fs time scale. In contrast, the red-side excitation (stronger H-bonding structures) results in a blue-shift and a recursion at 125±10 fs, indicating the presence of an underdamped intermolecular mode of interfacial water.

1. Introduction

Molecular properties of water adjacent to interfaces critically affect many biochemically, biophysically, and technologically important processes. The static and dynamic properties of water are largely determined by its hydrogen-bonding network. Surface-specific interactions make the thin interfacial layer of interfacial water significantly different from bulk water. Aqueous H-bond network is very dynamic, evolving on the sub-picosecond time scale. A complete characterization of the H-bond network of water at interfaces requires measurements of ultrafast dynamics to complement the time-averaged structure characterization by conventional frequency-domain spectroscopy. We present Spectrally- and Time-Resolved Sum Frequency Generation (STiR-SFG) vibrational spectroscopy, a new surface-selective technique capable of monitoring the ultrafast evolution of the hydrogen-bonding patterns at water interfaces through the spectral dynamics (vibrational frequency shift) of the OH (OD) stretch. Results for a simple liquid/solid interface, D_2O/CaF_2, are presented as a first example of application of this technique.

2. Experimental Method

The mixed time-frequency domain 3-wave mixing spectroscopy technique, STiR-SFG, builds upon the purely time-domain method of SFG Free Induction Decay (SFG-FID).[1,2] In SFG-FID, a short IR pulse excites the vibrational coherence, creating an oscillating first-order polarization, and a delayed visible pulse monitors its Free Induction Decay (FID) by up-converting the oscillating surface polarization into the SFG signal. The SFG-FID signal intensity is recorded as a function of the delay τ between the two pulses. In the STiR-SFG, the signal generated by a short IR and time-delayed visible pulses is dispersed through a monochromator and the SFG spectrum (rather than just overall signal intensity) is recorded as a function of IR-visible delay. The results are plotted as a two-dimensional image in (*SFG wavelength; time delay*) axes. The 1st order polarization $P^{(1)}(t)$ is a convolution of the molecular response function of the surface $S(t)$ with the IR field $E_{IR}(t)$; the 2nd order polarization $P^{(2)}(\tau,t)$ results from up-conversion of the $P^{(1)}(t)$ by the time-delayed visible pulse $E_{vis}(t-\tau)$,

$$P^{(1)}(t) = \int_{-\infty}^{+\infty} E_{IR}(t-t')S(t')dt' \quad , \qquad P^{(2)}(t,\tau) = E_{vis}(t-\tau)P^{(1)}(t) \qquad (1)$$

where τ is the IR-visible time delay (note that we assume a non-resonant visible field). In the STiR-SFG measurement, monochromator performs a Fourier transform of the SFG field emitted by the 2nd order polarization $P^{(2)}(\tau,t)$ with respect to time t before its intensity is detected by the CCD

$$I_{\text{STiR-SFG}}(\omega_{SFG},\tau) \propto \left| \int_{-\infty}^{+\infty} P^{(2)}(t,\tau)e^{-i\omega_{SFG}t}dt \right|^2 = \left| \int_{-\infty}^{+\infty} P^{(1)}(t)E_{vis}(t-\tau)e^{-i\omega_{SFG}t}dt \right|^2 \qquad (2)$$

The recorded signal is therefore a sliding window Fourier transform of the oscillating polarization $P^{(1)}(t)$, roughly measuring its instantaneous frequency around time $t=\tau$ (IR-visible delay), within the window provided by the visible up-conversion pulse. Such measurement therefore allows observation of ultrafast spectral diffusion.

The STiR-SFG measurements is an SFG analog of the Frequency Resolved Optical Gating (FROG). Correspondingly, it is extremely sensitive to the chirp in the IR and visible pulses. The instrument response function, i.e. the frequency-resolved IR-visible pulse cross-correlation was recorded by imaging SFG from a nonresonant substrate (dry surface of the CaF_2 slide) onto the CCD *simultaneously with the* STiR-SFG *signal*. This allows deconvolution of the probe laser fields form the observed dynamics.

3. Results and Discussion

The frequency-domain spectrum of ν_{OD} band of D_2O at the CaF_2 surface (Fig. 1), was recorded using a Broad-Band SFG technique.[3] The broad line (FWHM~200 cm^{-1}) indicates a distribution of H-bonding structures.

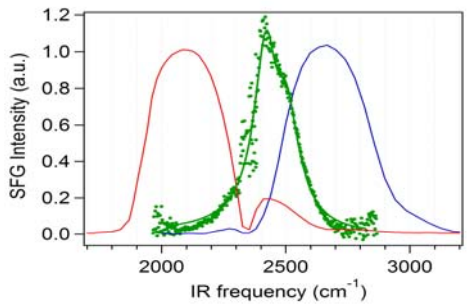

Fig. 1. Frequency-domain SFG spectrum of the ν(OD) transition of D_2O at CaF_2 interface (dots – experimental data, green line- fit). IR pulse spectra used for the Spectrally- and Time-Resolved SFG measurements (STiR-SFG) are shown in thin blue and red lines.

A more informative measurement for this system is the mixed frequency- and time-domain STiR-SFG experiment (Fig. 2), which shows rapid total dephasing of the OD-stretch on the ~150 fs time scale and the spectral dynamics underlying the broad frequency-domain spectrum in Fig. 1. Here, we take advantage of the fact that the transition is almost as broad as the IR pulse spectral width. Tuning the IR pulse to the first to the blue and then to the red side of the ν_{OD} band (Fig. 1), we record the ultrafast spectral dynamics of the OD-stretch indicating structural rearrangement on the sub-100 fs time scale. For IR excitation on the blue side (ν_{IR}=2650 cm^{-1}) of the ν_{OD} band (weaker H-bonding structures), the STiR-SFG signal shows monotonic decay and spectral shift to the red (Fig. 2, left), towards the equilibrium SFG spectrum peak 2450 cm^{-1}, on a 100 fs time scale. In contrast, stronger H-bond structures excited on the red side (ν_{IR} = 2200 cm^{-1}), show markedly different dynamics (Fig. 2, right): there is the blue shift towards the equilibrium distribution accompanied by a weak recursion at ~ 130 fs.

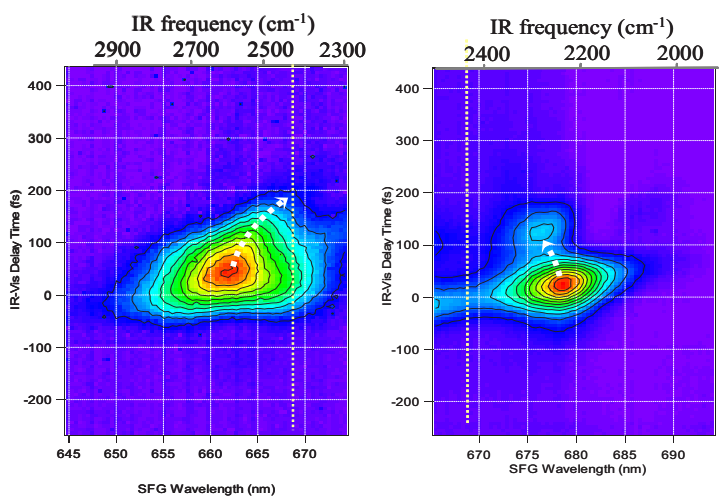

Fig. 2. Spectrally- and Time-Resolved SFG of D_2O at CaF_2 interface. Left: IR excitation 2650 cm^{-1} (blue side). Right: IR excitation 2200 cm^{-1} (red side). Vertical axis: IR-visible delay time (fs), horizontal axis: SFG wavelength.

The observed recursion in the frequency-resolved SFG-FID signal points to the existence of an underdamped oscillatory mode in the H-bond network, something that is not obvious from the featureless frequency-domain line

shape. Interestingly, our measurements indicate that the recurrence results only from the H-bond structures that are on the red side of the spectrum, i.e. the sub-ensemble with stronger-than-average hydrogen bonds selected by our excitation IR pulse.

In order to model the observed spectral dynamics of the OD-stretch at the D_2O/CaF_2 interface, we consider the molecular response function in the form

$$S(t) = -i\theta(t)\exp\left[-i\int\omega_{01}(t)dt - \Gamma(t)t\right] + c.c. \quad (3)$$

This 'toy' response function results from a Franck-Condon approximation[4] that separates the high-frequency ν_{OD} mode from the slow motions of the H-bond network that modulate the energy gap between ν_{OD}=0 and ν_{OD}=1 terms. $\omega_{01}(t)$ describes the fluctuating energy gap between $|v=0\rangle$ and $|v=1\rangle$ levels as a one-dimensional projection of the complex dynamics of the hydrogen bonding environment of the OD chromophore at the interface. $\Gamma(t)$ is (time-dependent) total dephasing rate. The fluctuating energy gap is conveniently described in terms of a time correlation function for the transition frequency

$$C_\omega(t) \equiv \frac{\omega_{01}(t) - \omega_{01}(\infty)}{\omega_{01}(0) - \omega_{01}(\infty)} \quad (4)$$

The IR pulse does not excite the whole ground state distribution of H-bond configurations, but rather selects a sub-ensemble on either the red or the blue side of the transition (Fig. 1). Correspondingly, $S(\omega_{IR},t)$ is not the complete response function of the system, but rather describes the dynamics of the selected sub-ensemble, hence it is dependent on the IR pulse excitation frequency ω_{IR}. Our model developed for calculation of the mixed time-frequency SFG spectroscopic signals explicitly takes into account the laser pulse fields that enter Eqs. (2) to reproduce the SFG-FROG cross-correlation, thus allowing extraction of the molecular response functions $S(\omega_{IR},t)$.

The dynamics observed for the blue side IR excitation (Fig. 2 left) can be well modeled using a time-dependent red-shift described by a monotonically decaying (overdamped) Gaussian correlation function

$$C_\omega^{blue}(t) = \exp(-t^2/\tau_\omega^2) \quad (5)$$

The recursion observed for the excitation on the red side of the ν_{OD} transition (Fig. 2 right) clearly indicates the presence of an oscillatory component in the dynamics, which can be qualitatively reproduced by using a damped cosine correlation function,

$$C_\omega^{red}(t) = \frac{1}{2}\{1+\cos(\Omega_\omega t)\}\exp(-t^2/\tau_\omega^2) \quad (6)$$

Similar recurrence was recently observed in bulk HOD/D_2O system by 3-pulse photon echo peak shift,[5] and predicted theoretically.[6-8] Interestingly, our measurement indicates that the recurrence results only from the H-bond structures that are on the red side of the spectrum (stronger-than-average hydrogen bonds). Qualitatively different dynamics observed for the different sub-ensembles in the distribution of the H-bond structures point to the dynamical heterogeneity of interfacial water.

In conclusion, STiR-SFG is a new technique that provides insight into the ultrafast H-bond dynamics at surfaces by mixing time- and frequency-domain. Ultrafast spectral dynamics of D_2O at CaF_2 interface indicate rearrangements of the hydrogen bond network on 100 fs time scale. *Dynamical heterogeneity* of aqueous H-bond network at interfaces is discovered.

References

(1) Owrutsky, J. C.; Culver, J. P.; Li, M.; Kim, Y. R.; Sarisky, M. J.; Yeganeh, M. S.; Yodh, A. G.; Hochstrasser, R. M. *J. Chem. Phys.* **1992**, *97*, 4421.

(2) Guyot-Sionnest, P. *Physical Review Letters* **1991**, *66*, 1489.

(3) Richter, L. T.; Petralli-Mallow, T. P.; Stephenson, J. C. *Optics Letters* **1998**, *23*, 1594.

(4) Mukamel, S. *Principles of Nonlinear Optical Spectroscopy*; Oxford University Press: New York, 1995.

(5) Fecko, C. J.; Eaves, J. D.; Loparo, J. J.; Tokmakoff, A.; Geissler, P. L. *Science* **2003**, *301*, 1698.

(6) Lawrence, C. P.; Skinner, J. L. *Journal of Chemical Physics* **2003**, *118*, 264.

(7) Steinel, T.; Asbury, J. B.; Corcelli, S. A.; Lawrence, C. P.; Skinner, J. L.; Fayer, M. D. *Chemical Physics Letters* **2004**, *386*, 295.

(8) Corcelli, S. A.; Lawrence, C. P.; Asbury, J. B.; Steinel, T.; Fayer, M. D.; Skinner, J. L. *Journal of Chemical Physics* **2004**, *121*, 8897.

Progress report from a neighbor of infrared – tracing “loose electrons” with femtosecond time-resolved near-infrared spectroscopy

Koichi Iwata
E-mail, iwata@chem.s.u-tokyo.ac.jp.
Research Centre for Spectrochemistry, School of Science, The University of Tokyo
Bunkyo-ku, Tokyo 113-0033, Japan.

”Loose electrons”

In chemical reactions, electrons escape from the attractive force of the nuclei and move to new locations where they form new chemical bonds. Electrons loosely bound to the nuclei, or “loose electrons”, play an essential role in the relocation process. It is vital to develop an experimental method that can specifically detect the “loose electrons”. It has been known that many “loose electrons”, such as electrons in charge transfer (CT) states, in the semiconductor conduction bands, in excited states delocalized in C=C conjugated chains, or solvated electrons show absorption bands in the near-infrared region. We develop a femtosecond time-resolved near-infrared spectrometer for tracing the fast dynamics of the loose electrons formed in chemical reactions.

Spectrometer

Our time-resolved near-infrared spectrometer covers the spectral range of 0.9 to 1.5 μm with the detection sensitivity of 10^{-4} in the absorbance unit [1]. The second or third harmonic of a femtosecond Ti:sapphire amplifier output is used as the pump light. The near-infrared portion of the white light continuum generated by the self phase modulation on a sapphire plate is used as the pump light. Two sets of 256-channel InGaAs array detectors are used for the detection of the near-infrared light. The first set is used for detecting the “sample” probe light, while the second set is used for the “reference” light.

Fast carrier dynamics in TiO_2 and Pt/TiO_2 powders [1]

It is difficult to directly measure the time-resolved ultraviolet or visible absorption spectra of samples that strongly scatter the visible light, such as photocatalytic powders. By using the near-infrared probe light, however, we can often measure the time-resolved spectra of the scattering samples with the transmission method.

When the TiO_2 photocatalytic particles are photoexcited, electrons and holes are generated. These

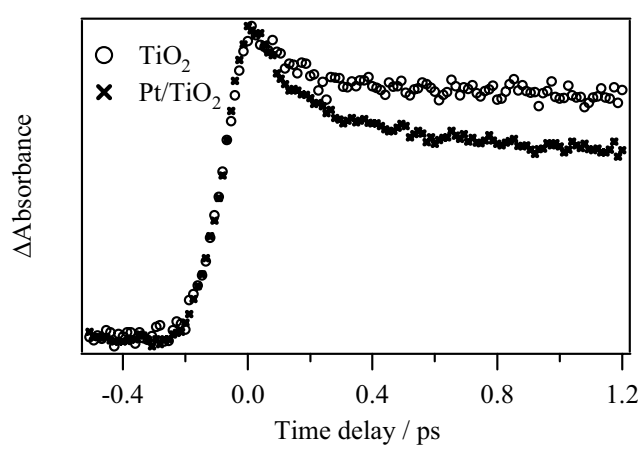

Fig. 1 Decay dynamics of charge carriers photogenerated in TiO_2 and Pt/TiO_2 probed at 1200 nm.

charge carriers eventually reach the surface of the particles and start a series of photocatalytic reactions by reducing or oxidizing other molecules there. We study the initial process of these photocatalytic reactions by monitoring the fast dynamics of the charge carriers generated in the TiO_2 particles.

We compared the decay kinetics of the charge carries in the TiO_2 powders (TIO4, diameter 21 nm) and in the Pt/TiO_2 powders that contain Pt as a co-catalyst. The decay kinetics observed for TiO_2 shows a fast component of 160 fs, which most probably reflects the trapping process of the electrons. For Pt/TiO_2, an additional decay component of 2.3 ps is also observed (Fig. 1). We think that the 2.3 ps process represents the migration of the electrons from TiO_2 to the loaded Pt co-catalyst. After the migration, the electron-hole recombination process becomes slower. The charge carriers have longer time for the reduction or oxidization reactions, which explains the activity increase by the Pt co-catalyst.

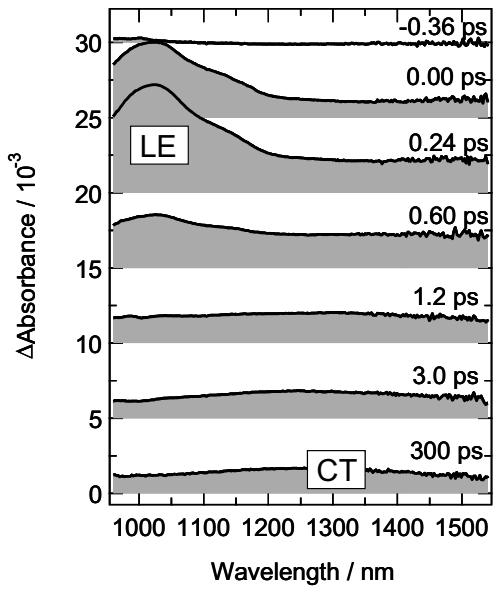

Fig. 2 Time-resolved near-infrared spectra of 9,9'-bianthryl photoexcited in acetonitrile.

CT state formation and solvation in 9,9'-bianthryl [2]

When 9,9'-bianthryl is photoexcited, the locally excited (LE) state is formed first. In polar solvents, the LE state is converted to the charge-transfer (CT) state. This reaction is one of the simplest and most basic photoelectron transfer reactions. Although the reaction has been studied intensively, its mechanism has not been fully understood. Detailed knowledge on the reaction kinetics is essential for understanding the reaction.

With time-resolved near-infrared spectroscopy, both of the decay of the LE state and the rise of the CT state have been successfully detected (Fig. 2). The CT state is formed in 0.4 ps in acetonitrile [2]. We can further separate the observed near-infrared absorption bands numerically by using the results of polarized absorption measurements. It has been expected that the transition dipoles for the LE band and the CT bands are parallel and perpendicular to the long axis of the anthracene ring, respectively. The observed "time-resolved absorption anisotropy spectra" confirms the expected directions of the transition dipoles. The analysis of the experimental data shows that "partially CT" state is formed immediately after the photoexcitation, both in acetonitrile and in heptane. Only in acetonitrile, more stabilized CT state is formed as the solvation process proceeds. We think that this simple model based on the observed time-resolved near-infrared spectra explains the basic mechanism of the photoelectron transfer reaction in 9,9'-bianthryl.

References

1. K. Iwata, T. Takaya, H. Hamaguchi, A. Yamakata, T. Ishibashi, H. Onishi, and H. Kuroda, J. Phys. Chem. B, **108**, 20233 (2004).

2. T. Takaya, H. Hamaguchi, H. Kuroda, and K. Iwata, Chem. Phys. Lett. **399**, 210 (2004).

Broadband CARS Microscopy

T.W. Kee and M.T. Cicerone

Polymers Division, NIST
Gaithersburg, MD 20899

We have developed an adaptation of coherent anti-Stokes Raman scattering (CARS) microscopy which uses only a single Ti:Sapphire laser, but gives > 2500 cm^{-1} bandwidth, sufficient for simultaneous identification of many distinct species in chemically complex samples. Using power levels that are not toxic to rapidly dividing cells, we are able to acquire a single hyperspectral pixel in milliseconds, so that the technique is potentially amenable to 3D imaging of live, developing cells and tissue. Development of this technique is a work-in-progress, and we will discuss progress along these lines.

Tracking excited state dynamics with coherent control: automated limiting of population transfer in LDS750.

Omer Nahmias, Oshrat Bismuth, Ofir Shoshana and Sanford Ruhman
Department of Physical Chemistry and the Farkas Center for Light Induced Processes,
The Hebrew University, Jerusalem 91904, Israel.

Shaping ultrashort laser pulses to control photoinduced molecular dynamics is the subject of active current investigation[1,2,3]. Starting more than a decade ago, theoretical studies demonstrated that properly chirped broad-band pulses could improve on the performance of their transform limited analogues in achieving a variety of dynamic goals[4,5,6,7]. Considering resonant excitation of a one dimensional photodissociative model, Ruhman and Kosloff showed that with the right amount of negative linear chirp, a single excitation pulse comprises a complete pump and dump sequence[8], enhancing the amplitude of ground state vibrational coherences. In a series of pioneering experiments, Shank and coworkers produced short enough pulses for testing these predictions on real molecular systems[9], showing that aside from enhancing ground state vibrational coherence, linear chirp also induces transparency via the same pump-dump mechanism, - leading to minimization of fluorescence from organic dye solutions.

In our experiments an automated pulse shaper based on a micromachined deformable mirror (DM) guided by a genetic algorithm were used in conjunction with a broad-band noncollinear optical parametric amplifier (NOPA), to investigate population transfer in LDS750 dye solutions in acetonitrile and in ethanol. We chose a laser dye whose spontaneous emission serves as a built in gauge for residual excited state population. In the case of this particular dye a large body of work concerning ultrafast photophysics exists which can be used to compare with the results of our study[10,11,12]. Contrary to the assertion of Cerullo et.al. that solvent relaxation contributes significantly to dynamic Stokes shifting of LDS750, much of the excited state dynamics recorded in those studies were dominated by intramolecular coordinates, with the steady state emission taking place from an isomer of the optically accessed excited state.

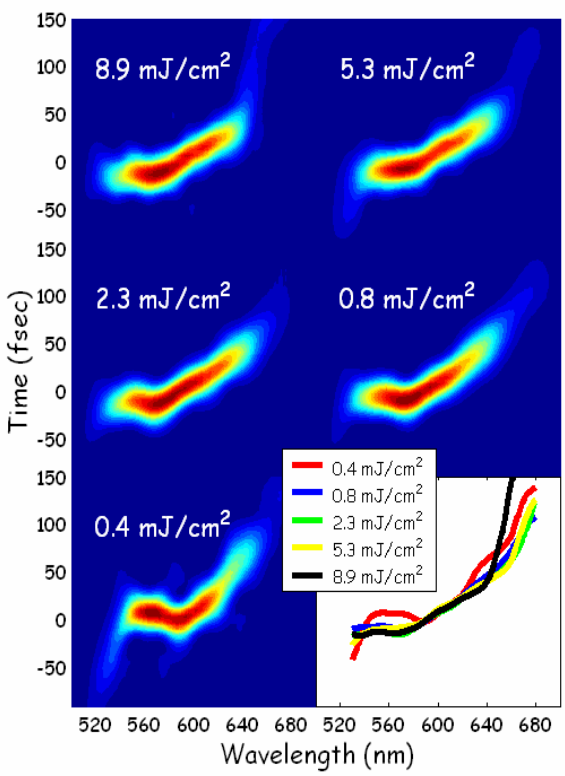

Figure 1

Our main objective here is to discover whether nonlinearly chirped pulses made available by flexible pulse-shaping methods can reduce population transfer in a polyatomic chromophore in solution below levels attained by linear chirp alone, and if so, whether the

resulting pulse shapes can be rationalized in terms of the underlying photoinduced molecular dynamics. We further aimed to test whether the optimal pulse shape for minimal population transfer is a function of the pulse fluence or of the solvent.

The control experiments were conducted using 7 fsec NOPA pulses extending from 520 to 700 nm which were pre-compressed in a fused silica prism pair in order to increase the negative GVD provided by our DM shaper. The beam fluence was adjusted to ~ 100 nJ and focussed into the sample with an off axis paraboloid. Fluorescence from the dye cell was detected by an amplified silicon photodiode through a 695 nm high pass cutoff filter to discriminate fluorescence from pump pulse scatter. The fluorescence signal from the photodiode, V_f, is digitized and used as feedback in a genetic algorithm which minimizes the fluorescence signal. Optimal pulses were characterized in a polarization gate FROG setup which uses a 0.5 mm fused silica flat as the Kerr medium.

Results of optimization runs in acetonitrile are presented in figure 1 where a series of FROG traces of the optimal pulses at various excitation fluences are shown. In the last panel a plot of the GDD curves obtained from the contour maps above are presented for comparison. The similarity of the GDD at the different fluences is obvious both from the FROG traces themselves, and from the GDD curves below. The optimal GDD for minimizing LDS750 fluorescence in acetonitrile exhibits a constant group delay below 580 nm comprises a nearly transform limited pulse in this region. At higher wavelengths the spectral components arrive at later and later delays. The chirp rate is nearly constant at first with a GDD of -140 $fsec^2$/rad up to $\lambda \sim 660$ nm, slowing even further beyond that wavelength. This general structure is conserved for ethanol solutions as well. The results show that the chirp rate is somewhat lower in ethanol, and the further falling off is slightly earlier in that solvent.

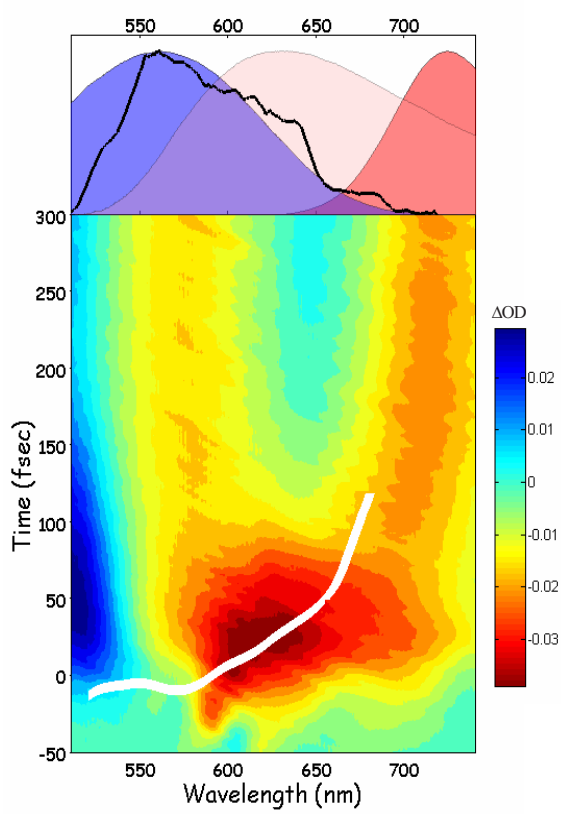

Figure 2

In order to assess the strategy by which minimal population transfer is achieved in these experiments, we compare the optimal GDD with multichannel transient transmission data measured in acetonitrile, as depicted in figure 2. The data was recorded with a similar laser system pumping a 20 fsec parametric amplifier (TOPAS), with transient spectra collected in a double spectrometer system described in the literature[13]. The upper panel shows the linear absorption and the time integrated fluorescence spectra of LDS750 in acetonitrile, along with the intensity spectrum of our NOPA pulses. The lower panel displays a contour plot of the transient spectral variations induced by 600 nm photoexcitation of LDS750 in acetonitrile as a function of pump-probe delay in the range from 500-900

nm. Increased transmission is depicted in shades of red and brown, with excess absorption in shades of blue (see ΔOD scale on color-bar).

As described by Ernsting and coworkers, excitation gives rise to an instantaneous excited state absorption band to the blue of that of the ground state. Emission and ground state bleach overlap at early delay times to produce a broad excess transmission feature which gradually separates into two distinct bands due to ground state relaxation, and excited state isomerization. Juxtaposed on this contour plot is the averaged optimal GDD obtained from the FROG scans in acetonitrile and depicted in figure 6. Even on a phenomenological level, the comparison of the GDD and multichannel data shows that the spectral components above 580 closely follow the Stokes shifting of the emission band.

In view of the compiled data in figure 6, our understanding of how these pulses realize maximal transparency is as follows: The blue transform limited portion builds up an impulsive "initiation" pulse, which serves to launch a focused wave packet on the excited surface. Following the blue “initiation” interaction, the remainder of the NOPA field comprises a "tracking" chirped red tail which follows the evolving excited population in frequency and in time, and efficiently stimulates emission as the excited state dynamics are underway. This GDD thus produces an ideal single pulse concerted pump-dump sequence which optimally obtains the control objective of inducing transparency and minimizing the ultimate population of the excited state. This spectral method accordingly provides a single pulse probe for covering ultrafast spectral evolution in the excited sample. Future efforts will be dedicated to appreciating why fluence has such a slight effect on the optimal pulse GDD, and exploring this process in a broader range of solvents.

---

[1] Brixner, T.; Gerber, G.; *CHEMPHYSCHEM* **2003**, *4*, 418.

[2] Rice, S. A.; Zhao, M.;*Optical Control of Molecular Dynamics*, Wiley, New York, **2000**.

[3] Kawashima, H.; Wefers, M. M.; Nelson, K.A.; *Annual Review of Physical Chemistry* **1995**, *46*, 627.

[4] Shi, S.; Woody, A.; Rabitz, H.; *J. Chem. Phys.* **1988**, *88*, 6870.

[5] Chelkowski, S.; Bandrauk, A. D.; Corkum, P. B.; *Phys. Rev. Lett.* **1990**, *65*, 2355.

[6] Krause, J. L.; Whitnell, R. M.; Wilson, K. R.; Yan, Y.; Mukamel, S.; *J. Chem. Phys.* **1993**, *99*, 6562.

[7] Melinger, J. S.; Gandhi, S. F. L.; Hariharan, A.; Goswami, D.; Warren, W. S.; *J. Chem. Phys.* **1994**, *101*, 6439.

[8] Ruhman, S.; Kosloff, R.; *J. Opt. Sot. Am. B* **1990**, *7 (8)*, 1748.

[9] Cerullo, G.; Bardeen, C. J.; Wang, Q.; Shank, C. V.; *Chem. Phys. Lett.* **1996**, *262*, 362.

[10] Kovalenko, S. A.; Ernsting, N. P.; Ruthmann, J.; *J. Chem. Phys.* **1997**, *106*, 3504.

[11] Bardeen, C. J.; Rosenthal, S. J.; Shank, C. V.; *J. Phys. Chem. A* **1999**, *103*, 10506.

[12] Knorr, F. J.; Wall, M. H.; McHale, J. L.; *J. Phys. Chem. A* **2000,** *104,* 9494.

[13] Ernsting, N. P.; Kovalenko, S. A.; Senyushkina, T.; Saam, J.; Farztdinov, V.; *J. Phys. Chem. A* **2001,** *105,* 3443.

Towards Vibrationally Mediated Chemistry in Solution

Leonid Sheps, Andrew C. Crowther, and F. Fleming Crim
Dept. of Chemistry, University of Wisconsin, Madison

Introduction

Chemical reactions involve rearrangement of atoms and the breaking and formation of chemical bonds. Many have significant energy barriers that need to be overcome, and often only a small fraction of the molecules have enough energy to react. In such cases vibrational enhancement of reaction rates is possible. The idea, sometimes called vibrationally mediated chemistry, is to deposit vibrational energy into a molecular motion that couples well to the reaction coordinate in order to surmount the reaction barrier and to enhance the rate much more than predicted by statistical heating.

Many elegant examples of this technique exist in the gas phase, where reaction dynamics is a mature field[1,2]. However, in solution vibrationally mediated chemistry remains an elusive goal for two reasons. First, vibrational lifetimes in condensed phase are extremely short compared to a gas, and therefore the window for vibrational enhancement of reaction rates is similarly small. Prior to attempting a vibrationally driven reaction, it is useful to study vibrational energy relaxation (VER) in liquids and understand the limits it imposes. Secondly, interaction with the solvent can influence the bimolecular reaction itself, resulting in reaction rates and mechanisms that are quite different from the gas phase. Before adding vibrational excitation, we need to develop a reliable methodology for monitoring thermal reactions in solution, including techniques to generate a reactive system, to probe both reactants and products, and to determine reaction rate constants and product yields.

To this end we have performed experiments on vibrational relaxation and bimolecular reactions in solution. The highlight of the VER work is a study of the fundamental CH stretch relaxation in a series of iodomethanes (CH_3I, CH_2I_2, CHI_3), where we measured the *intra-* and *inter*molecular vibrational energy redistibution lifetimes (IVR and IET, respectively), and explained the trends in terms of state-to-state relaxation pathways[3]. We have also investigated a series of hydrogen abstraction reactions by chlorine radicals in solution, $Cl + RH \rightarrow HCl + R$, where RH is one of sixteen different hydrocarbons[4].

Methods

All of our experiments employed time-resolved laser spectroscopic techniques with ~100 fs time resolution. For the VER experiments, we generated an infrared pump pulse, tunable in the 3000 cm^{-1} region, and a tunable near-UV probe pulse. The pump pulse excited the $v = 0 \rightarrow 1$ CH stretch transition in a dilute solution of iodomethanes (CH_3I, CH_2I_2, or CHI_3), while subsequent VER depopulated the CH stretch and populated low-frequency CI vibrations. The probe pulse, tuned to the red edge of the UV absorption of our chromophore, selectively monitored the population in these CI modes, thus allowing for observation of IVR and IET of these small molecules in solution.

For the bimolecular reaction experiments, we studied hydrogen abstraction by chlorine atoms in dichloromethane solutions of sixteen different organic molecules, including alkanes (pentane, hexane, heptane, and their cyclic analogues), alcohols

(methanol, ethanol, 1-propanol, 2-propanol, 1-butanol), and chlorinated alkanes (1-chlorobutane, 2-chlorobutane, 1,2-dichlorobutane, 1,4-dichlorobutane, cyclohexyl chloride). We generated chlorine radicals either by 2-photon dissociation of the solvent at 267 nm or by 1-photon photolysis of solvated molecular chlorine, Cl_2, at 350 nm, and probed the transient reactant population (Cl atoms) with a 330 nm laser pulse. For one of the reactions, $Cl + n\text{-}C_5H_{12} \rightarrow HCl + C_5H_{11}$ we also probed the nascent products (HCl) with an IR probe pulse tuned its vibrational transition, ~3.6 μm.

Vibrational Energy Redistribution

Figure 1 shows a set of normalized transients for the three iodomethanes (CH_3I, CH_2I_2, and CHI_3), dissolved in $CDCl_3$, a weakly-interacting solvent[3]. Similar data exist for $(CD_3)_2CO$, a strongly interacting solvent. In each case the transient signal rises with a time constant τ_{IVR} (reflecting transfer of population from the initially excited CH stretch to the lower frequency CI modes of the chromophore), and then falls with a time constant τ_{IET} (representative of vibrational energy leaving the molecule and transferring to the solvent). A fit of each transient to the product of a rising and a falling exponential gives the times for the vibrational energy redistribution in each molecule, summarized in table 1.

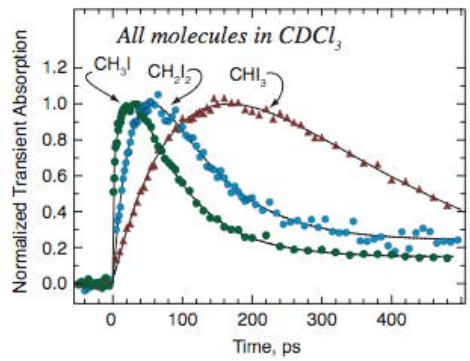

figure 1

Two obvious trends emerge from the data. First, the VER lifetimes of all three iodomethanes were much shorter in deuterated acetone than in chloroform, consistent with acetone being a more strongly interacting solvent. Secondly, the IVR rates in iodomethanes *increased* with *decreasing* number of iodine atoms. This trend is inconsistent with a statistical relaxation model, since a decrease in the number of iodines leads to fewer low frequency molecular vibrations and a lower overall vibrational state density. Instead, our non-statistical IVR rates indicate state-to-state relaxation pathways.[3] There are very few favorable low coupling order transitions in CHI_3, a molecule with a high vibrational density of states. By contrast, in CH_3I the overall state density is lower by a factor of 160, but there is a very fast state-specific relaxation pathway through Fermi resonance with the overtone of the CH bend ($2\nu_5$).

	$CDCl_3$		$(CD_3)_2CO$	
	τ_{IVR}(ps)	τ_{IET}(ps)	τ_{IVR}(ps)	τ_{IET}(ps)
CH_3I	17±5	70±10	8±3	19±5
CH_2I_2	35±3	80±5	15±2	21±3
CHI_3	170±20	170±20	90±12	10±2

table 1

A major finding that came out of our VER work and is relevant to vibrationally mediated chemistry is that vibrational lifetimes in solution can be quite long (170 ps for iodoform dissolved in chloroform). Thus in a vibrationally mediated experiment an initially excited molecular motion will survive for several potentially reactive collisions, a condition that is critical to the success of such an experiment.

Bimolecular Reactions in Solution

Figure 2 shows a set of transients from a reaction of chlorine radicals with pentane in dichloromethane. When no pentane is present, the chlorine signal exhibits a fast drop due to diffusive geminate recombination, which accounts for ~33% of the radicals, and a very slow decay due to hydrogen abstraction from the solvent with a rate constant[4] $k_{solvent}$ = 1.36 x10^7 $M^{-1}s^{-1}$. Upon addition of pentane the chlorine decays more quickly, reflecting the presence of a new hydrogen abstraction pathway with a bimolecular rate constant k_{bi} = 9.3 x10^9 $M^{-1}s^{-1}$. In addition to probing the decay of chlorine radicals, we have also monitored the appearance of the HCl reaction product, shown in figure 3. Both the reactant and product transients fit well to a diffusion-based model with the same bimolecular rate constant[5].

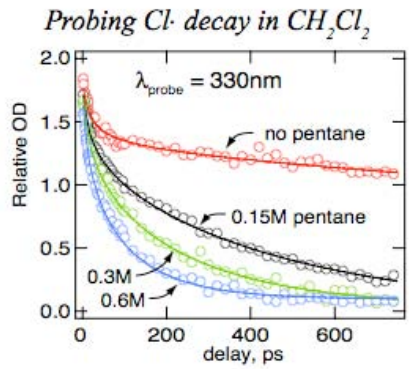

figure 2

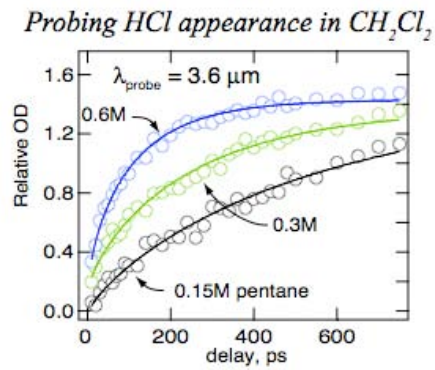

figure 3

We have also probed chlorine radical dynamics in reactions with fifteen other organic molecules[4] (listed above) and measured bimolecular reaction rate constants ranging from diffusion limited for alkanes and cyclic alkanes (k_{bi} ~ 10 x10^9 $M^{-1}s^{-1}$) to activation limited for chlorinated alkanes (k_{bi} ~ 1 x10^7 $M^{-1}s^{-1}$). For the reaction Cl + pentane in carbon tetrachloride solution, we measured a rate constant k_{bi} = 7.4 x10^9 $M^{-1}s^{-1}$, lower than in dichloromethane and consistent with a diffusion-limited reaction in a more viscous solvent.

This work shows that we can confidently monitor the progress of bimolecular reactions in solution. Although probing the reactants (in the UV) and the products (in the IR) yields equivalent information, UV probing is more sensitive, because the chlorine atom is a much stronger absorber than HCl, resulting in far better signal to noise ratio. In a vibrationally mediated experiment, the signal is likely to be small, necessitating use of such a sensitive probing technique.

(1) Yoon, S.; Holiday, R. J.; Crim, F. F. *J Phys Chem B* **2005**, *109*, 8388.

(2) Yoon, S.; Holiday, R. J.; Crim, F. F. *J Chem Phys* **2003**, *119*, 4755.

(3) Heckscher, M. M.; Sheps, L.; Bingemann, D.; Crim, F. F. *J Chem Phys* **2002**, *117*, 8917.

(4) Sheps, L.; Crowther, A. C.; Elles, C. G.; Crim, F. F. *J Phys Chem A* **2005**, *109*, 4296.

(5) unpublished results

A new ultrafast technique for measuring the terahertz dynamics of chiral molecules: The theory of Optical Heterodyne-Detected Raman-Induced Kerr Optical Activity (OHD-RIKOA)

Klaas Wynne
Department of Physics, University of Strathclyde, Glasgow G4 0NG, Scotland, UK

Optical Heterodyne-Detected Raman-Induced Kerr Optical Activity (OHD-RIKOA) is a non-resonant ultrafast chiroptical technique for measuring the terahertz-frequency Raman spectrum of chirally active modes in liquids, solutions, and glasses of chiral molecules. OHD-RIKOA has the potential to provide much more information on the structure of molecules and the symmetries of librational and vibrational modes than the well-known non chirally-sensitive technique Optical Heterodyne-Detected Raman-Induced Kerr-Effect Spectroscopy (OHD-RIKES). The theory of OHD-RIKOA is discussed and possible practical ways of performing the experiments are analysed.

Low frequency librational and vibrational modes in the condensed phase with a frequency of about a terahertz are important in understanding the fluctuations that drive and stabilise reactions. Terahertz frequency fluctuations in liquids control the rates of chemical reactions and similar motions in proteins control protein-folding rates and the rates of enzymatic reactions. Such low frequency modes have been studied with various forms of infrared absorption, Raman scattering, and other spectroscopies for decades.[1] One especially sensitive technique is based on the ultrafast Kerr effect and is often referred to as Optical Heterodyne-Detected Raman-Induced Kerr-Effect Spectroscopy (OHD-RIKES).[2] OHD-RIKES has been applied to a great variety of condensed-phase systems such as various liquids and liquid crystals,[3-5] liquid mixtures,[6,7] solutions,[8] protein solutions,[9-11] and other inhomogeneous media. Typical OHD-RIKES spectra cover the approximate range 0.3 to >500 cm^{-1} corresponding to timescales of about 50 fs to 100 ps. At very low frequencies (<~10 cm^{-1}), the signal is mostly due to diffusive reorientational motions of molecules or molecular side groups. At relatively high frequencies (>~200 cm^{-1}), intramolecular vibrational modes and hydrogen-bond motions are observed. The intermediate region is in some sense of most interest and represents underdamped or critically damped librational motions of individual molecules or groups of molecules (collective motions).

Fig. 1 shows a typical example of an OHD-RIKES spectrum of benzonitrile emphasising the intermediate frequency range. Such a spectrum is typically fitted with a number of analytical line shapes. Many groups have used combinations of Lorentzian, Ohmic, and Gaussian lineshapes[2] to fit such spectra, whereas others have used distributions of harmonic oscillators as in Fig. 1.[12,13] It is quite clear, however, that, despite the impressive signal-to-noise ratio achievable in the OHD-RIKES experiments, such fits are somewhat arbitrary as the results depend on the choice of fit functions.

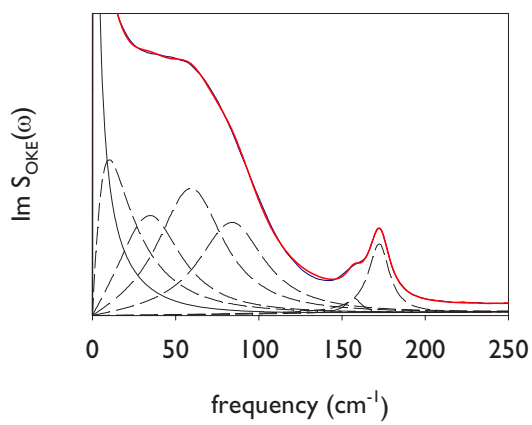

Fig. 1. *Optical heterodyne-detected Raman-Induced Kerr-Effect Spectrum (OHD-RIKES) of benzonitrile and analysis in terms of six Brownian oscillators.*[13]

Thus, the problem is that there is no reliable method to separate the various modes supposedly present in the intermediate frequency Raman spectrum of liquids and proteins. A similar problem exists for Raman scattering off high frequency modes in some cases. In 1969, Atkins and Barron predicted that the light scattered off chiral molecules contains a small degree of circular polarisation.[14] Further im-

provement of this idea led to the development of Raman Optical Activity (ROA),[15,16] which is now a mature technique used in commercial instruments. ROA and the related infrared-absorption technique of Vibrational Circular Dichroism (VCD) produce spectra with bands for those modes that change with the chirality of the molecule. ROA and VCD both require the sample to be optically active (rather than a racemic mixture). The strength and sign of the spectral bands is directly related to the structure and handedness of the molecule and can be used in conjunction with *ab-initio* computations to determine the absolute three-dimensional configuration of molecules.

It is well-known that spontaneous Raman scattering and OHD-RIKES are related and contain essentially the same information.[17] Both spontaneous Raman scattering and OHD-RIKES are four-wave mixing processes where the former involves vacuum fluctuations and the latter externally supplied pump and probe laser beams. Therefore, it is clear that an optical-activity version of OHD-RIKES ought to exist. We have derived a theory for an ROA analogue of OHD-RIKES,[1] named Optical Heterodyne-Detected Raman-Induced Kerr Optical Activity (OHD-RIKOA) and have shown that an optical-activity signal can be obtained in the forward direction under the right polarisation conditions. The interaction Hamiltonian used is[1]

$$H = -\mu_i E_i(\mathbf{r},t) - m_i B_i(\mathbf{r},t) - \tfrac{1}{3} Q_{ij} \nabla_j E_i(\mathbf{r},t), \qquad (1)$$

where $\boldsymbol{\mu}$ is the electric dipole-moment vector, $\boldsymbol{m}$ is the magnetic dipole-moment vector and $\mathbf{Q}$ the electric quadrupole-moment tensor.[18] Interactions with the magnetic-dipole and electric-quadrupole moments are about three to four orders of magnitude weaker than those with the electric-dipole moment. Since RIKOA is a four-wave mixing process like RIKES (see Fig. 2), it must therefore be based on **three** interactions with the electric dipole and **one** interaction with either the magnetic dipole or the electric quadrupole. In the OHD-RIKOA experiment as in a standard OHD-RIKES experiment, the field generated in third order is detected by heterodyning it with the probe field. With the use of wave plates in the probe beam, one can heterodyne with in-phase or out-of-phase fields resulting in the detection of dichroic or refractive effects respectively. The electromagnetic energy absorbed for an out-of-phase probe field is[1]

$$S_{refrac} = \mathrm{Im} \int dt \left(\mathbf{E} \cdot \frac{\partial \mathbf{P}}{\partial t} + \mu_0 \mathbf{H} \cdot \frac{\partial \mathbf{M}}{\partial t} \right) \qquad (2)$$

and the real part for an in-phase probe field.

In OHD-RIKOA, a pump pulse of any polarisation causes a difference in the refractive index for right versus left circularly polarised light. By choosing the appropriate polarisation conditions in the experiment, this circular retardation can be measured directly in a balanced detection set-up (see Fig. 3). The full expression for the OHD-RIKOA signal is:[1]

$$\begin{aligned} S_{RIKOA} = & -\frac{N\omega_0}{16} \frac{\left(E_0^{pump}\right)^2 \left(E_0^{probe}\right)^2}{c} \\ & \left[4\alpha^{iso}\gamma^{iso} + \tfrac{4}{45}\beta(\gamma) + \tfrac{4}{45}\beta(\theta) \right] \qquad (3) \\ & \mathrm{Re} \int_0^\infty d\tau G(\tau) \tfrac{i}{\hbar} \left\langle \left[q(\tau), q \right]_- \right\rangle_Q , \end{aligned}$$

which is essentially the same as the expression for depolarised Raman Optical Activity (ROA) scattering in the forward direction.[18]

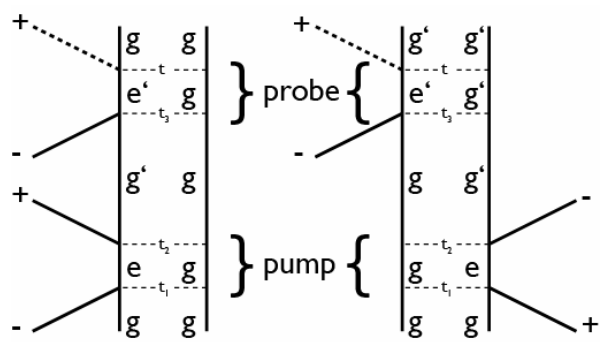

Fig. 2. *The two most relevant Feynman paths for Raman-Induced Kerr Optical Activity[1] (RIKOA) and Raman-Induced Kerr-Effect Spectroscopy (RIKES). In RIKES, all four field interactions are through the electric dipole-moment operator. In RIKOA, one interaction is instead through the magnetic-dipole or electric-quadrupole moment operator.*

In setting up an OHD-RIKOA experiment, it will be very important to suppress any OHD-RIKES signals, which could be three orders of magnitude larger. In the scheme proposed here (linearly polarised probe pulse), OHD-RIKES signals could be suppressed by either using a circularly polarised pump pulse or a linearly polarised pump pulse with the polarisation either parallel or perpendicular to that of the probe pulse. The relative polarisations of the pump and the probe pulses will have to be controlled with an accuracy better than 1:1000. Samples with significant linear optical rotatory dispersion or dichroism would rotate the polarisation of pump and probe fields equally and therefore it should be straightforward to cancel such effects by rotating either the input or the output po-

larisations in order to maintain balanced detection. A more detailed description of how an OHD-RIKOA signal could be measured in practice and how the much stronger OHD-RIKES signal can be suppressed can be found elsewhere.[1]

Acknowledgements

Discussions with Laurence Barron and Lutz Hecht of Glasgow University on Raman Optical Activity and related optical-activity phenomena are gratefully acknowledged. Without them, this work could not even have started. Discussions on the optical Kerr effect and other ultrafast polarisation spectroscopies with Neil Hunt and David Turton are also gratefully acknowledged. This research has been supported by grants from EPSRC and the Leverhulme Trust.

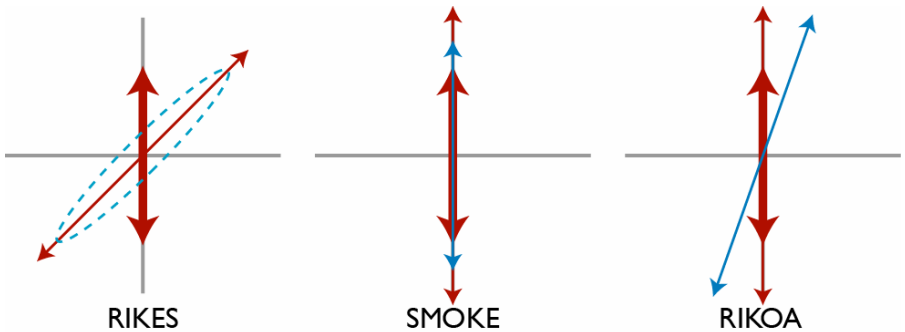

Fig. 3. *In OHD-RIKES, the pump pulse causes the sample to become birefringent, which can be measured as an induced ellipticity on a probe beam polarised at 45° with respect to the pump-beam polarisation. In SMOKE, a spatial mask is used after the sample to produce an intensity modulation of the probe beam. In OHD-RIKOA, the polarisation of the probe laser beam is rotated in a direction determined by the chiral sample.*

References

(1) Wynne, K. *J. Chem. Phys.* **2005**, *123*, xx.
(2) Smith, N. A.; Meech, S. R. *Int. Rev. Phys. Chem.* **2002**, *21*, 75.
(3) Cang, H.; Li, J.; Novikov, V. N.; Fayer, M. D. *J. Chem. Phys.* **2003**, *118*, 9303.
(4) Hyun, B.-R.; Quitevis, E. L. *Chem. Phys. Lett.* **2003**, *370*, 725–732.
(5) Hunt, N. T.; Meech, S. R. *J. Chem. Phys.* **2004**, *120*, 10828.
(6) Ernsting, N. P.; Photiadis, G. M.; Hennig, H.; Laurent, T. *J. Phys. Chem. A* **2002**, *106*, 9159.
(7) Wiewior, P. P.; Shirota, H.; Castner, E. W. *J. Chem. Phys.* **2002**, *116*, 4643.
(8) Idrissi, A.; Bartolini, P.; Ricci, M.; Righini, R. *J. Chem. Phys.* **2001**, *114*, 6774.
(9) Giraud, G.; Wynne, K. *J. Am. Chem. Soc.* **2002**, *124*, 12110.
(10) Eaves, J. D.; Fecko, C. J.; Stevens, A. L.; Peng, P.; Tokmakoff, A. *Chem. Phys. Lett.* **2003**, *376*, 20.
(11) Giraud, G.; Karolin, J.; Wynne, K. *Biophys. J.* **2003**, *85*, 1903.
(12) McMorrow, D.; Thantu, N.; Kleiman, V.; Melinger, J. S.; Lotshaw, W. T. *J. Phys. Chem. A* **2001**, *105*, 7960.
(13) Giraud, G.; Wynne, K. *J. Chem. Phys.* **2003**, *119*, 11753.
(14) Atkins, P. W.; Barron, L. D. *Mol. Phys.* **1969**, *16*, 453.
(15) Barron, L. D.; Buckingham, A. D. *Mol. Phys.* **1971**, *20*, 1111.
(16) Hecht, L.; Nafie, L. A. *Mol. Phys.* **1991**, *72*, 441.
(17) Mukamel, S. *Principles of Nonlinear Optical Spectroscopy*; Oxford University Press: New York, 1995; Vol. 6.
(18) Barron, L. D. *Molecular Light Scattering and Optical Activity*, 2nd ed.; Cambridge University Press: Cambridge, 2004.

TRVS XII

NIST National Institute of Standards and Technology

Washington, D.C.
May 23-27, 2005

Poster Presentations

Coherent Vibrational Quantum Beats as a Probe of Langmuir-Blodgett Monolayers

Andrey N. Bordenyuk, Himali Jayathilake, and Alexander V. Benderskii
Department of Chemistry, Wayne State University, Detroit, MI
anb@chem.wayne.edu

Abstract
We combine frequency- and femtosecond time-domain IR+visible 3-wave mixing measurements of vibrational coherences for spectroscopic characterization of surface monolayer films. Frequency-domain vibrational spectra in the CH-stretch region are obtained by Sum Frequency Generation (SFG). Time-domain coherences are measured using SFG Free Induction Decay, where a 75 fs IR pulse excites several vibrational modes, and a delayed 40 fs visible pulse probes the oscillating surface polarization. The time- and frequency-domain data are analyzed simultaneously within a unified framework based on optical Bloch equations. Information redundancy in the combined frequency- and time-domain measurement allows more accurate determination of the spectral parameters than purely frequency- or time-domain techniques. We compare molecular organization of monolayers in different two-dimensional phases.

1. Introduction

LB transfer is receiving increased attention as a method of manufacturing molecularly ordered monolayer materials for preparation of organic and molecular electronic materials and devices.[1,2] In the majority of these applications, molecular order plays crucial role in determining the performance characteristics. The Langmuir-Blodgett monolayers of Heptadecanoic acid (HDA) (C_{17} fatty acid) were chosen as a model system because the structure and two-dimensional (2D) phases of the precursor Langmuir films have been extensively characterized by various techniques such as surface tensiometry, X-ray diffraction, and Brewster angle microscopy.[3,4] Langmuir monolayers of heptadecanoic acid on water sub-phase have several phases and related mesophases at 21°C, corresponding to different ranges of surface pressure and area per molecule. [4,5] The liquid expanded (LE) phase corresponds to area 30 - 40 Å^2 per molecule. The liquid condensed (LC) phase has two mesophases: the lower pressure mesophase L_{2d} (upper bound pressure ~16 mN/m) with a collective tilt of the alkane chains towards the nearest neighbor (NN), and the higher pressure mesophase Ov (surface pressure range 16 – 26 mN/m) with alkane chain tilt towards the next-nearest neighbor (NNN). The transition $L_{2d} – O_v$ occurs without singularity on the pressure-area isotherm. The superliquid phase (LS), an untilted phase without regular twist angle orientation of alkane chain and backbone planes within the unit cell, corresponds to pressure range 26 – 40 mN/m.[5]

In this paper, we combine the frequency-domain SFG spectroscopy and the time-domain SFG Free Induction Decay (SFG-FID) technique for structural and dynamical characterization of Langmuir-Blodgett (LB) monolayers of HDA deposited onto the glass substrate at various surface pressures. We combine time- and frequency-resolved SFG in a unified framework which allows simultaneous analysis to utilize the redundant information of the time- and frequency-domain data. This redundancy helps combat measurement noise and achieve more accurate determination of the molecular response function parameters.

2. Experimental method

Monolayers of heptadecanoic acid (HDA) were prepared by standard Langmuir-Blodgett transfer onto IR-grade fused silica substrates. The films were prepared at surface pressure 30 mN/m (Sample 1), 15 mN/m (Samples 2 and 3), and 5 mN/m (Sample 4) representing different points on the 2D phase diagram. Our experimental setup capable of both frequency- and time-domain Sum Frequency Generation (SFG) spectroscopy was described in details elsewhere.[6] For the frequency-domain spectroscopy, broad-band SFG scheme[7] was employed which uses spectrally broad IR and narrow visible pulses to obtain the SFG spectrum by frequency-dispersing the signal. For the time-domain measurements the technique builds upon the purely time-domain method of SFG Free Induction Decay (SFG-FID),[8] in which a short IR pulse (75 fs FWHM) excites the vibrational coherence creating an oscillating first-order polarization, and a delayed visible pulse (40 fs FWHM) probes its Free Induction Decay by up-converting the oscillating surface polarization.

3. Results and Discussion

The results obtained for highly ordered sample 1 and disordered sample 4 are shown on Fig. 1 and 2 (parts (a) represent FID, parts (b) SFG spectra). The frequency-domain SFG spectrum for Sample 1 is dominated by two narrow transitions which can be assigned to the symmetric stretch of the terminal CH_3 group (CH_3-SS), $\nu(r^+)$ =

2875±1 cm^{-1} , and CH_3 asymmetric bend overtone split by Fermi resonance (CH_3-FR), $\nu(r^+_{FR})$ = 2935±1 cm^{-1} with weak manifestation of asymmetric CH_3 stretch $\nu(r^-)$ = 2956±5 cm^{-1}.[9] The time-domain SFG-FID signals exhibit a pronounced quantum beat pattern at the difference frequency between the two coherently excited vibrational modes ($\Delta\nu \approx 60$ cm^{-1} translates into ~540 fs period). The SFG spectrum for Sample 4 shows presence of 2 additional transitions. All 5 transitions are spectrally broader than for Sample 1. Both the appearance of new transitions and the broadening can be attributed to more disordered structure. The FID curve (Fig. 2a) shows fast decay of the vibrational coherence without pronounced quantum beats.

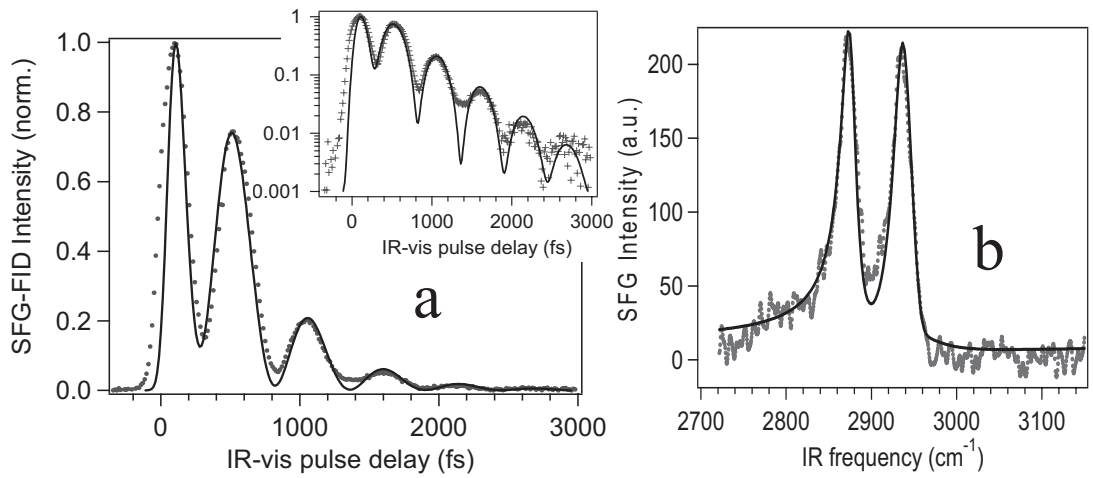

Fig. 1. (a) SFG spectrum of LB monolayer of Sample 1: monolayer of HDA transferred onto quartz substrate at surface pressure π=30 mN/m. **(b)** Time-domain SFG-detected vibrational Free Induction Decay (SFG-FID) for Sample 1.

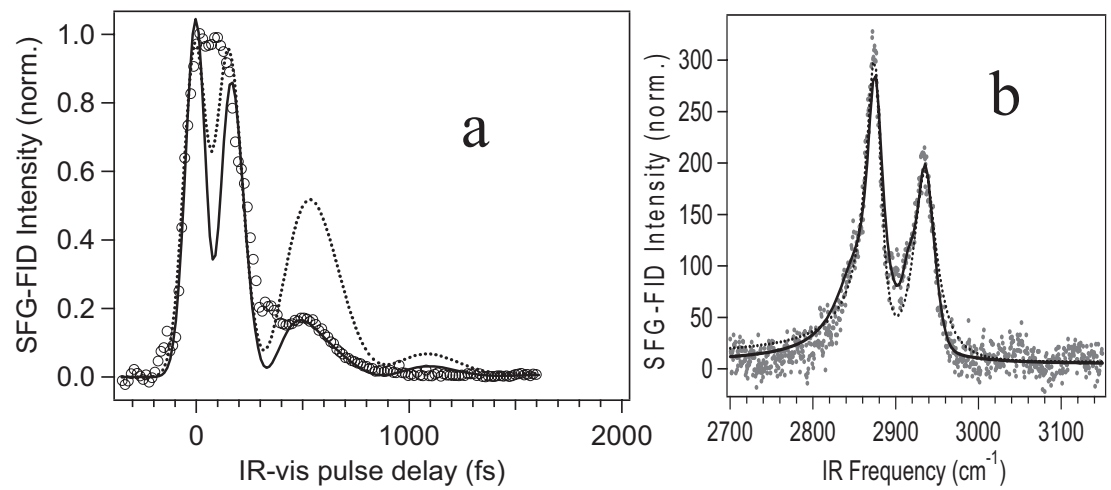

Fig. 2. (a) SFG spectrum of Sample 4: LB monolayer of HDA, transfer pressure 5 mN/m. **(b)** Time-domain SFG-FID signal of Sample 4. Dots - experimental data; Solid lines - simultaneous fit using the model with 5 vibrational modes; Dotted lines: model fit using 2 vibrational modes.

The additional transitions are related to the CH_2 symmetric and asymmetric stretch. The need to introduce the CH_2 stretch modes for disordered samples may be indicative of the increased amount of *gauche*- defects in this less-ordered monolayer, due to increased conformational freedom provided by a larger surface area per molecule. We also point out that the LC phase monolayers are composed of a heterogeneous mixture of mesophase domains.

We parametrize the spectroscopic response function for the LB monolayers using a model based on optical Bloch equations, which represents the monolayer as a collection of uncoupled vibrational modes with exponential relaxation. After solving the Bloch equations we calculate the time-domain response function:

$$S(t) = iA_{NR}e^{i\varphi_{NR}}\delta(t) + i\theta(t)\sum_i B_i\Gamma_i \exp\left(-i\omega_i t - \Gamma_i t\right) - i\left[c.c.\right] \qquad (1)$$

Here $\theta(t)$ is the Heaviside step-function. The first term is introduced to account for the nonresonant (instantaneous) part of the response with amplitude A_{NR} and phase φ_{NR} with respect to the vibrational resonances. The corresponding frequency-domain response function is given by the Fourier transform of (1)

$$G(\omega_{IR}) = A_{NR}e^{i\varphi_{NR}} + \sum_i \frac{B_i\Gamma_i}{\omega_{\mathrm{IR}} - \omega_i + \mathrm{i}\Gamma_{\mathrm{i}}} \qquad (2)$$

In the time-domain SFG-FID, the IR pulse $E_{IR}(t)$ interacts with the system setting up first order polarization

$$P^{(1)}(t) = \int_{-\infty}^{+\infty} dt' E_{IR}(t-t')S(t') . \qquad (3)$$

$P^{(1)}(t)$ is up-converted into the 2nd order polarization by the time-delayed nonresonant visible field $E_{vis}(t-\tau)$,

$$P^{(2)}(t,\tau) \propto E_{vis}(t-\tau)P^{(1)}(t) \qquad (4)$$

The component of this second-order polarization oscillating at the IR + visible sum frequency radiates the SFG signal into the phase-matched direction, so that $I_{SFG-FID}(\tau) \propto \int_{-\infty}^{\infty} \left|P^{(2)}(t,\tau)\right|^2 d\tau$.

In the frequency-domain, the broad-band SFG spectra are given by

$$I_{SFG}(\omega_{SFG}) \propto \left| \int_{-\infty}^{\infty} d\omega_{IR} E_{vis}(\omega_{SFG} - \omega_{IR})\left[E_{IR}(\omega_{IR})G(\omega_{IR})\right] \right|^2 \qquad (5)$$

The term in square brackets describes spectrum of the first order polarization $P^{(1)}(\omega_{\mathrm{IR}})$ resulting from interaction of the IR field $E_{\mathrm{IR}}(\omega_{\mathrm{IR}})$ with the system's response function $G(\omega_{IR})$. The convolution integral represents up-conversion of $P^{(1)}(\omega_{\mathrm{IR}})$ by the visible field $E_{vis}(\omega_{vis})$, resulting in SFG signal at frequency $\omega_{SFG}=\omega_{vis}+\omega_{IR}$.

From Figs. 1 and 2, one can see that the time-domain measurement is more sensitive to change of structure of monolayer than the SFG spectrum. We found that highly ordered samples could be successfully fitted using only 2 transitions (CH_3 symmetric stretch and CH3 Fermi resonance with weak participation of CH_3 asymmetric stretch) whereas up to 5 transitions are needed to fit FID and spectra for disordered samples.

In conclusion, a combination of frequency- and time-domain SFG techniques is a sensitive probe of the molecular structure and dynamics. Model calculations relate time- and frequency domain observables. Vibrational quantum beats observed in Langmuir-Blodgett films are sensitive to the molecular disorder in the monolayer. Redundant information obtained via simultaneous fit in the time- and frequency-domain allows more accurate determination of the parameters of the response function. The combined measurements prove advantageous over purely frequency- or time-domain techniques for samples with complex congested spectra or broad and overlapping transitions. Our measurements show the difference in the molecular orientation and conformation of Langmuir-Blodgett monolayers of heptadecanoic acid in different two-dimensional phases and mesophases. Measuring characteristics of SFG transitions for HDA mesophases well described by independent methods one can find fundamental constants for individual transitions and complete orientational information for specific molecular group. Such measurement can be performed using a single combination of polarizations, eliminating the necessity of using the Fresnel factors for surface layer which are usually unknown.

References

1. Katz, H. E.; Bao, Z. N.; Gilat, S. L. *Accounts of Chemical Research* **2001**, *34*, 359.
2. Reece, T. J.; Ducharme, S.; Sorokin, A. V.; Poulsen, M. *Applied Physics Letters* **2003**, *82*, 142.
3. Bohanon, T. M.; Lin, B.; Shih, M. C.; Ice, G. E.; Dutta, P. *Physical Review B* **1990**, *41*, 4846.
4. Riviere, S.; Henon, S.; Meunier, J.; Schwartz, D.; Tsao, M.; Knobler, C. *J. Chem. Phys.* **1994**, *101*, 10045.
5. Ramos, S.; Castillo, R. *Journal of Chemical Physics* **1999**, *110*, 7021.
6. Bordenyuk, A.N.; Benderskii A.V. *J. Chem. Phys*. **2005**, *122*, 134713.
7. Richter, L. T.; Petralli-Mallow, T. P.; Stephenson, J. C. *Optics Letters* **1998**, *23*, 1594.
8. Guyot-Sionnest, P. *Physical Review Letters* **1991**, *66*, 1489.
9. MacPhail, R. A.; Straws, H. L.; Snyder, R. G.; Elliger, C. A. *Journal of Physical Chemistry* **1984**, *88*, 334.

Nanosecond T-Jump Induced Unfolding Kinetics of α-Helical Peptide: A UV Resonance Raman Study

Gurusamy Balakrishnan, Ying Hu, and Thomas G. Spiro*
Department of Chemistry, Princeton University, Princeton, New Jersey 08544.

Gretchen M. Bender, Zelleka Getahun, and William F. DeGrado
Department Biochemistry and Biophysics, University of Pennsylvania, Philadelphia, Pennsylvania 19104.

The dynamics of protein folding and unfolding are of great current interest, and attention has focused on early events, on the ns-μs time scale, shorter than can readily be accessed with traditional mixing methods[1,2]. The folded short peptides (Fs) with α-helix secondary structure have been widely studied because of its common occurrence in proteins, understanding its folding dynamics expected to provide the basic principles involved in the first step of protein folding[3-8]. Although the helix-coil transition has been studied extensively by both experimental and theoretical methods, controversy still exits due to the complexity of the problem and the lack sufficient structural details of the available experimental data.

The laser induced temperature jump (T-jump) technique has emerged as a powerful relaxation method to study the protein folding on the ns-μs time scale. The T-jump response of the protein can be monitored by optical methods. Fluorescence[3], infrared[4-7], and Raman[8] signals have all been shown to provide useful information. Raman spectroscopy holds particular promise because of the structural specificity of the vibrational bands, and because the entire fingerprint region of the protein spectra can be probed, whereas IR spectroscopy is limited largely to the amide I (carbonyl stretching) vibration, because of strong IR absorption by water. UV excitation produces resonance enhancement of protein Raman bands[9,10] allowing discriminating studies on dilute solutions. Lednev et al. have pioneered T-jump/UV resonance Raman (UVRR) studies, applying the technique to polypeptides[8]. In this work, a α-helical peptide, Ac-GSPEAAAKAAAAKAAAA-CO-D-Arg-$CONH_2$ (GSP peptide), has been studied using a newly developed a laser T-jump / UV resonance Raman apparatus.

Synthesis and purification of the GSP peptide were described elsewhere[7]. In Raman and T-jump/time-resolved resonance Raman experiments, ~ 3 mg/ ml peptide was dissolved in 50 mM phosphate buffer at pH 7.4 in the presence of 0.2 M sodium perchlorate as Raman intensity standard. About 4 ml of the sample is circulated through a temperature controlled (± 0.5 ^{o}C) wire guided flow cell using a peristaltic pump to form a thin film.

The experimental set-up and the spectral acquisition scheme has been described elsewhere[11,12]. Nanosecond t-jump were induced using IR laser pulses at 1.9 μm (10 ns, 0.4-0.8 mJ/pulse, 1 kHz) obtained from a potassium titanyl arsenate (KTA) crystal-based optical parametric oscillator (OPO) operating under intracavity configuration of a diode pumped Nd-YLF laser (Photonics International Inc.). Raman spectra were excited using197 nm pluse (1 μJ/pulse, 20 ns, 1 kHz) obtained from a fourth harmonic output of a Ti:sapphire laser pumped by the second harmonic (12 W) of a Q-switched Nd:YLF laser (Photonics International). Raman scattered light was collected at 135° with a pair of fused quartz lenses, f-matched to a 1.26 m

spectrograph (Spex 1269), which was equipped with a holographic grating (3600 groove mm^{-1}) and intensified photodiode-array detector (Roper Scientific). The timing between pump and probe pulses were adjusted with a computer-controlled pulse generator (DG 535, Stanford Research Systems). Static UVRR spectra at different temperatures were obtained by equilibrating the sample for ~10 mins at each measured temperature. The spectra were calibrated using the standard Raman spectrum of acetone.

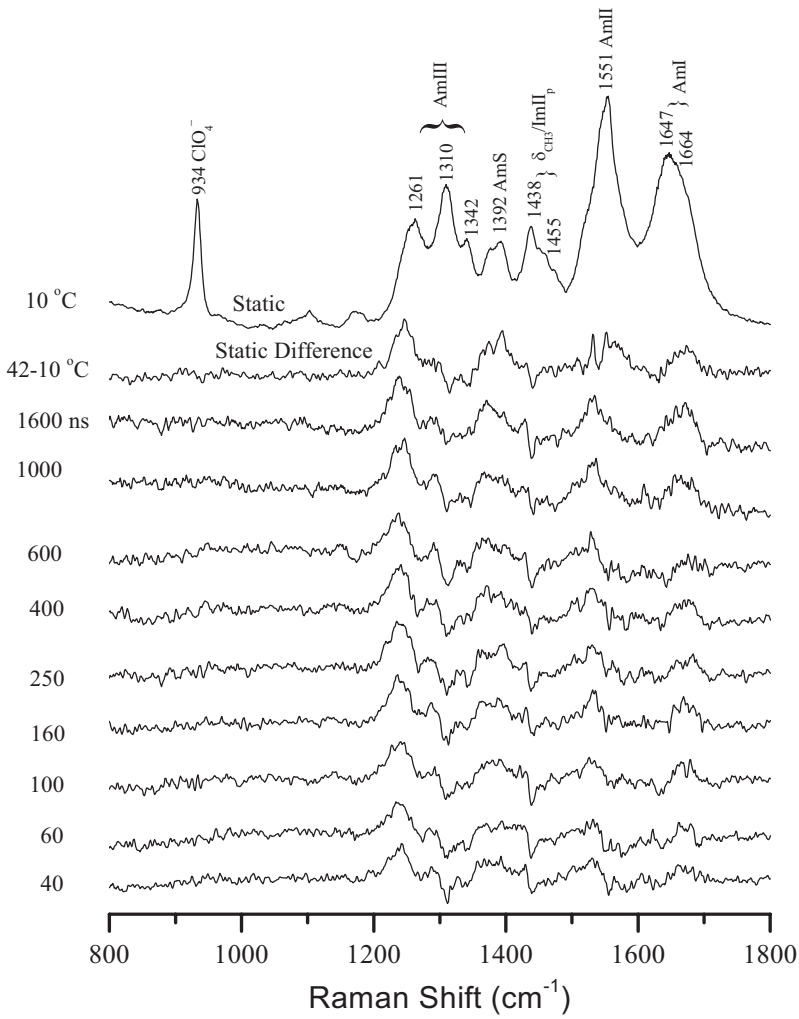

Static UVRR spectrum at 10 °C and the difference spectrum between 42 °C and 10 °C are shown at the top. T-jump/time-resolved UVRR difference spectra (pump+probe minus probe only) at the indicated delay times (ns) following the laser-induced t-jump of 31 °C (from 6 °C to 37 °C) in aqueous GSP (3mg/ml NaP buffer pH 7.4, 0.2 M ClO4-) . λpump= 1.9 μm, 1 kHz, 10 ns, 0.6 mJ and λprobe= 197 nm, 1 kHz, 20 ns, 1 μJ. Band positions are marked at the top.

Excitation of the π-π* transition of peptide bond at 197 nm gives resonance enhanced signals (Figure) for various amide modes such as CO stretching (AmI, 1630-1670 cm^{-1}) in and out-of-phase combinations of NH bending and CN stretching (AmIII,1230-1340 cm^{-1} and AmII,1520-1555 cm^{-1}), and $C_\alpha H$ (AmS ~1390 cm^{-1}) bending modes. Quantitative spectral analysis becomes difficult in the AmI and AmII regions due to the strong spectral overlap of the helix and unfolded states. Whereas AmIII bands at 1310 and 1342 cm^{-1} show clear decreases in intensity due to melting of helical content and increases in intensity for the AmIII band at 1261 cm^{-1} and AmS band 1392 cm^{-1} due to increase of unfolded conformations. The apparent two-state modeling of the AmS band intensity at different temperature gives Tm ~ 17.5 °C which is in agreement with the value obtained from CD melting profile at 222 nm. However, the helical content calculated from Raman shows significant residual population of the helix at higher temperature compared to CD spectroscopy. Such differences were noted before and are attributed to helical length dependent nature of the the CD signal[13].

The magnitude of the laser induced T-jump was obtained from the pre-calibrated temperature dependent Raman intensity of OH stretching band of water at 3400 cm^{-1}. The appearance of positive and negative features in the difference spectra (Figure) are due to the formation of coil and melting of helical structures respectively. It is clear that the onset of the unfolding reaction is as early as 40 ns. Following a thermal jump of 20 °C, the amide resonance Raman bands relax in a apparent single exponential process with a time constant of 118 ± 22 ns at 26 ^{o}C. This value is in reasonable agreement with the values reported from time resolved IR studies[5,6]. The activation energy was approximated by assuming the system is in a two-state equilibrium. Although this is a gross oversimplification, it allows comparison with studies from other laboratories. The activation energy obtained using observed unfolding rate constants at different temperatures and equilibrium constant are 2.06 kcal mol^{-1} for unfolding and -2.76 kcal mol^{-1} for folding. This value is lower than the 15.5 kcal mol^{-1} and 11.3 kcal mol^{-1} reported by Huang etal.[5] for the D-Arg peptide and 8 kcal mol^{-1} and -4 kcal mol^{-1} reported by Lednev et al.[8] for 21 residue α-helical peptide with mainly alanine residues. The differences among these values may arise due to various factors. For example, IR probes the CO band whereas Raman spectral changes were dominated by the AmIII modes which are uncoupled and local in nature. The other difference may arise due to difference experimental conditions; $T_{initial}$ is fixed and T-jump is varied in Raman experiments whereas in IR experiments, the T-jump is fixed the $T_{initial}$ and T_{final} is varied. Huang et al.[6] have noted a significant influence of the width of the temperature jump on observed rate constants. Further studies are in progress to resolve the above noted differences.

References

1. J. K. Myers and T. G. Oas, *Ann. Rev. Biochem.* **71**, 783 (2002).
2. H. Roder, K. Maki, H. Cheng, and M. C. R. Shastry, *Methods* **34**, 15 (2004).
3. P. A. Thompson, V. Munoz, G. S. Jas, E. R. Henry, W. A. Eaton, and J. Hofrichter, *J. Phys. Chem. B* **104**, 378 (2000).
4. S. Williams, T. P. Causgrove, R. Gilmanshin, K. S. Fang, R. H. Callender, W. H. Woodruff, and R. B. Dyer, *Biochemistry* **35**, 691 (1996).
5. C. Y. Huang, J. W. Klemke, Z. Getahun, W. F. DeGrado, and F. Gai, *J. Am. Chem. Soc.* **123**, 9235 (2001).
6. C. Y. Huang, Z. Getahun, Y. J. Zhu, J. W. Klemke, W. F. DeGrado, and F. Gai, *Proc. Natl. Acad. Sci. USA* **99**, 2788 (2002).
7. T. Wang, Y. J. Zhu, Z. Getahun, D. G. Du, C. Y. Huang, W. F. DeGrado, and F. Gai, *J. Phys. Chem. B* **108**, 15301 (2004).
8. I. K. Lednev, A. S. Karnoup, M. C. Sparrow, and S. A. Asher, *J. Am. Chem. Soc.* **121**, 8074 (1999).
9. J. C. Austin, K. R. Rodgers, and T. G. Spiro. "Protein-Structure from Ultraviolet Resonance Raman-Spectroscopy". in *Metallobiochemistry, Part C*, 1993; Vol. 226; pp 374-396.
10. Z. H. Chi, X. G. Chen, J. S. W. Holtz, and S. A. Asher, *Biochemistry* **37**, 2854 (1998).
11. G. Balakrishnan, Y. Hu, and T. G. Spiro, *(in prep.)*.
12. G. Balakrishnan, Y. Hu, S. B. Nielsen, and T. G. Spiro, *Appl. Spectrosc.* **59**, 776 (2005).
13. A. Ozdemir, I. K. Lednev, and S. A. Asher, *Biochemistry* **41**, 1893 (2002).

Vibrational Cooling in the Excited State: A Comparison of Femtosecond Transient Absorption and Picosecond Raman Spectroscopies

Gotard Burdzinski, Terry L. Gustafson, Christophe Lefumeux, Guy Buntinx and Olivier Poizat*

Department of Chemistry and Center for Chemical and Biophysical Dynamics, The Ohio State University, 100 West 18th Avenue, Columbus, OH 43221-1185, USA and Laboratoire de Spectrochimie Infrarouge et Raman (LASIR), UMR 8516 CNRS/USTL,Centre d'Etudes et de Recherches Lasers et Applications, FR 2416 CNRS, Bâtiment C5, Université des Sciences et Technologies de Lille, 59655 Villeneuve d'Ascq cedex, France

Relaxation processes in the excited state, including vibrational and conformational relaxation, provide insight into the fundamental interactions that occur between a solute and its solvent environment.[1-14] Experimentally, the approach for determining the effect of solvent on excited state relaxation processes is to generate the excited state photolytically and monitor the rate at which some property of the excited state changes while varying the solvent properties systematically. The reaction rates are then compared to bulk properties of the solvent, since the solvent is viewed as non-interacting from the perspective of statistical mechanics. (*i.e.*, The solvent molecules simply act as a heat bath that may be considered as a continuous viscous medium at liquid-phase densities.) The primary tools used to study these interactions have been time-resolved fluorescence and absorption spectroscopies.

We and others have shown that picosecond transient Raman spectroscopy provides a valuable tool for the examination of solute-solvent interactions.[2;4-7;9;11;12;15-21] An advantage of time-resolved Raman spectroscopy is that it provides mode-specific information about the probe molecule so that solvent induced structural effects may be observed directly. Dynamical effects are observed in transient Raman spectra as changes in bandwidth, peak position, and relative intensity with time delay. The transient spectra provide sensitive vibrational markers for solvation dynamics.

Several picosecond transient Raman studies have been performed by our group and others on *trans*-stilbene (tS) in various solvents to gain insight into the effect of solvent and excess vibrational energy on the S_1 tS molecule.[9;16;21-25] Derivatives of tS have also been examined in order to gain further insight into solute-solvent interactions and to gather more evidence for relaxation theories that have been proposed to describe the behavior of tS. Butler *et al.* have reported the picosecond transient Raman spectra of *trans*-4,4'-diphenylstilbene (DPS) in dioxane and methylene chloride.[15] They observe only small shifts in the peak positions and bandwidths of the transient Raman bands with time delay in both solvents at the excess vibrational energies used in their study. However, the relative intensities of S_1 Raman bands that have been assigned to the biphenyl portions of the molecule show significant changes with delay and are affected by variation of the solvent environment.[15] Butler *et al*. interpret the changes in relative intensity for these bands to indicate that the molecule is assuming a more planar conformation following photoexcitation. The rate of this change is affected by the solvent dielectric constant which, the authors suggest, helps to stabilize the increased electron density on the phenyl rings.[15] Leonard and Gustafson have shown that the conformation of DPS in aromatic solvents is affected by substituents on the solvent phenyl rings, while vibrational cooling is essentially identical in the solvents studied.[2]

DPS is an interesting molecule for probing solvent effects on excited state dynamics for several reasons. It has a long-lived S_1 state, making it possible to obtain high quality absorption and Raman spectra to long delays; the transient absorption cross section is large, based on the intensity

of the excited state Raman spectra; and there appear to be conformational changes (*i.e.*, nuclear coordinate changes in the excited state) that occur on time scales comparable to vibrational relaxation.[2;15;26] The steady-state absorption and emission spectra of DPS , along with the transient absorption spectrum, are shown in Figure 1. Our current understanding of the excited state dynamics has been based primarily on picosecond transient Raman data.[2;15;26] and femtosecond transient absorption.[27] The current picture for the photophysical processes of DPS in the S_1 electronic state is as follows.[26] After the initial photoexcitation the excess vibrational energy initially stored in the Franck-Condon modes of the molecule is redistributed in less than ~100 fs and deposited in the first solvent shell.[9;24;26;28;29] Following this relaxation, slower processes (~10-50 ps) ensue, including vibrational cooling in which the"hot" first solvent shell cools by transferring energy to the bulk solvent and conformational relaxation in which the solute changes its conformation along certain nuclear coordinates in order to relax to the optimum equilibrium geometry in the excited state.[2;9;15;24;26-29]

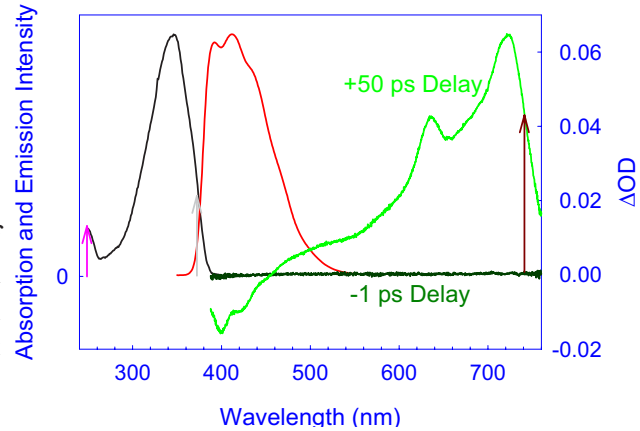

Figure 1 The steady-state absorption and emission spectra of DPS, along with the transient absorption spectra of the excited state of DPS. The arrows indicate the pump and probe wavelengths for the Raman experiment.

Vibrational cooling in the excited state manifests itself in slightly different ways, depending on the nature of the spectroscopy used to monitor the process. We have previously observed that the vibrational cooling rates were slightly different depending upon whether transient absorption or transient Raman was used to probe the cooling process.[26;27] In order to evaluate the basis for these differences, we have acquired transient (Stokes) Raman and transient absorption spectra of DPS, pumping near the 0-0 transition (~370 nm) where there is little excess vibrational energy, and at ~ 260 nm with ~12,000 cm^{-1} of excess vibrational energy. We have compared the dynamical changes in the spectroscopic observables (bandwidths and peak positions) of the Raman and absorption bands, to determine which of the observables provides a "true" indication of the vibrational cooling rate. (See Figure 2.)

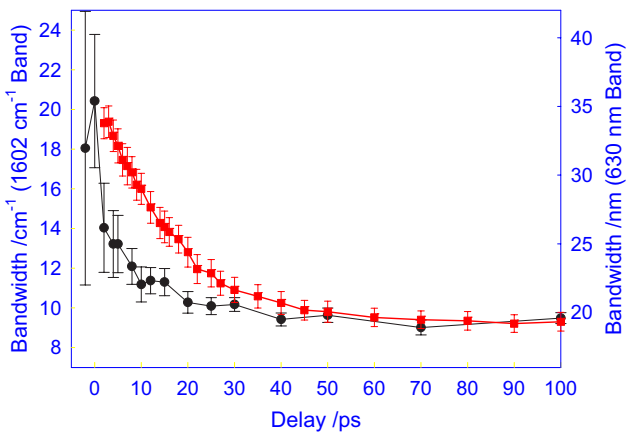

Figure 2 A comparison of the dynamical changes in the bandwidth of a Raman band (left axis, black line) and the bandwidth of a transient absorption band (right axis, red line) for DPS in methylene chloride, excited at 254 nm.

Based on our results we conclude that with excess vibrational energy the rate of vibrational cooling as observed with peak position changes in the transient Raman spectra agree with the bandwidth changes in the transient absorption spectra and that with excess vibrational energy the rate of vibrational cooling as observed with bandwidth changes in the transient Raman spectra do not agree with the bandwidth changes in the transient absorption spectra. We also observe that

conformational relaxation is evidenced by peak position changes in the transient absorption spectra and relative intensity changes in the picosecond transient Raman spectra.

References

(1) Tan, X.; Gustafson, T. L. *J.Phys.Chem.A* **2000**, *104*, 4469-4474.
(2) Leonard, J. D., Jr.; Gustafson, T. L. *J.Raman Spectrosc.* **2000**, *31*, 353-358.
(3) Hamaguchi, H.; Gustafson, T. L. *Annu.Rev.Phys.Chem.* **1994**, *45*, 593-622.
(4) Morris, D. L.; Gustafson, T. L. *J.Phys.Chem.* **1994**, *98*, 6725-6730.
(5) Morris, D. L.; Gustafson, T. L. *Appl.Phys.B* **1994**, *59*, 389-395.
(6) Kwok, W. M.; Ma, C.; Phillips, D.; Matousek, P.; Parker, A. W.; Towrie, M. *J.Phys.Chem.A* **2000**, *104*, 4188-4197.
(7) Kwok, W. M.; Ma, C.; Matousek, P.; Parker, A. W.; Phillips, D.; Toner, W. T.; Towrie, M. *Chem.Phys.Lett.* **2000**, *322*, 395-400.
(8) Iwata, K.; Hamaguchi, H. *Chem.Lett.* **2000**, 456-457.
(9) Iwata, K.; Hamaguchi, H. *J.Raman Spectrosc.* **1998**, *29*, 915-918.
(10) Iwaki, L. K.; Deak, J. C.; Rhea, S. T.; Dlott, D. D. *Chem.Phys.Lett.* **1999**, *303*, 176-182.
(11) Waele, V. D.; Buntinx, G.; Poizat, O.; Flament, J. P. *J.Raman Spectrosc.* **2000**, *31*, 275-281.
(12) Bremard, C.; Buntinx, G.; De Waele, V.; Didierjean, C.; Gener, I.; Poizat, O. *J.Mol.Struct.* **1999**, *480-481*, 69-81.
(13) Stratt, R. M.; Maroncelli, M. *J.Phys.Chem.* **1996**, *100*, 12981-12996.
(14) Voth, G. A.; Hochstrasser, R. M. *J.Phys.Chem.* **1996**, *100*, 13034-13049.
(15) Butler, R. M.; Lynn, M. A.; Gustafson, T. L. *J.Phys.Chem.* **1993**, *97*, 2609-2617.
(16) Qian, J.; Schultz, S. L.; Jean, J. M. *Chem.Phys.Lett.* **1995**, *233*, 9-15.
(17) Nakabayashi, T.; Okamoto, H.; Tasumi, M. *J.Raman Spectrosc.* **1995**, *26*, 841-845.
(18) Poizat, O.; Buntinx, G. *J.Phys.Chem.* **1995**, *99*, 9403-9407.
(19) Fujino, T.; Tahara, T. *J.Phys.Chem.A* **2000**, *104*, 4203-4210.
(20) Hogiu, S.; Werncke, W.; Pfeiffer, M.; Elsaesser, T. *Chem.Phys.Lett.* **1999**, *312*, 407-414.
(21) Nakabayashi, T.; Okamoto, H.; Tasumi, M. *J.Phys.Chem.A* **1998**, *102*, 9686-9695.
(22) Weaver, W. L.; Huston, L. A.; Iwata, K.; Gustafson, T. L. *J.Phys.Chem.* **1992**, *96*, 8956-8961.
(23) Hester, R. E.; Matousek, P.; Moore, J. N.; Parker, A. W.; Toner, W. T.; Towrie, M. *Chem.Phys.Lett.* **1993**, *208*, 471-478.
(24) Iwata, K.; Hamaguchi, H. *J.Mol.Liq.* **1995**, *65-6*, 417-420.
(25) Matousek, P.; Parker, A. W.; Phillips, D.; Scholes, G. D.; Toner, W. T.; Towrie, M. *Chem.Phys.Lett.* **1997**, *278*, 56-62.
(26) Leonard, J. D., Jr.; Gustafson, T. L. *Journal of Physical Chemistry A* **2001**, *105*, 1724-1730.
(27) Tan, X.; Gustafson, T. L.; Lefumeux, C.; Burdzinski, G.; Buntinx, G.; Poizat, O. *Journal of Physical Chemistry A* **2002**, *106*, 3593-3598.
(28) Iwata, K.; Hamaguchi, H. *J.Phys.Chem.A* **1997**, *101*, 632-637.
(29) Iwata, K.; Hamaguchi, H. *Laser Chem.* **1999**, *19*, 367-370.

Vibrational and electronic infrared absorption spectra of benzophenone in the lowest excited triplet state

Sohshi Yabumoto†, Shin Sato, Hiro-o Hamaguchi
Department of Chemistry, School of Science, The University of Tokyo, Tokyo, Japan
†E-mail: yabumoto@chem.s.u-tokyo.ac.jp

1. Introduction

Photochemical processes of carbonyl compounds are closely related to the nature of the involved excited electronic states. For example, the reactivity toward photoinduced hydrogen atom abstraction reaction is dependent on the electronic configuration of the T_1 state, i.e. n–π^*, π–π^* or charge transfer (CT). The rate of intersystem crossing is also governed by the nature of the involved singlet and triplet states, which is known as the El-Sayed rule. Because the electronic configuration is distinctly reflected in the molecular structure, vibrational spectroscopy can be used for elucidating the electronic structure of excited states and hence the mechanism of the photochemical processes taking place there. Though a significant number of the Raman and infrared spectra of π–π^* and the Raman spectra of n–π^* triplet states have so far been reported [1], infrared study for n–π^* is still scant [2].

Benzophenone (BP) is one of the most basic and most important aromatic carbonyl compounds. Moreover, the T_1 state of BP (T_1 BP) takes an n–π^* electronic configuration and hence shows very high reactivity. Therefore, the nature and the structure of T_1 BP are of great interest. Though the Raman spectrum of T_1 BP has already been reported [1a], its infrared spectrum has not been known and the structure of T_1 BP has not been fully. Thus the infrared spectrum of T_1 BP is strongly required. In the present study, we observed the transient infrared spectra of photoexcited BP in carbon tetrachloride and benzene-d_6 with nanosecond time-resolved infrared spectroscopy to obtain the infrared spectrum of T_1 BP.

2. Experimental

All transient infrared spectra were measured a with nanosecond time-resolved infrared spectroscopy system, detail of which was described previously [3]. BP was excited to the S_1 state with the third harmonic of a Spectra-Physics TFR Q-switched Nd:YLF laser (349 nm, ~6ns, 17μJ, 230Hz). The O_2 concentration of the sample solution was regulated with O_2 or Ar saturation.

3. Result and discussion

The time-resolved infrared spectra of photoexcited BP in carbon tetrachloride are shown in Figure 1. Both under O_2 and Ar saturated conditions, positive and negative peaks appear right after photoexcitation and decay synchronously. The negative peaks are apparently assignable to the depletion of the absorption of the BP in the ground state by comparison with a ground-state infrared spectrum. Since the intersystem crossing from the S_1 to T_1 states takes place in a few tens of picoseconds [4], which is much faster than the time-resolution of the apparatus, the positive peaks cannot be S_1 BP. In addition, the decay is much faster under O_2 saturated condition than under Ar saturated condition, which is the characteristic of excited triplet states. Therefore, the positive peaks are ascribable to T_1 BP. Furthermore, the same spectra

are also observed in benzene-d_6. This confirms the assignment of the positive peaks to T_1 BP; the possibility of the assignment to any other species like chlorine-adduct radical of BP generated by reaction with solvent carbon tetrachloride is excluded.

The infrared spectrum of T_1 BP, shown in Figure 2, is obtained from the time-resolved spectra by compensating the depletion of BP in the ground state. In this spectrum, the CO stretch band, which is known to be located at 1216 cm^{-1} by Raman spectroscopy [1a], is not observed. This seems strange because the CO stretching modes of the ground- state carbonyl compounds show very strong absorption bands. This infrared absence of the CO stretch mode is thought to reflect the reduced polarity of the CO bond of the n–π^* T_1 state of BP.

In addition to the vibrational absorption band, an extremely broad absorption is found in the wavenumber region higher than 2700 cm^{-1} extending to the near-infrared. Because this band is too broad to be attributed to vibrational transition, we assigned this broad absorption band to the $T_2 \leftarrow T_1$ electronic transition. The electronic configurations of S_1 and T_1 BP are both n–π^*, on the other hand, that of T_2 state is π–π^*. According to the El-Sayed rule, the intersystem crossing between both n–π^* states or both π–π^* states is slow and, in contrast, that between n–π^* and π–π^* is fast. The intersystem crossing from the S_1 BP, in fact, is known to be very fast, which means that the direct intersystem crossing from S_1 to T_1 BP is not likely to occur. In the case of long-conjugated aromatic compounds such as BP, the energy level of π–π^* triplet states are lowered coming close to that of n–π^* triplet states and. Consequently, the involvement of the π–π^* T_2 state in the intersystem crossing from S_1 BP has been suggested. However, a concrete evidence for this T_2 involvement has not been reported. The $T_2 \leftarrow T_1$ electronic transition band observed in the present study indicates the low wavenumber edge of the T_2 state band comes down to the energy level less than 2700 cm^{-1} from the T_1 state. The energy gap between the S_1 and T_1 state is about 2700 cm^{-1}. Therefore, the intersystem crossing from S_1 to T_1 BP is feasible. Thus, the involvement of the T_2 state in the intersystem crossing of BP is confirmed.

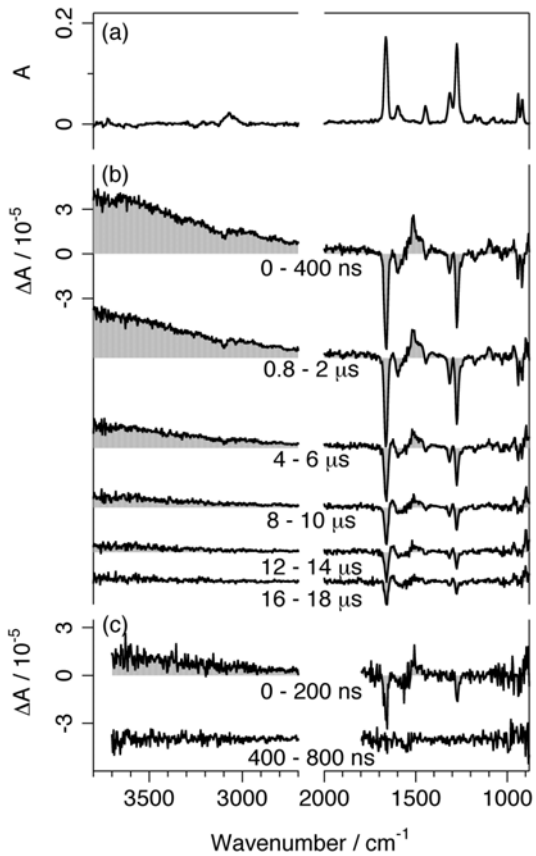

Fig. 1 Ground-state infrared spectrum of BP (a) and time-resolved infrared spectra of photoexcited BP in carbon tetrachloride under Ar saturation (b) and O_2 saturation.

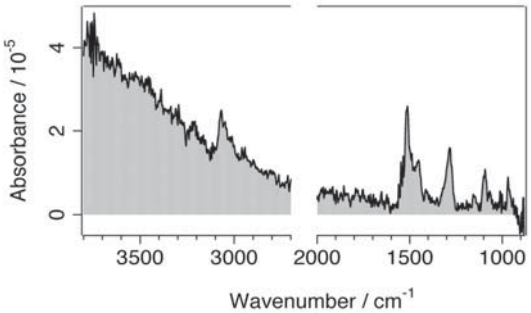

Fig. 2 Infrared spectrum of benzophenone in the T_1

As above, an electronic transition between very closely lying electronic states of a transient chemical species is observed in a transient infrared spectrum. Therefore, time-resolved infrared spectroscopy is useful for elucidating the mechanism of photophysical and photochemical process of aromatic carbonyl compounds, which are known to have many closely lying excited triplet states.

Reference

[1] (a) T. Tahara *et al*., Chem. Phys. Lett. 152 (1988) 135. (b) T. Tahara *et al*., J. Phys. Chem. 94 (1990) 170. (c) T. Tahara, H. Hamaguchi, Chem. Lett. (1992) 17. (d) M.J. van der Burgt *et al*., Chem. Phys. 196 (1995) 193. (e) W.S. Chan *et al*., J. Phys. Chem. A 109 (2005) 3454. (f) M.W. George *et al.*, Chem. Lett. (1993) 873. (g) S. Tanaka *et al.*, Chem. Phys. Lett. 381 (2003) 385.

[2] We have found only one report: S. Srivastava, E. Yourd, J.P. Toscano, J. Am. Chem. Soc. 120 (1998) 6173.
[3] T. Yuzawa, C. Kato, M.W. George, H. Hamaguchi, Appl. Spectrosc. 48 (1994) 684.
[4] D.E. Damschen, C.D. Merritt, D.L. Perry, G.W. Scott, L.D. Talley, J. Phys. Chem. 82 (1978) 2268.

Time-Resolved Resonance Raman Observations of Vibrational Dynamics in Heme Model Compounds

Jagannadha R. Challa, Tissa C. Gunaratne, M. Cather Simpson*

Center for Chemical Dynamics, Department of Chemistry, Case Western Reserve University, Cleveland, OH 44106-7078, USA. Phone: (216) 368-1911, email: mcs9@case.edu

We seek to obtain a basic understanding of vibrational dynamics in condensed phase systems of large molecules. As part of understanding these dynamical processes, we have focused upon the vibrational dynamics in deoxyHb model compounds, Fe^{II}OEP 2-MeIm and the photoproduct of Fe^{II}OEP $(Im)_2$. Only the results of the five-coordinate, high-spin model compound Fe^{II}OEP 2-MeIm are presented in this short paper. Soret band excitation of Fe^{II}OEP 2-MeIm, followed by ultrafast internal conversion results in a vibrationally hot ground electronic state which then undergoes vibrational relaxation. The ground electronic state depletion and recovery were monitored using femtosecond transient absorption spectroscopy. Transient vibrational populations on the ground electronic state were probed with femtosecond time-resolved Stokes and anti-Stokes resonance Raman spectroscopy. In particular, we present the mode-specific vibrational energy transfer in and out of the different vibrational modes with sub-picosecond resolution.

Introduction

The flow of vibrational energy in molecules is a fundamental physical process that is not yet well understood. In the condensed phase, this flow can be separated into two components: intramolecular vibrational energy redistribution (IVR) among the vibrational modes of the molecule and intermolecular vibrational energy relaxation (VR) to the surrounding solvent or bath. Vibrational dynamics deals with the role of vibrational motions in IVR and VR.

One motivation for studying vibrational dynamics is the possibility that they influence molecular function. Hemes are biologically important molecules with a large propensity for catalytic activity. The electronic and vibrational behavior of photoexcited hemes has not converged to a single model, despite the active research by several groups. Two different models, vibrationally hot ground electronic state model and multiple intermediate excited electronic state model, are found in the literature[1-3]. However all agree with a rapid non-radiative decay of the heme excited electronic state following photoexcitation.

Previous studies of deoxyhemoglobin and other five-coordinate, high spin hemes have shown that mode-specific vibrational energy distributions intrinsic to the porphyrin moiety can be generated[4-6]. Single pulse transient Raman experiments of Fe^{II}OEP-2MeIm[7] showed that the ν_4 vibrational mode retains more excess energy than the ν_7. In order to comprehend the observed behavior, ultrafast time-resolved absorption and resonance Raman experiments have been undertaken.

By using pulses in resonance with the heme Soret transition, excess energy was deposited in the vibrational manifold of the ground electronic state via efficient non-radiative electronic decay. The subsequent evolution of vibrational populations (i.e. IVR and VR) were probed using Stokes and anti-Stokes resonance Raman scattering.

Materials and methods

The heme model compound, Fe^{II} octaethyl porphyrin 2-methyl imidazole [Fe^{II}OEP-2MeIm] was prepared using a two phase method[7] as reported by Loparo *et al.* The concentration of the sample was 0.5-1.0 mM for the Raman experiments. The concentration for the transient absorption experiments was chosen so that the equilibrium ground state absorption was 0.5 at the pump wavelength. The sample was circulated through a 1 mm quartz flow cell using Teflon tubing under N_2 gas pressure. The transient absorption experiments were done in the Ohio Laboratory for Kinetic Spectrometry at Bowling Green state University and the experimental details can be found elsewhere[8]. The duration of the laser pulses employed for transient absorption were 200 fs or less. The one color pump-probe method and the experimental details used for Raman measurements were published elsewhere[9]. The duration of the laser pulses used for Raman measurements were 500 fs or less.

Results and Discussion

Excitation of the five-coordinate, high-spin heme leads to rapid deposition of excess vibrational energy in the ground electronic state. Figure 1 shows a set of transient absorption spectra generated by exciting the molecule in the Soret band and probing the spectrum as a function of time delay.

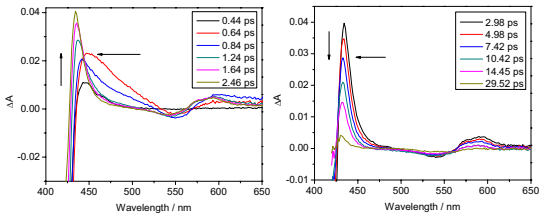

Figure 1. Femtosecond time-resolved transient absorption spectra of Fe^{II}OEP-2MeIm in CH_2Cl_2 using 400 nm pump-white light continuum probe.

Initially broad and red shifted transient absorption bands appeared on the red side of the equilibrium Soret and Q bands, which spectrally narrowed and blue shifted with time. The transients were assigned to the absorption of vibrationally hot ground electronic state formed by ultrafast internal conversion. The transient decay and thermal equilibration on the ground electronic state were complete within 30 ps. The transients exhibited wavelength dependent kinetics, as shown in Figure 2.

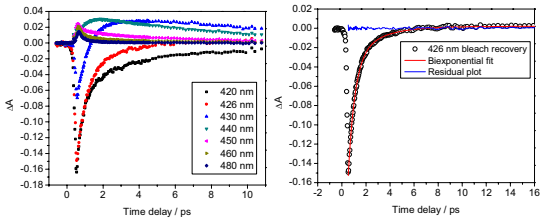

Figure 2. (A) Kinetic traces of transient absorption from Fe^{II}OEP-2MeIm (λ_{ex}=400 nm) in CH_2Cl_2 probed at different wavelengths. (B) Kinetics of the bleach recovery at 426 nm from Fe^{II}OEP-2MeIm in CH_2Cl_2 (λ_{ex}=400 nm).

The transient bleach recovery at the Soret band maximum had a 550 fs fast component (86%) due to internal conversion and a 2.2 ps slower component due to IVR and vibrational cooling on the ground electronic state. The recovery of the ground electronic state was also monitored using time-resolved Stokes resonance Raman spectroscopy, as shown in Figure 3. The recovery time from the transient Stokes Raman data matched well with the slow component of the transient bleach recovery at 426 nm.

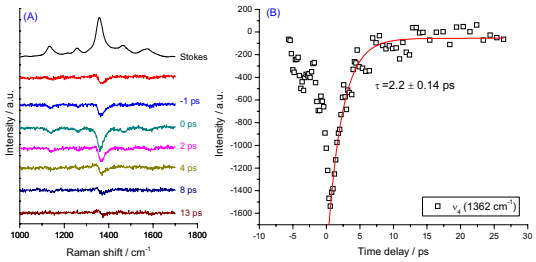

Figure 3. (A) Time-resolved Stokes resonance Raman spectra of Fe^{II}OEP-2MeIm in CH_2Cl_2 using 405 nm pump-probe. **(B)** Kinetics of the vibrational population recovery of the ν_4, a symmetric (A_{1g}) pyrrole breathing motion at 1362 cm^{-1}.

The time-resolved anti-Stokes resonance Raman (TRARR) spectra in Figure 4 show three peaks, one intense feature at 1364 cm^{-1} and the other two at 1565 and 1140 cm^{-1}. The 1565 cm^{-1} band is assigned to ν_2, an A_{1g} in-phase C_β-C_β stretch. By comparison to NiOEP spectral assignments, the 1140 cm^{-1} band is assigned to ν_5, an A_{1g} C_β-C_{ethyl} stretch.

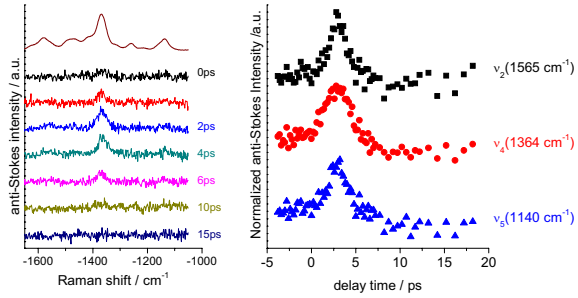

Figure 4. (A) TRARR spectra of Fe^{II}OEP-2MeIm in CH_2Cl_2 using 413 nm pump and 413 nm probe. **(B)** Decay kinetics of the vibrational mode population on the ground electronic state of Fe^{II}OEP-2MeIm using TRARR spectroscopy.

The TRARRS results of Fe^{II}OEP-2MeIm in CH_2Cl_2 show that the ν_4 and ν_5 vibrational modes decay exponentially with similar kinetics, with time constants of 2.6±0.2 ps and 2.8±0.2 ps respectively, whereas the ν_2 mode decays more rapidly with a 1.6±0.2 ps time constant. The decay time of 1.1±0.6 ps for the ν_4 vibrational mode observed by Mizutani *et.al* was slightly faster than our observation of 2.6±0.2 ps[6]. It could be due to a difference in the method of preparing the vibrationally hot ground state (internal conversion versus photolysis followed by internal conversion) and also in the amount of excess energy available (Soret band excitation versus Q-band excitation).

Conclusions

The transient absorption data supports the vibrationally hot electronic ground state model. We did not observe any spectroscopic evidence for the multiple intermediate electronic state model. These data are consistent with rapid, subpicosend decay of the excited electronic state to generate a vibrationally excited ground state. The observed vibrational modes and their lifetimes showed that the vibronic processes involved in direct internal conversion following photoexcitation and in internal conversion following the photolysis of a ligand were different. These transient absorption and time-resolved Raman experiments provided an important first step in unraveling the vibrational participation in internal conversion in hemes, and the nature of heme vibrational dynamics.

Acknowledgement

We thank the National Institutes of Health (GM056816; MCS) the Provost's opportunity fund (MCS, TCG) at Case Western Reserve University, the Ohio Laboratory for Kinetic Spectrometry at BGSU and Stephan Brunello for his help in analyzing time-resolved data.

References

1. Kholodenko, Y.; Volk, M.; Gooding, E.; Hochstrasser, R. M. *Chem. Phys.* **2000**, 259, 71-87.
2. Franzen, S.; Kiger, L.; Poyart, C.; Martin, J-L. *Biophys. J.* **2001**, 80, 2372-2385.
3. Ye, X.; Demidov, A.; Rosca, F.; Wang, W.; Kumar, A.; Ionascu, D.; Zhu, L.; Barrick, D.; Wharton, D.; Champion, P.M. *J. Phys. Chem. A.* **2003**, 107, 8156-65
4. Lingle, R. Jr.; Xu, X.; Zhu, H.; Yu, S-C.; Hopkins, J. B. *J. Phys. Chem.* **1991**, 95, 9320-9331.
5. Simpson, M. C.; Peterson, E. S.; Shannon, C. F.; Eads, D. D.; Friedman, J. M.; Cheatum, C. M.; Ondrias, M. R. *J. Am. Chem. Soc.* **1997**, 119, 5110-5117.
6. Mizutani, Y.; Kitagawa, T. *Science* **1997**, 278, 443-446.
7. Loparo, J. J.; Cheatum, C. M.; Ondrias, M. R.; Simpson, M. C. *Chem. Phys.* **2003**, 286, 353-374.
8. Gentili, P. L.; Danilov, E.; Ortica, F.; Rodgers, M. A. *Photochem. Potobiol. Sci,* **2004**, 3, 886-891.
9. Gunaratne, T.; Challa, J. R.; Simpson, M. C. *Chem. Phys. Chem.* **2005**, 6, 1157-1163.

The Dynamics of Enzyme-Inhibitor Interactions

Kenan Gundogdu, Jigar Bandaria, and Christopher M. Cheatum
Department of Chemistry, University of Iowa, Iowa City, IA 52242

We have measured the vibrational dynamics of pseudohalides bound as a substrate analog inhibitors at the active site of enzymes as a probe of the interactions between the protein and the pseudohalide inhibitor. We present both integrated photon-echo measurements and spectrally dispersed echoes that allow us to separate the ground-state and excited-state contributions to the signal. These results suggest that the pseudohalides can be used as probes of local interactions at enzyme active sites.

CHARACTERIZING COUPLED VIBRATORS WITH FIFTH-ORDER 2D-IR SPECTROSCOPY

Feng Ding, Eric C. Fulmer, and Martin T. Zanni

Department of Chemistry, 1101 University Avenue,

University of Wisconsin, Madison, WI 53706, USA

The vibrations of condensed phase molecules are a topic of great interest, because they provide a spectroscopic window into molecular structures, dynamics, and their surrounding solvent environments. But even though molecular vibrations are rich in information content, their complex nature creates significant challenges with regard to their measurement and interpretation. To better meet the experimental challenges, sophisticated new pulsed non-linear infrared spectroscopies, such as heterodyned 3rd-order spectroscopy, have been developed that improve the spectral resolution and directly measure dynamic timescales, among other capabilities. The clear advantages of heterodyned 3rd-order spectroscopy over linear spectroscopy suggest that 5th and higher order techniques should provide additional capabilities. A heterodyned 5th-order 2D IR spectrum of the model di-carbonyl system Ir(CO)2(C5H7O2) is reported. The pulse sequence used to generate this spectrum probes the eigenstate energies up to the 2nd overtone and combination bands and produces a 2D IR spectrum that correlates the fundamentals to the 1st overtone and combination bands. The pulse sequence is designed to generate and then rephase a two-quantum coherence so that the spectrum is line narrowed and the resolution improved for inhomogeneously broadened systems. Features arising from coherence transfer processes are identified, which are more pronounced than in 3rd-order 2D IR spectroscopy because the transition dipoles of the

2nd overtone and combination states are not rigorously orthogonal, relaxing the polarization constraints on the signal intensity for these features. The spectrum provides a stringent test of cascading signals caused by 3rd-order emitted fields and no cascading is observed.

Using 5th-order 2D IR spectroscopy, we measured the relative energies of the carbonyl stretch eigenstates up to the second overtone and combination bands. We found that if the local mode anharmonicity and coupling were determined solely from the first overtone and combination bands, the potential was insufficiently accurate to predict the 3Q eigenstates energies to within 8 cm^{-1}. To describe the potential up to the 3Q eigenstate energies, the local mode anharmonicity had to be adjusted and a coupling term β_4 that is quadratic in the two local modes had to be included. The β_4 term couples the first overtone states together. In systems with degenerate local modes such as IDC, even a small β_4 can have a measurable effect. For non-degenerate systems, β_4 will be less important. After including β_4 and adjusting the local mode parameters, the fits still do not reproduced the energy of the first combination band to within the experimental accuracy. As discussed above, this may indicate that the first combination band is coupled to some other lower frequency mode not included in the model Hamiltonian. Identifying states that are shifted because of coupling to unobserved modes presents an inherent challenge to extracting accurate local mode parameters from eigenstate energies. By including 3Q states in the fits, the chance that an outside coupling affects the extracted local mode parameters is minimized.

Besides obtaining a more accurate description of the potential energy surface of IDC, the 5th-order spectra also showed pronounced peaks arising from coherence transfer pathways. Coherence transfer is one mechanism for vibrational relaxation in condensed phase media that also includes population relaxation, dephasing, and population transfer. Fifth-order 2D IR spectroscopy is a potentially powerful tool for measuring the kinetics of these processes. In 3rd-order spectroscopies, there are three delay times that can be varied. Two of these delay times are needed to generate 2D IR spectra, while the third can be used as a "waiting time" to monitor population and coherence transfer processes.[6,13,39] Fifth-order pulse sequences have 5 delay times. As a result, there are three waiting times and the pulse sequence can be configured to solely measure coherence transfer processes during one of these waiting times, thereby removing population transfer effects and simplifying interpretation of the spectra. Furthermore, 5th-order spectroscopy is sensitive to the non-linear vibrational dynamics that results from dynamics between equilibrium states. Finally, the extra waiting times can also be used to generate 3D or 4D spectra, for higher resolution spectra and higher correlation of vibrational modes. Taken together, these attributes make 5th-order 2D IR spectroscopy a promising new tool to study vibrational couplings and dynamics of condensed phase molecules.

Time-Resolved Studies of Nitrosyl Halide Photoreaction Dynamics

Catherine C. Cooksey, Kevin J. Johnson, and Philip J. Reid
Department of Chemistry, Box 351700, University of Washington, Seattle, WA 98195
preid@chem.washington.edu Phone: (206) 543-6147 Fax: (206) 685-8665

Introduction. The photochemistry of chlorine-containing compounds is an important area in atmospheric chemistry due the participation of these species in chemical cycles involving atomic chlorine (Cl), a central species in stratospheric ozone depletion.[1] One such class of compounds are halooxides such as chlorine dioxide (OClO) and dichlorine monoxide (ClOCl). Transient absorption and time-resolved resonance Raman studies[2] of aqueous OClO have found that the dominant photochemical pathway is dissociation to form ClO and O followed by geminate recombination of these photoproducts resulting in reformation of OClO. The minor photochemical pathway is isomerization to form ClOO which appears with a time constant of ~30 ps and decays on the sub-nanosecond timescale. In comparison, transient absorption studies of ClOCl dissolved in perfluorohexane[3] have found that the dominant photochemical pathway is production of the isomer ClClO, with little evidence for Cl and ClO production and geminate recombination. The appearance and decay time constants of ClClO, ~10 ps and ~100 ps respectively, are similar to those of ClOO suggesting that photoisomerization is a general feature of halooxide photochemistry in condensed environments.

To extend our understanding of the condensed phase photochemistry of chlorine-containing molecules, we have initiated a series of studies involving nitrosyl halides, and in particular nitrosyl chloride (ClNO).[4] In the gas phase, photoexcitation of ClNO results in dissociation to form Cl and NO with a quantum yield near unity.[5] Matrix-isolation studies of ClNO have found that photoexcitation results in formation of the isomer, ClON.[6] The similarity of ClNO photochemistry to that of OClO and ClOCl, namely direct dissociation in the gas phase and photoisomerization in low-temperature matrices, suggests that the photochemistry of ClNO in solution should be similar as well. To see if this is the case, we have performed transient absorption studies of ClNO dissolved in two solvents, acetonitrile and chloroform. ClNO is photoexcited at 266 nm and the subsequent dynamics are probed throughout the UV.

Experimental. An amplified Ti:sapphire laser was used to produce 120-fs pulses (full width at half-maximum) centered at 800 nm with an energy of 750 μJ at a repetition rate of 1 kHz. The amplifier output was separated into two beams. The 266-nm pump field, was produced through third-harmonic generation (Spectra Physics TP-IA), and the probe field was produced by frequency doubling the second-harmonic of the signal output from an optical parametric amplifier (Quantronix, TOPAS). The pump polarization was oriented to 54.7^{o} relative to the probe in order to minimize rotational contributions to the measured evolution in optical density. The instrument response as measured by the optical Kerr effect in water was 350 ± 50 fs at all probe wavelengths. The sample was delivered to a fused-silica flow cell equipped with CaF_2 windows having a path of 0.2 cm. Pump and probe pulse energies of 5.0 and 0.3 μJ, respectively, were used in the ClNO studies reported here. ClNO samples were prepared as described in the literature, and concentrations of 1.2mM were employed.[7] For the studies of methyl hypochlorite (MeOCl) and ClNO dissolved in dichloromethane, the pump and probe pulse energies used were 0.27 and 0.08 μJ, respectively. Samples of MeOCl were prepared as described in literature, and concentrations of 1.1 M were employed.[8]

Results and Discussion. Figure 1 presents the contour plots of the transient absorption spectra of ClNO dissolved in (A) acetonitrile and (B) chloroform. Photolysis of ClNO in both solvents results in an initial decrease in optical density at 256 nm and 266 nm consistent with ground state depletion of ClNO. An increase in optical density at longer probe wavelengths due to photoproduct formation is also observed, with the maximum change in optical density occurring at ~295 nm in acetonitrile and at ~331 nm in chloroform. Examination of the color scales of the absolute change in optical density following ClNO photolysis demonstrates that photoproduct formation in chloroform results in a significantly larger change in optical density compared to acetonitrile (~2.7 times). In addition, the photoproduct produced in acetonitrile appears to be undergoing vibrational relaxation whereas similar evolution is not observed in acetonitrile.

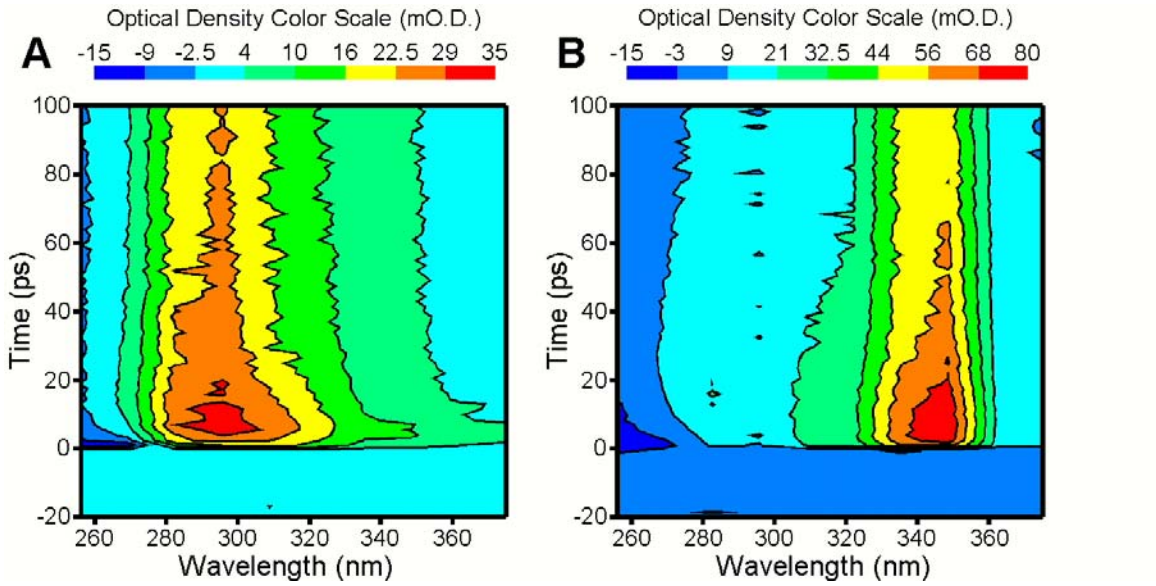

Figure 1. Contour plots of the transient absorption spectra of ClNO dissolved in (A) acetonitrile and (B) chloroform. The absolute change in optical density is indicated by the contour lines, with the color scale shown above the each plot.

The results presented here represent the first detailed measurements of ClNO photochemistry in solution. The measured evolution in optical density following ClNO photolysis in acetonitrile is consistent with the production of a photoproduct having an absorption band centered at 295 nm. In contrast, photolysis of ClNO dissolved in chloroform results in production of a photoproduct with an absorption maximum at 331 nm. There are two possible assignments for the photoproduct: the Cl:solvent charge-transfer complex or the structural isomer, ClON.

The first possibility is the formation of the Cl:solvent charge-transfer complex. To determine the location of the absorption band for the Cl:solvent charge transfer complex in chloroform, we performed a transient absorption study of methyl hypochlorite (MeOCl) in dichloromethane (Figure 2). The ionization potentials of dichloromethane and chloroform are roughly the same; therefore, the absorption maximum for the charge transfer complex in these solvents should be similar. Following photoexcitation of MeOCl in dichloromethane, a broad absorption band is observed centered at 340 nm, similar to the 331-nm band observed following ClNO photoexcitation in chloroform. However, the photoproduct absorption band derived from ClNO in dichloromethane is significantly different in comparison to that formed from MeOCl. The appearance kinetics of the ClNO photoproduct band are slower in comparison to MeOCl, while the decay kinetics are faster for the ClNO photoproduct. Additionally, the Cl:H_2O charge-transfer complex has a maximum absorption at 310 nm. The similarity of the ionization potentials for water and acetonitrile suggests that the Cl:acetonitrile charge-transfer complex would have a similar absorption maximum consistent with the observation of the photoproduct absorption at 295 nm.

The second possibility for the ClNO photoproduct is the isomer, ClON. Infrared spectroscopy confirmed the formation of ClON following photolysis of ClNO trapped in Ar and N_2 matrixes.[6] In addition, both theoretical and matrix isolation studies have suggested that the cross section for ClON is significantly larger than that of ClNO.[6a,9] The maximum optical density change observed for the photoproduct is consistent with a molar absorptivity for this species that is at least 3 times larger than that of ClNO at 256 nm given the depletion intensity observed at this wavelength. Therefore, the molar absorptivity of the photoproduct is $\geq$10,000 $M^{-1}cm^{-1}$. UV absorption spectra taken before and after photolysis of ClNO in a low-temperature matrix are consistent with a ClON absorption-band maximum at 417 nm. Both photoproduct bands in this experiment are blue-shifted 85 nm and 120 nm in chloroform and acetonitrile, respectively, relative to this value. However, theoretical calculations predict that the Cl-O bond in ClON is quite weak, and modification of this bond length in solution may have a substantial impact on the absorption spectrum. Therefore, it is possible that the ClON absorption band is shifted in solution relative to the matrix results.

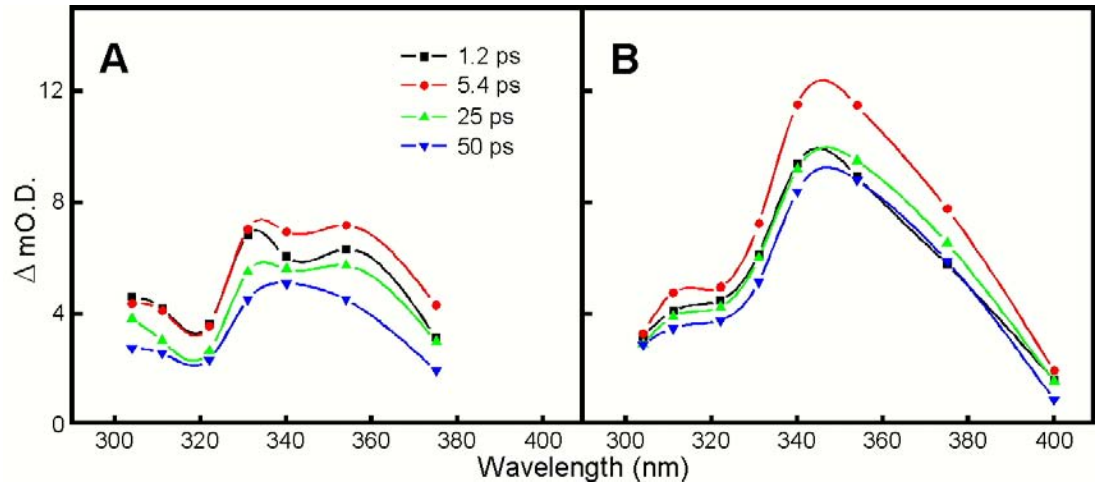

Figure 2. The transient absorption spectrum of (A) methyl hypochlorite and (B) ClNO dissolved in dichloromethane. The time delay for each spectrum is given in the figure.

In order to test the above photoproduct assignments, we plan to employ time-resolved vibrational spectroscopy. Time-resolved UV pump-IR probe can be used to probe the Cl:solvent charge transfer complex complementary pair, NO. In addition, production of the structural isomer, ClON, can be monitored with time-resolved resonance Raman spectroscopy.

Acknowledgement. The National Science Foundation is acknowledged for their support of this work (CHE-0350191). Acknowledgment is also made to the donors of the Petroleum Research Fund, administered by the American Chemical Society. CCC gratefully acknowledges support from the Ford Foundation.

References.

1. P. J. Reid, *J. Phys. Chem. A*, **106**, 1473-1482, (2002).
2. S. C. Hayes, C. L. Thomsen and P. J. Reid, *J. Chem. Phys*., **115**, 11228-11238, (2001).
3. C. C. Cooksey and P. J. Reid, *J. Phys. Chem. A*, **107**, 5508-5514, (2003).
4. C. C. Cooksey and P. J. Reid, *Photochem. Photobio*., **80**, 386-400, (2004).
5. C. B. Colburn, *Developments in Inorganic Nitrogen Chemistry* (Elsevier Scientific Publishing Company, New York, 1973).
6. a) G. Maier, H. P. Reisenauer, and M. DeMarco, *Chem. A. European J*., **6**, 800-808, (2000); b) A. Hallou, L. Schriver-Mazzuoli, A. Schriver, and P. Chaquin, *Chem. Phys*., **237**, 251-264, (1998).
7. B. P. Nyholm and P. J. Reid, *J. Phys. Chem. B*, **108**, 8716-8724, (2004).
8. C. G. Elles, M. J. Cox, G. L. Barnes, and F. Fleming Crim, *J. Phys. Chem. A*, **108**, 10973-10979, (2004).
9. T. J. Lee, *Chem. Phys. Lett*., **223**, 431-438, (1994).

Dissipative dynamics of a system passing through a conical intersection: ultrafast pump-probe observables

David Gelman and Ronnie Kosloff[1,*]

[1]*Fritz Haber Research Center for Molecular Dynamics,*

The Hebrew University, Jerusalem 91904, Israel

The Born-Oppenheimer separation of nuclear and electronic motions is the enabler of nearly all our knowledge of molecular structure and dynamics. The adiabatic separation on which this principle is based, however, is never exactly correct, and there are instances where it fails substantially. The simplest example is probably nonradiative decay, brought on by vibronic coupling. In the standard Landau-Zener approach motion along one coordinate modulates the nonadiabatic transition among electronic states. While the coupling is most easily envisaged along one coordinate, generalizing the Landau-Zener approach to multiple coordinates lies at the heart of contemporary models for electron transfer and for nonradiative decay.

Because of the different geometry of curve crossing between isolated Landau-Zener avoided crossings and higher-dimensional conical intersections, population transfer can be very rapid in the conical case. This is what led to the original interest in conical intersections, and it has been extensively discussed, particularly using density operator methods.

In our study, we focus on decay of photoexcited states, and on the experimental observables of luminescence, pump/probe spectra, and recovery of the bleach. All of these are governed not only by the population dynamics, but also by the value of the transition dipole moment and by energy redistribution. Hence it is necessary to deal not only with the electronic state population, but also with the energy distribution. In nearly all cases, then, we have in addition to the curve crossing problem an intramolecular vibrational relaxation (IVR) issue - the system must return to the starting configuration for bleach recovery to be observed, and back transfer (re-crossing) can occur in the excited state unless either IVR or effective dephasing make such recurrences impossible.

We use a direct propagation scheme to examine a two-mode model for conical intersec-

*Electronic address: `davg@fh.huji.ac.il`

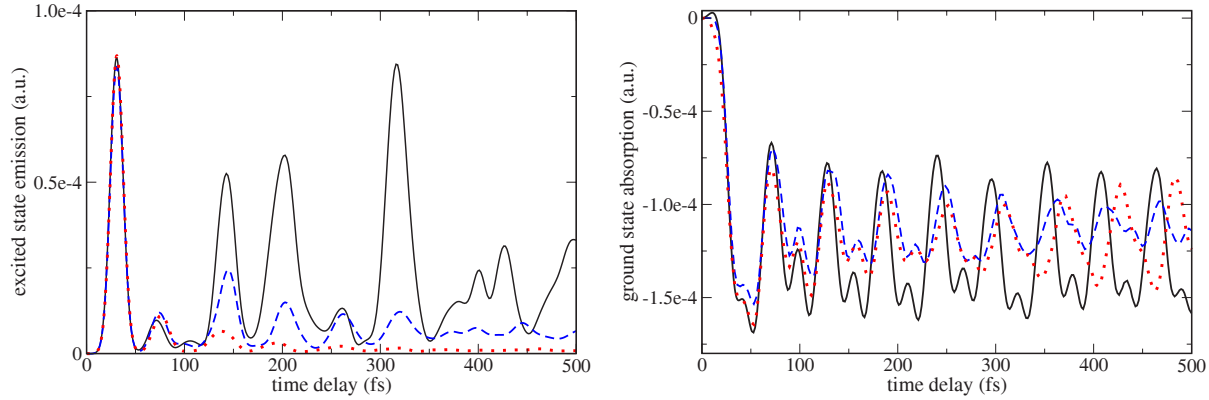

FIG. 1: Transient stimulated-emission (left) and absorption (right) signals for the two-mode system, incorporating a conical intersection. The pump and probe frequencies are chosen to correspond to vertical excitation from the bottom of the ground electronic potential. Solid lines: the isolated system; dashed lines: vibrational relaxation with weak system-bath coupling ($\eta_0 = \eta_c = 0.01, \gamma^{-1} = 750$ fs); dotted lines: vibrational relaxation ($\eta_0 = \eta_c = 0.01$) with medium electronic dephasing ($\bar{c}_e = 0.25$). The number of bath modes is $N = 30$ with two simultaneous excitations allowed.

tions. The aim is to investigate both population dynamics and bleach recovery, in order to relate them to experimental observations. Since the direct propagation of such a system scales exponentially with the number of modes, we use a system/bath approach, with two active vibrational modes and two electronic states chosen as the system, and a representation of the bath. We use two different treatments of this bath: first, a reduced description based on a density operator treatment where the dynamics is generated by the Lindblad formalism of semi-group dynamics; alternatively, we use a wavefunction propagation scheme with the so-called Surrogate Hamiltonian method, corresponding to an Ohmic distribution of spin modes in the bath. The focus is on photochemical dynamics, and the photochemical excitation is treated nonperturbatively - a system/electromagnetic field determination is included in the time-dependent Hamiltonian.

Widely discussed adiabatic electronic state populations can only be partially connected to experimental pump-probe signals. Therefore the present study emphasizes the transient modulations of optical observables, which are a direct signature of the ultrafast dynamics, measured in the pump-probe experiments. The non-perturbative approach has been employed for describing the dynamics induced by the pump pulse, while the weak probe has been treated within a perturbative picture. This allows us to associate a quantum mechani-

cal window operator to the absorption of the probe pulse centered at time t. The stimulated emission and absorption have been calculated as expectation values of this window operator.

The stimulated emission signals (left panel, Fig. 1) show a rapid initial decay on a time-scale of tens of femtoseconds, which can be associated with an ultrafast nonadiabatic transition via a conical intersection. This initial decay is almost unaffected by vibrational relaxation and the electronic dephasing. The dissipation becomes important in the following stage: it prevents a back transfer (re-crossing) leading to a sub-picosecond relaxation of the excited state population.

At the same time, it is clear that the pump/probe spectra are governed not only by the population dynamics, but also by the energy redistribution. After the initial curve crossing, the system may return close to its initial pre-pump configuration. Experimentally this is associated with the recovery of the bleach observed in the transient absorption signal. The *ground* state recovery dynamics, i.e. the bleach recovery and the cooling of the hot vibrational population, are not reflected in the electronic population probabilities. In our model the absorption signal (right panel, Fig. 1) shows coherent oscillations of the slightly perturbed ground state wave packet and apparently no fast recovery of the bleach up to 500 fsec. We can conclude that the energy relaxation, dominated by an intramolecular vibrational relaxation, proceeds much more slowly. The origin of the fast bleach recovery, measured in charge-transfer experiments remains unclear, but might well arise from simple avoided crossing with a sufficiently strong local diabatic coupling and efficient IVR.

SPECTRA/STRUCTURE CORRELATIONS AND TEMPORAL BEHAVIOUR OF DOVE 2D-IR SPECTRA

Paul M. Donaldson, Laura M.C. Barter, Elizabeth M. Gardner, Jason D. Palmer and David R. Klug
Molecular Dynamics Group, Biological and Biophysical Chemistry Section, Department of Chemistry, Imperial College of Science Technology and Medicine, Exhibition Road, London SW7 2AZ, U.K.

INTRODUCTION

Finding new analytical probes for studying proteins and associated biological systems that combine sensitivity, structural information and high throughput is of great importance in solving outstanding issues in cell biology. We are exploring a 2D-IR technique known as DOVE-FWM[1] (Doubly Vibrationally Enhanced Four Wave Mixing). We show in this paper that DOVE-2D-IR combines the following important properties:

- The ability to simplify vibrational spectra by mapping coupled vibrations into 2 or more dimensions.
- High sensitivity by mixing resonant infrared fields with a visible field to give an output in the visible part of the spectrum, with the possibility of visible resonance enhancements.
- Reduction of non resonant background, line narrowing and selection of resonant processes with time ordered picosecond pulse sequences.
- Flexible sample preparation schemes for reducing the non resonant background contribution to the FWM signal.

Figures 1 sketches our DOVE-2D-IR experiment, the wave mixing diagrams and pulse delay definitions. Note in the wave mixing diagrams that steps 1 to 2 for DOVE-Raman and steps 3 to 4 for DOVE-IR only occur if the vibrational levels are coupled. By varying ω_1 and ω_2, and measuring the FWM intensity, a 2D map can be made with DOVE signal appearing as cross peaks.

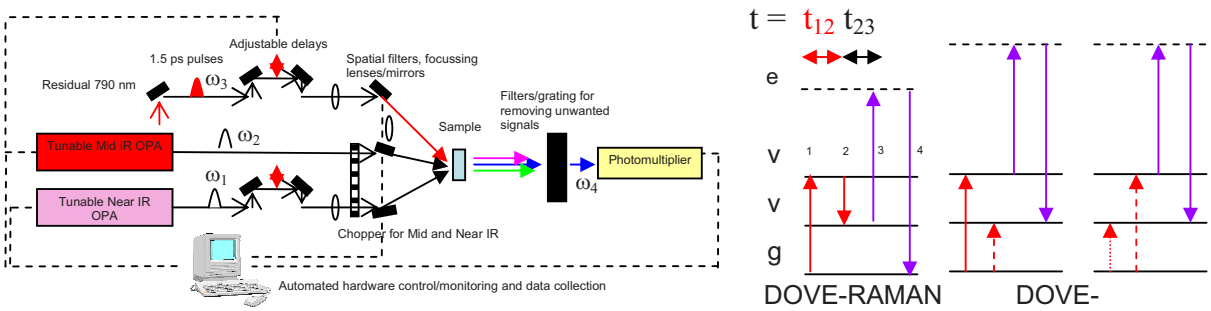

Figure 1 Experimental setup and Wave Mixing diagrams for DOVE-FWM spectroscopy.

SPECTRA/STRUCTURE CORRELATIONS

All DOVE 2D-IR spectra in this paper explore the correlation of combination bands in the near-IR (4200-5000 cm^{-1}) with bands in the mid-IR (1320-1690 cm^{-1}). We use plastics, peptides and proteins in the solid phase as model systems to identify and interpret DOVE features. Shown in Figure 2 are some examples of 2D spectra we have collected.

Assignments can be straight forward. The well understood linear infrared absorption spectra for polyethylene (PE - 2A) and polystyrene (PS - 2B) are shown along their 2D spectra's axes. The CH_2 deformation and wag modes of PE (1350-1450 cm-1) clearly correlate with their respective stretch combination bands (4200-4400 cm^{-1}). The ring breathing modes (1570-1690 cm^{-1}) of the aromatic side chain in PS are clearly involved in generating DOVE peaks with the Ar(C-H) stretch/ring breathing combination bands (4500-4800 cm^{-1}). The extra peaks in the LDPE (2B) are possibly due to increased CH_3 content.

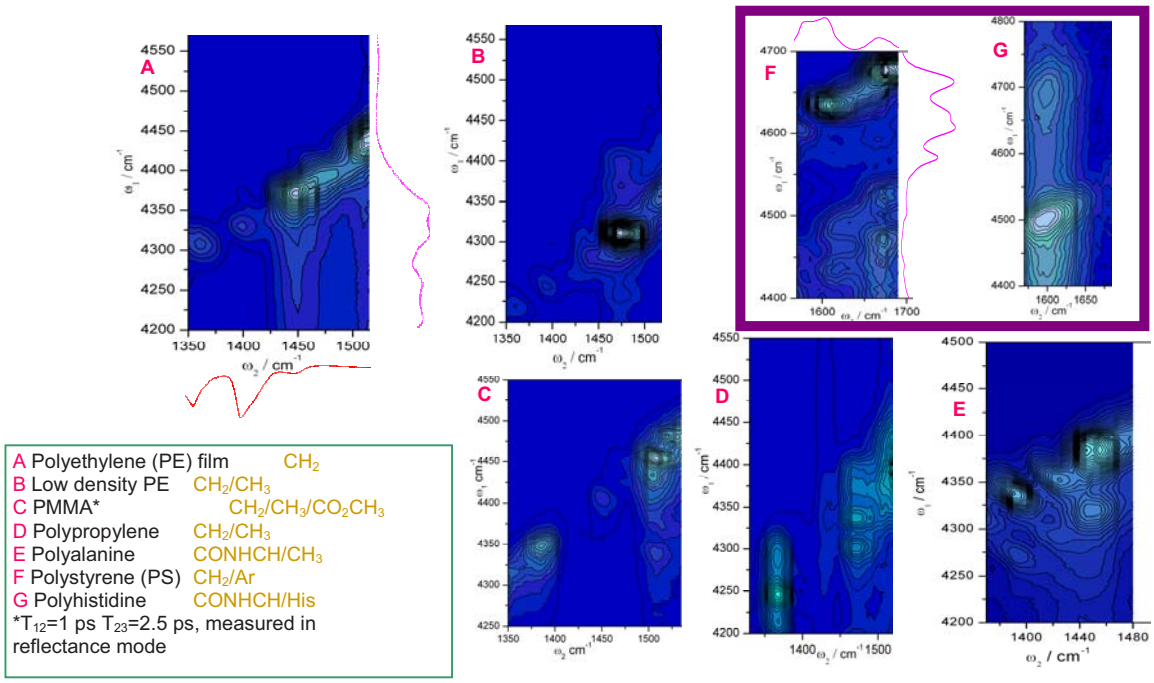

Figure 2 2D DOVE spectra for plastics and peptides in the solid phase. With mid–IR first T12=1.5ps T23=1.5ps.

TEMPORAL STUDIES OF DOVE-2D-IR SIGNAL

A very useful feature of sub-picosecond FWM techniques is the ability to select coherence pathways and remove non resonant four wave mixing processes. Non resonant background can only be generated when all beams are temporally overlapped. The lifetime of vibrational coherences that generate DOVE-FWM are typically > 1 ps. Using laser pulses of 1.5 ps duration, DOVE signal can thus be generated with pulse delays greater than the temporal width of each pulse. Figure 3 shows 2D spectra of gelatine (B,C and D) taken at three different sets of pulse delays. When the beams are temporally overlapped, peaks are obscured by non resonant background and competing DOVE processes. 1.5 ps delays are enough to resolve the cross peaks.

The time ordering of ω_2 and ω_2 is important and in our case determines whether a single DOVE-IR process occurs, or DOVE-IR and DOVE-Raman occur (see Figure 1). The DOVE-Raman signal occurs at values of ω_2 shifted slightly from the DOVE-IR signal by the anharmonicity of the combination band. These can be observed in the Near-IR pulse first spectrum of Gelatine in Figure 3D. Many samples give unwanted CARS signals, such as polystyrene (Figure 6.). Reducing the overlap between the IR pulses eliminates CARS (see Figure 3A). We found that for T_{12}=10 ps, the polystyrene DOVE signal was only 14 times smaller than the T_{12}=T_{23}=0 signal.

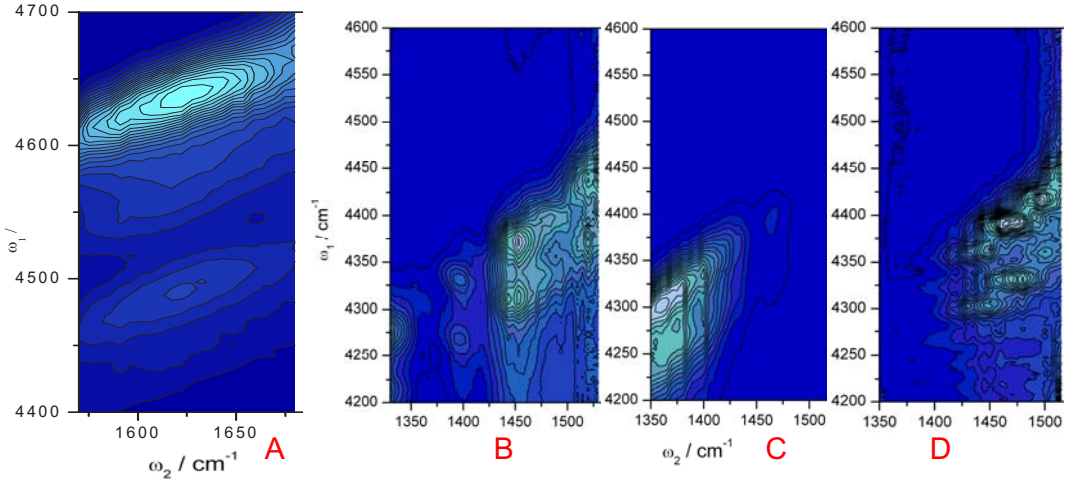

Figure 3 2D Spectra taken at various pulse delays of A: polystyrene T_{12}=T_{23}=0 (c.f Figure 2F) and B-D: Gelatine B: T_{12}=1.5ps, T_{23}=1.5ps, C: T_{12}=1ps, T_{23}=1ps (Mid IR first), D: T_{12}=-1.5ps, T_{23}=1.5 ps (Near-IR first).

TOWARDS FULL VIBRATIONAL FINGERPRINTS OF PROTEINS

Our current method of exploring protein 2D-IR spectra is to drop coat and dry a sample onto glass (Figure 4C). This method eliminates the need for a front window and concentrates the sample in a small area. The glass backing is a strong IR absorber and generates very little background signal. With this method we achieve extremely high signal to noise ratios (see Figure 4B). We have studied a wide range of proteins with this method. Figure 4A shows an example protein fingerprint of Liver Alcohol Dehydrogenase. Future work will include scanning wider spectral ranges and Mid-IR/Mid-IR DOVE 2D-IR studies.

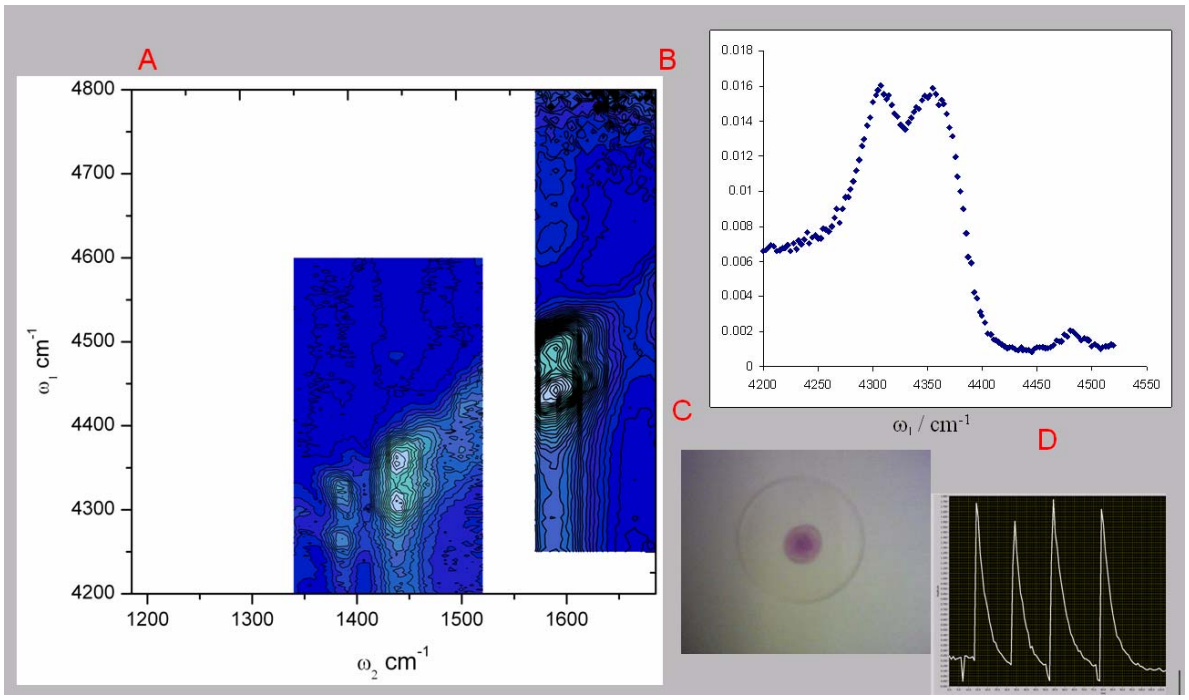

Figure 4 Liver Alcohol Dehydrogenase 2D DOVE spectrum (A) and a 1D cut (B) for T12=T23=1.5 ps. Each data point is collected in 150 ms (150 laser shots). Shown in C is Bacteriorhodopsin drop coated on glass. D shows the reflection FWM signal v.s time for a TiO_2 film with adsorbed Indo-cyanine green. The film is moved periodically, exposing fresh dye to the beams.

ω_3 VISIBLE RESONANCE ENHANCEMENT AND REFLECTION SIGNALS

We have been exploring methods of improving the sensitivity of DOVE-2D-IR. Tuning ω_3 near to electronic absorption features gives orders of magnitude more signal and adds a third dimension for spectral simplification, as only vibrations that couple to electronic excitations will give triply enhanced signal. Measuring DOVE-FWM in reflection from films or porous substrate such as TiO_2 eliminates non resonant background from support materials and greatly reduces the amount of protein required for analysis. Figure 4D. shows transient reflection FWM signals from a dye adsorbed in a nanoporous 4 mm TiO_2 film. Its electronic absorption coincides with our 790 nm ω_3 beam. Upon irradiation, the dye falls apart. The film is moved repeatedly, exposing fresh dye and thus demonstrating a four wave mixing visible resonance enhancement in reflection.

REFERENCES

1) Wei Zhao and John C. Wright, Physical Review Letters, 2000, **84**(7), 1411-1414
Doubly vibrationally enhanced four waving: The optical analogue of 2D NMR

ACKNOWLEDGEMENTS

We thank Chris Barnett for his invaluable support in the design and construction of the electrical equipment necessary for our measurements.

CONTACTS: **paul.donaldson@ic.ac.uk, d.klug@ic.ac.uk**

Vibrational Energy Flow in Push-Pull Chromophores: A Time Resolved anti-Stokes Resonance Raman Study

Tissa C. Gunaratne, J. Reddy Challa and M. Cather Simpson

Center for Chemical Dynamics and Department of Chemistry, Case Western Reserve University, Cleveland OH 44106

Abstract

Push–pull chromophores are a useful class of molecules for understanding electronic and vibrational energy dynamics, and are good candidates for non-linear optical and molecular electronics applications. A prototype push-pull chromophore, *para*-nitroaniline (PNA), and its analogs (2-methyl-4-nitroaniline (MPNA) and 2,6-dimethyl-4-nitroaniline (DMPNA)) have been probed with ultrafast time-resolved anti-Stokes Resonance Raman spectrometry (TR^3S). The successive addition methyl rotors on the benzene ring has a measurable accelerating effect upon the vibrational redistribution and/or relaxation processes of the central benzene ring.

Introduction

Photoinduced electronic excitation of a molecule initiates a sometimes quite complex chain of photophysical and photochemical events. Push-pull chromophores, in which an electron donor is covalently attached to an electron acceptor via a conjugated linker, exhibit many properties that confer utility for elucidating how fast dynamical events depend upon the details of the structure, environment, and energy deposition conditions. Our studies have focused upon exploiting the PNA system to study the effects upon vibrational dynamics of (1) photoexcitation of different subpopulations of ground state conformations[1] and (2) addition of peripheral degrees of freedom to the main chromophore unit.

It has been suggested that the UV/Vis absorption of PNA is broadened by a distribution of NO_2 twist angles.[2-4] As this coordinate is thought to play a major role in the electronic excited state dynamics of the system[2-4], our hypothesis was that the initial NO_2 conformation or subset of conformations electronically excited should have an impact on the subset of electronic and vibrational dynamics This was tested by using three different excitation wavelengths within the UV/Vis absorption lineshape of PNA, and measuring the subsequent vibrational dynamics with anti-Stokes TR^3 spectroscopy. The lifetimes of the major modes observed were consistent with those published by others[2-8], and no wavelength dependence was observed[1]. The results suggest that either the UV/Vis lineshape is not broadened conformationally or the dynamics are sufficiently rapid on the electronic excited state that the system crosses back to S_0 in a thermalized state.

The new hypothesis presented here explores the proposal that the addition of methyl groups to the PNA chromophore should decrease the vibrational relaxation lifetime. These methyl rotors are envisioned as efficient moities through which vibrational energy can flow from the chromophore to the solvent. Single and double methyled PNA analogs were studied and their anti-Stokes TR^3 kinetics were compared to those of the bare PNA. The changes in kinetics of ν_{29} (1310 cm^{-1}) band will be looked at in detail. No evidence for wavelength specific kinetics was

observed. The vibrational cooling kinetics (peak shift and linewidth changes) were observed and analyzed quantitatively.

Methods

Transient Raman spectra were obtained by subtracting pump-only and probe-only spectra from pump-probe spectra and once lifetimes were estimated a spectrum at a reference point with long delay time was subtracted from pump-probe spectra.

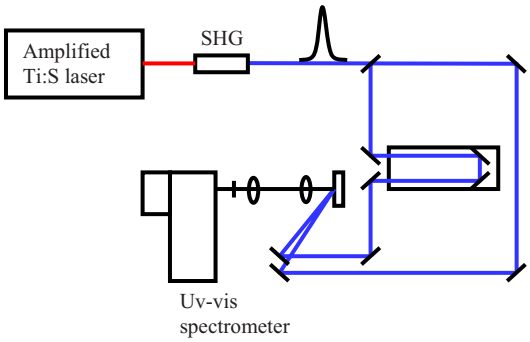

Figure 1. The scmatics of the current system with short b/w pulses for both pump and probe derived from 30 mm long KDP crystal.
λ=385-420 nm, ~500 fs, 17-25 cm^{-1}

To find the temporal overlap (time zero), coherent processes do not hold much promise; the pulses are too long in duration. Therefore, a method based on the temporal symmetry of a one-color pump/probe experiment was used to find the temporal overlap. Since both arms have the same wavelength, both can act as pump or probe (see Figure 2(b) for an example). When two beams are made equal in flux, the kinetic trace is symmetric around time zero. This method can comfortably be extended to find instrument response function when a molecule with fast rise time (faster than the instrument response) is used[9].

Results and Discussion

The influence of peripheral methyl substitution upon the vibrational lifetime of the high frequency NO_2 stretch mode (ν_{29}, 1310 cm^{-1} in PNA) is shown in Figure 2. A systematic decrease in vibrational lifetimes on the ground electronic state was observed with increasing number of methyl groups. Thus the results are consistent with the idea that the methyl rotors facilitate vibrational energy relaxation from the PNA chromophore to the solvent. Studies are underway to explore this effect. In particular, we will examine mode selectivity and the extension of the methyl group to larger substituents with additional degrees of freedom.

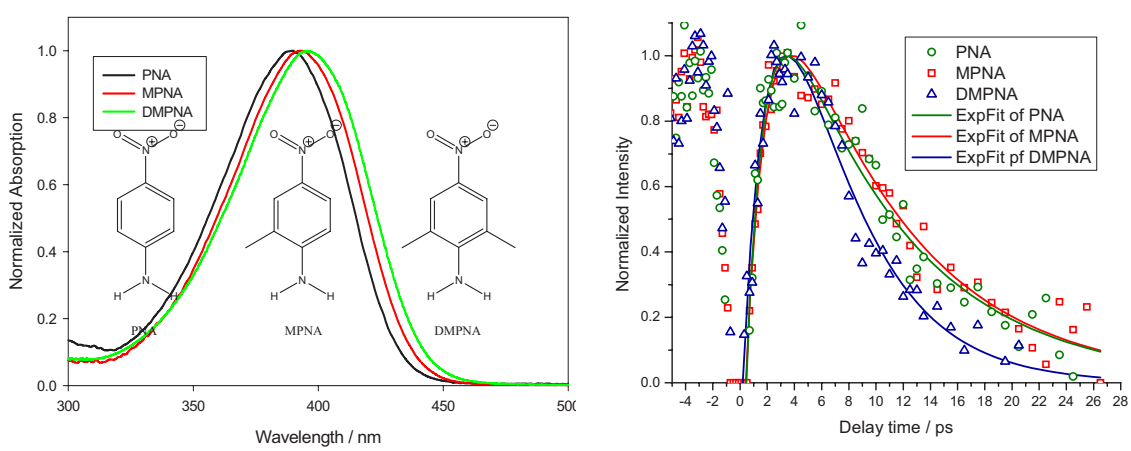

Figure 2. (a) Absorption spectra and structures of PNA, MPNA and DMPNA. (b) Kinetic decay profiles for PNA, MPNA and DMPNA at ~1300 cm^{-1}. Note that the excitation event occurs at 6.5 ps on the time scale in (b).

References

[1] T. Gunaratne, J. R. Challa, M. Cather Simpson, *Chem. Phys. Chem*. **2005,** 6(6), 1157-1163

[2] S. A. Kovalenko, R. Schanz, H. Hennig, N. P. Ernsting, *J. Chem. Phys*. **2001**, 115, 3256 – 3273.

[3] S. A. Kovalenko, R. Schanz, V. M. Farztdinov, H. Hennig, N. P. Ernsting, *Chem. Phys. Lett*. **2000**, 323, 312 –322.

[4] V. M. Farztdinov, R. Schanz, S. A. Kovalenko, N. P. Ernsting, *J. Phys. Chem. A* **2000**, 104, 11 486 –11496.

[5] C. L. Thomsen, J. Thogersen, S. R. Keiding, *J. Phys. Chem. A* **1998**, 102,1062 –1067.

[6] Q. An, P. Gilch, *Chem. Phys. Lett*. **2002**, 363, 397 –403.

[7] V. Kozich, W. Werncke, J. Dreyer, K.-W. Brzezinka, M. Rini, A. Kummrow, T. Elsaesser, J. *Chem. Phys*. **2002**, 117, 719 –726.

[8] V. Kozich, W. Werncke, A. I. Vodchits, J. Dreyer, *J. Chem. Phys.* **2003**, 118, 1808 –1814.

[9] T. C. Gunaratne, M. Milliken, M. C. Simpson. *Applied Optics* **2005** (in revision)

Acknowledgements

Authors acknowledge the National Institutes of Health (GM056816; MCS) and the Provost's Opportunity Fund at Case Western Reserve University (MCS & TCG) for support of this work.

Transient Terahertz Spectroscopy of Trans-Azobenzene

Okan Esenturk and Edwin J. Heilweil

Optical Technology Division, National Institute of Science and Technology
Gaithersburg, MD 20899
e-mail: okanesenturk@gmail.com

Abstract

Application of ultrafast optical pump-THz probe experiments on solid and liquid trans-azobenzene is presented. Large differences in UV excitation (400 nm between S_1 and S_2 absorption) and THz absorption cross-sections for azobenzene make these pump-probe experiments extremely difficult. Preliminary results shows a fast decay on the order of ~1 ps, as observed in previous transient UV-visible and Raman studies. The longer lived ~10 ps decay observed in other studies has not yet been captured due to extremely low S/N levels. Further improvements on the instrument and experimental conditions are in progress.

Introduction

In this study the isomerization mechanism of azobenzene have been investigated by UV-pump THz-probe spectroscopy to demonstrate the application of THz spectroscopy to determine transient properties of molecules. Due to its high sensitivity transient THz spectroscopy is widely applied to semiconductors. This is the first known study on transient behavior of molecules to authors' knowledge.

Azobenzene is a simple molecule consisting of two benzene rings attached by a diazo bridge (Figure 1). It has two stable isomers (trans and cis) and exhibits color dependent photoisomerization from one form to the other. It is a system that mimics the behaviour of more complex systems that are

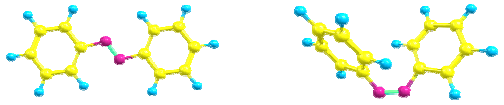

Figure 1. Trans-azobenzene and cis-azobenzene

used for image storage and light switches.[1] Transient properties of azobenzene has been investigated by many techniques such as UV-VIS, Raman, and IR in addition to extensive theoretical work.[2-9] According to the reported studies of azobenzene isomerization reaction there two photisomerization process. The isomerization path is determined by the color that excites the azobenzene molecules. Azobenzene undergoes isomerization via an in-plane inversion at a single N atom if it is excited to S1 state or via a rotation around the N=N double bond when it is excited to S2 state.[6] The reported quantum yields are 0.2 for the first isomerization pathway and 0.1 for the second pathway.[7] The reported studies suggest two time constants as ~1 ps (in solvents like toluene) and ~10 ps.[7-9] Both but especially the former is highly depend on the solvent viscosity.[9]
The main advantage of THz spectroscopy over the other commonly used techniques is that it observes the vibrational behavior of the molecules on the low frequency range, 10-300 cm^{-1}. These vibrational modes involves the whole structure rather than a specific local mode such as N=N stretch. Potentially, this gives a unique advantage to THz spectroscopy to follow the dynamic behavior of the molecules that undergoes large scale structural changes, such as isomerization, folding, etc. In addition, the pulsed THz method is inherently a time domain spectroscopic technique meaning the interferogram not only contains amplitude but also phase information. These qualities allow one to calculate the real and imaginary part of the dielectric constant and precise measurements of refractive index and absorption coefficient. However, THz spectroscopy lacks a strong theoretical understanding of the molecular motions, which is a significant drawback for its application.

Experimental

Trans-azobenzene was purchased from Aldrich and used as received.[10] FT-IR spectra were collected with a Nicolet FT-IR spectrometer specially modified for the THz range. Time-resolved THz spectra were collected with a home-built THz spectrometer and the optical design of the UV pump-THz probe apparatus is given in Figure 2. THz probe pulses were generated by difference frequency mixing the spectral components of an ultrafast ~60 fs, 800 nm (~50 nm FWHM) laser pulse in a 150 μm thick GaP crystal (110). The generated THz probe pulse has ~110 fs pulsewidth and 3 THz FWHM band-width. It has usable power spanning 0.3 THz (~10 cm^{-1}) and 8 THz (~250 cm^{-1}) in dry air. The typically used spectral range is 0.3-7 THz with a frequency resolution of ~0.3 THz (due to the reflections of the thin GaP crystals). The generated THz beam is collimated, focused onto the sample, re-collimated, and directed to a THz detector crystal by off-axis parabolic silver mirrors. The THz field is detected by the electro-optic effect using a 150mm thick GaP crystal (110). The THz detector is gated with a weak portion of the ultrafast 800 nm laser pulse and the electric field of the THz pulse is mapped as a function of time via an optical delay line and detected by silicon photodiodes (NIST calibrated). The fast Fourier transform of the THz pulse waveform yields the THz power spectrum. Second harmonic of the 800 nm pulses is used for photoexcitation of trans-azobenzene.

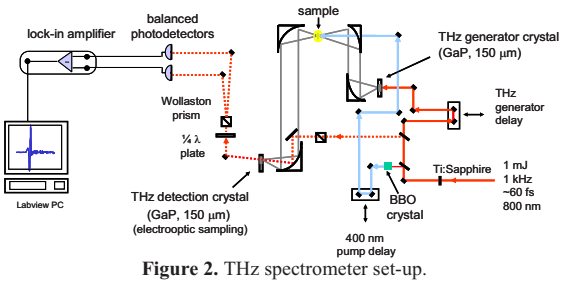

Figure 2. THz spectrometer set-up.

Discussion and Conclusion

Steady state FTIR studies showed that solid trans-azobenzene (t-azo) has two low frequency features at ~2.6 and ~2.9 THz and a higher frequency feature at 9.1 THz (Figure 3, solid line) that falls within our spectral bandwidth of the pulsed THz spectrometer. DFT calculations (Gaussian 03) on isolated gas-phase t-azo molecule with B3LYP/cc-pvdz combination reproduced the two low frequency modes at 1.9 and 2.6 THz, and the higher frequency mode at 9.3 THz (Figure 3, dashed line). Although the low frequency modes are slightly red shifted, and high frequency mode is slightly blue shifted, the overall calculated spectrum of t-azo is consistent with the FTIR spectrum. However, the calculated spectrum of cis-azobenzene (c-azo) (Figure 3, dotted line) is comparably different than that of t-azo. The calculated c-azo modes below 9 THz are 1.4, 2.3, 4.4, 5.6, and 8.4 THz. The all three features observed in t-azo are red-shifted in c-azo spectrum. Therefore, after a photo-isomerization of t-azo to c-azo a loss in t-azo absorptions at all of its absorption bands (i.e. 2.6 and 2.9 THz)should occur, and new features of cis-azo (i.e. 1.4, 2.3 and 4.4 THz) should appear.

The UV-visible spectrum of t-azo has two absorption bands: one centered at 320 nm is much stronger than the one centered at 450 nm. These bands correspond to the excitation of the molecules to S1 and S2 states, respectively. Therefore, photoexcitation with a 400 nm pulse mainly excites molecules to their low lying S1 state rather than to the S2 state. Another facet of UV excitation is that 400 nm falls on the blue edge of the low energy S1 absorption band. The absorption coefficient is comparably lower (~100 cm^{-1} @ 400 nm) with respect to the center of the band (~1000 cm^{-1} @ 320nm). In order to observe IR transients, it is very important to have closely matching pump-probe absorption coefficients. Unfortunately, the THz absorption coefficient for t-azo is extremely low (≤ 1 cm^{-1}). Therefore, the lowest absorption coefficient for optical pumping is preferred.

Figure 4 shows results for optical pump-THz probe experiments on the photoisomerization of solid azobenzene. Figure 4A compares the time-domain spectrum of t-azo with its pump-induced response spectrum at ~0.5 ps after the pump pulse. The transient response overlays very well with the THz spectrum. Figure 4B is the fast Fourier transform spectrum of the transient response shown in A. Although the signal-to-noise level is very low, the results are promising. The broad feature centered at 3 THz most likely corresponds to the loss of absorption at ~2.6 and 2.9 THz of t-azo molecules and absorption at 2.3 THz from c-azo molecules, as discussed above. The spectra also suggest the possibility of new c-azo absorption features such as the low frequency band at ~1.4 THz and higher frequency bands at 4.4 and 5.6 THz. However, the noise level (i.e @ ~8 and ~11 THz) is similar to the signals of these features. We are currently working on improving the signal-to-noise level of our instrument for improved studies of the azobenzene and other systems.

In conclusion, this study explored the use of optical pump-THz probe spectroscopy to study the photoisomerization of azobenzene molecules. Results to date yielded a transient response due to loss of t-azo parent absorption and absorption increase from c-azo molecules formed by photoisomerization. Due to extremely low signal-to-noise levels, the isomerization path has not been determined. Future work will concentrate on signal-to-noise improvement of the instrument.

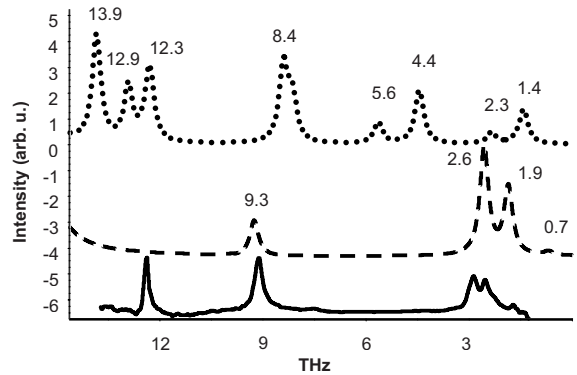

Figure 3. THz spectra of solid trans-azobenzene (solid line) is compared to calculated trans (dashed line) and cis-azobenzene (dotted line).

References

[1] Ikeda, T. and Tsutsumi, O. *Science* **1995**, 268, 1873; Liu, Z.F., Hashimoto, K., and Fujishima, A. *Nature* **1990**, 347,658.
[2] Morgante, C.G., Struve, W.S. *Chem. Phys. Lett.* **1979**, 68, 267.
[3] Armstron, D.R. et.al. *J. Phys. Chem.* **1995**, 99,17825.
[4] Cembran, A. et.al. *JACS* **2004**, 126, 3234.
[5] Hamm, P., Ohline, S.M., Zinth, W. *J. Chem. Phys.* **1996**, 106, 519.
[6] Rau, H. and Luddecke, E. *JACS* **1982**, 104, 1616.
[7] Lednev, I.K. et.al. *J. Phys. Chem.* **1996**, 100, 13338.
[8] Lednev, I.K. et.al. *Chem. Phys. Lett.* **1998**, 290, 68.
[9] Fujino. T. and Tahara, T *J. Phys. Chem. A* **2000**, 104,4203.
[10] Certain commercial equipment, instruments, or materials are identified but in no case imply recommendation by NIST.

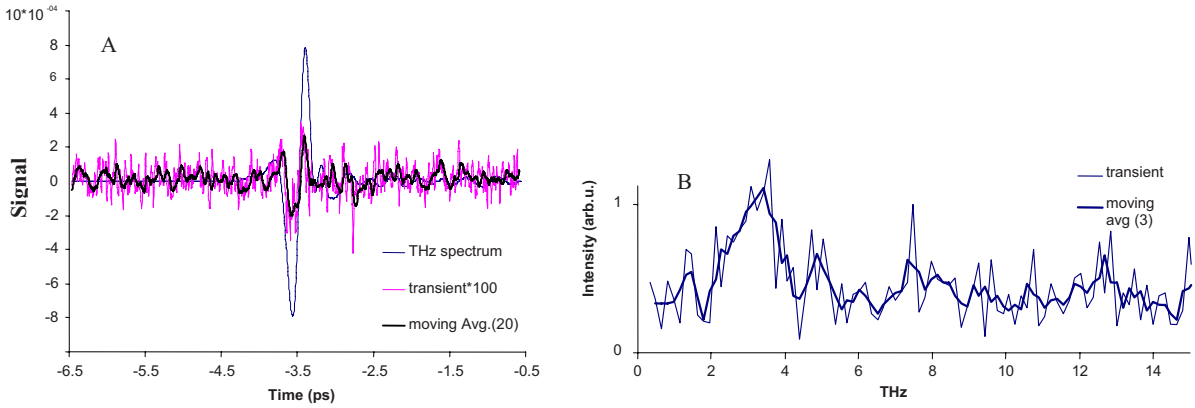

Figure 4. A) Time-domain THz spectrum of solid t-azo and transient spectrum (purple). B) FFT of the transient time-domain spectrum given in A. The feature ~3 THz is mainly due to the loss in trans-azobenzene absorption.

Inter- and Intra-Molecular Hydrogen Bonding in Phenol Derivatives: A Model System for Polypeptides

Neil T. Hunt, Andrew R. Turner and Klaas Wynne
Department of Physics, University of Strathclyde, John Anderson Building, 107 Rottenrow East, Glasgow G4 0NG, Scotland, UK

Abstract The ultrafast dynamics of solutions of phenol and two phenol derivatives – hydroquinone (1,4-benzenediol) and pyrocatechol (1,2-benzenediol) – have been studied using Optically Heterodyne-Detected Optical Kerr-Effect (OHD-OKE) spectroscopy. The solvents, methanol and acetonitrile, were selected to provide strong and weak solvent-solute hydrogen bonding interactions respectively while pyrocatechol features an intra-molecular hydrogen bond. Together these provide a series of model systems for polypeptides such as polytyrosine, which facilitate the direct study of inter- and intra-molecular hydrogen bonding. A broad contribution to the Raman spectral density of the methanol solutions at frequencies between 150 and 300 cm^{-1} has been observed that is absent in acetonitrile. This contribution has been assigned to solvent-solute hydrogen-bond stretching vibrations. The OHD-OKE response of poly-L-tyrosine has been measured and was found to contain a similar contribution.

Density functional theory geometry optimizations and normal mode calculations have been performed using the B3LYP hybrid functional and 6-311++G** basis set. These have yielded a complete assignment of the low frequency Raman and far-infrared spectra of pyrocatechol for the first time, which has provided information on the nature of the intra-molecular hydrogen bond of pyrocatechol.

I. Introduction

Hydrogen bonding in liquids plays an important role in the structure and chemistry of biomolecules. From stabilising of biopolymer molecules into structures such as the α-helix or β-sheet to the reversible bond formation that allows the action of enzymes, the hydrogen bond is central to all biological processes. Understanding the dynamics of these interactions is therefore crucial to our exploitation of such systems. Despite much study, however, this understanding remains incomplete.

The aim of this study is to determine directly the contribution of hydrogen bonding to the ultrafast dynamics and low frequency Raman spectrum of the polypeptide poly-L-tyrosine. This is achieved through the use of model systems featuring a range of phenol derivatives: phenol, hydroquinone (1,4-benzenediol), and pyrocatechol (1,2-benzenediol) (see Scheme 1) dissolved in the two solvents methanol and acetonitrile. The phenolic side group of the tyrosine molecule makes these an obvious choice of model system. The solvents have been chosen to provide strong and weak hydrogen bonding interactions with the solute molecules respectively while avoiding the broad low frequency absorptions that hinder aqueous studies.

II. Results

FTIR spectra of the OH stretching region showed that the absorptions of the phenol derivatives dissolved in methanol are broader and red-shifted in comparison to those in acetonitrile. This indicates stronger solvent-solute Hydrogen bonding in methanol.

a.OHD-OKE Results – Frequency Domain

Fourier transforms of the OHD-OKE data for each of the solutions studied, with the solvent contributions subtracted, are displayed in Figure 1.

A sharp spike at low frequency dominates the complete spectral densities of the six samples, which is due to the rotational diffusive dynamics. In all cases, the broad band below 150 cm^{-1} that is assignable to librational motion[1] is clearly observed. At frequencies in excess of 200 cm^{-1} are low amplitude, narrow bands due to intra-molecular vibrations of the solute.

The spectral densities of the methanol solutions containing either phenol or hydroquinone show an additional contribution between 150 and 300 cm^{-1}. That of pyrocatechol shows a broadband offset of the baseline that persists to beyond the scope of the spectrometer at frequencies above 700 cm^{-1} (the latter feature is both repeatable and scales with pyrocatechol concentration). Neither of these features is present in the acetonitrile samples.

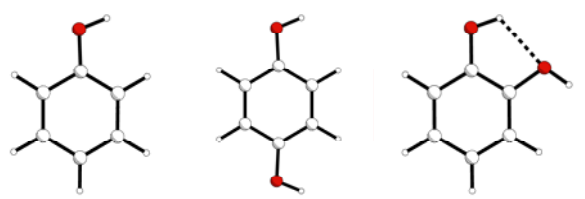

Scheme 1: Equilibrium structures of phenol, hydroquinone, and pyrocatechol calculated using DFT (see text).

The additional amplitude in the spectral densities in the phenol and hydroquinone in methanol samples is apparently due to some interaction between the solvent and the solute. As such it is instructive to study the dependence of the effect on methanol concentration. This is shown in Figure 2 where methanol was added to concentrations of 0.5, 1, and 2 M to a 1 M solution of hydroquinone in acetonitrile. All spectra were normalised to the sharp, low frequency rotational-diffusion feature although similar results were achieved by normalising to an acetonitrile intra-molecular mode and subsequent subtraction of the solvent response. As can be clearly seen, the broad component between 150 and 300 cm^{-1} persists for all methanol concentrations studied. This result shows that the addition of even small amounts of methanol leads to a modification of the spectral density of hydroquinone in this frequency region that can only be ascribed to solvent-solute interaction.

a. Librational and Inter-molecular Dynamics

For further analyses, it is advantageous to separate the Raman spectral densities into two regions at this stage. The high frequency (>300 cm^{-1}) portion, which is dominated by

intra-molecular vibrational modes will be discussed in a separate subsection. Presented below is a more quantitative analysis of the low frequency portion, which is dominated by librational motions and inter-molecular interactions.

The broad and somewhat featureless nature of the low frequency spectral density of most liquids means that fitting of the data is, to a certain extent, an arbitrary process. In this work, the spectral densities of the 1-M solutions of phenol and hydroquinone in methanol and phenol, hydroquinone and pyrocatechol in acetonitrile were fit to the sum of a Bucaro-Litovitz function and a set of anti-symmetrised Gaussian (ASG) profiles. In all cases, the non-diffusive spectral density without solvent subtraction was used for the fit. This approach removes the need for an additional function to fit the rotational dynamics and ensures that no artefacts from the solvent subtraction complicate the fitting process. Furthermore, the solvent subtraction approach assumes separability of the solvent and solute responses. This is not necessarily valid when considering solutions that exhibit strong solvent-solute interactions and it is thus more rigorous to consider the spectral density as a whole.

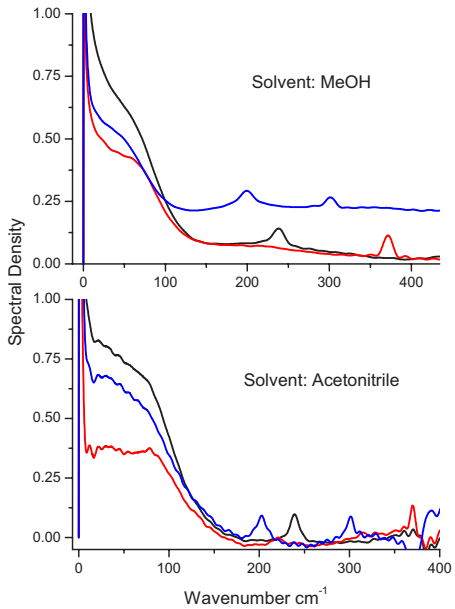

Figure 1. Solvent subtracted spectral densities of 1M solutions of phenol (black), hydroquinone (red) and pyrocatechol (blue).

Figure 3 displays example fits for phenol dissolved in methanol and acetonitrile. The results of the fitting process show that all of the spectral densities can be fit by a similar range of functions: the broad lineshape at low frequency is well described by a Bucaro-Litovitz lineshape with ω_{BL} = 11 cm^{-1} ± 2 cm^{-1} and one ASG lineshape centred at 35 cm^{-1} ± 5 cm^{-1} with a width parameter (σ_G) of around 115 cm^{-1}. In addition, the samples in methanol require a second ASG function with $\omega \sim 90$ cm^{-1} and $\sigma_G \sim 275$ cm^{-1}. Phenol and pyrocatechol also require a narrow ASG profile to account for a low-lying intra-molecular vibrational mode.

b. Intra-molecular Vibrational Modes and DFT Calculations

Despite the mid infrared spectra of phenol, hydroquinone and pyrocatechol being much studied[2-6] and well understood, some confusion still exists at low frequencies. While agreement seems to have been reached in the cases of phenol and hydroquinone, assignment of the low frequency modes of pyrocatechol remains unclear. In order to establish fully any effects of hydrogen bonding on the low frequency Raman spectral densities recovered here, it was first necessary to obtain a complete assignment of all observed bands. In the cases of phenol and hydroquinone, assignment was relatively straightforward using existing studies.[3,6] For pyrocatechol, however, specific problems existed that related to observed modes at 289 and 301 cm^{-1}. These appeared not to agree, even closely, with previous studies.[6] It seemed that the two modes were probably due to the symmetric out-of-plane and in-plane bending modes of the two hydroxyl groups, however, the latter was predicted to be Raman inactive while the former had not been previously assigned.

In order to solve this problem, DFT calculations of the equilibrium structure and vibrational modes of phenol, hydroquinone, and pyrocatechol were performed. The equilibrium structures are as shown in Scheme 1 and the intra-molecular modes and their assignments were obtained. The phenol and hydroquinone results were impressive with accuracy generally better than ±5 cm^{-1} even though the calculations were performed on gas phase molecules.

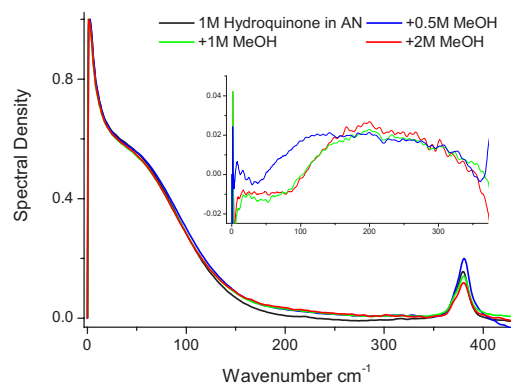

Figure 2. Spectral densities of 1 M hydroquinone dissolved in acetonitrile with 0 (black), 0.5 (blue), 1 (pink) and 2 M (red) of methanol added. Inset shows the result of subtracting the neat acetonitrile spectral density from that of each of the solutions.

In the case of pyrocatechol, the agreement with experiment is also very good; to the extent that a complete assignment of the low frequency modes has been possible for the first time. It is also apparent that the symmetric and asymmetric in-plane bends, predicted to be Raman inactive, [6] are in fact weakly visible. This is due to the presence of the intra-molecular hydrogen bond in the equilibrium structure of pyrocatechol, which lowers the symmetry of the molecule and which was apparently neglected in previous studies.

c. Poly-L-Tyrosine

Figure 4 shows the OHD-OKE response of poly-L-tyrosine (PLT) dissolved in water and in methanol. In both cases, sodium hydroxide was added to a concentration of 100 mM to facilitate PLT solubility. The PLT concentration was ~15 mg/ml in water and approximately twice that in methanol. In both cases, this was approaching a saturated solution.

In the basic solutions used, PLT has been shown by vibrational circular dichroism studies to assume a random coil rather than α-helical structure.[7] Previous studies of

polymers with large side groups[8] have shown a tendency for a shift away from long rotational relaxation timescales toward relaxation through low frequency intra-molecular modes with increasing chain length. These observations appear to hold for PLT (mol. wt. ~ 10-40,000), which shows no apparent slow rotational decay but exhibits many low frequency vibrational modes.

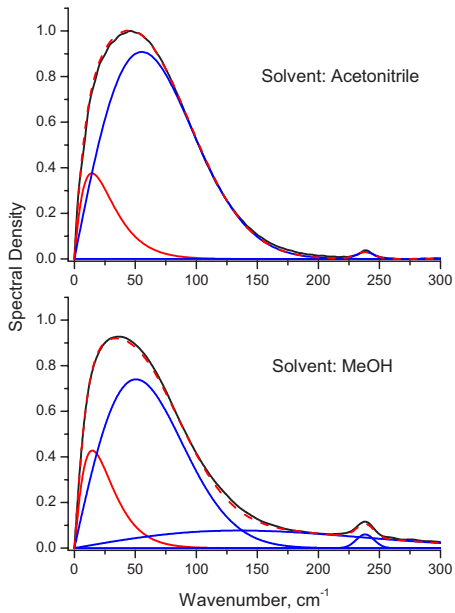

Figure 3. Fits (red dashed line) to reduced spectral densities (black line) of phenol dissolved in methanol and acetonitrile. Solid red lines show component due to Eq (3) and blue lines those due to Eq (4).

It is also noteworthy that, when dissolved in methanol, the PLT Raman spectral density displays non-zero amplitude between 150 and 300 cm^{-1} similar to that of the model systems discussed above. This qualitative assessment is further supported by fitting the PLT spectral density using the same approach as that discussed above involving Bucaro-Litovitz and ASG functions. The result is shown in Figure 4.

III. Conclusions

OHD-OKE studies have been carried out on a variety of solutions of phenol derivatives in methanol and acetonitrile. FTIR spectroscopy has been used to show that solutions involving the former feature significantly stronger solvent-solute hydrogen bonding than the latter. Analysis of the Raman spectral density of these solutions has shown that an extra component appears in the methanol samples that is not present when acetonitrile is the solvent. This feature is a broad lineshape centred at around 100 cm^{-1} and is analogous to that observed in gas phase studies of phenol(methanol)$_n$ clusters for large n.[9] It is assigned to an inhomogeneously broadened transition due to solvent-solute inter-molecular hydrogen bonds.

The studies of phenol derivatives have been used as a model system for an OHD-OKE study of poly-L-tyrosine. The low frequency Raman spectral density of this species dissolved in methanol and water also shows a similar feature, as have previous studies of other polypeptide and protein-based systems.[10]

The low frequency intra-molecular modes of phenol, hydroquinone and pyrocatechol have been assigned, the latter for the first time, with the aid of DFT calculations. It has been shown that the equilibrium structure of pyrocatechol features an intra-molecular hydrogen bond, which significantly influences the low frequency vibrational Raman spectrum.

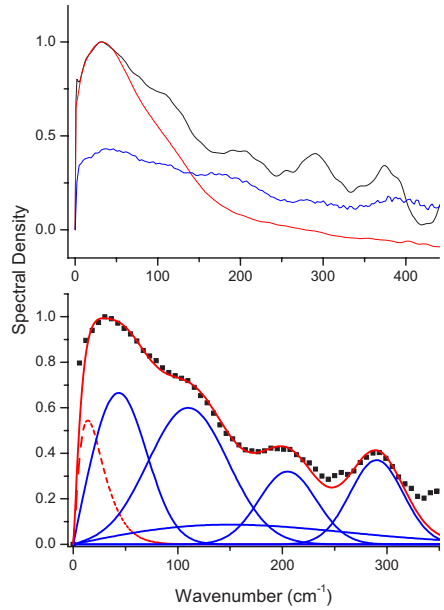

Figure 4. Top: Complete spectral densities of PLT dissolved in basic solutions of methanol (black line) and water (blue). Red line shows complete spectral density of methanol. Bottom: Comparison of experimental (black dots) and simulated (solid red line) spectral density of PLT dissolved in methanol using Eq (3) (red dashed line) and five ASG functions (Eq 4, solid blue lines).

IV. Acknowledgements

The authors would like to acknowledge funding provided by EPSRC and the Leverhulme Trust.

V. References

(1) Smith, N. A.; Meech, S. R. *J. Phys. Chem. A* **2000**, *104*, 4223.
(2) Evans, J. C. *Spectrochimica Acta* **1960**, *16*, 1382.
(3) Tripathi, G. N. R. *J. Chem. Phys.* **1979**, *71*, 4025.
(4) Kubinyi, M. J.; Keresztury, G. *Mikrochimica Acta* **1997**, *14*, 525.
(5) Rao, R.; Sakuntala, T.; Arora, A. K.; Deb, S. K. *J. Chem. Phys.* **2004**, *121*, 7320.
(6) Varsanyi, G. *Assignments for Vibrational Spectra of 700 Benzene Derivatives*; Wiley: New York, 1974.
(7) Watanabe, K.; Muto, K.; Ishii, T. *Biospectroscopy* **1997**, *3*, 103.
(8) Hunt, N. T.; Jaye, A. A.; Hellman, A.; Meech, S. R. *J. Phys. Chem. B* **2004**, *108*, 100.
(9) Schmitt, M.; Muller, H.; Henrichs, U.; Gerhards, M.; W.Perl; Deusen, C.; Kleinermanns, K. *J. Chem. Phys.* **1995**, *103*, 584.
(10) Giraud, G.; Karolin, J.; Wynne, K. *Biophys. J.* **2003**, *85*, 1903.

Nonlinear Solvation Dynamics: Beyond the Two-Point Frequency Fluctuation Correlation Function

Peter Hamm, Jens Bredenbeck, Jan Helbing

Physical Chemistry Institute, University of Zurich, Switzerland

Transient 2D-IR spectroscopy is used to investigate the solvation of the photo-induced metal-to-ligand charge transfer (MLCT) of the rhenium carbonyl complex [Re(CO_3Cl(dmbpy)]. 2D-IR spectra of the a'(1) C=O stretching mode of the molecule are measured 'on-the-fly' while the system still is highly in non-equilibrium after excitation to the electronically excited state. Their evolution as a function of time is analyzed. We model the data based on a Langevin-equation in a two-dimensional 'solvation-space' and show that the experimental spectra cannot be explained in the framework of linear response theory. Rather we show that transient 2D spectroscopy is sensitive to higher order frequency fluctuation correlation functions and gives insights into the coupling of fast and slow solvation degrees of freedom [1].

[1] J. Bredenbeck, J. Helbing, P. Hamm, Phys. Rev. Lett. submitted

Evidence of Excited State Proton Transfer in the Green Fluorescent Protein from Picosecond IR Spectroscopy

Andrew A. Jaye,[1,2*] Deborah Stoner-Ma,[1] Pavel Matousek,[3] Michael Towrie,[3] Stephen R. Meech[2] and Peter J. Tonge[1]

[1] Department of Chemistry, Stony Brook University, Stony Brook, NY 11794-3400, USA.
[2] School of Chemical Sciences and Pharmacy, University of East Anglia, Norwich, NR4 7TJ, UK.
[3] CCLCR Central Laser Facility, Rutherford Appleton Laboratory, Chilton, Didcot, Oxon, OX11 0QX, UK.
[*] email: ajaye@notes.cc.sunysb.edu

Introduction. Understanding the photochemistry of green fluorescent protein (GFP) remains an important goal across many disciplines. This arises due to the wide ranging applications for which GFP is suitable, such as fluorescence imaging *in vivo*. In particular, there has been much interest in elucidating the structural changes which occur in the chromophore and the surrounding protein residues in the excited state. This is with a view to the production of specific protein mutants, in which the excited state chemistry can be controlled. It has been hypothesized from fluorescence and crystallography studies that photoexcitation with 400 nm light results in an excited state proton transfer (ESPT) from the chromophore phenol hydroxyl group, through a hydrogen-bonding network, to a buried protein residue, Glu222. In this report, we describe the use of picosecond time-resolved IR spectroscopy to provide the first direct evidence that Glu222 is the terminal proton acceptor in the ESPT reaction.[1]

The absorption spectrum of wild-type GFP (wtGFP) reveals two characteristic bands at 395 and 475 nm (see below) arising from two separate ground state structures of the chromophore; protonated (neutral) and deprotonated (anionic). Taking into account the different extinction coefficients, the relative intensities of these bands represent the populations of the A and B structures of the protein respectively (fig. 1). Excitation into either band results in strong green fluorescence at 508 nm (Φ = 0.8).

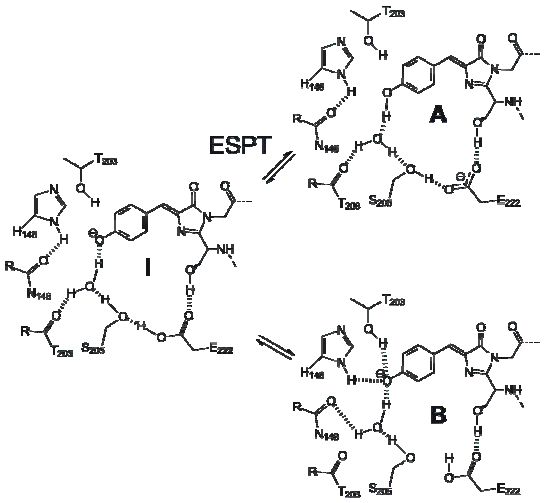

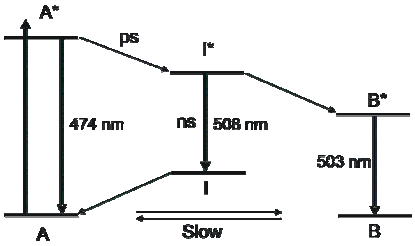

Figure 1. A schematic showing the light-driven conversion from the neutral (A form) and anionic (B form) chromophore via an intermediate state, I. Adapted from Brejc *et al*[2]. Also shown is a simplified photocycle of wtGFP upon photoexcitation with 400 nm light

Using fluorescence upconversion techniques, Boxer and co-workers[3] were able to show that photoexcitation at 400 nm resulted in conversion from the A-form of the protein to the I- form (fig. 1). The I-form may then convert to the B-form, but this is an infrequent process, even in the excited state. The photophysics of this process are represented by the cycle in figure 1.

Also illustrated in figure 1 is the hydrogen-bonding network that links the phenol hydroxyl group and Glu222. This network was first proposed by Remington[4] on the basis of crystal structures. Based on these studies, when GFP is excited with 400 nm light to the A* state, the system can undergo non-radiative decay, fluoresce back to A or transfer a proton through the hydrogen-bonding network to form I*. Time resolved fluorescence dynamics have shown that decay from A* is a multi-exponential process occurring

on the picosecond time scale[4]. Although the fluorescence kinetics of GFP are well characterized, the spectral evolution, which may contain information on local structure changes during the ESPT reaction, has not received much detailed attention. Using a Kerr-gated fluorescence spectrometer, we recorded the entire fluorescence spectrum of GFP on the picosecond time scale, leading to the conclusion that the local environment surrounding the chromophore is rigid (see ref 5 and TRVS XII Conference Proceedings by S.R. Meech).

Although time-resolved fluorescence studies are expected to be a sensitive probe of chromophore-protein interactions, they are unable to probe specific structural changes following photoexcitation. Therefore we have used time-resolved IR as a means to monitor vibrational modes of the chromophore and protein during the ESPT reaction. Steady state IR has been used previously to monitor these changes,[6] but failed to see evidence of proton acceptance by Glu222. It was later discovered that the reason for this was the decarboxylation of Glu222, occurring at high power densities of the pump laser and preventing the observation of a protonated Glu222 band.[7] The time-resolved measurements below are performed at power densities which minimize the effects of this phototransformation.

Experimental. The PIRATE apparatus and the TRIR technique are described in detail elsewhere.[8] Protein samples were concentrated to 2 mM and placed in 50 µm pathlength IR cells. Under these conditions, samples had an absorbance of ~0.2. The excitation energy was <1 µJ per pulse and the wavelength was 400 nm for wtGFP, the synthetic model chromophore and Ser65Thr (at pH 5.5). For Thr203Val/Glu222Gln, 500 nm excitation was used. For the purposes of clarification, the local structure around the chromophore of each protein is represented in figure 2 along with their characteristic absorption spectra. The relative intensity of the A form peak (~400 nm) to the B form (~470 nm) is representative of the neutral and anionic chromophore populations

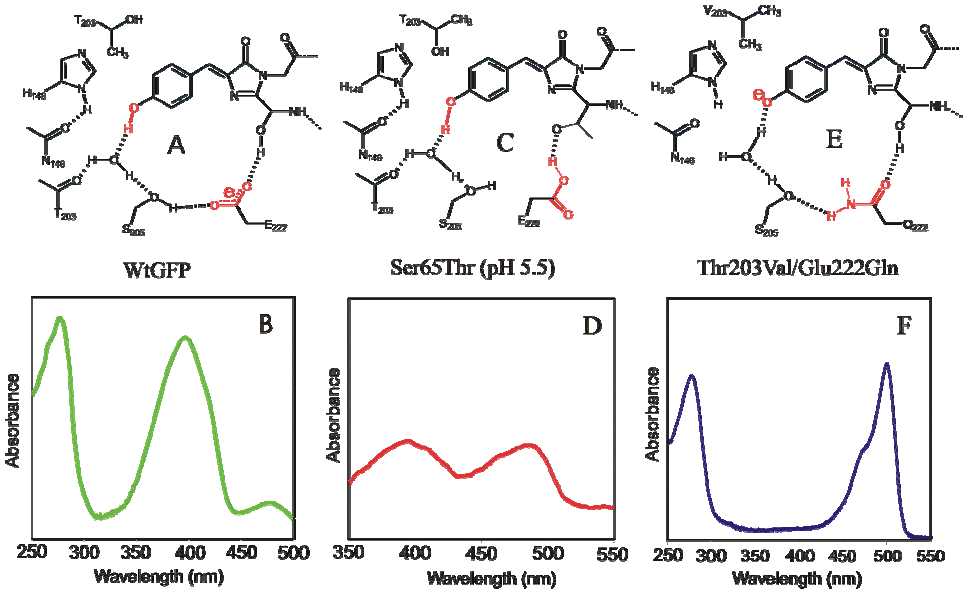

Figure 2. A, C and E represent the local chromophore structure before excitation, while B, D and F are the corresponding absorption spectra of each protein.

Results and Discussion. Time-resolved IR spectra of wtGFP are shown in figure 3B. Immediately apparent from these data is the spectral complexity, arising from overlap of instantaneous ground state bleaches and transient absorption. Fortunately, the modes of the chromophore structure are well understood and facilitate analysis of these TIR spectra. In particular, we can assign modes at 1596, 1637 and 1680 cm^{-1} to the phenol ring mode, exocyclic C=C and C=O respectively, from the basis of the TIR model chromophore spectra (fig 3A). Two long-lived modes that are not present in the chromophore are those at 1565 and 1706 cm^{-1}. These can thus be assigned to modes resulting from the protein. Significantly, these two bands appear with a fall or rise time (respectively) of ~50 ps and persist for over 500 ps, however, the original ground state is recovered in < 1 ms. The appearance of these modes on this time scale could be assigned to the ESPT reaction but in principle, they may arise from another competing process, or from the formation of I*. To rule out these possibilities, we measured the TIR spectra of

Ser65Thr (fig. 3C) which does not undergo ESPT and Thr203Val/Glu222Gln (fig 3D), which exists solely in the I form ground state. Neither of these mutants showed any long lived features at 1565 or 1706 cm^{-1} (see ref 1). The positions of these modes are consistent with titration of carboxylate to carboxylic acid in the protein. It has been demonstrated, by difference FTIR experiments, that irreversible photoconversion of wtGFP results in the loss of a band at 1565 cm^{-1}, assigned to the antisymmetric stretch of the Glu222 carboxylate (unpublished results). From these TIR studies, we can additionally assign the 1706 cm^{-1} band to the protonated Glu222 group, which grows at the expense of the Glu222 carboxylate band.

Further information on the mechanism of ESPT can be obtained from comparing the dynamics of the 1565/1706 cm^{-1} modes with the excited state fluorescence dynamics of A* reported previously[4]. We find that the exponential decay and rise for the 1565 and 1706 cm^{-1} bands respectively, are in good agreement with the fluorescence decay (see ref 1). This is indicative of the rate determining step arising from initial deprotonation at the chromophore hydroxyl.

Thus we have shown evidence for the first time that Glu222 is the terminal proton acceptor in the ESPT reaction. We have also confirmed that the dynamics of bands associated with Glu222 are consistent with the fluorescence decay of A*. We are currently expanding our IR studies by incorporating site-specific isotopic labels into GFP and manufacturing mutants with different excited state properties.

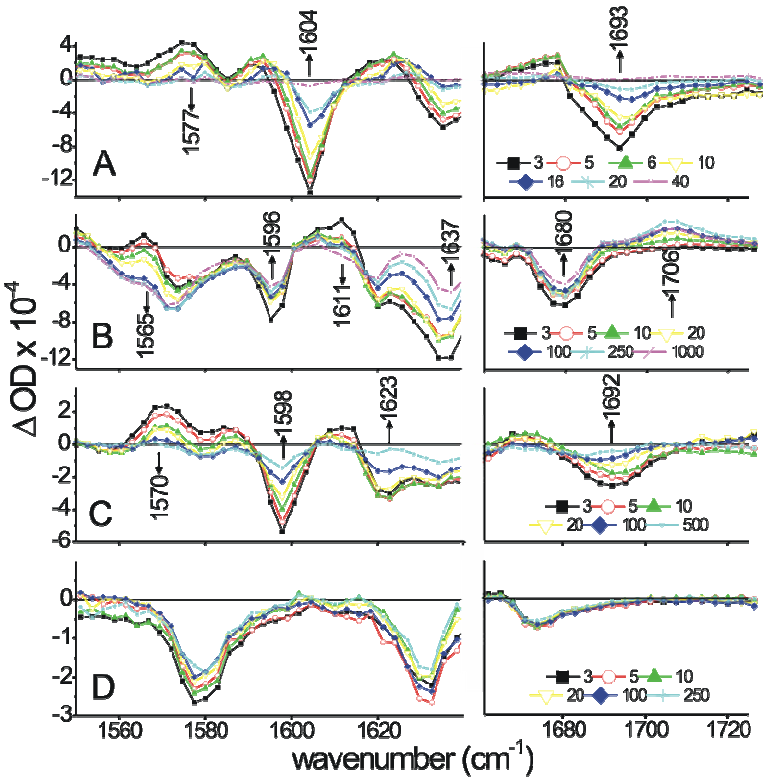

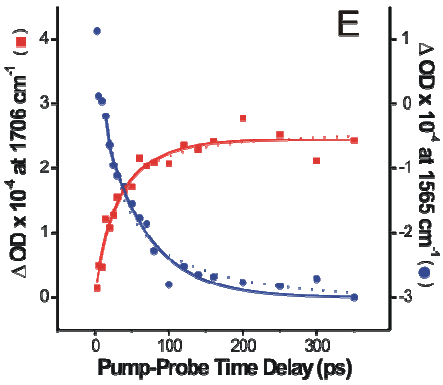

Figure 3. Time resolved IR spectra of A, model chromophore, B, wtGFP C, Ser65Thr and D, Thr203Val/Glu222Gln. E shows the kinetcs at 1565 and 1706 cm^{-1} of wtGFP. Both biexponential fits are statistically the same as the fluorescence decay data from A* (time constants of 22 and 116 ps[4]).

References

[1] Stoner-Ma, D.; Jaye, A.A.; Matousek, P.; Towrie, M.; Meech, S.R.; Tonge, P.J., *J. Am. Chem. Soc.* **127**, 2864, 2005.

[2] Brejc, K.; Sixma, T.K.; Kitts, P.A.; Kain, S.R.; Tsien, R.Y.; Ormo, M.; Remington, S.J., *Proc. Natl. Acad. Sci. U.S.A.*, **94**, 2306, 1997.

[3] Chattoraj, M.; King, B.A.; Bublitz, G.U.; Boxer, S.G., *Proc. Natl. Acad. Sci. U.S.A.*, **93**, 8362, 1996.

[4] Kummer, A,D.; Wiehler, J.; Rehaber, H.; Kompa, C.; Steipe, B.; Michel-Beyerle, M.E., *J. Phys. Chem. B.*, **104**, 4791, 2000.

[5] Jaye, A.A.; Stoner-Ma, D.; Matousek, P.; Towrie, M.; Tonge, P.J.; Meech, S.R., *Photochem. Photobiol.*, In Press, 2005.

[6] van Thor, J.J.; Pierik, A.J.; Nugteren-Roodzant, I.; Xie, A.H.; Hellingwerf, K.J., *Biochemistry*, **37**, 16915, 1998.

[7] van Thor, J.J.; Gensch, T.; Hellingwerf, K.J.; Johnson, L.N., *Nat. Struct. Biol*, **9**, 37, 2002.

[8] Towrie, M.; Grills, D.C.; Dyer, J.; Weinstein, J.A.; Matousek, P.; Barton , R.; Bailey, P.D.; Subramaniam, N.; Kwok, W.M.; Ma, C.S.; Phillips, D.; Parker, A.W.; George, M.W. *Appl. Spectrosc.,* **57**, 367, 2003.

Ultrafast Pump-Probe Absorption Study of Reactive Excited State of *cis*-Stilbene: Wavelength-Dispersed Measurement of Quantum Beat

Kunihiko Ishii, Satoshi Takeuchi, and Tahei Tahara*

Molecular Spectroscopy Laboratory, RIKEN (The Institute of Physical and Chemical Research)
2-1 Hirosawa, Wako, Saitama 351-0198, Japan

Introduction: Quantum beat observed in transient absorption signal of *cis*-stilbene

Studies of vibrational coherence in the excited state of photoreactive molecules provide information about the nuclear motion in the course of the reaction. We have observed a vibrational coherence of photoexcited *cis*-stilbene by ultrafast pump-probe absorption spectroscopy with ~40-fs time resolution.[1] *Cis*-stilbene shows photoisomerization reaction upon UV irradiation in ~1 ps (solution). This very fast reaction rate implies a nearly barrierless S_1 potential. The observed time profile showed a rapidly dephasing quantum beat on an exponential population decay (Fig. 1). The Fourier transformed spectrum of the quantum beat had a broad band at ~220 cm^{-1}. This spectrum well corresponded to the spontaneous Raman spectrum of the S_1 state.[2] The 220 cm^{-1} mode had been assigned to a mixture of C=C torsion, C-Ph torsion and C-Ph in-plane bending motions,[3] and it was dominant in both time-domain and frequency-domain data. In addition, unusually strong overtones were observed in the spontaneous Raman spectrum.[2] In order to identify the origin of such strong and peculiar signals, we investigated the time-domain signal using a wavelength dispersion method.

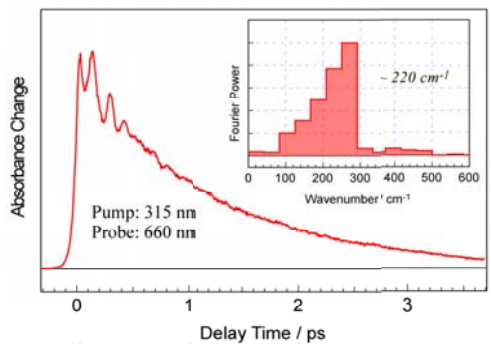

Figure 1. Time-resolved absorption signal of *cis*-stilbene in cyclohexane. Inset: Fourier transform power spectrum of the oscillatory component.

Wavelength-dispersed measurement of the quantum beat

Our apparatus for ultrafast absorption measurement is based on two NOPAs (non-collinear optical parametric amplifiers) as a light source for pump (~315 nm) and probe (~640 nm) pulses.[4] The spectrum of the ultrashort probe pulse from NOPA has a broad bandwidth that covers the $S_n \leftarrow S_1$ absorption peak of *cis*-stilbene at ~640 nm. By spectrally dispersing the probe pulse transmitted through the sample, we achieved observation of the time-dependent spectral change of $S_n \leftarrow S_1$ absorption over the probe bandwidth. There was no reduction of the time-resolution by the wavelength dispersion because the probe pulse kept its ultrashort pulsewidth at the sample point.

Figure 2 shows wavelength-dispersed time-resolved absorption data of *cis*-stilbene. A quantum beat with a ~150 fs period is clearly seen over all the wavelength range observed. No phase flip is found in the oscillation around the absorption peak, and its amplitudes are similar at the blue-edge, peak and red-edge. This behavior indicates that the origin of the quantum beat is not a transition energy modulation but a transition intensity modulation by the wavepacket motion. This kind of quantum beat was also observed in other systems previously.[5,6]

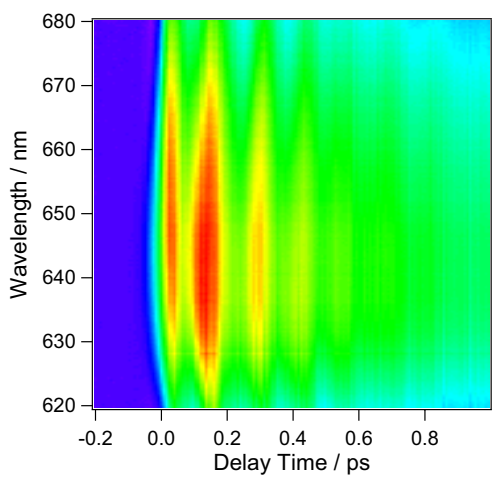

Figure 2. Time-wavelength 2D plot of the time-resolved wavelength-dispersed absorption signal of *cis*-stilbene in cyclohexane.

* Corresponding author. E-mail: tahei@riken.jp.

Numerical simulation

To theoretically reproduce the observed signal, we carried out a numerical simulation. The observed quantum beat in the wavelength-dispersed data can be treated as the temporal change of the optical response that has the imaginary part (known as the extinction coefficient) and the real part (refractive index). Strictly speaking, because the real and the imaginary parts are mixed to give the spectroscopic signal, we cannot simply treat the wavelength-dispersed data as time-resolved "absorption" using the extinction coefficient. Thus, we performed a numerical simulation including both of the real and the imaginary parts of the optical response.

We adopted effective linear response theory introduced by Kumar et al.[7] In this theory, nonlinear optical response is modeled as a time-dependent linear response ($S_n \leftarrow S_1$ absorption spectrum) modulated by coherent nuclear wavepacket motions. The coherent nuclear motion is described as time-dependent changes of moments (typically the first-order moment: the center of mass) of the nuclear wavepacket. In the original treatment, they only considered the modulation of the optical response due to the displaced potentials (Franck-Condon type transition energy modulation). In order to explain our experimental results, we introduced Herzberg-Teller type modulation by assuming the coordinate dependence of the $S_n \leftarrow S_1$ transition intensity, which was represented as $\mu(Q)=\mu_0\exp[cQ]$.[8] Figure 3 shows the results of simulations based on the two modulation mechanisms. In these simulations, the experimentally observed equilibrium absorption spectrum and the probe pulse spectrum were taken into account. As can be seen in Fig. 3, the observed behavior is well reproduced by the Herzberg-Teller type modulation that assumes the coordinate dependence of the $S_n \leftarrow S_1$ transition intensity.

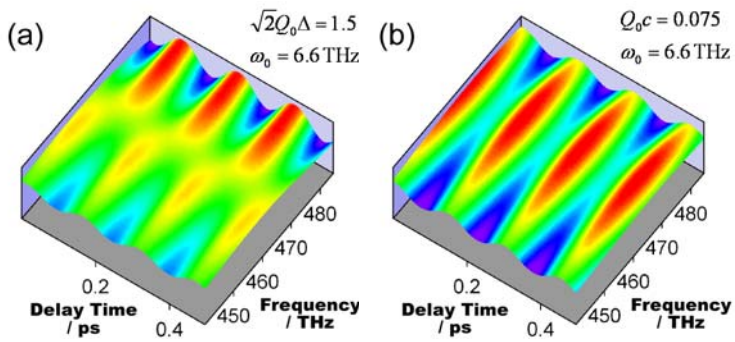

Figure 3. Results of numerical simulation of wavelength-dispersed absorption signal assuming (a) Franck-Condon type and (b) Herzberg-Teller type modulation. Q_0: Displacement of potential curves between S_1 and S_0 states. Δ: Displacement of potential curves between S_n and S_1 states. ω_0: Frequency of the vibrational mode. c: Non-Condon parameter (see text).

References

1. K. Ishii, S. Takeuchi, and T. Tahara, *Chem. Phys. Lett.* **398**, 400 (2004).
2. W. M. Kwok, C. Ma, D. Phillips, A. Beeby, T. B. Marder, R. L. Thomas, C. Tschuschke, G. Baranoviζ, P. Matousek, M. Towrie, and A. W. Parker, *J. Raman Spectrosc.* **34**, 886 (2003).
3. G. Baranoviζ, *J. Raman Spectrosc.* **32**, 293(2001).
4. S. Takeuchi and T. Tahara, *J. Chem. Phys.* **120**, 4768(2004).
5. I. V. Rubtsov and K. Yoshihara, *J. Phys. Chem. A* **103**, 10202 (1999).
6. H. Kano, T. Saito, and T. Kobayashi, *J. Phys. Chem. A* **106**, 3445 (2002).
7. A. T. N. Kumar, F. Rosca, A. Widom, and P. M. Champion, *J. Chem. Phys.* **114**, 701 (2001).
8. Y. Tanimura and S. Mukamel, *J. Opt. Soc. Am. B* **10**, 2263(1993).

Early events in β-sheet formation:

Nanosecond temperature-jump time-resolved UV resonance Raman studies

Renee D. JiJi, Ying Hu, Gurusamy Balakrishnan and Thomas G. Spiro

Princeton University, Department of Chemistry

Princeton, NJ 08544, USA

Conformation change is a common motif of amyloid diseases; the α-helix to β-sheet conformation change of the Alzheimer's Aβ peptide being one of the most infamous. The Aβ peptide and select homo-polypeptides, such as poly(L-lysine) have been shown to go through temperature dependent conformation changes to β-sheet structure. Temperature-jump (T-jump) UV time-resolved resonance Raman ($UVTR^3$) spectroscopy was used to monitor the first 3 μs of the α-helix to β-sheet conformational transition of poly(L-lysine). Poly(L-lysine) is primarily α-helical at high pH and low temperature (<25°C), undergoing a relatively rapid conformational change to β-sheet structure at higher temperatures. A positive feature in the amide III (1235 cm^{-1}) and amide S (1388 cm^{-1}) regions of the T-jump $UVTR^3$ difference spectra indicate the loss of a small fraction of α-helical structure prior to the formation of β-sheet structure. The relaxation time constant for this process is ~200-300 ns.

Poly(L-lysine) adopts three major conformations found in proteins, unfolded (extended), α-helix and β-sheet. Thus, it is often used as a protein conformation reference[1]. At low pH, the lysine residues are protonated and the peptide adopts a primarily extended helical structure (3_1-helical)[2], often referred to as polyproline II

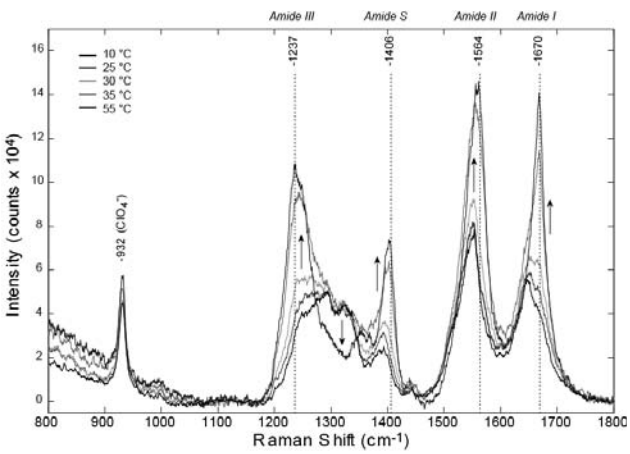

Figure 1. Temperature dependent UVRR spectra of poly(K) at a concentration of 2-3 mg/ml and pH 11.6, arrows indicate direction of intensity change upon going from 10°C to 55°C.

(PPII) type structure. At high pH and low temperatures, poly(L-lysine) is predominantly α-helical with a small fraction of non-helical structure. Finally, at high pH and temperature, the peptide rapidly transforms to β-sheet structure. The three conformers are easily distinguished by their UVRR spectra.

The temperature dependent α-helix to β-sheet conformation change of poly(L-lysine) is both concentration and pH dependent. Under the conditions of these experiments, the largest degree of conformation change occurred between 30°C and 35°C (Figure 1). A least-squares fit of the CD difference spectrum of α-helical poly(L-lysine) at pH 11.6 between 4°C and 20°C, both below the critical temperature for β-sheet formation (T_β > 30°C), indicates that ~10% of the helical structure is lost as a result of the 16° temperature increase. Furthermore, the emerging non-helical conformation appears

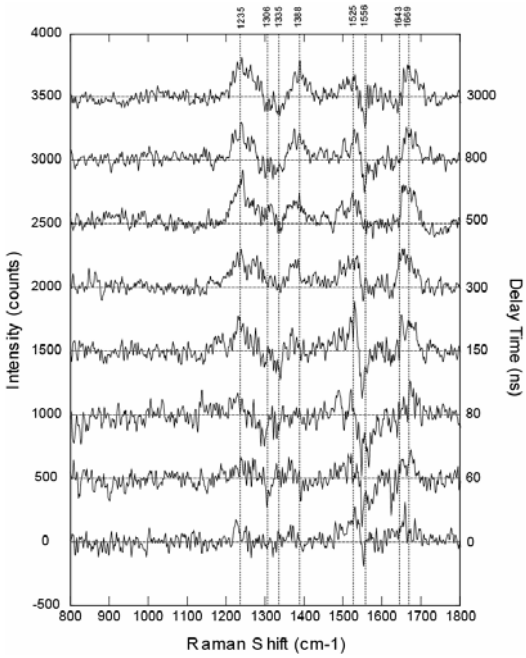

Figure 2. UVRR T-jump difference spectra of poly(K) at several delay times between 0 and 3μs during the α-helix to β-sheet conformational transition. Sample conditions were as follows pH = 11.6, T_i = 21°C-22°C and ΔT = 22°C -23°C.

to be most similar to the extended structure of the low pH conformer. The difference spectrum was well reproduced by a combination of the "pure" extended (pH 4.3) and α-helical (pH 11.6) CD spectra (data not shown).

The time dependence of the ΔT induced α-helix to β-sheet conformation change of poly(L-lysine) was examined by utilizing a nanosecond T-jump and monitoring the UVRR spectra at several time delays through 3 μs. Development of positive features at 1235, 1388 and 1669 cm^{-1} in the T-jump difference spectra indicate an increase in the non-helical fraction (Figure 2) within the first 3 μs of this conformation change.

The relaxation time constants for the amide III and S bands are 192 ns and 302 ns, respectively (Figure 3). These values are quite similar to the time constant for the melting of α-helices in short alanine peptides, which is ~200 ns[3]. Hence the earliest events in the α-helix to β-sheet transition of poly(L-lysine) involve the unfolding of a small fraction of the α-helical secondary structure. This is the first short time scale spectroscopic study of the α-helix to β-sheet conformational transition, which reveals that the poly(L-lysine) begins to unfold prior to β-sheet formation.

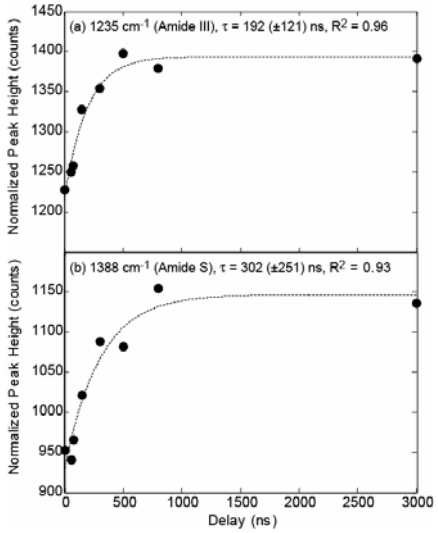

Figure 3. Exponential fit of the normalized peak intensities of the amide III band at 1242 cm-1 and the amide S band at 1394 cm-1. Data were normalized to the probe only amide III band at 1242 cm-1.

References

1. N. Greenfield and G. D. Fasman, *Biochemistry*, **1969**, *8*, 4108-4116.
2. M. L. Tiffany and S. Krimm, *Biopolymers*, **1968**, *6*, 1379-1382.
3. I. K. Lednev, A. S. Karnoup, M. C. Sparrow and S. A. Asher, *Journal of the American Chemical Society*, **2001**, *123*, 2388-2392.

Determination of the excited state twisting angle of the chromophore of green fluorescent protein

Anwar Usman[1], Omar F. Mohammed[1], Jian Dong[2],

Kyryl M. Solntsev[2], Laren M. Tolbert[2], and Erik T. J. Nibbering[1,*]

[1]: *Max Born Institut für Nichtlineare Optik und Kurzzeitspektroskopie,*

Max Born Strasse 2A, D-12489 Berlin, Germany

[2]: *School of Chemistry and Biochemistry, Georgia Institute of Technology, Atlanta, GA, USA*

*: Corresponding Author E-mail: nibberin@mbi-berlin.de

In wild type green fluorescent protein (GFP), an important photosensor protein used in bioimaging, the photochemical dynamics of the chromophore consists of a Förster cycle, where excitation of the photoacid chromophore is followed by proton transfer to the side groups of the protein pocket. Fluorescent emission with high efficiency (quantum yield = 0.8) occurs from the chromophore in its photobase form. In contrast, the chromophore of GFP, p-hydroxybenzylidene-imidazolidinone (HBDI) shows markedly different behaviour, in which the ground state is recovered within picoseconds with high internal conversion (IC) quantum yield (> 0.999). We report on ultrafast polarization-sensitive infrared (IR) spectroscopy of the excited state structure of HBDI, from which we draw conclusions on the importance of twisting motions. Our focus is on the orientation of the transition moment of the IR-active carbonyl stretching vibration of HBDI relative to that of the electronic transition dipole moment, which indicates that the C=O vibration acts as a spectator mode for the relative orientation of the phenolate and imidazolidinone groups. We have determined the anisotropy of the C=O vibration of HBDI in the S_0 and S_1 states for three charged configurations (anionic, neutral and cationic form). We find that our estimated value for the C=O bond vector in the S_1-state can only be explained by a single twist of 120 degrees or a hula twist of 150 degrees. These values are much larger than the twisting angle of 90 degrees found in quantum chemical calculations, from which conical intersections at this twisting angle have been assigned as the efficient IC channel. Although according to our findings the equilibrium structure of HBDI in the S_1-state is even more displaced along the twisting coordinate upon electronic excitation than in the reported calculations, we conclude that the twisting coordinate is a likely candidate for the efficient coupling between S_1 and S_0, leading to IC.

Excited state dynamics of PYP chromophore model systems explored with ultrafast infrared spectroscopy

Anwar Usman[1], Omar F. Mohammed[1], Karsten Heyne[1],

Jens Dreyer[1], Erik T. J. Nibbering[1,*] and Michael A. Cusanovich[2]

[1]: *Max Born Institut für Nichtlineare Optik und Kurzzeitspektroskopie,*

Max Born Strasse 2A, D-12489 Berlin, Germany

[2]: *Department of Biochemistry and Molecular Biophysics, University of Arizona, Tucson,*

Arizona 85721, USA

*: Corresponding Author E-mail: nibberin@mbi-berlin.de

Ultrafast mid-infrared spectroscopy enables the determination of dynamically evolving structures in the liquid phase by monitoring vibrational marker modes. We perform ultrafast polarization sensitive visible pump-mid infrared probe spectroscopy on deprotonated *trans*-S-thio-*p*-hydroxycinnamate derivatives, that are model compounds for the photoinduced *trans-cis* isomerization of photoactive yellow protein. We derive structural information from the observed bleach signals by comparison of the experimentally found frequency positions and anisotropies with those obtained from quantum chemical calculations. The electronic excited state decays with 8 ps or 15 ps time constants in 1:1 or 10:1 DMSO:H_2O-buffer, respectively, for the phenyl derivative, and a 15 ps time constant in 1:1 DMSO:H_2O-buffer for the methyl derivative. The quantum yield for isomerization product formation is less than 5 %. Comparison of our results with earlier reported work on model compounds and on PYP suggests an intricate tuning mechanism for the relaxation dynamics of PYP.

[1]. A. Usman, O. F. Mohammed, K. Heyne, J. Dreyer and E. T. J. Nibbering, Chem. Phys. Lett. **401** , 157 (2005).

Photoexcited state studies on Re(bipy)(CO)$_3$ in the solid state by ps-TRIR

K.L. Ronayne[1*)], K. Bowes[2)], M. Towrie[1)], P. Raithby[3)], and A. W. Parker[1)]

1) Central Laser Facility, CCLRC Rutherford Appleton Laboratory, Didcot, Oxfordshire, OX11 0QX, UK
2) Department of Chemistry, University of Cambridge, Lensfield Rd, Cambridge, CB2 1EW, UK
3) Department of Chemistry, University of Bath, Claverton Down, Bath, Avon, BA2 7AY, UK

Solid materials in crystalline and amorphous states are currently finding applications in molecular photonic devices such as LEDs and displays. Development and optimisation of these devices requires detailed knowledge of the electronically excited states of the materials in the solid state. Vibrational spectroscopic techniques such as TR[3] and TRIR have been extensively used to probe photophysical and photochemical properties of excited states in the solution phase. However, they have only rarely been applied to solids due to experimental factors mainly relating to photo-degradation and the relatively low sensitivity of the instruments employed. In this light we have recently developed methods to employ ps-TRIR to investigate the excited state and chemical intermediates within the solid state.

[Re(bipy)(CO)$_3$Cl] was chosen as a prototype compound for these investigations as its solution phase photochemistry is well understood.[1] The ps-TRIR spectra of the excited state decay of a thin film of this complex on a CaF_2 plate are compared with those recorded in solution. The characteristic carbonyl bleaches are visible in both the solution and thin film as shown in Figure 1 below. The high frequency transient, at c, 2055 cm^{-1}, is downshifted in the thin-film data with respect to the solution suggesting a decrease in the extent of Re→bpy charge transfer in the ^{3}MLCT. The thin film showed marked sensitivity to the peak power and polarisation of the photo-excitation beam. These results and the methods used will be presented.

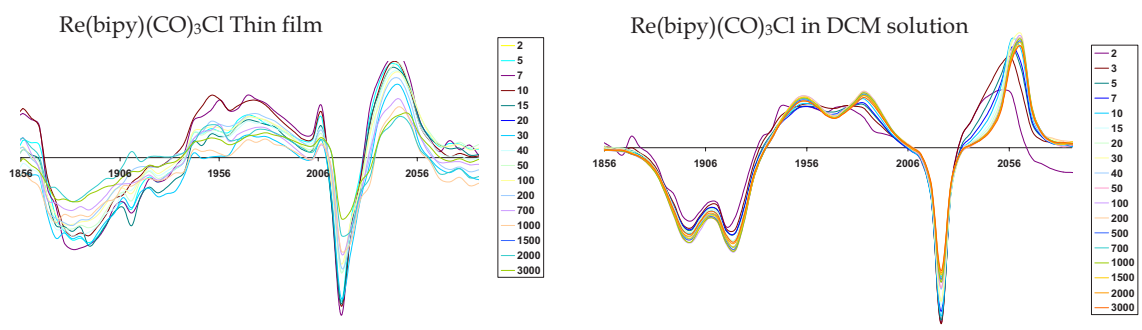

Figure 1: ps-TRIR spectra of Re(bipy)(CO)$_3$Cl in thin film and dichloromethane solution recorded on the PIRATE apparatus[2] using 400 nm excitation.

References
[1] D.R. Gamelin, M.W. George, P. Glyn, F-W. Grevels, F.P.A. Johnson, W. Klotzbücher, S.L. Morrison, G. Russell, K. Schaffner and J.J. Turner, *Inorg. Chem.*, **33**, 2346-3250, 1994.
[2] M. Towrie, D.C. Grills, J. Dyer, J.A. Weinstein, P. Matousek, R. Barton, P.D. Bailey, N. Subramanian, W.M. Kwok, D. Phillips, A.W. Parker and M.W. George, *Appl. Spectrosc.*, **57**, 367-380, 2003.

Observation of vibrational relaxation processes of S_1 *trans*-stilbene in ionic-liquids

Yuta Takada†, Koichi Iwata, and Hiro-o Hamaguhi

Department of Chemistry and Research Centre for Spectrochemistry, School of Science, The University of Tokyo, 7-3-1, Hongo, Bunkyo-ku, Tokyo, 113-0033, Japan

†E-mail: takada@chem.s.u-tokyo.ac.jp

Ionic liquids exist as liquids at the room-temperature while they are composed solely of ions. They attract much attention as "designers' liquids" that serve as a new class of solvents for solution-phase chemistry and also as electrolytes with wide potential windows. There have been only a small number of studies, however, on their physicochemical properties. In this study, we examine the vibrational relaxation process of the first excited singlet (S_1) state of *trans*-stilbene in ionic liquids by using picosecond time-resolved Raman spectroscopy. Vibrational relaxation is a sensitive measure of the solute-solvent interaction. We measure the cooling rate of the central C=C stretch vibration in ionic liquids and compare results with ordinary solvents.

Picosecond time-resolved Raman spectra are measured with the standard pump-probe medhod. A block diagram of our apparatus is shown in Fig. 1. We use a mode-locked Ti:sapphire laser system (Quantronix, Integra, 800 nm, 1 kHz, 2.5 W) as the light source. Its output is divided into two and are introduced into two separate OPA's (Light conversion, Topas) to generate independently wavelength-tunable picosecond pulses. The pump light (300 nm, 5 μJ/pulse, 2 ps) and the probe light (595 nm, 1 μJ/pulse, 2 ps,) are focused on the sample solution contained in a rotating quartz cell. We use five kinds of ionic liquids, [emim]Tf_2N [1], [bmim]Tf_2N [2], [bmim]PF_6 [3], [C7mim]BF_4 [4], and [C10mim]BF_4 [5], as well as heptane for the solvents. Typical accumulation time is 40 minutes.

Transient Raman spectra of S_1 *trans*-stilbene were measured at 50 ps in the five ionic liquids as well as in heptane. The results are shown in Fig. 2. It is clear from the figure that the width of the C=C stretch band at 1570 cm^{-1} is larger in the ionic liquids, indicating faster vibrational dephasing compared with ordinary solvents. We think that the strong Coulomb interaction between the solute and the monopoles in the ionic liquids contributes to the acceleration of the vibrational dephasing of S_1 *trans*-stilbene.

For studying the solute-solvent interaction further, time-resolved Raman spectra of S_1 *trans*-stilbene were measured at eight time delays between 0 ps and 50 ps. The results are shown in Fig. 3. The vibrational cooling rates estimated from the time-dependence of the C=C stretch peak position [6] are similar among the six solvents. By studying the origin of the marked difference between the effects of ionic liquids on vibrational dephasing and on vibrational

cooling, we should be able to clarify the structure and dynamics of ionic liquids. In our recent study, we have suggested that ionic liquids have small domains which have structures similar to the crystal.[7] As a reference, the solid state X-ray structure of a [bmim]Cl crystal at room temperature is shown in Fig. 4.[8] This column like ordered structure may also exists in the liquid phase, and this anomalous structure which has an ionic region and an alkane chain region simultaneously determines the properties of ionic liquids as solvents. With more time-resolved Raman experiments, we will be able to clarify the liquid state structure and its dynamics of ionic liquids.

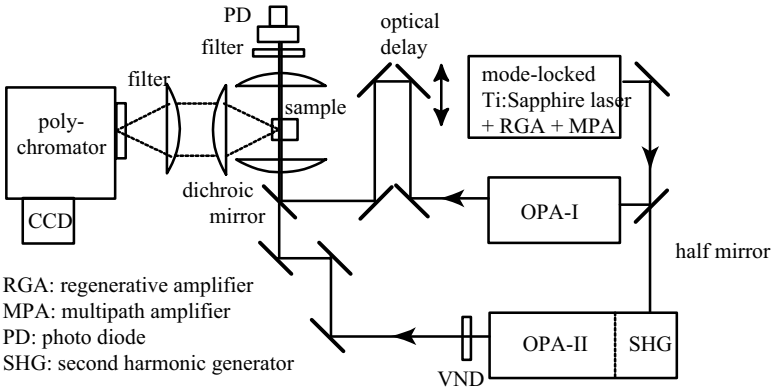

Fig. 1 Block diagram of picosecond time-resolved Raman spectrometer.

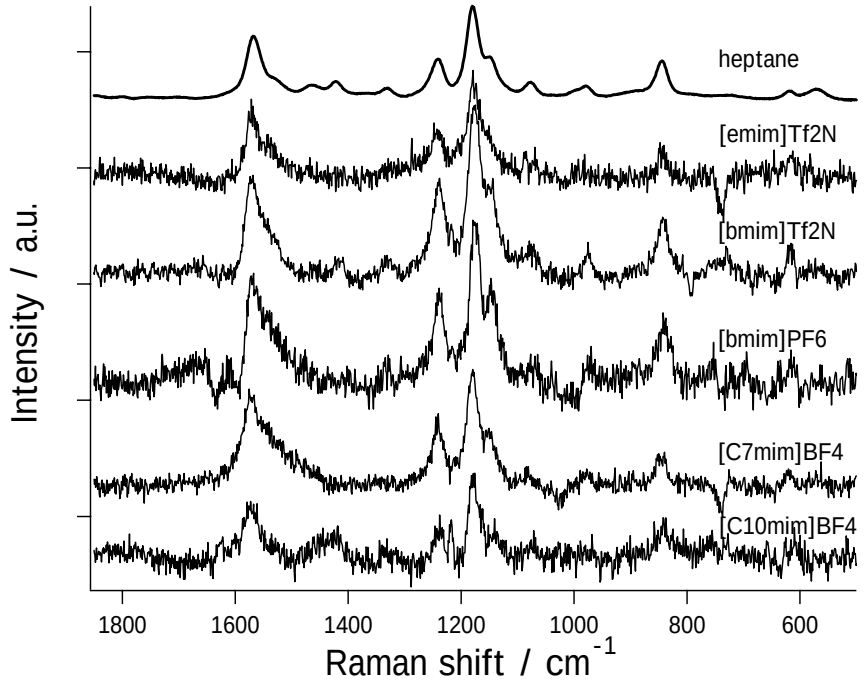

Fig. 2 Transient Raman spectra of S_1 *trans*-stilbene in five ionic liquids and in heptane at 50 ps.

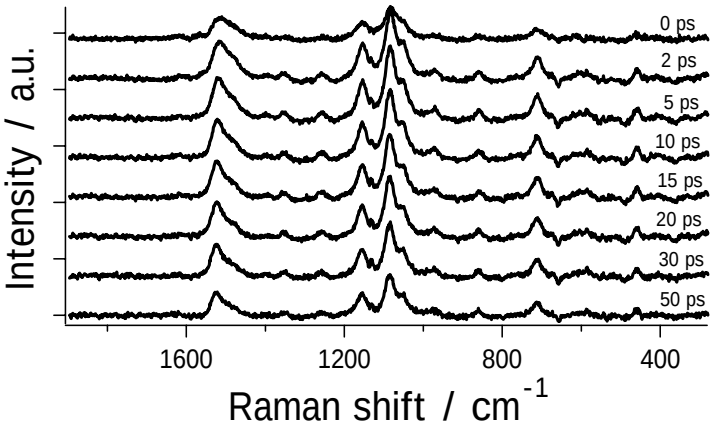

Fig. 3. Time-resolved Raman spectra of S_1 *trans*-stilbene in [bmim]Tf_2N at various time delays.

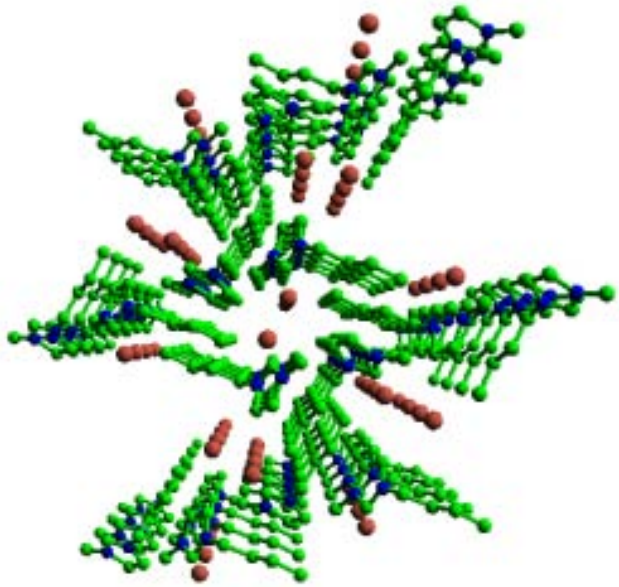

Fig. 4. Structure of a [bmim]Cl crystal obtained by X-ray diffraction.

---

[1] 1- ethyl -3-methylimidazolium bis(trifluoromethane sulfonyl)imide
[2] 1- butyl -3-methylimidazolium bis(trifluoromethane sulfonyl)imide
[3] 1- butyl -3-methylimidazolium hexafluorophosphate
[4] 1-heptyl-3-methylimidazolium tetrafluoroborate
[5] 1-decyl-3-methylimidazolium tetrafluoroborate
[6] K. Iwata and H. Hamaguchi, *J. Phys. Chem.* A 101, 632 (1997).
[7] R. Ozawa, S. hayashi, S. Saha, A. Kobayashi, and H. Hamaguchi, *Chem. Lett.,* **32**, 948 (2003).[8] S. Saha, S. Hayashi, A. Kobayashi, and H. Hamaguchi, *Chem. Lett.,* **32**, 740 (2003).

Vibrational Relaxation of Anions in Ionic Liquids

Gerald M Sando, Kevin Dahl, and Jeffrey C. Owrutsky
Naval Research Laboratory, Code 6111, Chemistry Division, Washington, DC 20375

Abstract: Ultrafast infrared spectroscopy has been used to measure vibrational energy relaxation (VER) times for high frequency modes of small ions in ionic liquid solutions. The ions studied include NCS^-, $N(CN)_2^-$, N_3^-, and $Fe(CN)_5NO^{2-}$. The VER rates of these ions generally depend on solvent polarity and hydrogen bonding ability. From a comparison of static spectra and VER rates, the ionic liquids appear to behave as typical polar aprotic solvents for most cases. VER rates are slower than expected for $Fe(CN)_5NO^{2-}$, and this is related to results for neutral $W(CO)_6$, where the solvent dependent behavior differs from that of small ions. We extended VER measurements to IR active ionic liquids in nonionic reverse micelles. The VER rates are faster in the bulk ionic liquids than in the reverse micelles, consistent with a mixed solvation environment of ionic liquid and surfactant. Effects of the micelle size were also evident.

Bulk Ionic Liquids

Vibrational energy relaxation (VER) of small ions in solution has been shown to be a good measure of solute-solvent interaction strength.[1] In particular, azide (N_3^-) has been well studied and shown to exhibit a strong correlation between the vibrational frequency and the VER rate in typical bulk solvents.[2] We have extended these studies to characterize the solvation properties of room temperature ionic liquids. Room temperature ionic liquids (ILs) are a relatively new class of solvents that have the potential to exhibit unique solvation properties. ILs consist solely of ions and are liquids at or near room temperature. This results in solvents with high polarity and extremely low vapor pressures. These properties suggest a possible use of ILs as "green" replacement solvents for traditional polar organic solvents. However, the ionic nature of ILs suggests that the solute-solvent interactions may be significantly different in ILs than in tradition solvents. The utility of ILs as replacement solvents depends on how similar the solute-solvent interactions are to traditional solvents.

Spectroscopic studies of solvatochromatic dyes in ILs have been used to characterize their solvation properties.[3] Apparent polarities can vary from DMSO to ethanol, depending on the dye. Overall, the IL solvent properties are not well described by a single parameter.[3] We have used infrared spectroscopy of small ions in ILs to study the local solute-solvent interactions important for determining vibrational properties using static and ultrafast infrared spectroscopy to measure vibrational frequencies and VER times for the high frequency modes of small ions in ionic liquid solutions. The ions studied include NCS^-, $N(CN)_2^-$, N_3^-, and $Fe(CN)_5NO^{2-}$. We also extended these studies to IR active ILs in nonionic reverse micelles. The ILs studied include [BMIM][BF_4], [BM_2IM][BF_4], [BM_2IM][$N(CN)_2$], and [BM_2IM][NCS], where BMIM and BM_2IM are

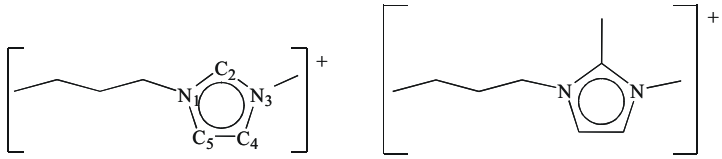

[BMIM]$^+$ [BM$_2$IM]$^+$

The IR active ions are either the majority anion in the IL or added as a solute.

For most of the ions studied, the vibrational frequencies in the ionic liquids are between those in NMF and DMSO, and generally lie closer to DMSO. NCS^- is an exception where the vibrational frequency shows little solvent dependence. The vibrational frequencies are consistent with the ILs behaving as a polar aprotic solvent. The VER rates for the smallest ions (NCS^-, $N(CN)_2^-$, and N_3^-) are also between those in NMF and DMSO and are consistent with a polar aprotic solvent. As shown in Figure 1, the rate-shift correlation observed in typical solvents for $N(CN)_2^-$ and N_3^- is followed by the ILs.[4] These results suggest that ILs behave as typical polar aprotic organic solvents, at least for the small ions, with little evidence of hydrogen bonding.

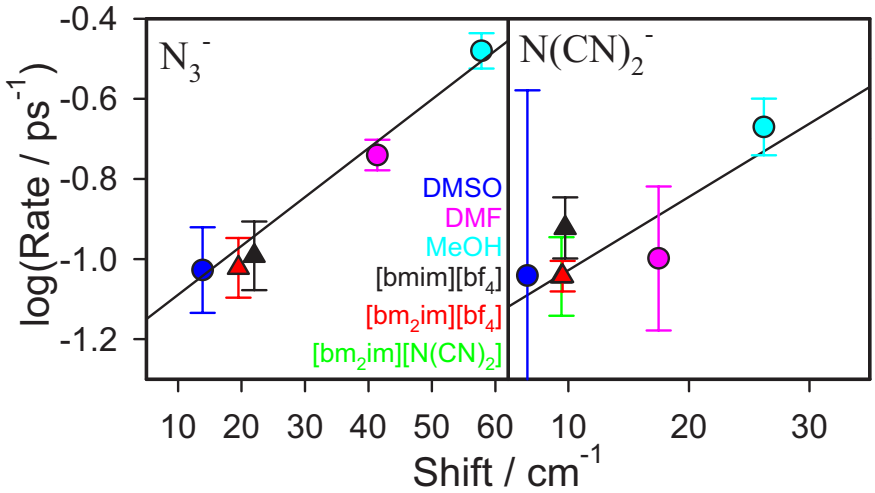

Fig 1 Rate-Shift correlation for $N(CN)_2^-$ and N_3^-

For the NO band near 1940 cm^{-1} of the larger ion $Fe(CN)_5NO^{2-}$ (SNP) in [BMIM][BF$_4$], [BM$_2$IM][BF$_4$], and [BM$_2$IM][N(CN)$_2$], somewhat different behavior is observed. The additional normal modes of the larger SNP ion open up the possibility of more complex VER dynamics. In most typical solvents, the VER rate also scales with the vibrational frequency, with VER times of 30 to 40 ps.[5] Although the vibrational frequencies in the ILs fall within the range of polar aprotic solvents, the VER rates are slower (44 to 49 ps) meaning that the rate-frequency correlation is not followed in the ILs. The VER rate of neutral $W(CO)_6$ was also studied in [BMIM][BF$_4$]. $W(CO)_6$ has a similar geometry to SNP and may have a similar VER mechanism, but the VER rate in conventional solvents depends little on the solute-solvent interaction strength.[6] In this case, as for SNP, the vibrational frequency in the IL is between that in methanol and DMSO, but the VER rate is slower than both in the IL. This suggests that the solute-

solvent interaction may be different in ILs and that the small ion results cannot be generalized to larger species, possibly due to differing VER mechanisms.

IL Reverse Micelles

Reverse micelles (RMs) are nanosized pools of a polar solvent in a nonpolar solvent stabilized through the use of a surfactant. RMs were formed with $[BM_2IM][N(CN)_2]$ and $[BM_2IM][NCS]$ ILs with IR active anions, in 45% (by weight) Brij-30 in cyclohexane. For each IL, reverse micelles were formed with $\omega = 0.5$ and 1, where ω is the IL to surfactant molar ratio. For $N(CN)_2^-$ and NCS^-, the vibrational frequencies in the RMs were between those in the neat IL and those in MeOH. In addition, the VER rates are faster in the RMs than the neat ILs, but slower than in methanol. In most polar solvents, RM confinement results in slower solute VER rates.[7] These results suggest a mixed solvation environment that contains contributions from both the IL and Brij-30 poly-ox headgroups. In addition, a dependence on ω is seen for the NCS^- VER rate, with a slower rate for the lower ω, suggesting an effect of confinement on the dynamics.

Acknowledgements. This work was supported by the Office of Naval Research at the Naval Research Laboratory. G.M.S. acknowledges the NRL-ASEE Postdoctoral Fellowship program. K.D. acknowledges the NRL-NRC Postdoctoral Fellowship program

1. Owrutsky, J. C.; Raftery, D.; Hochstrasser, R. M. *Annu. Rev. Phys. Chem.* **1994**, *45*, 519.
2. Dahl, K.; Sando, G. M.; Owrutsky, J. *in preparation* **2004**.
3. Muldoon, M. J.; Gordon, C. M.; Dunkin, I. R. *J. Chem. Soc., Perkin Trans. 2* **2001**, *2001*, 433.
4. Dahl, K.; Sando, G. M.; Fox, D. M.; Sutto, T. E.; Owrutsky, J. C. *J. Chem. Phys.* **2005**, *accepted.*
5. Sando, G. M.; Zhong, Q.; Owrutsky, J. C. *J. Chem. Phys.* **2004**, *121*, 2158.
6. Heilweil, E. J.; Cavanagh, R. R.; Stephenson, J. C. *Chem. Phys. Lett.* **1987**, *134*, 181.
7. Sando, G. M.; Dahl, K.; Zhong, Q.; Owrutsky, J. *J. Phys. Chem. A* **2005**, *109*, ASAP.

Probing the Q-Proton Pathway and Docking site Dynamics of *ba*$_3$-Oxidoreductase by Time-Resolved Step-scan Fourier Transform Infrared Spectroscopy

Costas Varotsis and Costas Koutsoupakis
Department of Chemistry, University of Crete, Heraklion, Crete, Greece
e-mail:varotsis@edu.uoc.gr

Time-resolved vibrational spectroscopy is a powerful technique that has been applied to study the structure and kinetics of transient species which are essential for the mechanistic understanding of biological and chemical processes. Of the two major techniques available, time-resolved resonance Raman (TR^3) and time-resolved step-scan (TRS^2)-FTIR, the former has dominated thus far the field of heme protein dynamics. Over the last ten years however, the TRS^2-FTIR technique has been used extensively to probe optical transitions which are too short wavelengths for monitoring by optical or resonance Raman spectroscopies, and to add time-domain information to the structural information gained from static FTIR spectra of proteins.

In this presentation we will report recent results of experiments using TRS^2-FTIR spectroscopies to examine the dynamics of heme-copper oxidases. Our results over the past several years, together with advances by others in structural and functional understanding of heme-copper oxidases, have led us to specific suggestions as to how docking site dynamics near the metal centers of cytochrome oxidases play key roles in the function of this enzyme. The extension of the TRS^2-FTIR spectroscopy into the nanosecond regime is a

relatively recent accomplishment that bears mention because of its relevance to the determination of motional correlation functions for the various chemical bonds in the structure of a protein.

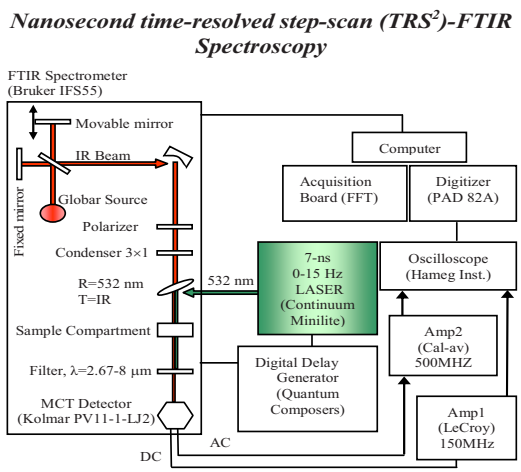

Fig.1 Schematic diagram of the nanosecond (TRS^2)-FTIR experiment.

We have applied FTIR and time-resolved step-scan Fourier transform infrared (TRS^2-FTIR) spectroscopies to investigate the protonation/deprotonation events in the Q-proton pathway of ba_3-oxidoreductase at ambient temperature. The photolysis of CO from heme a_3 and its transient binding to Cu_B is dynamically linked to structural changes that can be attributed to ring A propionate of heme a_3 (1695/1708 cm^{-1}) and to deprotonation of Asp372 (1726cm^{-1}). The implications of these results with respect to the role of the ring A propionate of heme a_3-Asp372-H_2O site as a proton carrier to the exit/output proton channel (H_2O pool) that is conserved among all structurally known heme-copper oxidases, and is part of the Q-proton pathway in ba_3-cytochrome *c* oxidase, will be presented.

The description of reaction regulation in enzymes responsible for activating and catalyzing small molecules (O_2, NO) requires identification of ligand movement into the binding site and out of the enzyme through specific channels and docking sites. We show that upon dissociation, the photolyzed CO becomes trapped within a ligand docking site located near the ring A propionate of heme a_3. Two trajectories of CO that are distinguished spectroscopically and

kinetically (ν_{CO}=2131 cm^{-1}/t_d=10-35 μs and ν_{CO}=2146 cm^{-1}/ t_d=60 μs) are observed. The 2131 cm^{-1} mode of the "docked" CO we have detected corresponds to the B_1 state of Mb and persists for 35 μs. The release of CO from the docking site is not followed by recombination to the heme a_3 Fe. Our analysis indicates that this behavior reflects a mechanism in which the protein near the ring A of heme a_3 propionate reorganizes about the released CO from the docking site, and establishes a transient barrier that inhibits the recombination process to the heme a_3 Fe for a few ms. Rebinding to heme a_3 occurs with k_2 = 29.5 s^{-1}. The time-dependent shift of the CO trajectories we observe is attributed to a conformational motion of the docking site surrounding the ligand. The implications of these results with respect to the ability of the docking site to constrain ligand orientation, and the reaction dynamics of the docking site will be discussed.

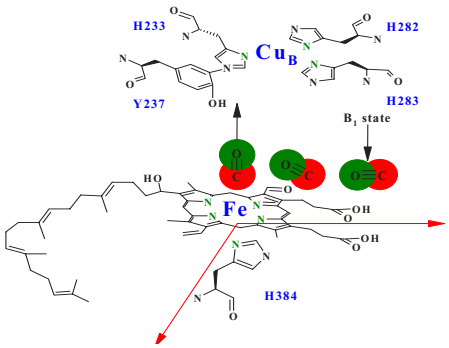

Fig.2 Schematic view of the proposed ligand trajectory (B_1 state, 2131 cm^{-1} mode).

References:1.Docking Site Dynamics of *ba*$_3$-cytochrome *c* oxidase from *Thermus thermophilus*, C. Koutsoupakis, T. Soulimane, and C. Varotsis, *J. Biol. Chem. 278*, 36806-36809 **(2003)**. 2. Ligand Binding in a Docking Site of Cytochrome *c* Oxidase: A Time-Resolved Step-Scan Fourier Transform Infrared Study, C. Koutsoupakis, T. Soulimane, and C. Varotsis, *J. Am. Chem. Soc. 125*,14728-14732 **(2003)**.3. Probing the Q-Proton Pathway of *ba*$_3$-cytochrome *c* oxidase by Time-resolved Fourier Transform Infrared Spectroscopy, C. Koutsoupakis, T. Soulimane, and C. Varotsis, *Biophys. J. 86*, 2438-2444 **(2004).** 4.TRS^2 Investigation of Heme-Copper Oxidases: Implications for O_2 Input and H_2O/H^+ Output Channels C. Koutsoupakis, E. Pinakoulaki, S. Stavrakis, V. Daskalakis, and C. Varotsis *Biochim. Biophys. Acta, 1655*, 347-352 **(2004).** Pinakoulaki et al. *J.Raman Spectroscopy* **(2005)** *in press*.

Anisotropy-Resolved Near-IR Absorption Study of Photoinduced Electron Transfer Reaction in 9,9'-Bianthryl

Tomohisa Takaya[1], Hiro-o Hamaguchi[1], and Koichi Iwata[2]
[1]*Department of Chemistry and* [2]*Research Centre for Spectrochemistry, School of Science, The University of Tokyo*

Time-resolved near-IR spectroscopy is a powerful tool for tracing the dynamics of "loosely bound" electrons, as well as for monitoring the dynamics of anharmonic vibrations. The photoinduced electron transfer is one of the elemental reactions which involve these electrons. As a prototype of the photoinduced electron transfer processes, the intramolecular electron transfer reaction in 9,9'-bianthryl (BA) has been extensively investigated by using time-resolved fluorescence and UV–visible absorption spectroscopy [1–3]. It is widely accepted that BA is photoexcited to the locally excited (LE) state by UV light and that the charge transfer (CT) state is successively formed in polar solvents [4]. Time-resolved near-IR spectroscopy is expected to provide information on its reaction mechanism by closely monitoring the dynamics of the loosely bound electrons.

We have recorded time-resolved near-IR spectra [5] and time-resolved near-IR absorption anisotropy spectra of BA in acetonitrile in the 950–1550 nm region. The obtained spectra are shown in Figures 1 and 2. An LE band similar to that of S_1 anthracene is observed at 0 ps, although its anisotropy between 1200–1550 nm is not consistent with that of S_1 anthracene. By 3 ps, the LE band disappears and a broad and structureless CT band appears. Its anisotropy is 0.25 at 3 ps and is 0.4 at 0 ps when the reorientation is taken into account. The anisotropy value of 0.4 indicates that the transition dipole involved in the CT absorption has the direction along the central C–C bond. It suggests the presence of strong inter-ring interaction in the CT state.

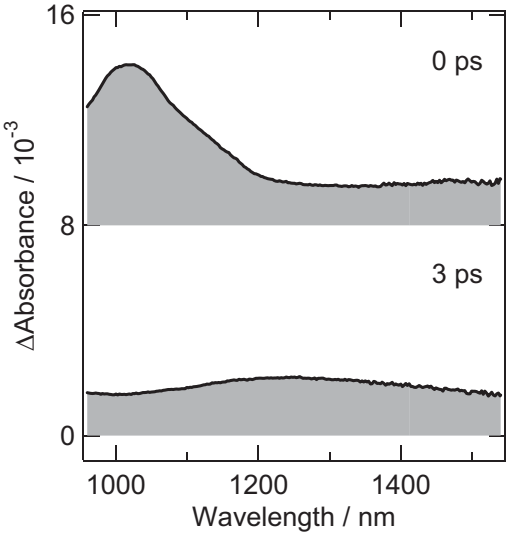

Figure 1. Time-resolved near-IR spectra of BA in acetonitrile.

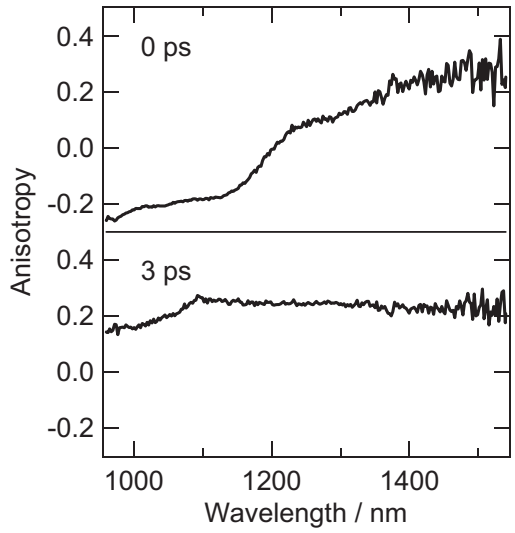

Figure 2. Time-resolved absorption anisotropy spectra of BA in acetonitrile in the near-IR region.

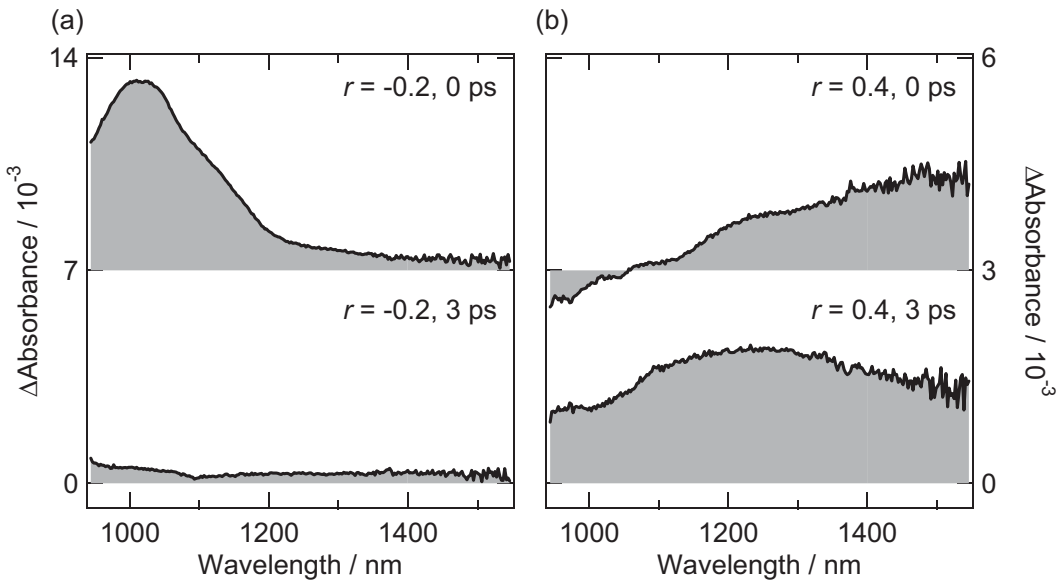

Figure 3. Decomposed transient near-IR absorption bands of BA in acetonitrile. Their anisotropy values are -0.2 (a) and 0.4 (b), respectively.

By using the observed anisotropy spectra, $r^{\mathrm{obs}}(\lambda,\tau)$, we decompose the time-resolved near-IR spectra $A^{\mathrm{obs}}(\lambda,\tau)$ into two components $A^{(-0.2)}(\lambda,\tau)$ and $A^{(0.4)}(\lambda,\tau)$, which have anisotropy of –0.2 and 0.4 respectively. The decomposition procedure is expressed as follows:

$$A^{\mathrm{obs}}(\lambda,\tau) = A^{(-0.2)}(\lambda,\tau) + A^{(0.4)}(\lambda,\tau), \tag{1}$$

$$\begin{aligned} r^{\mathrm{obs}}(\lambda,\tau) &= \frac{r^{(-0.2)}(\lambda,\tau)A^{(-0.2)}(\lambda,\tau) + r^{(0.4)}(\lambda,\tau)A^{(0.4)}(\lambda,\tau)}{A^{(-0.2)}(\lambda,\tau) + A^{(0.4)}(\lambda,\tau)} \\ &= -0.2\frac{A^{(-0.2)}(\lambda,\tau)}{A^{\mathrm{obs}}(\lambda,\tau)} + 0.4\frac{A^{(0.4)}(\lambda,\tau)}{A^{\mathrm{obs}}(\lambda,\tau)}. \end{aligned} \tag{2}$$

The decomposed spectra are shown in Figure 3. The 0-ps component with the anisotropy of 0.4 is broad and structureless, not identical but similar to the CT band. We suggest that the two anthracene rings in BA interact with each other in the LE state due to the interaction with the solvent molecules. We think that the different dynamic solvation structure for each of the two anthracene rings is essential for the electron transfer in BA.

[1] P. F. Barbara and W. Jarzeba, Adv. Photochem. **15**, 1 (1990).
[2] N. Nakashima, M. Murakawa, and N. Mataga, Bull. Chem. Soc. Jpn. **49**, 854 (1976).
[3] M. Jurczok, P. Plaza, M. M. Martin, Y. H. Meyer, and W. Rettig, Chem. Phys. **253**, 339 (2000).
[4] F. Schneider and E. Lippert. Ber. Bunsen-ges. Phys. Chem. **72**, 1155 (1968).
[5] T. Takaya, H. Hamaguchi, H. Kuroda, and K. Iwata, Chem. Phys. Lett. **399**, 210 (2004).

Ultrafast polarization and coherent charge motions in bacteriorhodopsin observed by infrared emission interferometry

Anne Colonna[1], Jean-Christophe Lambry[1], Géza I. Groma[2], Manuel Joffre[1], Jean-Louis Martin[1] & Marten H. Vos[1]

1. Laboratory for Optical Biosciences, INSERM U451, CNRS UMR 7645, Ecole Polytechnique, 91128 Palaiseau cédex, France
2. Institute of Biophysics, Biological Research Centre of the Hungarian Academy of Sciences, Szeged, H-6726, Hungary

Bacteriorhodopsin is a membrane protein acting as a light-driven proton pump in the purple membrane of the bacterium *Halobacterium salinarium*. Following absorption of a photon by the retinal cofactor, bacteriorhodopsin goes through a photocycle during which protons are pumped across the membrane. Its capacity to withstand a high photon flux and its simple photosynthetic system make it a convenient model for understanding light-driven processes involving retinal proteins, such as vision and energy transduction. The conversion of light energy in bacteriorhodopsin involves both isomerization of the retinal chromophore and charge separation, but their respective roles are subject of debate.

Our work aims at showing the interplay between the sudden macroscopic polarization appearing upon visible excitation and vibrational motions involving charge displacements. Making use of the second order nonlinear properties of bacteriorhodopsin, we have used 11 fs visible pulses in resonance with the optical transition to generate infrared emission by optical rectification (frequency down-conversion) in dried oriented bacteriorhodopsin samples[1]. This optical rectification radiation is interferometrically detected using a reference emission from a semiconductor sample. The time delay between both infrared beams is varied up to 5 ps.

As in optical rectification processes in semiconductors, a strong broadband THz radiation is emitted, which is detected interferometrically (figure 1).

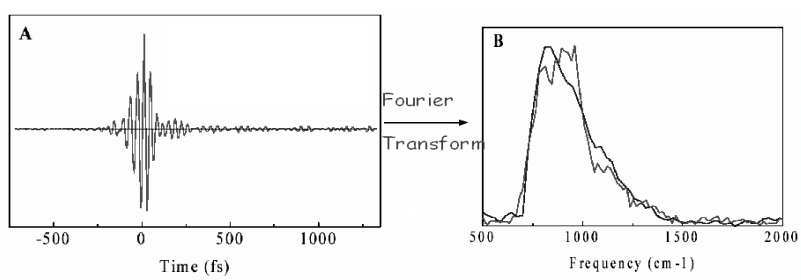

Fig. 1 : Interferometric detection of the infrared emission of bR (A) and the corresponding spectrum (B).

This implies that ultrafast (<11 fs) membrane polarization occurs upon absorption of a photon. In addition to the electronic response, long-lived infrared emission at specific frequencies is observed for t>0, reflecting charge movements associated with vibrational motions, whose coherence persists for several picoseconds, i.e. beyond retinal isomerization.

A simple two-level model is used to simulate the electronic response of bacteriorhodopsin for a resonant excitation. The vibrational part is analysed by multi-exponential decay and Fourier transform sliding window. The simultaneous and phase-sensitive observation and analysis of both the electronic and vibrational signals opens the way to study the transduction of the initial polarization into structural dynamics.

1 Groma, G. I., Colonna, A., Lambry, J.-C., Petrich, J. W., Varo, G., Joffre, M., Vos, M. H. & Martin, J.-L. (2004) *Proc. Natl. Acad. Sci. U.S.A.* **101,** 7971-7975

Ultrafast TRIR Chelation Studies Help Design Ultrafast Molecular Switches

Tung To[1], Jake Yeston[2], Edwin Heilweil[2] and Theodore Burkey[1]

[1]*Department of Chemistry, University of Memphis, Memphis, TN 38152*
[2] *Optical Technology Division, National Institute of Standards and Technology, Gaithersburg, MD 20899*

Previous TRIR experiments indicate that chelation of cymantrene derivative with pendant mono-sulfide side chain, **S1** ($[\eta^5\text{-}C_5H_4C(O)R]Mn(CO)_3$, where R = CH_2SCH_3)[1] occurs via two reaction pathways depending on the conformation of the side chain (Scheme 1). The first reaction pathway is direct ultrafast chelation if the CO dissociates when the sulfur is near the metal center. The second reaction pathway occurs through a formation of solvated intermediate if the CO dissociates when the sulfur is away from the metal center. To eliminate the competing solvation pathway, we increased the probability for the sulfur to be near the metal center by adding more sulfide groups on the Cp (cyclopentadienyl) side chain (**S2** and **S3** in Chart 1).

Scheme 1

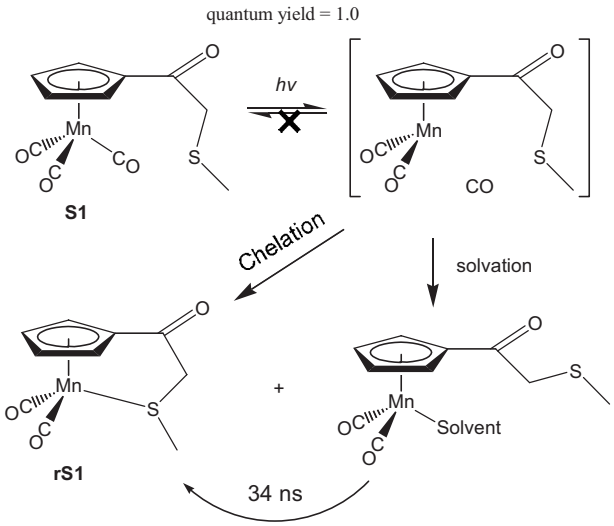

Chart 1

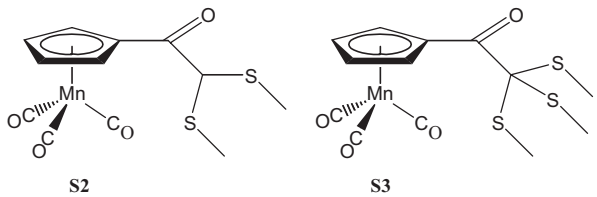

Figure 1 shows results from the ultrafast TRIR chelation dynamics of **S2** and **S3** in heptane. Similar to **S1**, chelation of **S2** occurs via two reaction pathways. However, chelation of **S3**, under identical conditions, occurs only via direct chelation.[2]

The chelation of **S2** and **S3** and ring opening of their isolated chelates in acetonitrile will also be discussed. Our preliminary results from FTIR experiments are shown in Figure 2. The nitrile coordinated product is stable and has lifetime beyond FTIR experimental timescale.

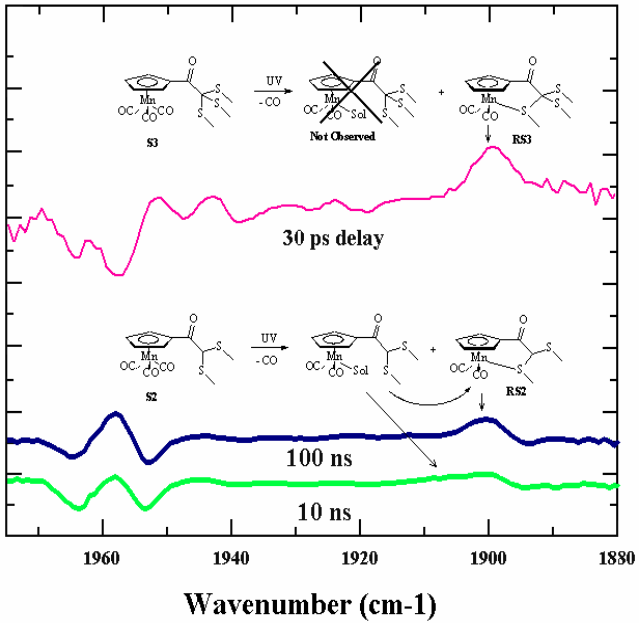

Figure 1: TRIR spectra upon irradiation of **S2** and **S3** in heptane

UV irradiation of **S2** or **S3** in acetonitrile results in the formation of chelates with no evidence for the formation of the nitrile solvated product. UV irradiation of **rS2** (chelate of **S2**) yields the nitrile coordinated product, but irradiation of **rS3** (chelate of **S3**) only leads to decomposition of the starting chelate with no evidence of the nitrile solvated product.

We further prepared the first reversible photo-molecular switches based on non-competing chelation as shown in Figure 3. Visible irradiation of purple **rA1N** results in the formation of blue **rA1O**. Subsequently, **rA1O** returns to **rA1N** by thermal conversion at room temperature.

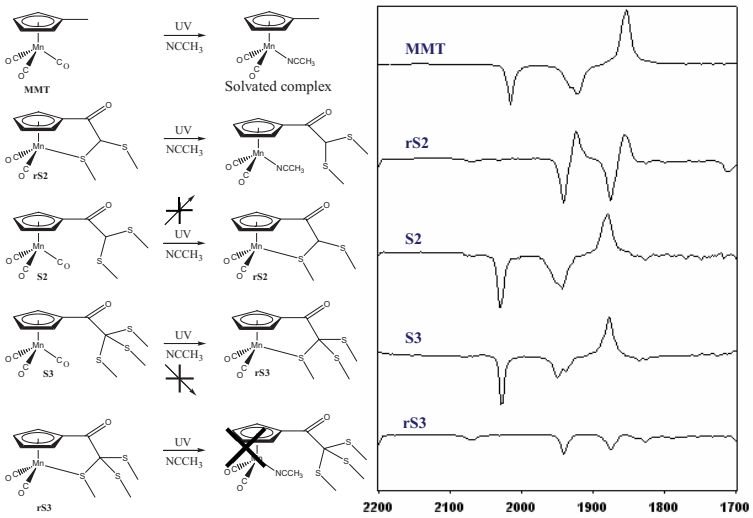

Figure 2: FTIR different spectra upon irradiation of **MMT** (methylcyclopentadienyl manganese tricarbonyl) , **S2**, **S3**, **rS2**, and **rS3**

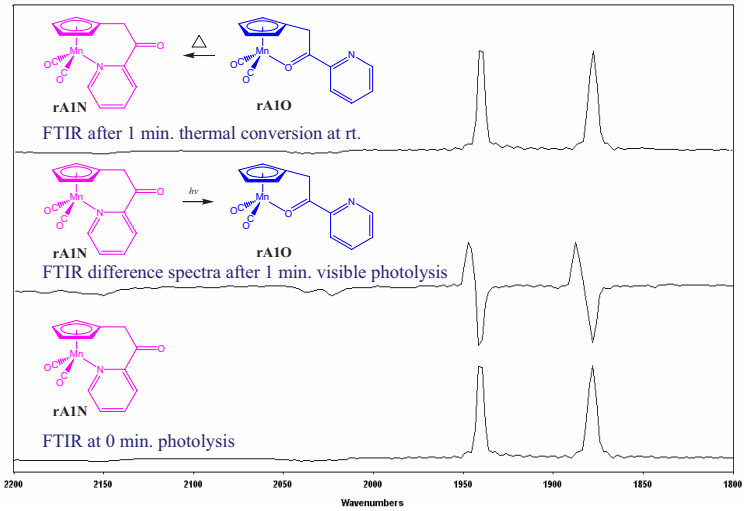

Figure 3: Reversible FTIR spectral changes upon reversible photo and thermal isomerization of **rA1N** and **rA1O**

---

[1] Jiao,T.; Pang, Z.; Burkey, T. J.; Johnston, R. F.; Heimer, T. A.; Kleiman, V. D.; Heilweil, E. J. *J. Am. Chem. Soc*. **1999**, *121*, 4618-4624.

[2] Yeston, J. S., To, T. T., Burkey, T. J., Heilweil, E. J. *J. Phys. Chem. B*, **2004**, 108, 4582-4585.

Polarisation spectroscopy of chiral molecules: First attempts at OHD-RIKOA on phenylethanol and quartz

David A. Turton, Neil T. Hunt, Andrew R. Turner, and Klaas Wynne
Department of Physics, University of Strathclyde, Glasgow G4 0NG, Scotland, UK

Time-domain polarisation spectroscopies such as Raman-induced Kerr-effect spectroscopy (RIKES) have been successfully used to probe low frequency vibrations and librations in liquids.[1] However, in all but the simplest systems individual modes cannot be resolved impeding meaningful analysis. A technique sensitive only to modes that change the chirality of the molecule would greatly simplify the spectrum allowing individual assignments to be made. We have derived the theory[2] of a new time-domain technique called optical heterodyne-detected Raman-induced Kerr optical activity (OHD-RIKOA) which is equivalent to Raman Optical Activity (ROA) in the frequency domain.[3] Like ROA, RIKOA depends on interactions with the electric-quadrupole and magnetic-dipole moments in addition to the electric-dipole moment of the molecules and therefore RIKOA is applicable only to non-racemic samples of chiral molecules. Our experimental RIKOA set-up and preliminary results on phenylethanol and crystalline quartz are described here. Normal-mode analysis is also being undertaken to allow the measured spectra to be assigned.

According to the theory of RIKOA, the four-wave mixing interaction results in transient optical activity of the sample inducing a rotation in the plane of polarisation of the probe beam, which can be detected by balanced detection following a polarising beamsplitter (Fig. 1). Due to the much lower interaction strength of the magnetic-dipole and electric-quadrupole moments compared to the electric-dipole-moment interaction of RIKES, this signal is expected to be at least three orders of magnitude smaller. This pushes the limit of achievable signal-to-noise ratios but also means that the signal must be measured in the presence of potentially much larger interfering signals. However, the ellipticity induced by RIKES does not generate a signal in the RIKOA configuration and since the theory shows that the RIKOA signal is generated for any polarisation of the pump-laser field, the pump and probe fields can be polarised parallel, suppressing any RIKES signals. This makes the experimental geometry equal to that of SMOKE (spatially-masked optical-Kerr effect).[4] The SMOKE signal can be used to optimise the experimental set-up but is easily removed by avoiding any aperturing of the probe beam and is further suppressed by the balanced detection used to measure RIKOA.

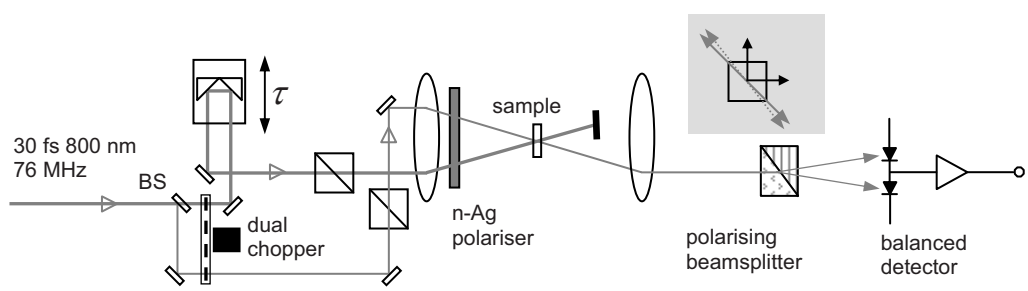

Fig. 1 RIKOA experimental setup

The polarisation of pump and probe beams is defined by a pair of cube prisms followed by a silver-nano-particle polariser, which has an extinction ratio of $>10^4$. With a diameter of 25 mm, both beams can be accommodated enabling a high degree of parallelism, and with a thickness of 1 mm it can be placed after the focusing lens to remove any strain-induced birefringence. The first (doublet) lens focuses the two beams to a diffraction-limited spot in the sample. The probe beam is then recollimated and analysed by a Wollaston prism and a balanced photodiode detector.

For lock-in detection, a dual frequency optical chopper reduces the noise due to scattering of the pump in the sample. In addition, an RTP Pockels cell can be used. RTP has a very low piezo-electric response allowing it to be switched rapidly without inducing ringing. This will allow us to increase the modulation frequency to at least 100 kHz, reducing background noise levels, and allowing more elaborate schemes of polarisation control. As the RIKOA signal arises from a rotation of the probe polarisation, inserting a half-wave plate between the sample and

the analyser changes the polarity of the measured signal. Implementing the half-wave plate by the Pockels cell will allow us to modulate the signal at high frequency without the inefficiency of a chopper.

For initial studies, molecular liquids were chosen with a large expected RIKES signal. Chosen for study were the small chiral molecules 1-phenylethanol and 1-phenylpropanol, which have a large polarisability anisotropy (producing a large RIKES signal) and a previously measured ROA spectrum. The ROA spectra[3] for 1-phenylethanol show a strong mode at ~320 cm^{-1}, which is well within the bandwidth of our 30 fs duration laser pulse . This 320 cm^{-1} mode is visible in our RIKES spectrum (Fig. 2), which also shows a much stronger mode at ~145 cm^{-1} beyond the low-frequency cut-off of the ROA instrument.

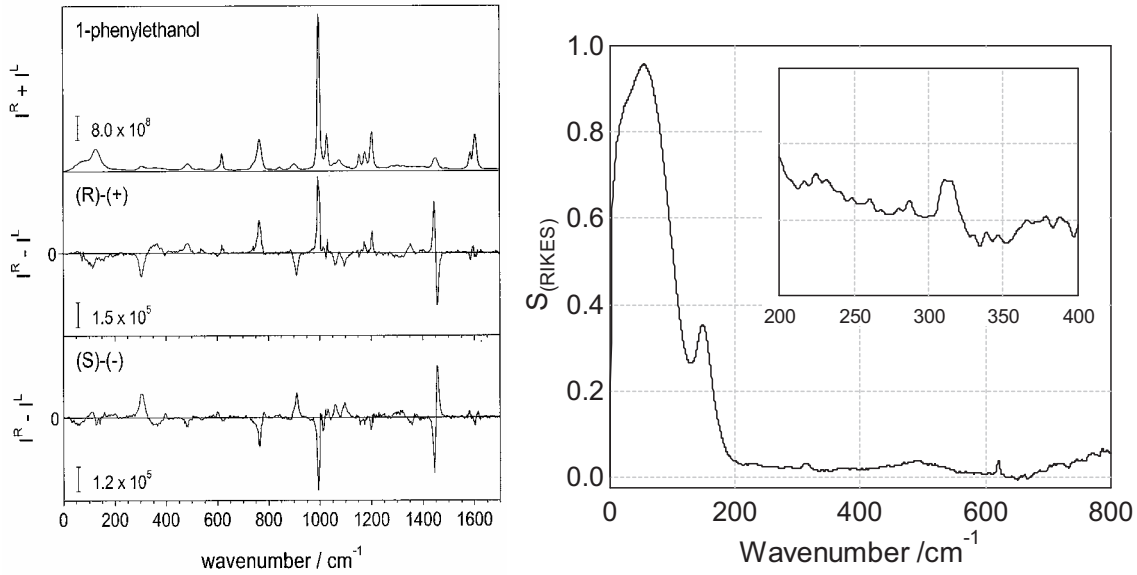

Fig. 2. (left) The Raman (top panel) and ROA spectra (lower two panels) of 1-phenylethanol.[3] (right) The OHD-RIKES spectrum of 1-phenylethanol.

Measurements were performed in the RIKOA configuration (Fig. 3) but did not exhibit the expected oscillations due to the vibrational mode at 320 cm^{-1}. Instead, we observed an exponential decay on a 100-fs timescale, which appears to change sign depending on the enantiomer used. This could be due to chirally active librational motions. Further work is needed to improve the SNR and repeatability of these signals.

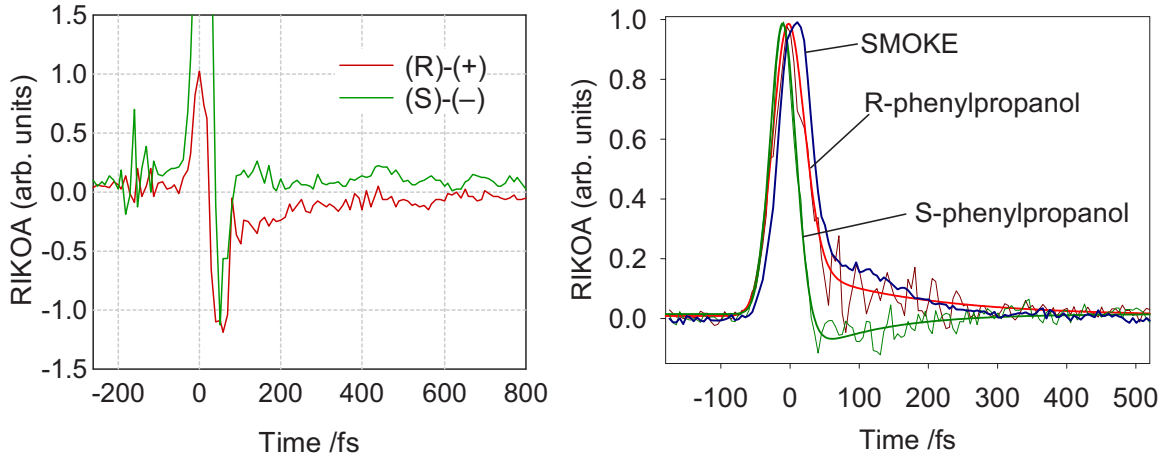

Fig. 3 RIKOA signals for both enantiomers of (left) 1-phenylethanol and (right) 1-phenylpropanol

The absence of a strong RIKOA signal from vibrational modes could have a simple explanation: The theoretical expression for the RIKOA signal in the forward direction is[2]

$$S_{RIKOA} = -\frac{N\omega_0}{16}\frac{\left(E_0^{pump}\right)^2\left(E_0^{probe}\right)^2}{c}\left[4\alpha^{iso}\gamma^{iso} + \tfrac{4}{45}\beta(\gamma) + \tfrac{4}{45}\beta(\theta)\right]\mathrm{Re}\int_0^\infty d\tau G(\tau)\tfrac{i}{\hbar}\left\langle\left[q(\tau),q\right]\right\rangle_Q . \quad (1)$$

In the simplest model for predicting ROA intensities, where it is assumed that the molecular bonds are axially-symmetric, the three bracketed terms sum to zero for forward-scattering and the ROA signal can only be seen in back-scattering, whereas our experimental RIKOA configuration is equivalent to ROA scattering in the forward direction. The possibility of overcoming this by using counter-propagating pump and probe beams will be investigated although this would inevitably compromise both time resolution and signal strength. This zero-signal condition is, however, lifted if the vibrational mode involves a non-axially symmetric bond.[5]

"Giant" ROA signals have been reported from crystalline quartz.[6] For light propagating along the *c*-axis, quartz is optically active and non-birefringent. Our RIKES signal shows vibrational normal modes at 128, 265, and 406 cm^{-1} agreeing with literature values[7] for the frequencies of the Raman-active *E* modes. The experimental RIKOA spectrum, however, shows strong modes at 206, 355, and 465 cm^{-1} corresponding to the A_1 (totally symmetric) modes of crystal quartz. These modes appear to generate artefacts with derivative lineshape character in the RIKES spectrum. The cause of these cross contaminations between RIKOA and RIKES are currently under investigation.

The RIKOA signals shown in Figure 3 are weak and clearly of a very preliminary nature. However, there are good reasons to believe that the signal-to-noise ratio can be improved considerably. With improvements such as this, RIKOA will be a very interesting and useful technique for the study of chiral liquids and proteins.

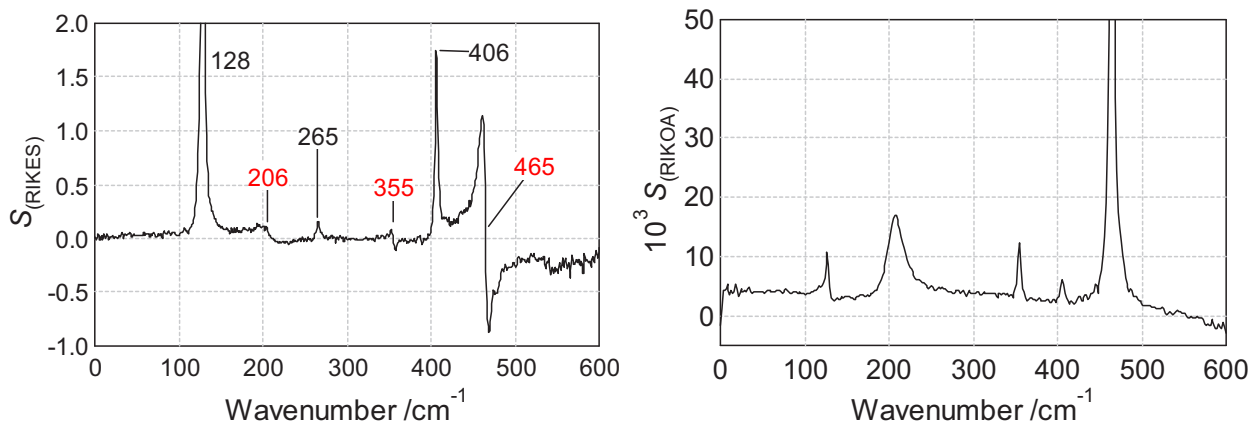

Fig. 4 RIKES and RIKOA spectra for crystalline quartz

1 G. Giraud, J. Karolin, and K. Wynne, Biophysical Journal **85**, 1903 (2003); N. A. Smith and S. R. Meech, International Reviews in Physical Chemistry **21**, 75 (2002).

2 K. Wynne, Journal of Chemical Physics **in press** (2005); K. Wynne, presented at the Time resolved vibrational spectroscopy, Gaithersburg M.D., 2005 (unpublished).

3 L. D. Barron, L. Hecht, I. H. McColl, and E. W. Blanch, Molecular Physics **102**, 731 (2004).

4 C. J. Fecko, J. D. Eaves, and A. Tokmakoff, Journal of Chemical Physics **117**, 1139 (2002).

5 L. D. Barron, L. Hecht, A. R. Gargaro, and W. Hug, Journal of Raman Spectroscopy **21**, 375 (1990).

6 M. Klein and M. Maier, Optics Communications **44**, 411 (1983).

7 J. D. Masso, C. Y. She, and D. F. Edwards, Phys. Rev. B **1**, 4179–4181 (1970).

Direct Observation of the Ultrafast Intersystem Crossing in Tris(2,2'-bipyridine)ruthenium(II) using Femtosecond Stimulated Raman Spectroscopy‡

SANGWOON YOON, PHILIPP KUKURA and
RICHARD A. MATHIES*

Department of Chemistry
University of California
Berkeley, California 94720
U.S.A.

Time-resolved femtosecond stimulated Raman spectroscopy (FSRS) is used to explore the ultrafast intersystem crossing between the metal-to-ligand charge transfer (MLCT) states of tris(2,2'-bipyridine)ruthenium(II) ($Ru(bpy)_3^{2+}$). Excitation at 480 nm by a ~35 fs actinic pump pulse initiates electron transfer from the metal to the bipyridine ligands and the subsequent changes in the vibrational structure of the ligands are probed by FSRS with high spectral (10 cm^{-1}) and temporal (70 fs) resolution. The unique Raman spectral features of the ^{3}MLCT state of $Ru(bpy)_3^{2+}$ appear with rise times from 100 to 130 fs. An upper limit for the initial ^{1}MLCT state lifetime of < 30 fs is determined by the spontaneous emission spectra and quantum yield. The ultra short lifetime of the ^{1}MLCT state is attributed to fast Franck-Condon vibrational and solvent relaxation of the excited singlet state into near degeneracy with the triplet state, leading to fast and efficient intersystem crossing.

1. Introduction

Polypyridyl ruthenium complexes are key elements of solar energy conversion devices.[2]. A key question in achieving high conversion efficiencies concerns the rate of intersystem crossing (ISC) among the electron transfer states of the sensitizer molecule.[3] Tris(2,2'-bipyridine)ruthenium(II) ($Ru(bpy)_3^{2+}$) is a prototype sensitizer that absorbs in the visible (λ_{max} = 453 nm, ε = 14 650 $M^{-1}cm^{-1}$) and emits in the red (λ_{max} ~ 620 nm). The prominent absorption band with a maximum at ~450 nm (Fig. 1) is due to a charge transfer transition from a metal-centered d-orbital to a ligand-centered π^*-orbital to form a singlet metal-to-ligand charge transfer (^{1}MLCT) state. The ^{1}MLCT state then undergoes intersystem crossing to a triplet MLCT state (^{3}MLCT) with a near unity quantum yield.[4] The absence of significant fluorescence from the ^{1}MLCT state and the large spin-orbit coupling of ruthenium (878 cm^{-1})[5] suggests that ISC to the ^{3}MLCT state occurs very rapidly and efficiently.

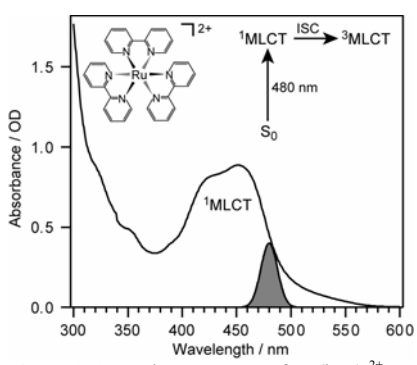

Figure 1. Asorption spectrum of $Ru(bpy)_3^{2+}$.

Here we present time-resolved vibrational structural measurements of the formation of the ^{3}MLCT state of $Ru(bpy)_3^{2+}$ using time-resolved femtosecond broadband stimulated Raman spectroscopy (FSRS).[6-10] FSRS allows one to follow the evolution from reactant to product by observing the changes in *vibrational structure* with both high temporal (70 fs) and spectral (10 cm^{-1}) resolution. In FSRS experiments, a femtosecond actinic pump pulse prepares molecules in the excited electronic state. Subsequently, the structural evolution of the excited molecules is probed at various time delays by coupling a narrow-band picosecond Raman pump pulse with a broadband femtosecond Raman probe pulse that gates the stimulated Raman signals.[10,11] Here, we use FSRS to structurally resolve the appearance of the triplet state of $Ru(bpy)_3^{2+}$ as the ISC from the ^{1}MLCT state to the ^{3}MLCT state occurs.

‡ A complete version of this work has been submitted to *Molecular Physics* (ref [1]).

* Corresponding author. E-mail: rich@zinc.cchem.berkeley.edu

2. Experimental Section

Crystalline $Ru(bpy)_3Cl_2$ (Aldrich) was dissolved in deionized water to give an absorbance of ~0.8 at 480 nm in 0.2 mm-pathlength cell. The FSRS apparatus and methods have been described in detail elsewhere.[9] Briefly, we used the actinic pump pulses at 480 nm (400 nJ/pulse) with 34 fs pulse duration. Raman pump was ~5 ps long, 1.5 μJ/pulse at 801 nm and broadband Raman probe was 20 fs, 830-960 nm, 6 nJ/pulse. The instrument response, 70 fs, was determined by optical Kerr cross-correlation between the actinic pump and Raman probe.

3. Results

Femtosecond stimulated Raman spectra of $Ru(bpy)_3^{2+}$ at selected time delays after 480 nm excitation into the ^{1}MLCT state reveal the evolution of the excited state features. At short time delays between 0 and 50 fs, we observe small features at 1308 and 1482 cm^{-1} shifted from the two largest ground state peaks by about 8 cm^{-1}. These features appear and decay with the temporal characteristics of the cross correlation. Similar downshifts and kinetics were observed for the solvent peaks in CH_3CN and C_3H_7CN experiments. It is most likely that these peaks are caused by slight frequency shifts of the Raman probe field caused by cross phase modulation.

At longer times, six new vibrational bands grow in until ~300 fs and remain unchanged up to 10 ps. These spectral and temporal features are independent of solvent since they are reproduced in CH_3CN, and C_3H_7CN spectra. The vibrational frequencies of these features exactly match those of picosecond[12] and nanosecond[13] time-resolved resonance Raman (TR^3) spectra which have been assigned to the ^{3}MLCT state. Normal mode analysis by Kincaid and coworkers[14] provides the vibrational characters of each peak from the ^{3}MLCT state as denoted in Fig. 2. The strongly dispersive lineshape of the 1169 cm^{-1} mode persists regardless of Raman pump wavelength or use of different solvents, suggesting that it arises from unique vibrational dynamics associated with this mode. Similar lineshapes are observed when the phase of the vibrational coherence changes during the dephasing[15] and also when time delay between the Raman pump and Raman probe is altered.[11]

The growth of the amplitudes of the three vibrational bands at 1548 (C=C stretch), 1498 (C=C stretch), and 1208 cm^{-1} (C-H in-plane wag) as a function of time delay are plotted in Fig. 3 along with the transient absorption kinetics at ~870 nm, which shows a rise similar to the kinetics of the vibrational bands. Kinetic analysis was performed based on the upper limit of the ^{1}MLCT state lifetime from quantum yield experiments (< 30 fs, , ref [1]) and the rise of the transient absorption and the vibrational features that belong to the ^{3}MLCT state.

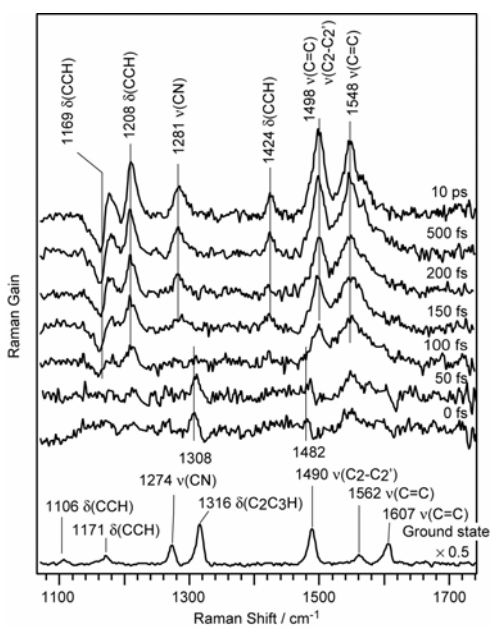

Figure 2. Excited state FSRS spectra of $Ru(bpy)_3^{2+}$ in water at selected time delays compared to the ground state FSRS spectrum.

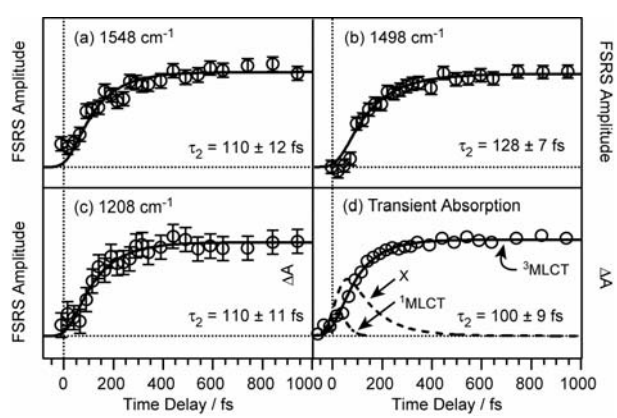

Figure 3. Kinetic analysis of the Raman bands at 1548, 1498, and 1208 cm^{-1} and transient absorption at 870 nm. Open circles represent the amplitudes of the signal and lines are best fit to the data using the model in Eq. (1). The time constant, τ_1, is fixed at 20 fs to meet the requirement of the lifetime of the ^{1}MLCT state (<30 fs) from the quantum yield measurements. The time constants (τ_2) from the fits are given in each panel.

The discrepancy between the short-lived ^{1}MLCT state (< 30 fs) measured by fluorescence and the relatively slow rise of the ^{3}MLCT state indicated in the FSRS spectra invokes a 3-state model:

$$^1MLCT \xrightarrow{k_1} X \xrightarrow{k_2} {}^3MLCT . \quad (1)$$

The rise of the intensities of the three vibrational bands arising from the ^{3}MLCT state and of the transient absorption kinetics were fit after convolution with a Gaussian instrument response function (FWHM ~70 fs). Due to the ultrafast kinetics of the ^{1}MLCT state, compared to the instrument response time, we fixed the time constant k_1 = (20 fs)$^{-1}$. The nonlinear least square fits yield the time constant k_2 ranging from 100 to 130 fs, suggesting that the ^{3}MLCT state is formed on a ~100-fs time scale. Although not directly observed, the predictions of the model for the population of the ^{1}MLCT state and of the intermediate X are given in the last panel of Fig. 3.

4. Discussion

The transition of $Ru(bpy)_3^{2+}$ from the ^{1}MLCT state to the ^{3}MLCT state is probed by monitoring the evolution of fs time resolution vibrational Raman spectra. The short lifetime of the ^{1}MLCT state is consistent with the fluorescence upconversion measurements by Okada and coworkers[16] who reported a lifetime of 40±15 fs. They also reported a fluorescence quantum yield of 9×10^{-5} from the emission spectrum which is 30-fold too high for their measured lifetime in the fluorescence upconversion study. This inconsistency may be due to their incorrect assignment of the shoulder in the emission spectrum to fluorescence.

We obtained a ~110 fs time constant for the formation of the ^{3}MLCT state from the vibrational kinetics of the FSRS spectra. The increase in vibrational intensities in FSRS spectra is unambiguously assigned to the formation of the ^{3}MLCT state since the vibrational frequencies between 100 fs and 10 ps agree with those of the ^{3}MLCT state known from previous ns and ps TR^3 studies. The lack of the vibrational features arising from the ^{1}MLCT state at short time delays is related to its ultrashort lifetime which would produce very broad bands (530 cm^{-1} full width for a 20 fs lifetime) and poor detectability.

The time constant for the formation of the ^{3}MLCT state obtained from time-resolved FSRS and transient absorption at NIR agrees with the time scale determined by transient absorption experiments in visible region by McCusker and coworkers.[17] They suggested that the formation of the ^{3}MLCT state is completed in ~300 fs. However, their probe window was limited to the 440-520 nm spectral region where the transient absorption spectra at time delays > 300 fs show only bleach of the strong ground-state absorption. Without the presence of the excited state features in the spectra, their results produce only a lower bound for the ^{3}MLCT state formation time. Our FSRS results provide definitive structural evidence that the ^{3}MLCT is indeed formed with a ~110 fs time constant. This result illustrates the value of a time-resolved structural technique over solely electronic transient absorption.

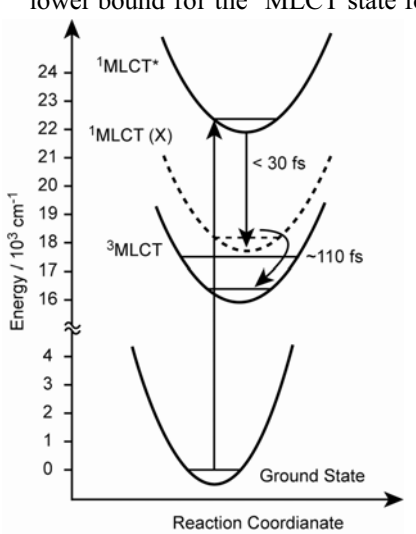

Figure 4. Schematic of the MLCT state dynamics in $Ru(bpy)_3^{2+}$.

We propose the model in Fig. 4 to explain our observations. Upon absorption at 480 nm, metal-to-ligand charge transfer reaction of $Ru(bpy)_3^{2+}$ creates a large dipole moment change (8.8 D)[18] Fast response of the solvent around this dipole as well as Franck-Condon vibrational relaxation stabilizes the excited state and lowers its energy rapidly into near degeneracy with triplet state. This rationalizes strong singlet oscillator strength with the fast loss of resonance emission (< 30 fs) in the 400-500 nm fluorescence probe window. Such a short lifetime is also consistent with the time scale of the inertial response of water solvent in charge transfer systems that has been predicted by molecular simulations[19] and measured by femtosecond fluorescence upconversion.[20] The internal vibrational reorganization energy of ~900 cm^{-1} that can be calculated from the resonance Raman intensities[21] together with the solvent reorganization energy of ~3200 cm^{-1}[12] bring the singlet state down by a total of 4100 cm^{-1} which is 2/3 of the singlet-triplet energy gap of ~6000 cm^{-1}.[22] This Stokes-shifted ^{1}MLCT state is presumably the species X in our kinetic

modeling. In this near resonant condition, the small energy gap and corresponding good Franck-Condon factors lead to rapid ISC although it is not clear whether the ~110 fs time constant is dominated by the rate of solvation, spin conversion or vibrational relaxation in the ^{3}MLCT state or a convolution of all three processes since they are expected to occur on similar time scales.

Acknowledgements

We gratefully acknowledge the support of the National Institutes of Health (EY02051) in setting up the FSRS apparatus and the Mathies Royalty Fund for supporting this research.

References

[1] S. Yoon, P. Kukura, C. M. Stuart, R. A. Mathies, *Mol. Phys.*, Submitted (2005).
[2] A. Hagfeldt, M. Graetzel, *Acc. Chem. Res.* **33**, 269 (2000).
[3] G. Benko, P. Myllyperkio, J. Pan, A. P. Yartsev, V. Sundstrom, *J. Am. Chem. Soc.* **125**, 1118 (2003).
[4] F. E. Lytle, D. M. Hercules, *J. Am. Chem. Soc.* **91**, 253 (1969).
[5] J. S. Griffith. *The Theory of Transition Metal Ions*, Appendix 6, Cambridge University Press, Cambridge (1971)
[6] M. Yoshizawa, Y. Hattori, T. Kobayashi, *Phys. Rev. B* **49**, 13259 (1994).
[7] M. Yoshizawa, M. Kurosawa, *Phys. Rev. A* **61**, 013808/1 (2000).
[8] D. W. McCamant, P. Kukura, R. A. Mathies, *J. Phys. Chem. A* **107**, 8208 (2003).
[9] D. W. McCamant, P. Kukura, S. Yoon, R. A. Mathies, *Rev. Sci. Instrum.* **75**, 4971 (2004).
[10] S.-Y. Lee, D. Zhang, D. W. McCamant, P. Kukura, R. A. Mathies, *J. Chem. Phys.* **121**, 3632 (2004).
[11] S. Yoon, D. W. McCamant, P. Kukura, R. A. Mathies, D. Zhang, S.-Y. Lee, *J. Chem. Phys.* **122**, 024505/1 (2005).
[12] P. J. Carroll, L. E. Brus, *J. Am. Chem. Soc.* **109**, 7613 (1987).
[13] R. F. Dallinger, W. H. Woodruff, *J. Am. Chem. Soc.* **101**, 4391 (1979).
[14] D. P. Strommen, P. K. Mallick, G. D. Danzer, R. S. Lumpkin, J. R. Kincaid, *J. Phys. Chem.* **94**, 1357 (1990).
[15] P. Kukura, S. Yoon, R. A. Mathies, Manuscript in preparation (2005).
[16] A. C. Bhasikuttan, M. Suzuki, S. Nakashima, T. Okada, *J. Am. Chem. Soc.* **124**, 8398 (2002).
[17] N. H. Damrauer, G. Cerullo, A. Yeh, T. R. Boussie, C. V. Shank, J. K. McCusker, *Science* **275**, 54 (1997).
[18] D. H. Oh, S. G. Boxer, *J. Am. Chem. Soc.* **111**, 1130 (1989).
[19] J. S. Bader, D. Chandler, *Chem. Phys. Lett.* **157**, 501 (1989).
[20] R. Jimenez, G. R. Fleming, P. V. Kumar, M. Maroncelli, *Nature* **369**, 471 (1994).
[21] V. I. Baranovski, O. O. Lubimova, A. A. Makarov, O. V. Sizova, *Chem. Phys. Lett.* **361**, 196 (2002).
[22] J. V. Caspar, T. J. Meyer, *J. Am. Chem. Soc.* **105**, 5583 (1983).

Time-Resolved Infrared Absorption Studies of the Solvent Dependent Vibrational Relaxation Dynamics of Chlorine Dioxide

Joshua C. Bolinger, Teresa J. Bixby, and Philip J. Reid

Department of Chemistry, Box 351700, University of Washington, Seattle WA 98195, USA
preid@chem.washington.edu Phone: (206) 543-6147

Introduction. Halooxides are an important class of compounds in atmospheric chemistry. The halooxide chlorine dioxide (OClO) has received interest due to its potential as a reservoir species for atomic chlorine (Cl) in the stratosphere.[1,2] Photoexcitation of gaseous OClO results predominately in dissociation to form ClO and O. In solution, the quantum yield for Cl production increases relative to the gas phase, but the predominant photochemical pathway remains the formation of ClO and O. However, the presence of solvent results in recombination of the primary photofragments resulting in the production of ground-state OClO with 17,000 cm^{-1} of excess vibrational energy. Time-resolved resonance Raman and UV-visible transient absorption studies have suggested that the initial energy available to OClO upon recombination is deposited along the asymmetric-stretch coordinate; however, a direct measure of energy deposition and vibrational relaxation along this coordinate has yet to be obtained. To address this issue, we have performed a series of time-resolved infrared (TRIR) absorption studies on OClO dissolved in H_2O, D_2O, and acetonitrile.[3,4] By using infrared absorption spectroscopy, the role of the asymmetric stretch in the geminate recombination and vibrational relaxation dynamics of OClO can be determined.

Experimental. The output of a regenerative Ti:sapphire amplifier (Spectra Physics) was split into two beams using a 60/40 beamsplitter. The higher energy beam was used to pump an optical parametric amplifier (OPA, Quantronix TOPAS), and the signal and idler beams from the OPA were used for difference frequency generation (DFG) in $AgGaS_2$ (type I), to produce the probe field centered at 9.5 µm. The lower energy beam derived from the amplifier output was frequency doubled using a 100-mm thick BBO crystal (type I) to provide the 401-nm pump field. The 9.5-µm probe field was collimated using two parabolic off-axis reflectors, then passed through a ZnSe 50/50 beamsplitter. The transmitted beam used as a reference while the reflected beam was used as the probe. The spatial and temporal overlap of the pump and probe fields was measured using the change in optical density in a Si wafer following 401-nm photoexcitation. The Si response was used to determine the instrument response (120 ± 50 fs full width half maximum). After passing through the sample, the probe field was delivered to a 0.25-m spectrograph (Jarrell Ash) equipped with a 100 groove/mm grating blazed at 5.6 µm to isolate individual probe frequency components with a resolution of 30 cm^{-1}. The reference field also passed through the spectrograph to ensure that identical spectral components of the probe and reference were measured. Detection of the probe and reference intensities was accomplished using two LN_2 cooled MCT detectors (Infrared Products).

Results and Discussion. The evolution in optical density for frequencies corresponding to asymmetric-stretch of OClO (~1100 cm^{-1}) following 401-nm photoexcitation is presented in Figure 1. The figure illustrates that for probe frequencies resonant with the fundamental transition, a pump-induced reduction in optical density is observed corresponding to ground-state depletion due to photolysis. As the probe frequency is reduced, higher-energy levels along the asymmetric-stretch vibrational manifold are probed. The appearance and subsequent decay in optical density observed at lower frequency is consistent with population and subsequent relaxation of these higher-energy levels. Therefore, modeling of the optical density evolution provides an approach by which to study the vibrational relaxation dynamics of OClO.

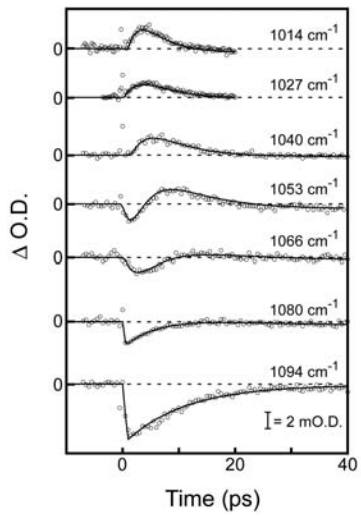

Figure 1. Evolution in optical density for aqueous OClO following photoexcitation at 401 nm measured at probe frequencies ranging from 1094 cm^{-1} to 1014 cm^{-1}. The probe wavelength at which the data were obtained is indicated. The data are presented as the circles, and the solid lines represent the best fit to the data by a sum of exponentials.

A comparison of the experimental evolution in optical density to two models for the vibrational-relaxation dynamics of OClO are presented in Figure 2. The left panel presents the prediction evolution in optical density using a simple collisional model to describe the vibrational-relaxation dynamics. In contrast, the right panel demonstrate the good agreement between the experimental and predicted optical-density evolution employing a description of the vibrational-relaxation dynamics derived from the molecular dynamics studies of Benjamin and co-workers.[5] In this approach, the relaxation rate constants as defined in the collisional model are augmented by an additional term corresponding to the frequency-dependent coupling between the solvent and solute. The superior agreement between theory and experiment for the MD treatment demonstrates that this approach represents a more accurate description of the OClO vibrational-relaxation dynamics.

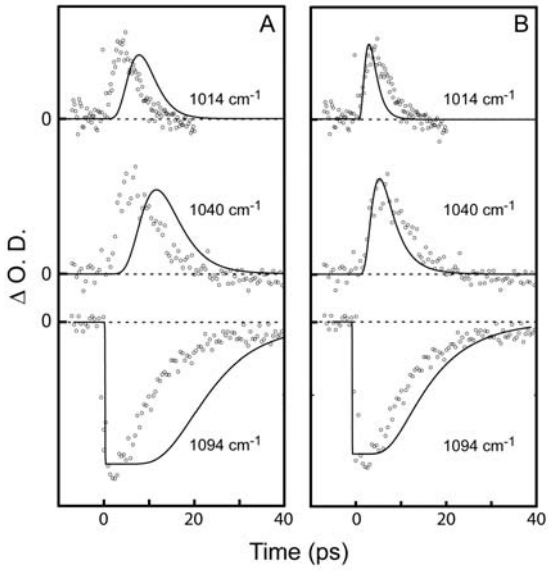

Figure 2. **(A)** Comparison of the experimental evolution in optical density of aqueous OClO (circles) to that predicted using the collisional model for vibrational relaxation along the asymmetric-stretch coordinate (solid line). **(B)** Comparison of the experimental evolution in optical density of aqueous OClO (circles) to that predicted using the perturbation model for describing the vibrational relaxation dynamics along the asymmetric-stretch coordinate (solid line). Comparisons are presented for probe wavelengths of 1094 cm^{-1}, 1040 cm^{-1}, and 1014 cm^{-1} to represent the entire vibrational dynamics across the probed asymmetric-stretch manifold.

The evolution in optical density following photoexcitation of OClO dissolved in D_2O is presented in Figure 3. Kinetic analysis of these data reveals that the vibrational-relaxation rates in D_2O are reduced by a factor of three relative to H_2O consistent with the predictions of molecular dynamics (MD). This difference reflects modification of the frequency-dependent solvent-solute coupling accompanying isotopic substitution of the solvent.

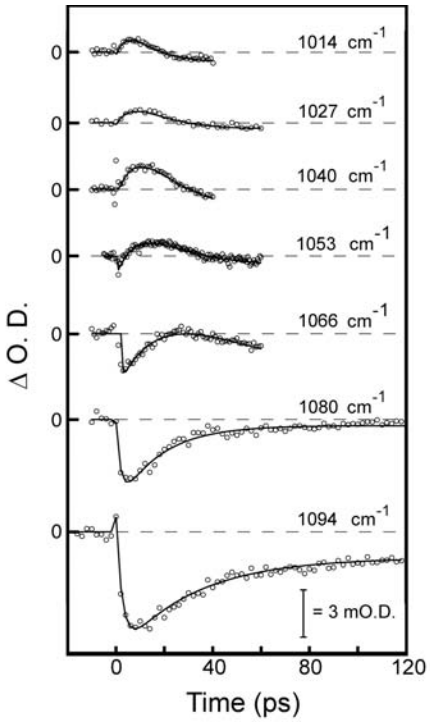

Figure 3. Evolution in optical density for OClO dissolved in D_2O following photoexcitation at 401 nm measured at probe frequencies ranging from 1094 cm^{-1} to 1014 cm^{-1}. The probe wavelength at which the data was obtained is indicated. The data are presented as the circles, and the solid lines represent the best fit to the data by a sum of exponentials

Finally, in contrast to H_2O and D_2O, modeling of the vibrational-relaxation dynamics in acetonitrile required significant modification of the frequency dependence of the solvent-solute coupling derived from MD. It is proposed that this modification reflects mode-specific vibrational-energy transfer from the asymmetric-stretch of OClO to the methyl rock of aceonitrile. In total, the results presented here provide a detailed description of the role of the asymmetric-stretch coordinate in the solvent-dependent geminate-recombination and vibrational-relaxation dynamics of OClO in solution.

Acknowledgement. The National Science Foundation is acknowledged for their support of this work (CHE-0350191). Acknowledgment is also made to the donors of the Petroleum Research Fund, administered by the American Chemical Society. JCB gratefully acknowledges support from the Rabinovich Fund administered by the Department of Chemistry at the University of Washington.

References

1. C. C. Cooksey and P. J. Reid, J. Photochem. Photobio. A **80**, 386 (2004).
2. V. Vaida and J. D. Simon, Science **268**, 1443 (1995).
3. J. C. Bolinger, S. C. Hayes and P. J. Reid, J. Chem. Phys. **121**, 4795 (2004).
4. J. C. Bolinger, T. J. Bixby and P. J. Reid, J. Chem. Phys., in press.
5. I. Chorny, J. Vieceli, and I. Benjamin, J. Chem. Phys. **116** , 8904 (2002).